Targeting DNA damage repair deficiency in pancreatic cancer

Thesis submitted to Trinity College Dublin, The University of Dublin for the degree of Doctor of Philosophy by

Jojanneke Stoof, MSc.

2025

Supervisor: Prof. Maeve Lowery

School of Medicine

Trinity College Dublin

DECLARATIONS

I declare that this thesis has not been submitted as an exercise for a degree at this or any other university and it is entirely my own work, except for the bioinformatic analysis of the DNA sequencing data found in table 4.25 which was performed by Charlotte Andrieu.

I agree to deposit this thesis in the University's open access institutional repository or allow the Library to do so on my behalf, subject to Irish Copyright Legislation and Trinity College Library conditions of use and acknowledgement.

I consent to the examiner retaining a copy of the thesis beyond the examining period, should they so wish (EU GDPR May 2018).

ACKNOWLEDGEMENTS

First of all, I want to give my sincere thanks to my supervisors Maeve and Naomi for giving me the opportunity to work on this project. Maeve, I have enjoyed our meetings these last three-and-a-half years, your guidance and clinical perspective were greatly appreciated. It can be easy to lose track of who we are doing all this research for, and you helped me to put everything in perspective – whether you were aware of it or not. Naomi, thank you for offering me a place in your lab. Your support and guidance on the laboratory side of this project as well as my professional development have been invaluable. The both of you have become role models for female researchers and have helped me to develop the skills and confidence to the next step in my own scientific career.

To the rest of the lab at LSI (or should I say NICB), it has been a pleasure to work with you and to get to know you. Charlotte, thank you for your help with the DNA sequencing – and for being a fellow liquorice and crochet enthusiast. Sara and Letizia, thank you for helping me get started in the lab when everything was chaotic due to Covid and you were still first-year PhD students yourselves. I've enjoyed working and learning (and troubleshooting, complaining, gossiping, celebrating…) alongside you. Panos and Karla, you've quickly made a place for yourselves in the lab, and I've been honoured by the trust you've put in me to help you – whether that was to train you on a technique, answer questions, or find something that I'd hoarded during the latest lab clean up.

At TTMI I would like to thank Jacintha and Fiona. Jacintha, for suggesting the Seahorse experiments and then also letting me use the machine. Fiona, for teaching me how to perform the experiments.

I also want to thank the members of the PRECODE consortium. This consortium was supported by the European Union's Marie Skłodowska-Curie Actions programme which also funded my PhD. PRECODE has not only provided me with a PhD position, training, and meetings, but has also given me access to an EU-wide network of fellow pancreatic cancer researchers. In this context I can't forget to mention Prof. Pilarsky who hosted me in his lab in Erlangen, Germany, for three months to perform the CRISPR/Cas9 screens. Special thanks here go to Isabella and Yanxi who showed me around, prepared the viral sgRNA library, and helped me with the data processing.

Back in Dublin, my thanks go to the people at Saint Vincent's University Hospital. To the surgical team who enrolled the patients and acquired the samples for the organoids. To the pathology team who processed the samples and provided the FFPE slides. But above all, to the patients who selflessly donated blood and tissue. It is humbling to realise that these samples have helped us to establish new models that will continue to help us study this terrible disease while so many of the donors have already passed away.

To all the friends that I've made these last three years – I don't think you realise how much your honest interest in my research, confused enthusiasm about the results that I was so excited about, or your heartfelt prayers when I was struggling or stressed mean to me.

Lastly, to my parents who have supported me all the way and remained curious throughout – asking for updates every Sunday evening. I don't think you had ever expected you hear so much about such a specific topic, but I am glad you did.

PUBLICATIONS

DNA damage repair deficiency in pancreatic ductal adenocarcinoma: preclinical models and clinical perspectives. J. Stoof, E. Harrold, S. Mariottino, M.A. Lowery, N. Walsh. *Frontiers in cell and developmental biology* (2021), 9, 749490.

Pancreatic Cancer 3D Cell Line Organoids (CLOs) Maintain the Phenotypic Characteristics of Organoids and Accurately Reflect the Cellular Architecture and Heterogeneity In Vivo. S. Noorani, S.R. Nelson, N.T. Conlon, J. Meiller, E. Shcheglova, A. Usai, J. Stoof, L. Palanga, F. O'Neill, S. Roche, M.B. Cotter, N. Swan, N. Walsh. *Organoids* (2022), 1, 2.

POSTER PRESENTATIONS

CRISPR screen identifies alternative synthetic lethality combinations in PDAC. J. Stoof, Y. Lu, C. Pilarsky, M. Lowery, N. Walsh. Irish Association for Cancer Research / European Association for Cancer Research Joint Annual Meeting, Dublin, Ireland. February 2024. Poster presentation

Development of a co-culture model to study the effect of cGAS/STING immune activation pathway in pancreatic periampullary intestinal adenocarcinoma. P. Sarametidis, J. Stoof, L. Ivers, J. Murphy, L. Benigno, N. Swan, M. Lowery, P. Mullan, N. Walsh. Irish Association for Cancer Research / European Association for Cancer Research Joint Annual Meeting, Dublin, Ireland. February 2024. Poster presentation

MicroRNA-31 modulates chemosensitivity via ATOX1 in pancreatic ductal adenocarcinoma. D. Hackett, J. McGrath, L. Kane, X. Lin, J. Stoof, B. Bibby, R. Hilger, M. Lowery, A. Prina-Mello, S. Maher. Irish Association for Cancer Research / European Association for Cancer Research Joint Annual Meeting, Dublin, Ireland. February 2024. Poster presentation

Mechanisms of Resistance to PARP Inhibitors in Homologous Recombination Repair-Deficient Pancreatic Ductal Adenocarcinoma J. Stoof, M. Lowery, N. Walsh. Precision Oncology forum. Nordic Oncology Forum, Stockholm, Sweden. June 2023. Poster presentation

Mechanisms of Resistance to PARP Inhibitors in HR-Deficient Pancreatic Ductal Adenocarcinoma. J. Stoof, M. Lowery, N. Walsh. EACR-AACR Basic & Translation Research Conference – Immune Responses and DNA Repair, Florence, Italy. March 2023. Poster presentation

Comparison of 2D and 3D culture systems in established and patient-derived pancreatic ductal adenocarcinoma cellular models on sensitivity to DNA damage repair targeting agents. J. Stoof, S. Noorani, S.R. Nelson, E. Zollbrecht, M. Lowery, N. Walsh. Irish Association for Cancer Research Annual Conference, Cork, Ireland. March 2022. Poster presentation

TABLE OF CONTENTS

List of Figures

List of Tables

Abbreviations

AUC	Area under the curve
BER	Base-excision repair
BME	Basement membrane extract
CAF	Cancer-associated fibroblast
CI	Combination index / confidence interval
CRISPR	clustered regularly interspaced short palindromic repeats
DDR	DNA damage repair
DM	Digestion media
DMEM	Dulbecco's Modified Eagle Medium
DMSO	Dimethylsulfoxide
DSB	Double-strand break
ECAR	Extracellular acidification rate
ECM	Extracellular matrix
FBS	Foetal bovine serum
FFPE	Formaldehyde-fixed paraffin-embedded
hCPLT	Human complete feeding media
HR	Homologous recombination
HRD	Homologous recombination deficient
HRP	Homologous recombination proficient
HTS	High-throughput screening
ICL	Interstrand cross-link
IPMN	Intraductal papillary mucinous neoplasm
MMR	Mismatch repair
MOI	Multiplicity of infection
NER	Nucleotide-excision repair
NGS	Next-generation sequencing
NHEJ	Non-homologous end-joining
OCR	Oxygen consumption rate
OCT	Optimal cutting temperature compound
ORR	Objective response rate
OS	Overall survival
OS	Overall survival
OxPhos	Oxidative phosphorylation
PanIN	pancreatic intraepithelial neoplasia
PARPi	PARP inhibitor
PBS	Phosphate-buffered saline
PDAC	Pancreatic ductal adenocarcinoma
PDCL	Patient-derived cell line
PDO	Patient-derived organoid
PFS	Progression-free survival
polyHEMA	Poly(2-hydroxyethyl methacrylate)

ROS	Reactive oxygen specifies
RPM	Rotations per minute
SOP	Standard operating procedure
SSB	Single-strand break
SV	Structural variant
TNM	Tumour, node, metastasis classification
UHP	Ultra-high pure water

ABSTRACT

Pancreatic ductal adenocarcinoma is a lethal disease with a 5-year survival of <12%. Approximately 5-10% of the patients have *BRCA1/2* mutations which cause homologous recombination (HR) deficiency and sensitise to cisplatin and PARP inhibitors (PARPi). However, intrinsic and acquired resistance are common and not well understood.

Lack of representative *in vitro* models is a challenge in treatment development, and research is shifting from the use of 2D monolayer cultures to more representative 3D spheroid and organoid cultures. Yet, the effect of culture method on drug sensitivity remains largely unexplored. In this thesis, I developed six isogeneic 2D and 3D models and investigated their sensitivity to cisplatin, olaparib, and talazoparib. I observed significant differences in sensitivity between the isogeneic models, but sensitivity did not correlate with culture method which highlights the importance of using multiple models to test drugs. Additionally, I developed and characterised four novel patient-derived organoids from rare periampullary adenocarcinomas that are suitable for toxicity assays.

To investigate the mechanism of acquired platinum and PARPi resistance, I developed cisplatin (Capan-1CisR) and PARPi (olaparib, Capan-1OlaR; and talazoparib, Capan-1TalR) mt*BRCA2* Capan-1 cells. Resistant cells had significant cross-resistance to PARPi and oxaliplatin, but not to 5-FU or gemcitabine, suggesting that 5-FU and gemcitabine may be effective second-line treatments. The resistant cells had significant metabolic alterations which may contribute to resistance. Interestingly, the metabolomic profile of Capan-1OlaR was different from that of Capan-1CisR and TalR, suggesting a different mechanism of resistance.

To investigate if loss of other DNA damage repair genes can also sensitise to PARPi, I performed two CRISPR/Cas9 knockout screens which identified *PTEN, BRCC3,* and *XRCC3* as potential targets. Validation by siRNA knockdown in a viability assay confirmed synthetic lethality. Additionally, I investigated if the combination of ATM or ATR inhibitor with PARPi can overcome resistance in the previously developed resistant Capan-1 cells. Combination of ATRi (Ceralasertib) and PARPi (Lynparza and Saruparib) was synergic in the parental and olaparib-resistant Capan-1 cells, suggesting that Ceralasertib may help to prevent or overcome olaparib-resistance in the clinic.

LAY ABSTRACT

Pancreatic ductal adenocarcinoma is a deadly disease where just one in nine patients survive longer than five years after the discovery of the disease. A small group of patients have changes in the *BRCA1* or *BRCA2* genes. This makes their cancer more sensitive to the chemotherapy agent cisplatin and PARP inhibitors. However, loss of sensitivity to treatment is common and not well understood.

One problem in the development of better treatments is the lack of good laboratory models. Traditionally, researchers have used 2D models where cancer cells are grown in a single layer. Recently, researchers have started using more 3D models that are more life-like. However, it is unclear how 2D and 3D models affect treatment sensitivity. I made six matched 2D and 3D models to test this. I saw that the model changes how sensitive cells are to medicines but that it differs per model whether the 2D or the 3D model is more sensitive. It is therefore important that researchers use multiple models when they test medicines.

To investigate how cancer cells become resistant to treatment I made cells resistant to cisplatin and two PARP inhibitors (olaparib and talazoparib) and compared how they had changed from the original, sensitive cells. The resistant cells were also resistant to chemotherapeutic drug oxaliplatin, but not to 5-FU and gemcitabine. I also discovered that the resistant cells had changes in what energy sources they use to grow.

To investigate if loss of genes other than *BRCA1/2* can also make tumour cells sensitive to PARP inhibitors I performed a CRISPR/Cas9 knockout screen. This screen showed that the genes *PTEN*, *BRCC3*, and *XRCC3* are potential targets. By using a different technique to reduce the presence of these genes from the cells (called siRNA knockdown) I confirmed that loss of these three genes makes cells sensitive to PARP inhibitors.

Lastly, I tested if the combination of ATR inhibitor and PARP inhibitor is effective in resistant cells. Combination of ATR inhibitor Ceralasertib with PARP inhibitor Lynparza or Saruparib was effective in sensitive and olaparib-resistant cells and was more effective than each medicine on its own. This suggests that addition of Ceralasertib to olaparib-treatment may prevent or overcome resistance in patients.

1 INTRODUCTION

1.1 PANCREATIC DUCTAL ADENOCARCINOMA

Pancreatic Ductal Adenocarcinoma (PDAC) is the predominant form of pancreatic cancer and is one of the most lethal cancers worldwide, accounting for 2.6% of all new cancer cases each year but causing 4.8% of all cancer deaths (Bray et al., 2024). The incidence of PDAC is rising and PDAC is projected to become the second leading cause of cancer-related death in the US by 2030, accounting for 671,000 deaths (Rahib et al., 2014). In Ireland, approximately 540 new patients are diagnosed yearly (NCRI, 2024).

Despite recent advances in personalised and targeted therapy, little progress has been made to improve disease outcome and the 5-year survival rate remains at just below 12% (Luo et al., 2023). Additionally, survival rates are strongly correlated with the disease stage at the time of diagnosis (NCRI, 2024). For patients in Ireland with stage I or II disease, the 5-year survival rate is 33% and 17%, respectively. However, for patients with stage III or IV disease this is less than 5%. Due to the cancers rapid growth, high metastatic potential, and lack of clear symptoms, over 80% of the patients are diagnosed at an advanced disease stage where curative treatment is no longer possible (Bray et al., 2024; Partyka et al., 2023).

1.1.1 The pancreas

The pancreas is a vital organ that is involved in food digestion and glucose homeostasis and is located in the upper part of the abdomen, between the duodenum and the spleen (Fig. 1.1). The regions of the pancreas can be divided into the head, body, and tail. Functionally, a distinction can be made between the endocrine and the exocrine pancreas (Cano et al., 2007; Johansson & Grapin-Botton, 2002; Pandol, 2010; Rhim & Stanger, 2010). The exocrine pancreas accounts for approximately 95-99% of the volume of the mature pancreas and produces digestive enzymes and sodium bicarbonate which are released into the duodenum to aid digestion and nutrient absorption. These enzymes are produced by acinar cells that are organised in clusters (acini) which drain into a ductule. These small ductules drain into larger interlobular ducts, which in turn drain into the main pancreatic duct. The pancreatic duct leads to the head of the pancreas where it connects with the common bile duct and releases its content in the duodenum through the ampulla of Vater.

The endocrine pancreas accounts for the remaining 1-5% of the pancreas and is structured as highly organised and well-vascularised groups of cells called the Islets of Langerhans (Cano et al., 2007; Ro et al., 2013). These islets are composed of α, ß, δ, and PP cells which produce insulin, glucagon, somatostatin, and pancreatic polypeptide, respectively.

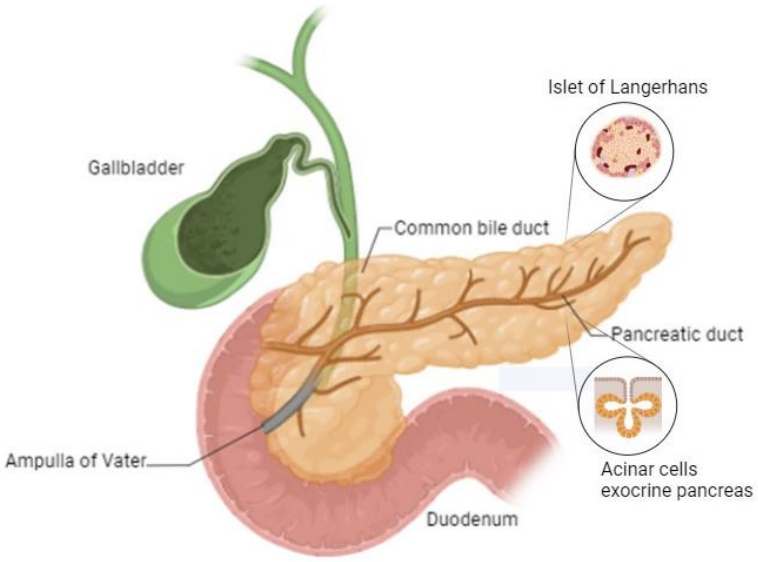

Figure 1.1. Diagram of the pancreas and associated duodenum. *Created in BioRender.*

1.1.2 Development of PDAC

PDAC arises from non-invasive precursor lesions such as pancreatic intraepithelial neoplasia (PanIN), intraductal papillary mucinous neoplasm (IPMN), or mucinous neoplasm (Distler et al., 2014; Hruban et al., 2004; Ren et al., 2019).

PanIN can be classified in three grades based on the morphology of the lesion (Hruban et al., 2004). PanIN-1 are epithelial lesions that are rich in mucin and have no cytologic abnormalities. PanIN-2 are mostly papillary epithelial lesions that have some cytologic abnormalities, such as loss of polarity, enlarged nuclei, and nuclear crowding. PanIN-3 are usually papillary or micropapillary lesions that have a high level of cytologic abnormalities, including complete loss of cell polarity, nuclear abnormalities, luminal necrosis, and cribriforming (ie. small clusters of epithelial cells into the lumen).

IPMNs are intraductal papillary growths that arise from the main pancreatic duct or its main branches (Machado et al., 2015). Consequently, the majority of the IPMNs are found in the pancreatic head. The cells are rich in mucin, especially mucin-2. Like PanIN, cytological abnormalities and cribriforming are seen in higher grades IPMNs. In contrast to PanIN, lesions are macroscopically visible (>5mm).

Mucinous neoplasms form well-defined cysts with a mucin-producing epithelium and an ovarian-type stroma (Fukushima & Fukayama, 2007). The epithelial cells are columnar and have varying degrees of cytological abnormalities. The ovarian-type stroma distinguishes mucinous neoplasms from IPMN and forms a band of spindle-shaped cells under the epithelial layer.

1.1.2.1 Driver mutations of PDAC

Progression from normal pancreas to precursor lesion to PDAC is commonly driven by sequential acquisition of driver mutations in *KRAS, CDKN2A, TP53,* and *DPC4 (Hu et al., 2021; Olaoba et al., 2024).*

KRAS is a proto-oncogene that can activate several signalling pathways that promote proliferation, metastasis, and metabolic reprogramming (Luo, 2021; Zhang et al., 2023). Constitutive activation of *KRAS* due to a missense mutation is found in 80-95% of PanIN-1 lesions and is considered to be the most common initiating event. The majority of *KRAS* mutations are found in one of three hotspots: $KRAS^{G12D}$ (40%), $KRAS^{G12V}$ (33%), or $KRAS^{G12R}$ (15%). While a lot of research is ongoing to target these KRAS mutations, currently only targeted inhibitors for $KRAS^{G12C}$, which occurs in 1-2% of PDAC, have received approval for clinical use (Oya et al., 2024; Wu et al., 2023).

The next mutation is generally loss of tumour suppressor gene *CDKN2A.* This gene encodes for protein p16, which is a negative regulator of the G1 to S phase transition. Mutations are found in 11.5% of PanIN-1/2 and 50% of PDAC (Kanda et al., 2012; Lin et al., 2020).

TP53 is a major tumour suppressor gene that encodes for p53 and regulates cell division. Loss of p53 expression due to missense or truncating mutations promotes proliferation (Kanda et al., 2013). Mutations are found in 18% of PanIN-2, 48% of PanIN-3, and in 75% of PDAC.

The latest common driver mutation is loss of *SMAD4* expression. *SMAD4* is encoded by *DPC4* and is a mediator of the TGFβ pathway which controls proliferation, differentiation, and apoptosis. Loss of *SMAD4* is rarely found in low-grade PanIN but occurs in 32-60% of PDAC (Dardare et al., 2020; Yokose et al., 2020).

1.1.3 PDAC histology and staging

PDAC is a highly heterogeneous disease that is mostly found in the pancreatic head. It is characterised by irregular glands that resemble pancreatic ducts which are embedded in desmoplastic stroma (Guillén-Ponce et al., 2017; Mostafa et al., 2018; Ren et al., 2019; Taherian et al., 2022). The stroma is rich in stromal cells, such as fibroblasts and inflammatory cells, as well as extracellular matrix (ECM) proteins. The tumour is highly invasive and has commonly infiltrated the surrounding tissues by the time it is diagnosed. At a cellular level, PDAC has nuclear abnormalities such as nuclear pleomorphism, macronucleoli, irregular nuclear membranes, and a high nucleus to cytoplasm ratio. Like it's precursor lesions, low-grade PDAC is rich in mucin, but this disappears in high-grade, poorly differentiated PDAC.

The TNM classification system is used for staging (Guillén-Ponce et al., 2017). In this classification, T describes the size and location of the main tumour, N describes the involvement of lymph nodes, and M describes the presence of metastases. At the lowest stage, stage I, the tumour is confined to the pancreas (T1/2), and there is no involvement of lymph nodes (N0) or metastases (M0). At stage II, the tumour may grow outside of the pancreas but does not infiltrate local major nerves or blood vessels (T1-3, N0, M0). At stage III, the tumour does affect local major nerves or blood vessels and may have invaded local lymph nodes (T4, N0/1, M0). At the highest stage, stage IV, the tumour has metastasised (M1). Grading is important because it provides valuable information about treatment possibilities and disease prognosis.

1.1.4 Treatment

Currently, curative treatment is limited to low-stage, resectable disease but over 80% of patients present with advanced or metastatic disease (Bilimoria et al., 2007; Ilic & Ilic, 2016; Stathis & Moore, 2010).

The most common form of resection is pancreaticoduodenectomy, also known as Whipple procedure. This surgery is used for the removal of periampullary tumours, including tumours located within the head of the pancreas (D'Cruz et al., 2024; Wei & Hackert, 2021). During the procedure the head of the pancreas, the first section of the small intestine, the gallbladder, and the bile duct are removed. The pancreatic duct in the remaining section of

the pancreas, the hepatic duct, as well as the stomach are connected to the beginning of the remaining section of the small intestine.

Current standard of care treatment for advanced PDAC consists of systemic chemotherapy, generally either combination treatment of nab-paclitaxel with gemcitabine or FOLFIRINOX (5-fluorouracil, leucovorin, irinotecan, oxaliplatin)(Adel, 2019; Mohammad, 2018; Mohammed et al., 2014). In 2013, the MPACT trial showed that nab-paclitaxel with gemcitabine improved overall survival by 1.8 months compared to gemcitabine alone (8.5 vs. 6.7 months, $p<0.001$)(Von Hoff et al., 2013). The PRODIGE trial found that FOLFIRINOX improved overall survival by 4.3 months compared to gemcitabine alone (11.1 vs. 6.8 months, $p<0.001$)(Conroy et al., 2011). While these trials show that FOLFIRINOX has a greater OS benefit, it is also associated with higher toxicity profiles and is therefore generally reserved for patients with a good performance status and given as a modified regimen. Alternative systemic treatment options for PDAC include: gemcitabine with cisplatin, nano-liposomal irinotecan with 5-FU, gemcitabine with erlotinib (for patients with activating EGR mutations), pembrolizumab (for patients with microsatellite instability), laratrectinib/entrectinib (for patients with NTRK-fusion), and olaparib (for patients with germline *BRCA1/2* mutation).

Genomic analyses have revealed a complex mutational landscape that is predominated by mutations in *KRAS, TP53, SMAD4*, and *CDKN2A* (Aguirre et al., 2018; Bailey et al., 2016). Despite extensive research, targeted therapies for TP53, SMAD4, and CDKN2A mutations have not reached clinical practice. (Linehan et al., 2024; Oya et al., 2024; Qian et al., 2020). For KRAS, the $KRAS^{G12D}$ inhibitors sotorasib and adagrasib have been approved for clinical use, but inhibitors for other KRAS mutations that are more common in PDAC are still in clinical trials (Oya et al., 2024).

In addition, PDAC is characterised by genome instability (Alexandrov et al., 2013). Genome instability has been described as one of the enabling hallmarks of cancer by Hanahan and Weinberg and can be attributed to multiple sources, including increased sensitivity to mutagenic agents, defects in the genomic maintenance machinery, loss of telomeric DNA, and aberrant surveillance mechanisms (Hanahan & Weinberg, 2011). While these aberrations can partly be attributed to the aforementioned mutated genes, additional pathway deficiencies are also involved. The DNA damage response (DDR) pathway plays a central role in genome maintenance and repair. In contrast to *TP53,* DDR deficiency is

targetable, with PARP inhibitor olaparib already available in the clinic as maintenance therapy following treatment with platinum-based chemotherapy for patients with advanced germline *BRCA* mutated PDAC (Kasi et al., 2020).

1.2 DDR PATHWAYS IN PDAC

To combat the development of mutations and the effects these may have on the cell, a complex network of DNA damage repair (DDR) pathways exists (Giglia-Mari et al., 2011). At the core of this network are the pathways for base excision repair (BER), nucleotide excision repair (NER), mismatch repair (MMR), interstrand crosslink repair (ICL), and double strand break repair (both homologous recombination (HR) and non-homologous end-joining (NHEJ)) (Fig. 1.3). Each pathway can roughly be divided into three steps: recognition of the damage, excision or processing of the damaged strand(s), and the actual repair.

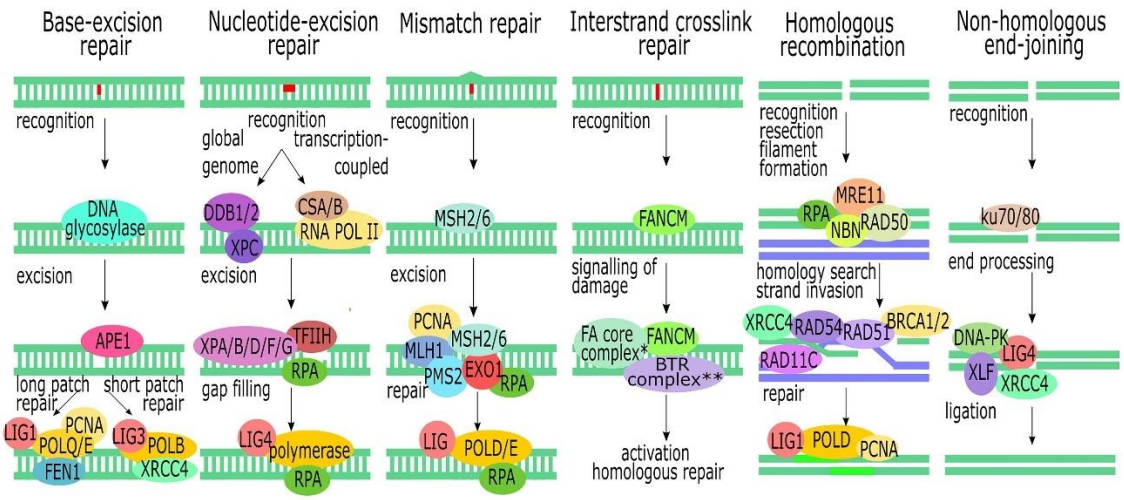

Figure 1.2. Overview of the major DNA damage repair pathways. *Based on (Deans & West, 2011; Gupta & Heinen, 2019; Lee & Kang, 2019; Ranjha et al., 2018; Yang et al., 2016). ⁎The Fanconi anemia core complex consists of FANCA, FANCB, FANCC, FANCD, FANCE, FANCF, FANCG, and FAAP100. ⁎⁎The BTR complex consists of BLM, TOPOIII, RMI1, and RMI2. This image was published in (Stoof et al., 2021).*

BER removes non-bulky single-base lesions that are caused by oxidative, deamination, and dealkylation events (Lee & Kang, 2019). The main type of damage that is repaired by BER is the removal of the cytosine deamination product uracil. The damaged base is recognised by one of multiple specific DNA glycosylases (UNG, SMUG1, NEIL1) which remove the damaged base leaving an abasic site (Caldecott, 2008, 2024; Gohil et al., 2023; Lee & Kang, 2019). The newly created abasic site is excised and processed by AP endonuclease 1 (APE1) to generate a single-strand break with a 3'-hydroxyl end. From there, two repair pathways can fill in the gap: long and short patch repair. In short-patch BER, polymerase β (POLB) fills in the missing nucleotide and ligase 1/3 (LIG1/3), aided by X-ray repair cross-complementing protein 1 (XRCC1, and possibly also PARP1), ligates the DNA backbone. In

long-patch BER, the gap is extended by removal of several additional nucleotides by flap endonuclease 1 (FEN1) which is stimulated by PARP1 and proliferating cell nuclear antigen (PCNA). The gap is filled by polymerase δ/ε (POLD/E).

The BER pathway has a lot of overlap with the single-strand break repair pathway (which is occasionally also referred to as a sub-pathway of BER). SSBs are recognised by PARP1 which is suggested to aid recruitment of repair proteins, in particular XRCC1 (Abbotts & Wilson, 2016; Beek et al., 2021). From here the ends of the DNA backbone are processed and repaired by the same machinery that is responsible for short and long-patch BER.

NER is the main pathway for the removal of bulky lesions and intrastrand crosslinks. Bulky lesions are mainly covalent base adducts that are produced by UV or ionising radiation (Lee & Kang, 2019)(Alhmoud et al., 2020; Naumenko et al., 2022). While two sub-pathways can be distinguished,global genome NER (GG-NER) for the whole genome and transcription-coupled NER (TC-NER) for the transcribing strand of active genes, the general repair process is similar to BER. GG-NER recognises distortions of the DNA helix through DNA damage-binding protein 1 and 2 (DDB1, DDB2) and Xeroderma pigmentosum complementation group C (XPC), whereas TC-NER ERCC excision repair 6 and 8 (ERCC6 and ERCC8 also known as CSB and CSA) recognise blockage of the RNA polymerase. General transcription factor IIH (TFIIH) opens up the DNA to enable ERCC excision repair 2 (ERCC2/XPD) to verify the lesion upon which several other XP endonucleases and replication protein A1 (RPA) are recruited to excise the lesion. Finally, the resulting 22 to 32 nucleotide long gap is filled and ligated to the original DNA strand by DNA polymerases and ligases.

The mismatch repair (MMR) pathway removes single nucleotide mismatches and small insertions or deletions created by DNA polymerase during DNA synthesis (Gupta & Heinen, 2019). The lesions are recognised by the heterodimer MutS homolog 2/6 (MSH2/MSH6). The dimer recruits another heterodimer, MutL homolog 1/PMS1 homolog 2 (MLH1/PMS2), and together they recruit several other proteins including Exonuclease 1 (EXO1) to excise the damage. Finally, polymerase eta or delta fills the newly created gap.

Interstrand crosslinks (ICLs) are caused by bifunctional alkylating agents that form covalent bonds between the two DNA strands (Deans & West, 2011; Hashimoto et al., 2016). In quiescent cells, the lesion is recognised and repaired by the NER pathway, but during S-phase several steps take place to activate the HR pathway. When a DNA replication fork

encounters an ICL the fork stalls and, through a complex containing FA complementation group M (FANCM), the lesion is recognised and the Fanconi anemia complex and BTR complex are recruited. These complexes create a DSB which is subsequently recognised and repaired by the HR pathway.

Double-strand breaks (DSBs) are caused by ionising radiation, DNA replication stress, and failed repair of other DNA lesions. Breaks are repaired through two main pathways: homologous recombination (HR) and non-homologous end-joining (NHEJ) (Foo & Xia, 2022; Giglia-Mari et al., 2011; Ranjha et al., 2018; Wu et al., 2020). HR can take place during the S- and G2-phases of the cell cycle when it can use the homologous sequence of a sister chromatid to accurately repair the break. The DSB is recognised by the MRN complex consisting of MRE11 homolog (MRE11), RAD50 double-strand break repair protein (RAD50), and Nibrin (NBN). The MRN complex recruits ATM which phosphorylates H2AX, and recruits the machinery to resect the ends of the break. RPA binds to and forms a filament between the newly resected single-stranded DNA section. Next, partner and localizer of BRCA2 (PALB2) is phosphorylated by ataxia telangiectasia and Rad3 related (ATR) / checkpoint kinase 1 (Chk1) and recruits BRCA2. The combination of PALB2 and BRCA2 recruit RAD51 recombinase (RAD51) to replace the RPA-filament and, assisted by several other proteins, homology search and strand invasion of the sister chromatid takes place. Using the sister chromatid as a template, polymerase delta synthesises the missing nucleotides of the broken strand, and the ends are ligated.

NHEJ, in contrast, can take place during every phase of the cell cycle and is quicker than HR but is also error-prone and commonly results in small deletions. The break is recognised by the Ku70/80 heterodimer which subsequently recruits DNA-protein kinases, non-homologous end joining factor 1 (XLF), X-ray repair cross complementing 4 (XRCC4), and DNA ligase 4 (LIG4) to process and ligate the broken ends of the DNA strands.

In recent years, important progress has been made in deciphering the molecular underpinnings of PDAC due to the unparalleled power of next generation sequencing (NGS) technologies. Constitutive mutations of PDAC have been described as selective DDR pathways in PDAC, however the main problem encountered is the heterogeneity of somatic alterations among patients outside of the four most frequently mutated genes (*KRAS, TP53, CDKN2A,* and *SMAD4*) and the ubiquity of mutant *KRAS* as an oncogenic driver which poses a challenge to the identification of potential predictive and prognostic biomarkers.

1.2.1 Germline mutations in PDAC

Approximately 10% of all PDAC cases are considered familial; defined as a family with at least two first-degree relatives with PDAC (Turati et al., 2013). While several germline pathogenic alterations that increase an individual's lifetime risk of PDAC (e.g., hereditary pancreatitis and Lynch syndrome) have been characterised, the causative germline mutation of most familial cases remains unclear (Klein, 2012). The most commonly mutated genes in familial pancreatic cancer are *BRCA2*, *CDKN2A*, *BRCA1*, and *PALB2* (Perkhofer et al., 2020). Pathogenic germline alterations have also been identified in patients who do not meet criteria for familial PDAC and may involve genes beyond those previously associated with hereditary pancreatic cancer. These pathogenic germline alterations are therapeutically considered actionable in 5% to 10% of patients, and clinical guidelines now support routinely offering germline genetic testing with a broad panel of known hereditary cancer predisposition genes to all PDAC patients (Stoffel et al., 2019).

1.2.2 Somatic mutations in PDAC

The presence of DDR gene mutations has been reported in 17-43% of all sporadic PDAC patients (Aguirre et al., 2018; Waddell et al., 2015). However, these studies focused on a limited selection of well-characterised DDR genes and potentially actionable DDR mutations may be more prevalent. In our recently published review (Stoof et al., 2021), we queried the GENIE cohort (The AACR Project GENIE Consortium, 2017) containing 3706 PDAC patients with somatic mutation profiling for the presence of mutations in any of the genes of the six major DDR pathways (BER, NER, HR, NHEJ, ICL, and MMR) (Deans & West, 2011; Gupta & Heinen, 2019; Lee & Kang, 2019; Ranjha et al., 2018; Yang et al., 2016). A comprehensive list of 352 genes was collated based on the gene lists of the respective pathways in the Gene Ontology database. Mutations were reported in 117 (33%, excluding *TP53*) of the queried genes, with 46 (13%) and 14 (4.0%) genes being mutated in more than 1% and 2% of the patients, respectively. The most commonly mutated genes were *TP53* (68.9%), *BRCA2* (4.4%), *ATM* (4%), and *PRKDC* (3.9%). An overview of these genes and associated pathways can be found in (Fig. 1.4 and Suppl. Table 1).

The relatively high prevalence of DDR gene mutations opens up opportunities for targeted therapies based on the synthetic lethality principle: tumours with a DDR pathway deficiency are more dependent on alternative DNA repair pathways to repair double-stranded DNA breaks and can therefore be targeted with drugs that inhibit these

alternative repair pathways (Guo et al., 2011; Topatana et al., 2020). Synthetic lethality has been applied successfully in cancers harbouring *BRCA1/2* mutations (HR pathway) by treating with PARP inhibitors (PARPi; PARP is involved in the single-strand break repair pathway) (Lord & Ashworth, 2017). Unrepaired SSBs may progress into DSBs. This can occur spontaneously when two opposed SSBs are in close vicinity, or due to collision with the DNA replication fork machinery which may result in fork collapse and the formation of a DSB (Caldecott, 2024; Cannan & Pederson, 2016). While SSBs are common lesions and these events therefore also occur in healthy cells, the accumulation of SSBs due to PARPi drastically increases the likelihood of developing DSBs. DSBs are considerably more cytotoxic and, due to HRD, will accumulate to the point of cell death.

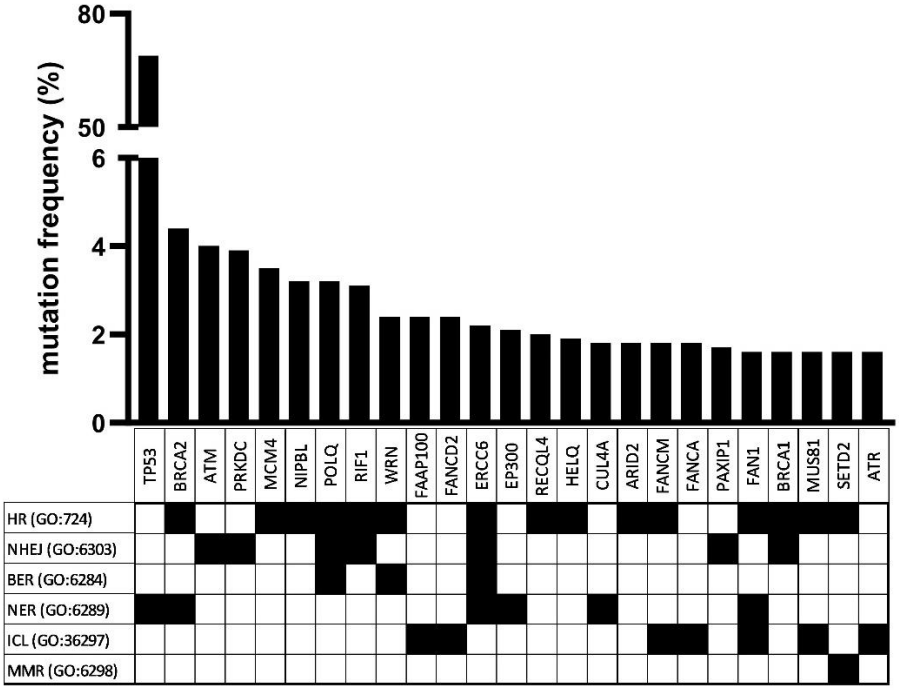

Figure 1.3. Prevalence of the top 25 most frequently found somatic DDR gene mutations and associated pathways in a cohort of 3706 PDAC patients. *Abbreviations: HR: homologous recombination, NHEJ: non-homologous end-joining, BER: base-excision repair, NER: nucleotide-excision repair, ICL: interstrand crosslink repair, MMR: mismatch repair. (Stoof et al., 2021)*

1.3 DDR Pathways Genomic Profiling/Biomarkers

Multiple research groups have classified molecular PDAC subtypes using next-generation sequencing and expression profiling to help tailor therapies and guide clinical decision making (Bailey et al., 2016; Collisson et al., 2011; Moffitt et al., 2015; Puleo et al., 2018). At its simplest, a distinction is made between classical and basal-like subtypes, though most classifications include more specific subtypes as well (Fig. 1.5). The classical subtype is characterised by the expression of epithelial markers, whereas the basal-like subtype has a higher expression of mesenchymal markers. In general, basal-like tumours are more aggressive and have a poorer prognosis (Suurmeijer et al., 2022; Zhou et al., 2021).

Bailey et al. defined four PDAC subtypes (Immunogenic, Pancreatic Progenitor, ADEX, and Squamous) based on ten discriminatory gene programs found by transcriptional network analysis (Bailey et al., 2016). Over fifty DDR genes were included in the gene program 'proliferation' which is associated with the squamous subtype. Functionally, the squamous subtype is associated with histological adenosquamous carcinoma and poor survival. The classifications by Collisson, Moffitt, and Puleo found no associations with DDR deficiency (Collisson et al., 2011; Moffitt et al., 2015; Puleo et al., 2018).

Instead of mutational signatures, Waddell et al. based their classification on structural variation (Waddell et al., 2015). Using a dataset of 75 primary samples and 25 patient-derived cell lines they defined four subtypes: stable, locally rearranged, scattered, and unstable. The unstable subtype co-segregated with inactivation of *BRCA1, BRCA2*, and *PALB2*, as well as with a mutational signature of DDR deficiency. Mutations of *ATM* and other genes involved in DNA maintenance (e.g. *XRCC4/6* and *FANCM*) were also regularly found in these tumours.

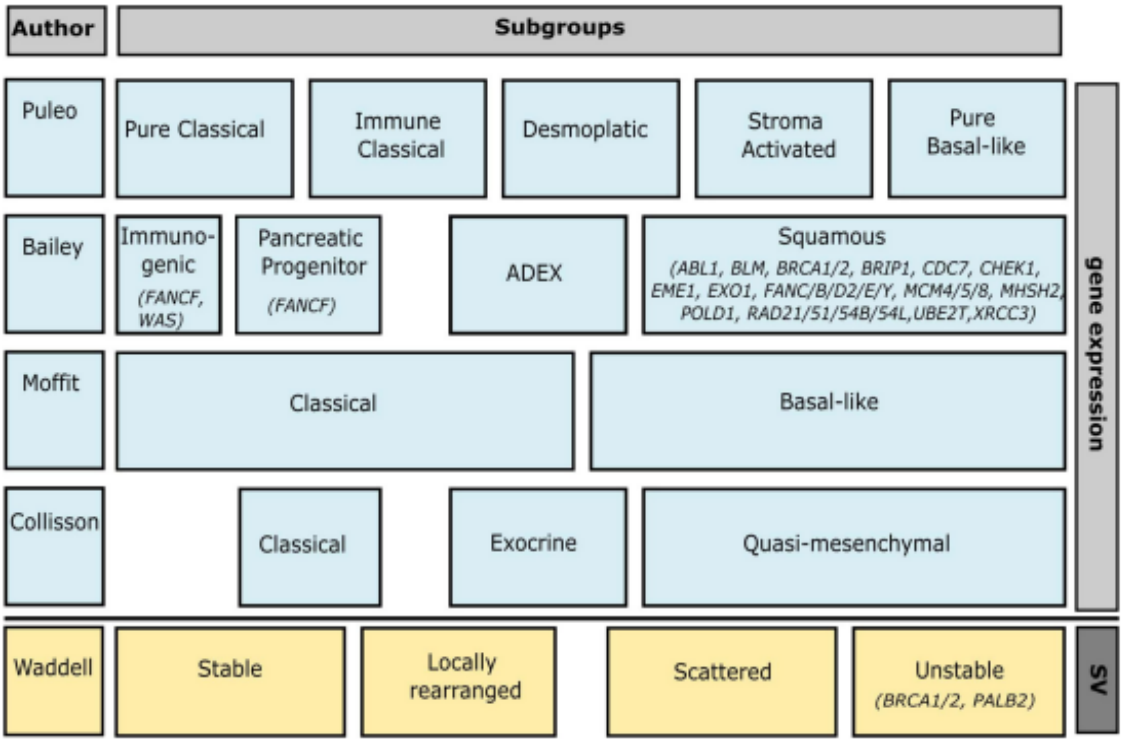

Figure 1.4. Overview of genomic pancreatic subtypes. *Associated DDR genes of which mutations have been found in PDAC patients (Suppl. Table 1) are included under their respective subtypes. The bar on the right indicates whether the classification is based on gene expression or structural variation (SV). Associated DDR genes not mutated in patients include CDC45, FEN1, GINS2/4, MAD2L2, MCM2/3/6/7, RMI2, RPA3, TIMELESS, HMGB2, POLA1, LIG1, DNA2, RDC2/3/4/5, PCNA, COPS5, BRIP1, HMGA2M, CETN2, UBC, TP73, PSMD14, POLR2D, and CDK7 for Bailey's squamous subtype, and USP7 for Bailey's Pancreatic Progenitor subtype.*

Currently only g*BRCA* is used in the clinic as a biomarker for sensitivity to PARPi olaparib. Our query of somatic DDR mutations found that *BRCA2* is mutated in 4% and *BRCA1* in 1.6% of all PDAC patients indicating that a larger group of patients may benefit from targeted therapy. In addition, multiple clinical trials are recruiting patients for treatment with DDR inhibitors based on a larger selection of DDR mutations, including but not limited to *PALB2, CHEK2, ATM,* and *RAD51* (Suppl. Table 2).

Already, DDR deficiency has been associated with a significantly better patient survival compared to DDR proficiency independently of tumour subtype classification (Zimmermann et al., 2021). However, it should be noted that analysis of the interaction with precise treatment regimens is limited, and this can be a considerable confounder. In addition, a small retrospective study in 36 patients treated with first line FOLFIRINOX in a

metastatic setting found that DDR deficiency, as based on a 14-gene panel, was significantly associated with improved survival (p=0.04) (Sehdev et al., 2018). While the DDR deficient patient group also had a better median overall survival (14 vs. 5 months) this difference was not significant (p=0.08). A similar retrospective study in 40 patients with metastatic PDAC treated with first-line platinum chemotherapy in combination with FOLFIRINOX was published a year later (Palacio et al., 2019). Based on a 35-gene panel, the patients with DDR deficiency had a significantly longer progression-free survival (18.5 vs. 6.9 months, p=0.003), with a trend towards superior median overall survival as well. Further research is needed to confirm these findings in a larger cohort and to investigate whether DDR deficiency is associated with response to FOLFIRINOX treatment or overall survival in general.

DDR deficiency has also been associated with sensitivity to cisplatin. In a phase II clinical trial patients with untreated germline *BRCA* or *PALB2* mutations and stage III to IV PDAC were treated with gemcitabine and cisplatin, or with gemcitabine, cisplatin, and PARPi veliparib (O'Reilly et al., 2020). While addition of veliparib did not significantly improve treatment, the 2-year (30.6%) and 3-year (17.8%) survival rates of the cohort exceeded expectations and are among the longest reported in any PDAC trial.

1.3.1 DNA damage repair deficiency and homologous recombination deficiency

DNA damage repair deficiency is a broad term that encompasses deficiency of any of the DDR pathways. A more precise, and often more useful, term is homologous recombination deficiency (HRD) which is limited to deficiency of the homologous recombination repair pathway. Yet, the definition of HRD varies between studies and can be based on either genotype or phenotype (Stewart et al., 2022). HRD based on genotype is the presence of pathogenic alterations in HR genes. At its narrowest, this includes just the core HR genes *BRCA1* and *BRCA2* but can be expanded to include other HR genes such as *PALB2, ATM, RAD50*, and *RAD51* (Casolino et al., 2021; McIntyre et al., 2020; Park et al., 2020). Alternatively, HRD can be defined on the phenotype, or the functional effect of HRD as seen by the presence of genome instability or mutational signatures. In this thesis, HRD is defined as the presence of pathogenic alterations in one of the 17 HR genes that are in the MSK-IMPACT sequencing panel (*ATM, BAP1, BARD1, BLM, BRCA1, BRCA2, BRIP1, CHEK2, FAM175A, FANCA, FANCC, NBN, PALB2, RAD50, RAD51, RAD51C,* and *RTEL1)* and which has been used in other PDAC studies (McIntyre et al., 2020; Park et al., 2020).

1.4 PARP INHIBITORS

One of the main targeted therapies used in PDAC is PARP inhibition. PARP (polyADP-ribose polymerase) is a protein family with 17 members of which PARP1 is both the most prevalent and best characterised (Chaudhuri & Nussenzweig, 2017; Kraus, 2015). PARP1 recognises DNA damage in the form of DNA nicks through its DNA binding domain which results in a conformational change and activation of its catalytic domain (Spiegel et al., 2021; Zhao et al., 2020). Using NAD^+ as a substrate, it adds ADP ribose chains to itself and protein substrates (PARylation), releasing nicotinamide in the process. PARylation recruits repair proteins to the site of the DNA damage and helps initiate repair. PARP1 is best known for its role in SSB repair but is also involved in DSB repair and BER. Inhibition of PARP1 in a HRD setting is synthetic lethal due to the loss of effective SSB and HR repair and consequent accumulation of DSBs (Zhao et al., 2020; Zheng et al., 2020). Several PARPi have been approved for clinical use in multiple cancers (olaparib, rucaparib, veliparib, niraparib, talazoparib) although only olaparib has been approved for PDAC.

In addition to catalytic inhibition of PARP1, PARPi have also been shown to create cytotoxic PARP-DNA complexes in a process called PARP-trapping. The exact effect of these complexes is still under debate but is thought to contribute to replication fork stalling and collapse (Hopkins et al., 2019) and impeded maturation of nascent DNA during replication (Petropoulos et al., 2024; Vaitsiankova et al., 2022), both of which can result in the formation of DSBs.

1.5 Clinical Trials Targeting DDR Deficiency Pathways

The past decade has seen a rising interest in the combination of cytotoxic chemotherapy, with targeted approaches to exploit the synthetic lethality of this combinatorial approach. As of January 2024, there are 73 clinical trials registered on clinicaltrials.gov that investigate DDR targeted therapies alone or in combination with chemotherapy in PDAC (either in PDAC alone or as part of a larger cancer patient cohort). The majority of these trials (79%, n=58) focus on *PARP* inhibitors, although *ATM/ATR, CHK1, DNA-PK*, and *WEE1* inhibitors are also being investigated (Suppl. Table 2). Except for two trials, all trials are either phase I or II, with limited numbers of patients and often single-arm treatment protocols, which renders efficacy analysis more challenging. The next section provides an overview of clinical trials with published results for DDR inhibitors in PDAC.

1.5.1 PARP inhibitors

The pivotal phase III trial leading to FDA approval for the use of PARP inhibition in metastatic PDAC was conducted by Golan et al. and evaluated olaparib as maintenance therapy in metastatic PDAC patients with germline mutation of *BRCA1/2* (NCT02184195) (Golan et al., 2019). Patients were eligible if their tumour had not progressed on first-line platinum-based chemotherapy (e.g. cisplatin or oxaliplatin). Treatment with olaparib was compared to placebo and a significant increase in progression-free survival was observed (PFS; 7.4 vs. 3.8 months, p=0.004), but at interim analysis (data maturity 46%) no significant difference was found in median overall survival (OS; 18.9 vs. 18.1 months, p=0.68). The updated results of this study were presented in January 2021 (Golan et al., 2021). Disappointingly, there was again no difference in median OS between the groups (OS 19.0 vs. 19.2 months, p=0.35). Notably, however, PFS2, i.e., the time from randomisation to second disease progression or death, was significantly longer in the olaparib-treated group (PFS2, 16.9 vs. 9.3 months, p=0.0061). This trial has led to the approval for the use of olaparib as maintenance treatment in *mtBRCA1/2* PDAC in the clinic.

A comparable phase I trial (NCT00515866) in PDAC patients with locally advanced or metastatic PDAC being treated in the first-line setting included a comparison of olaparib combined with gemcitabine versus gemcitabine alone in the expansion phase (n=22) (Bendell et al., 2015). Patients were eligible for inclusion regardless of genetic/molecular status. No significant benefit was found regarding objective response rate (ORR), OS, or PFS for the combination treatment. While the researchers noted that nine patients had *BRCA*

mutation status available, analysis of response by *BRCA* mutation status was not performed due to the small number of patients for whom this data was recorded.

The phase IB trial on the addition of the PARPi veliparib to first line chemotherapy (cisplatin, gemcitabine) demonstrated a striking ORR of 78% in patients with stage III/IV PDAC with *BRCA1/2* germline mutations and an equally impressive median OS of 23.3 months (O'Reilly et al., 2018). The investigators then proceeded to a phase II trial of this combination in patients with PDAC and germline *BRCA1/2* or *PALB2* mutations but could not reproduce these results (O'Reilly et al., 2020). Response rate in the combination arm was 79% versus 65.2% in the chemotherapy alone arm (p=0.02). There was no statistically significant difference in PFS or OS between the groups (PFS 10.1 vs. 9.7 months, p=0.73; OS 15.5 vs. 16.4 months, p=0.6). The 2- and 3-year OS of 30.7% and 17.8%, respectively, in this study are the longest ever reported in a clinical trial in this cohort. Notably a phase II study of veliparib alone in the second line setting in patients with *BRCA1/2* mutant PDAC reported no confirmed responses; 4 patients (4/16) had stable disease for 4 months (Lowery et al., 2018).

Two additional phase II trials have published results on the addition of veliparib to 5-FU based chemotherapy. The first study (NCT02890355) compared the combination of veliparib with modified FOLFIRI versus FOLFIRI alone as second line treatment in metastatic pancreatic cancer patients (Chiorean et al., 2021; Chiorean et al., 2019). In total, 108 patients were included in the analysis. The addition of veliparib to FOLFIRI treatment was shown to increase toxicity. Moreover, veliparib did not improve either OS (5.1 vs. 5.9 months in combination versus monotherapy arm, respectively, HR 1.3, p=0.21) or PFS (2.1 vs. 2.9 months, HR 1.5, p=0.05). Additionally, blood and tumour biopsies were collected at baseline to explore HR or DDR biomarkers. Twenty-two of the tumours (19%) had HR deficiency (*BRCA1/2, ATM, PALB2, ATM*, or *CDK12* mutation), and an additional 10 tumours (9%) had mutations in other DDR genes (*FANC, BLM, SLX4, CHEK2, POLD1, RIF1, MSH2/6)*. The patients with HR deficiency had a significantly longer PFS (7.3 vs 2.5 months, p=0.05), but OS was not significantly different (10.1 vs 5.9 months, p=0.17) compared to patients without DDR mutations when treated with FOLFIRI. When veliparib was added to mFOLFIRI no significant differences were found in either PFS (2.0 vs 2.1 months, p=0.62) or OS (7.4 vs 5.1 months, p=0.10).

Pishvaian et al. performed a phase I/II clinical trial (NCT01489865) to evaluate the safety and response of PDAC patients to combination treatment of veliparib with modified FOLFOX (Pishvaian et al., 2020). For the phase I portion of the study patients were not selected based on genetic history; however, for the phase II part of the trial, patients were selected based on the presence of HR-DDR deficiency or family history suggesting breast or ovarian cancer syndrome, and a distinction was made between previously treated and untreated patients. The ORR was 20% in the phase I unselected cohort (n=23) and 31% in the phase II cohort (n=33) selected for HR-DDR deficiency. Further analysis of the phase II cohort showed that treatment-naïve patients had a better objective response rate (ORR) and OS than previously treated patients (40% vs. 22%, and 13.0 vs. 4.5 months, respectively). In the treatment-naïve HR-DDR patients, the ORR was 57%. However, due to the lack of a placebo or control arm the magnitude of benefit attributable to the addition of veliparib is difficult to quantify. Previously reported OS of metastatic PDAC patients receiving FOLFOX as second-line treatment are in a similar range (3.3 and 6.3 months) (Hecht et al., 2020; Yoo et al., 2009).

Multiple trials for PARP inhibitors are currently recruiting or preparing for recruitment of patients with DDR deficiency (either for *BRCA* mutations specifically, or for a panel of DDR genes). This includes phase I and II trials for niraparib both as monotherapy and in combination with other drugs (NCT04673448, NCT04764084, NCT03601923, NCT04493060), olaparib (NCT04548752), rucaparib (NCT04171700), talazoparib (NCT04550494), and NMS-03305293 (NCT04182516).

1.5.2 CHK1 inhibitors

Laquente et al. performed a phase I/II clinical trial for the *CHK1* inhibitor rabusertib (LY2603618) combined with gemcitabine versus gemcitabine alone in patients with locally advanced or metastatic PDAC (NCT00839332) (Laquente et al., 2017). Although no significant differences were found in the number and severity of adverse events, no significant differences in OS, PFS, ORR, or duration of response were found either.

1.5.3 DNA-PK inhibitors

A phase II trial on the safety and efficacy of the combination of the *DNA-PK* inhibitor LY3023414 with abemaciclib in previously treated metastatic PDAC patients compared to

standard-of-care gemcitabine or capecitabine found that the combination treatment had a significantly worse PFS (1.81 vs. 3.25 months, p=0.012) (NCT02981342).

1.5.4 Patient selection

Preclinical models have shown that several targeted therapies are more effective in models that have defects in complementary DNA repair pathways and this principle of synthetic lethality has been adapted by clinical trials. Multiple trials are currently running which select patients based on the presence of *BRCA1/2* mutations. While the application of targeted therapy in patients with *BRCA1/2* mutations has had success in other cancer types (most notably in breast and ovarian cancer), the fraction of patients with *BRCA* mutations is relatively small and patients with other DDR gene mutations may also benefit from these therapies. Several studies have included additional mutations in their selection criteria but based on Table 1.1 these panels could be extended upon. However, preclinical trials might be needed to warrant this.

Alternatively, DDR deficiency might serve as a biomarker for response to non-targeted therapies. One study that is currently investigating this is the Precision Panc trial which recruits PDAC patients for molecular profiling and allows patients to enrol in a PRIMUS trial (NCT0461417), one of which aims to test a DDR deficiency biomarker for response to FOLFOX-A treatment (NCT04176952).

1.6 PRECLINICAL *IN VITRO* MODELS

Despite the promising results for many targeted therapies in other solid tumours, the use of targeted therapies in PDAC has had limited survival benefit in the clinic. Target discovery and successful development of targeted therapies is highly dependent on the relevance of the preclinical models used and therapies frequently fail at the transition to clinical trials. Multiple recent papers are available which review the preclinical models used in PDAC research (Garcia et al., 2020; Moreira et al., 2018; Swayden et al., 2020; Yu et al., 2021).

In vitro models can be classified into three different categories with increasing complexity: 2D cell lines, 3D spheroids and tumoroids, and 3D organoids (Fig. 1.6). Cell lines are the oldest and least complex model. They can be established from tissue but this can be a difficult and time consuming process (Mirabelli et al., 2019). Fortunately, many established, well-characterised cell lines are currently available from tissue culture collections such as the American Type Culture Collection (www.atcc.org). Once established, most cell lines are easily maintained in tissue culture flasks in commercially available media supplemented with foetal bovine serum.

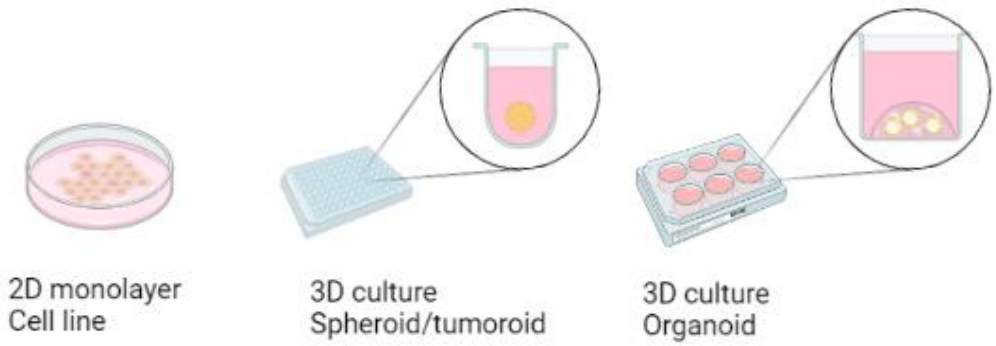

Figure 1.5. Overview of in vitro model systems for PDAC*. Cells lines are grown in a 2D monolayer in a petri dish or culture flask. Spheroids are a form of 3D culture and are often grown as dense clusters of cells that cannot adhere to the culture plate. Organoids are another form of 3D culture and are self-organising structures that are grown in a supporting extracellular matrix in media supplemented with organ-specific growth factors. Created in Biorender.*

Spheroids are a form of cell line culture in a 3D model. Sometimes spheroids are also referred to as tumoroids to highlight their tumour origin. However, the term tumoroid is also used to refer to organoids and to avoid confusion will therefore not be used in this work. There are numerous different spheroid models available each with their own

characteristics and applications (Białkowska et al., 2020; Costa et al., 2016; Gündel et al., 2021; Sant & Johnston, 2017). These models can be grouped into two categories: non-adherent and adherent culture. In non-adherent culture, cells are cultivated under conditions where the cells are unable to attach to the culture flask by using low-attachment plates or hanging drops, forcing the cells attach to each other and form cell clumps or aggregates. An advantage of this method is that it is cheap, easily scalable, and reproducible. Adherent or anchorage-dependent cell culture provides a scaffold that simulates the extracellular matrix and provides support to form a 3D structure. This method provides a microenvironment that mimics the *in vivo* situation but also introduces additional variation. Depending on the cell line used and the cell density at seeding spheroids can grow up to several hundred µm in size to the point that the centre turns necrotic due to lack of oxygen and nutrient perfusion (Ware et al., 2016; Wen et al., 2013).

Organoid culture is a more recent development with the first organoids being developed a little over a decade ago (Sato et al., 2009). Organoids can be established from stem cells and organ-specific progenitor cells. The cells are seeded in a supporting extracellular matrix such as basement membrane extract (BME) or Matrigel and the media is supplemented with growth factors that stimulate stem cell maintenance and organ-specific differentiation. The exact media formulation for PDAC organoids tends to differ between labs but usually contains at least EGF, FGF10, Wnt, R-spondin, and Noggin (Frappart & Hofmann, 2020). Like spheroids, organoids self-organize into 3D structures but unlike spheroids, their morphology is more similar to that of the tissue or cancer subtype of origin (Hirt et al., 2022; Shi et al., 2022) .

1.6.1 The application of cell lines in studying DDR in PDAC

Cell lines remain the most commonly used preclinical model for cancer research. Their widespread use has ensured that they are readily available and most commercial cell lines are well-characterised (Deer et al., 2010). The main advantages of cell lines are that they are cheap, require little maintenance, and are easy to manipulate. In addition, cell lines are considered to be more homogenous than other preclinical models, thus contributing to a better reproducibility which makes them well-suited for high-throughput drug screening. However, this also means that cell lines lack the complexity and heterogeneity typical of tumours. At the same time, clonality and adaptation to 2D culturing conditions as well as immortalisation and repeated passaging can all contribute to genomic drift which can

significantly affect drug responses (Hughes et al., 2007; Monberg et al., 2021). Other disadvantages of 2D culture include loss of part of the normal 3D morphology, cell polarity, and cell-cell or cell-stroma interactions, especially the interaction with cancer-associated fibroblasts (CAFs) and immune cells (Feig et al., 2012). While some of these disadvantages can be resolved or diminished by adapting the culture methods (e.g. using early passage patient-derived cell lines instead of established cell lines, or co-culturing with fibroblasts) other disadvantages are inherent to the model system itself. While the possible applications of cancer cell lines are diverse, ranging from biomarker discovery to functional studies, the use of cell lines to study the DDR pathways in PDAC has mainly been limited to drug sensitivity studies.

1.6.1.1 PARP inhibition

DDR pathway deficiency has been shown to confer sensitivity to PARP inhibition (PARPi). Multiple studies found that the *BRCA2*-deficient cell line Capan-1 is significantly more sensitive to several PARP inhibitors and cisplatin, but not to gemcitabine, compared to the *BRCA2*-proficient cell lines MiaPaCa-2 and Panc-1 (Andrei et al., 2015; de Soto, 2020; Porcelli et al., 2013). In addition, restoration of *BRCA2* expression in Capan-1 cell lines was shown to reduce sensitivity to PARP inhibitors olaparib and HYDAMTIQ (Mini et al., 2017; Sullivan-Reed et al., 2018). Similarly, shRNA-mediated knockdown of *BRCA2* in Panc-1 cells impaired homology-directed repair and conferred sensitivity to the PARPi BMN-673 (but not veliparib) (Andrei et al., 2015). Furthermore, increased sensitivity to PARPi (olaparib, BMN-673, rucaparib) and cisplatin has been found in DDR deficient patient-derived cell lines (PDCLs) (Dreyer et al., 2021).

Acquired drug resistance is a problem in many cancer treatments and one of the main causes of treatment failure. Long-term treatment of Capan-1 cells with low dose PARPi can induce resistance, including cross-resistance to other PARPis and cisplatin. Several mechanisms have been suggested for the development of resistance in the Capan-1 *BRCA2*-deficient cell line, one of these being the restoration of *BRCA2* expression. Sakai et al. found that 7 out of 14 Capan-1 clones that developed resistance to cisplatin treatment had additional mutations in the *BRCA2* gene which corrected the original frameshift mutation found in Capan-1 (Sakai et al., 2008). The truncated protein was also still present suggesting that these restorative mutations were preceded by gene duplication. However, the amplification of the truncated protein might in itself also contribute to resistance. Park et

al. investigated PARPi resistant Capan-1 clones and did not detect reversion mutations, though several clones had additional copies of the mutant *BRCA2* allele as well as an increased BRCA2 protein expression (Park et al., 2020). Immunoprecipitation of BRCA2 followed by mass spectrometry showed enrichment of PALB2, RAD51, MLLT10, and DOT1L in the resistant clones, but not in the parent cells, which may contribute to resistance. Alternatively, Chen et al. also found additional mutations in *BRCA2* in PARPi resistant Capan-1 clones, but these mutations resulted in truncated splice isoforms (Chen et al., 2020). In addition, they found overexpression of the anti-apoptotic proteins COX-2 and BIRC3. Depletion of either *BRCA2, COX-2*, or *BIRC3* partially restored PARPi sensitivity. In contrast, combined depletion had no additive effect, suggesting that additional mechanisms contribute to PARPi resistance.

Guo et al. established olaparib-resistant cell lines by exposing the cells in six 35-day cycles with increasing concentrations of olaparib (Guo et al., 2022). The resistant cells had a higher migration and invasion capacity which correlated with increased expression of mesenchymal markers ZEB1, Twist, and N-Cadherin. RNA sequencing revealed activation of the CXCL3-ERK1/2 signalling pathway, but while inhibition of CXCL3 decreased the migration of the resistant cells it did not alter the sensitivity to olaparib.

In a study conducted by Sasaki et al. MiaPaCa-2 cells with *BRCA1* knockout were created using CRISPR/Cas9 (Sasaki et al., 2024). Mutant cells were exposed to 0.75 mM of the alkylating agent methyl methanesulfonate for one hour to induce mutagenesis and were then cultivated in an increasing concentration of olaparib (1 to 20 µM) for approximately 5 months. The resultant resistant clone showed resistance against olaparib and talazoparib. In other cancers, loss of *PARP1* or *PARG* (which reverses the Poly ADP-ribosylation done by PARP) as well as the upregulation of drug efflux pump MDR1 have been reported as possible resistance mechanisms. However, the authors found no significant alterations in the expression of any of these three proteins. They also found no restoration of *BRCA1* expression. RNA sequencing revealed activation of the NAD^+ pathway, caused by the overexpression of NAMPT and NMNAT2. This resulted in a higher intracellular NAD^+ concentration. NAD^+ is a major PARP substrate and upregulation of NAD^+ by addition of nicotinamide conferred resistance to olaparib and talazoparib in the parental cells.

1.6.1.2 WEE1 inhibition

Sensitivity to the *WEE1* inhibitor AZD-1775 has been evaluated in multiple studies, but due to contradicting findings its role in DDR deficiency remains unclear. Two studies found that Capan-1 is markedly more sensitive to AZD-1775 than other (PDAC) cell lines, suggesting that *BRCA2* deficiency might play a role (Dréan et al., 2017; Parsels et al., 2018). However, while restoration of the *BRCA2* open reading frame due to secondary mutations induced by CRISPR-Cas9 reduced the sensitivity to PARP inhibitors olaparib and BMN-673, it did not affect the sensitivity to AZD-1775. On the other hand, Lal et al. investigated sensitivity to AZD-1775 in a panel of nine PDAC cell lines and reported a medium sensitivity for Capan-1 (Lal et al., 2016). In addition, they found that knockdown of *BRCA2* by siRNA in MiaPaCa-2 and PL5 induced resistance to AZD-1775.

1.6.1.3 ATR inhibition

The application of ATR inhibitors in PDAC has been investigated in multiple *in vitro* studies in both human PDAC cell lines and mouse KPC and KPCB cell lines, but so far, these drugs have shown limited potential and sensitivity to treatment does not correlate with DDR status (Dreyer et al., 2021; Elliott et al., 2019; Wallez et al., 2018). However, multiple studies have found that ATRi (VE-821 and VE-822) sensitises to gemcitabine and radiotherapy through impairment ofDNA repair (Fokas et al., 2012; Wallez et al., 2018). siRNA knockdown of another major signal transducer, ATM, in combination with ATRi in MiaPaCa-2 was able to prevent gemcitabine-induced activation of ATR completely (Wallez et al., 2018), suggesting that ATM-mutant tumours may be especially sensitive to this combination treatment. In addition, combination treatment with chloroquine, an autophagy inhibitor that is used in the treatment of malaria, significantly reduced proliferation in the majority of 26 tested PDAC cell lines compared to VE-822 (24 out of 26) or chloroquine (17 out of 26) alone (Elliott et al., 2019).

1.6.1.4 Combination treatment

A disadvantage of DDR targeted therapy is that it is not inherently cytotoxic. By inhibiting multiple DNA repair proteins, cancer cells will accrue DNA damage, but whether this results in cell death or senescence depends on additional factors, such as the proliferation rate and how well the cells tolerate replicative stress. Combination treatment with chemo- or radiotherapy can increase the anti-tumour effect by inducing additional DNA damage (Porcelli et al., 2013). Perkhofer et al. generated stable mouse cell lines from tumours with

pancreas-specific loss of *Kras* (KC), and *Kras* and *Atm* (AKC) (Perkhofer et al., 2017). *Atm*-deficient AKC cells showed a significant increase in DNA damage markers 53BP1 and γH2AX upon treatment with 5 Gy of ionising radiation compared to KC cells ($p<0.03$), indicating impaired double-strand break repair, and decreased proliferation. No significant differences were observed in sensitivity to cisplatin, 5-FU, or gemcitabine. Treatment with olaparib or niraparib reduced viability in an *Atm*-dependent manner and was potentiated by combination with gemcitabine or radiation ($p<0.01$), showing that combination of PARPi and ATM loss is effective but is potentiated by addition of gemcitabine or radiation.

Azorsa et al. used an RNAi screen to identify which genes, when silenced, sensitised pancreatic cancer cells to gemcitabine (Azorsa et al., 2009). Silencing of *CHK1* was found to be most effective and was further validated with additional siRNAs and two small molecule inhibitors (SB218078 and PD407824) in MiaPaCa-2 and BxPC3 cell lines.

1.6.1.5 DDR status in PDAC cell lines

The cell lines used for DDR pathway studies in PDAC are mainly limited to Capan-1 as a model for DDR/*BRCA2*-deficiency, and MiaPaCa-2, BxPC-3 and Panc-1 for DDR-proficiency (while MiaPaCa-2 is generally considered to be DDR proficient, it does have a missense mutation of unknown significance in *PALB2*). Studies in additional cell line models are required to analyse the role of the DDR pathways in more depth. Table 1.1 provides an overview of the mutations found in the ten most frequently mutated DDR genes (excluding *TP53*) as per Table 1.1 for all PDAC cell lines found in the Cancer Cell Line Encyclopaedia. Twenty of the 46 cell lines had a mutation in one or more of the investigated genes, of which three (Capan-1, PL18, and SNU-324) had a mutation annotated as pathogenic or likely pathogenic in the ClinVar or COSMIC database.

Capan-1 was established in 1974 from a PDAC liver metastasis found in a 40-year-old Caucasian male with a PDAC in the head of the pancreas (Fogh et al., 1977; Kyriazis et al., 1982). The cell line is well differentiated and when implanted in nude mice forms tumours that are morphologically similar to the tumour of origin.

Apart from Capan-1, SNU-324 is the only other available cell line with a suspected deleterious *BRCA2* mutation (Ku et al., 2002). SNU-324, established in 2001, is derived from a poorly differentiated primary pancreatic tumour of a 50-year-old male. The cells are mainly adherent, but a fraction of the cells grow in suspension and frequently form

aggregates. SNU-324 does not contain mutations in *KRAS* or *TP53*, but is microsatellite instable (Ku et al., 2002). Despite its usefulness for *BRCA2*-deficiency studies no other publications are available which have used this cell line and this model is not commercially available. Therefore, there is a need for additional well-defined *BRCA2*-deficient PDAC cell lines.

Table 1.1. Mutation status of DDR genes in cell lines. *Representation of the top ten (excluding TP53) most frequently mutated DDR genes in PDAC cell lines. The genes WRN and FANCD2 were not found to be mutated in any PDAC cell line. When available the pathogenicity status/score is included in the table. n/a: not available.*

Cell line	Gene	Nucleotide change	Protein change	ClinVar	COSMIC FATHMM
BXPC3	*POLQ*		p.ILL1421fs	n/a	n/a
Capan-1	*BRCA2*	c.5946del	p.S1982fs	pathogenic	n/a
	ATM	c.4755A>C	p.R1585S	n/a	n/a
CFPAC1	*PRKDC*	c.1945T>C	p.F649L	Uncertain significance	n/a
HPAC	*NIPBL*		p.T735I	n/a	n/a
HuP-T3	*BRCA2*	c.6131G>T	p.G2044V	Benign/likely benign	n/a
	NIPBL		p.1532_1532E>DK	n/a	n/a
KP2	*PRKDC*		p.G2261S	n/a	n/a
	FAAP100		p.K333R	n/a	n/a
MZ1PC	*PRKDC*		p.W1355C, p.W1355l, p.F1028V	n/a	n/a
Panc-02.03	*POLQ*		p.L1430fs	n/a	n/a
Panc-03.27	*ATM*	c.7052A>G	p.E2351G	Uncertain significance	n/a
Panc-04.03	*NIPBL*		p.S2389I	n/a	n/a
Panc-08.13	*ATM*		p.F1234S	n/a	n/a
PATU8988S/T	*ATM*		p.R919M	n/a	n/a
PK-45H	*POLQ*		p.G2225R	n/a	n/a

PK-59	*BRCA2*	c.6131G>T	p.G2044V	Benign/likely benign	n/a
PL18	*NIPBL*	c.3G>T	p.M1I	pathogenic	n/a
			p.S1517*	n/a	n/a
PL4	*RIF1*	c.1331C>T	p.A444V	n/a	Neutral (0.12)
PSN1	*NIPBL*		p.K601fs	n/a	n/a
SNU-324	*BRCA2*	c.7480C>T	p.R2494*	Pathogenic	n/a
	ATM		p.Q2809fs	n/a	n/a
	MCM4	c.1579G>A	p.V527I	n/a	Pathogenic (0.96)
SW-1990	*NIPBL*		p.K1180*	n/a	n/a
TCCPAN2	*POLQ*		p.R6P	n/a	n/a

1.6.2 Spheroids

Numerous studies have used PDAC spheroids to study tumour biology and drug response (Hwang et al., 2019; Matsushita et al., 2019; Minami et al., 2021; Ware et al., 2016), but to our knowledge only one group has used PDAC spheroids to evaluate DDR inhibition. Dufau et al. created spheroids by growing Capan-2 cells in DMEM/F12 media supplemented with EGF and B27 in plates coated with polyHEMA to prevent cell adhesion (Dufau et al., 2012). Spheroids were treated for three days with gemcitabine and/or CHK1 inhibitor CHIR-124. Combination treatment at EC_{20} concentration of both drugs had a synergistic effect resulting in a 79% ATP decrease as a measure of viability compared to 15% or 10% for CHIR-124 or gemcitabine alone. Addition of CHK1 inhibitor was associated with potentiation of gemcitabine-induced DNA damage through cell cycle checkpoint abrogation.

1.6.3 Organoids

Patient-derived organoids are still a relatively new model for pancreatic cancer and there are few studies published that focused on the DDR of PDAC organoids. However, there is limited information on patient derived organoid (PDO) sensitivity to DDR-targeted drugs.

Driehuis et al. performed high-throughput drug screening of 76 drugs in 24 PDOs and found that, in general, PDOs have a similar response to agents that target the same biological process or molecular pathway (Driehuis et al., 2019). Drug response was found to be PDO-

specific, thus reflecting patient heterogeneity. Of the 24 PDOs, one PDO had a *BRCA2* indel and was among the most sensitive PDOs for most of the tested drugs.

Tiriac et al. performed pharmacotyping on 66 PDOs for the drugs gemcitabine, paclitaxel, irinotecan, 5-FU, and oxaliplatin (Tiriac et al., 2018). Like Driehuis et al., they found that PDO response reflected interpatient variability. For nine patients, the PDO response was similar to patient response. Eight out of nine patients exhibited an outcome consistent with their matched PDO. Additionally, they investigated the correlation between AUC distribution and genotype for a range of drugs, including olaparib. The three samples with the lowest AUC, indicating highest sensitivity, had *ATM* loss, *PALB2* loss, and *ATM* frameshift plus *BRCA2* loss, respectively. The researchers observed a trend between olaparib sensitivity and complete loss of *PALB2*, but these data must be interpreted cautiously as there were just four PDOs with complete *PALB2* loss. In addition, they stated that single-copy losses of a range of genes involved in homologous recombination deficiency do not correspond with olaparib sensitivity. This suggests that loss of a single gene copy might not be sufficient to completely aberrate a DDR pathway and sensitise to targeted inhibitors.

In line with these findings Dreyer et al. reported that they found no correlation between DDR status and the response to *ATR* or *WEE1* inhibition in the six PDOs they investigated (Dreyer et al., 2021). They also showed that DDR deficiency correlated with sensitivity to platinum and PARP inhibitor (talazoparib, rucaparib) therapy in patient-derived cell lines and xenograft models. This suggests that even though cell cycle regulation is important for DNA repair, inhibition might not be synthetic lethal with DDR deficiency, possibly due to compensatory mechanisms of alternative repair pathways.

Based on genomic, transcriptomic, and histologic data, organoids are representative models of PDAC (Driehuis et al., 2019; Gendoo et al., 2019; Tiriac et al., 2018). While limited studies have been published highlighting their use in the study of DDR deficiency in PDAC, drug screening and correlation to patient response studies are promising and suggest that organoids are good models to determine drug sensitivity for targeted therapies and might also be used to identify biomarkers for drug sensitivity.

1.7 NEXT GENERATION SEQUENCING

The main method for performing molecular profiling is next-generation sequencing (NGS). NGS is a massively parallel technology that is used to read the nucleotide order of DNA and RNA samples. One of the most used NGS technologies is Illumina sequencing which uses a four-step process (Fig. 1.6)(Hu; et al., 2021; Illumina, 2017; McCombie et al., 2019). DNA can be used immediately in the first step for library preparation, but RNA needs to be transformed into cDNA by RT-PCR before use.

1. Library preparation. Purified DNA or cDNA samples are fragmented using enzymatic digestion or mechanical shearing to create ~500 base pair long fragments. For whole exome sequencing probes are used to isolate the exome fragments from the complete DNA pool. The fragmentation process creates overhanging fragments that must be trimmed. Next, 5' and 3' adapters are ligated to fragments. Each adapter contains at least a flow cell binding sequence and a sequencer primer binding site. Additionally, the adapter may contain an index or barcode that allows for multiplexing of different samples.
2. Clonal amplification. The library is loaded onto a flow cell covered with oligos that hybridise to the library fragments. Polymerase and nucleotides are added to create the complementary strand starting from the oligos. The double stranded fragment is denatured, and the template strand is washed away. The newly synthesised fragment folds over to hybridise to an unused oligo forming a bridge with a short double-stranded section that serves as starting place for another round of amplification. After several bridge-amplification cycles, clones with up to 1000 identical fragments have formed. The reverse strands are cleaved and washed off, leaving only the forward strands.
3. Sequencing. Primers, polymerase, and fluorescently labelled nucleotides are added onto the flow cell. The nucleotides contain a reversible termination signal that prevents incorporation of more than one nucleotide at a time. Once the first nucleotide has been incorporated, the flow cell is excited with a laser and the emitted fluorescent signal of each individual clone is captured. The termination signal is removed, and the cycle is repeated.

4. Data analysis. The order of fluorescent signals is translated into the nucleotide sequence per read. The reads are aligned with a reference allowing for the identification of sequencing differences and copy numbers.

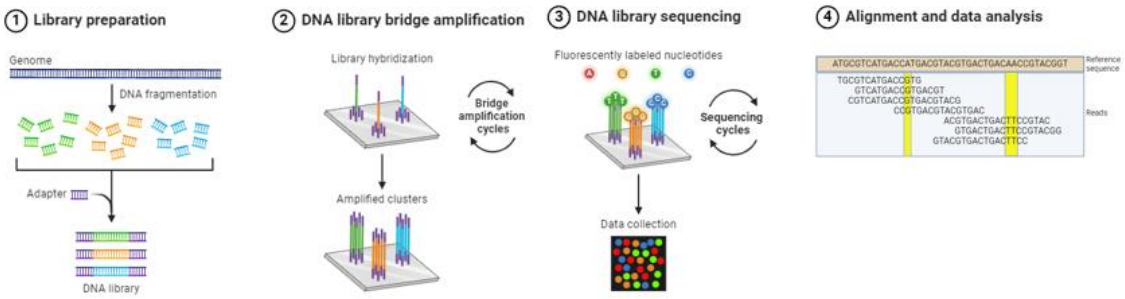

Figure 1.6. Next-generation sequencing. *1) DNA or cDNA is fragmented and annealed to an adapter to form a DNA library. 2) The DNA library is amplified using a process called bridge amplification which results in cluster of the same DNA clone. 3) All clones are sequenced simultaneously using fluorescently labelled nucleotides that emit a signal when they are incorporated. 4) The fluorescent signals are translated into nucleotide sequences, aligned to a reference genome, and analysed using bioinformatics. Created in BioRender.*

1.8 CRISPR/CAS-9 GENOME EDITING

To investigate the function of genes and the effect specific mutations have on cell behaviour, genes can be altered *in vitro*. One of the most adaptable and precise techniques to do this is CRISPR/Cas-9 genome editing.

Clustered regularly interspaced palindromic repeats (CRISPR)/CRISPR-associated protein (Cas) is a form of adaptive immune system found in bacteria and archaea that protects the cells against phage infection and plasmid transfer (Ma et al., 2014; Terns & Terns, 2011; Wiedenheft et al., 2012). The system uses short nucleotide sequences of the invading organism to recognise and cleave the invading genome to neutralise the threat. CRISPR/Cas has been adopted for highly specific genome editing in bacterial (Arroyo-Olarte et al., 2021), plant (El-Mounadi et al., 2020), and mammalian cells and organisms (Li et al., 2020; Yu & Yusa, 2019; Zhao et al., 2019).

The CRISPR/Cas immune response can be divided into three phases: incorporation; expression of Cas protein and crRNA; and recognition and cleavage of target (Fig. 1.7) (Rath et al., 2015; Terns & Terns, 2011). The first phase takes place during the initial infection. Fragments of the invading genome are incorporated into the host CRISPR locus as spacers between palindromic CRISPR-RNA (crRNA) repeats. During the second phase the resultant sequence is transcribed as pre-crRNA and processed to form mature crRNA. The Cas protein, or Cas protein complex depending on the organism, is also expressed. The crRNA and Cas protein are combined to form the active complex. During the last phase the crRNA guides recognition of the target sequence while Cas cleaves the sequence. To prevent cleavage of the host genome, many CRISPR systems require a specific protospacer-adjacent motif (PAM) sequence adjacent to the crRNA target site that does not occur in the host genome.

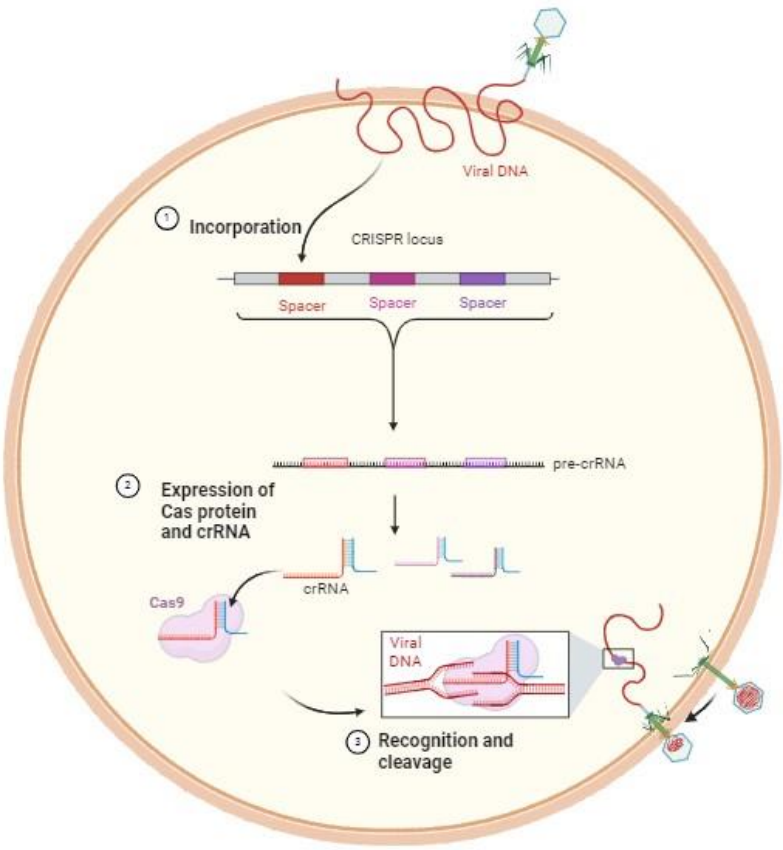

Figure 1.7. CRISPR/Cas immune response. *During the initial infection fragments of the invading genome are incorporated in the host CRISPR locus (1). The Cas protein and crRNA is expressed and assembled (2). The active complex recognises the invading genome using the crRNA and cleaves it to inactivate it. Created in BioRender.*

The CRISPR system can be divided into two classes: class 1 requires a complex of effector proteins, whereas class 2 uses single RNA-guided endonuclease. CRISPR/Cas9 is a class 2 system that has been adapted for gene editing (Liu et al., 2020). Orthologs of this variant can be found in multiple bacterial species, but the most used system is derived from S. pyogenes (spCas9).

Cas9 has a bilobular structure that is composed of a recognition (REC) and nuclease (NUC) lobe (Fig. 1.8) (Nishimasu et al., 2014). The REC lobe contains the REC1 and REC2 domains. The NUC lobe contains the RuvC, HNH, and PAM-interacting (PI) domains. The REC1 domains associates with the guide RNA which in turn activates the protein. In bacteria, this is a hybrid complex of a target complimentary region RNA (tracrRNA) and crRNA, but for gene editing purposes these two RNAs are fused as a single guide RNA (sgRNA). The activated sgRNA/Cas9 complex binds to the PAM sequence in the DNA using the PI domain. The PI domain is essential for the recognition of the PAM, and alterations of the PI domain

affect what PAM is can recognise. Binding to PAM initiates the hybridisation of sgRNA with the target DNA which results in a conformational change and cleavage of the DNA three nucleotides upstream of the PAM. The HNH domain cleaves the complementary DNA strand while the RuvC domain cleaves the non-complementary strand.

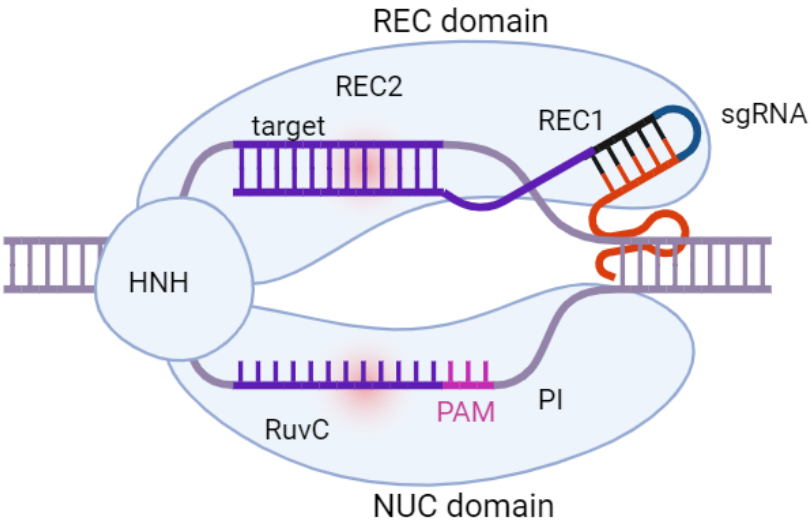

Figure 1.8. Cas-9 protein with associated DNA. *The Cas-9 protein has a bilobular structure with a recognition (REC) and nuclease (NUC) lobe. The REC1 domain associates with the guide RNA, the PI domain binds to the PAM sequence in the target DNA. The activated complex cleaves the target DNA using the HNH and RuvC domains. Created in BioRender.*

1.8.1 Applications of CRISPR/Cas9

CRISPR/Cas9 is a very flexible system and has been adapted for multiple applications, including but not limited to gene knockout, gene knock-in, and transcriptional regulation. Gene knockout is arguably the most common application. It is similar to the original function of CRISPR but instead of targeting an invading agent, cells are transfected or transduced with Cas9 protein or RNA and an sgRNA that targets the hosts own genome. The resulting double-strand break of the target region is repaired by homologous recombination (HR; ~25%) or non-homologous end-joining (NHEJ; ~75%) (Mao et al., 2008). While HR is considered to be error-free, NHEJ creates small indels that can cause frameshifts or early stop codons which abolish protein function and result in gene knockouts (Guirouilh-Barbat et al., 2014).

Gene knock-in is either the one-for-one substitution of nucleotides (e.g. to correct or create a SNP), or the insertion of a nucleotide sequence at a specific DNA locus (Lau et al., 2020;

Li et al., 2016). Similar to gene knockout, the cell is provided with the Cas9 protein and an sgRNA, and the DNA is cleaved at the targeted location. In addition, a DNA template with homology arms to the cleaved region and with the desired DNA alteration in the middle is added. This template is used by the HR pathway to repair the double-strand break and replaces the original sequence at the site of the break. Depending on the size of the template, the altered region can range from a single nucleotide to the inclusion of entire exons.

Lastly, sgRNAs can be combined to form a library that can be used for a CRISPR screen (He et al., 2021; Shalem et al., 2015). There are many variations and applications of CRISPR screens but at its simplest a pool of cells that express Cas9 protein is transduced with the CRISPR library at such a level that each cell receives at most a single sgRNA (a common guideline is a multiplicity of infection (MOI) of 0.3). The cells are cultivated for a period of time, collected, and sequenced. sgRNAs that are essential under the culturing conditions will be depleted, whereas sgRNAs that target inhibiting genes will be amplified. By combining this screen with different growth conditions or drug treatments it can be used to study biological processes, synthetic lethality, and more.

1.9 CANCER CELL METABOLISM

One of the hallmarks of cancer is deregulation of the cellular metabolism that supports growth, proliferation, and survival (Pavlova & Thompson, 2016). Due to their high proliferation rate cancer cells have a large demand for energy and nutrients required to generate new biomass. Two main catabolic pathways can be distinguished in cells.

1.9.1 Glycolysis

The first major catabolic pathway is glycolysis (Bar-Even et al., 2012; Chandel, 2021). Glycolysis is the breakdown of glucose into pyruvate and produces 2 ATP molecules per glucose molecule. The pathway consists of a series of ten enzymatic reactions that all take place in the cytoplasm. Under anaerobic conditions pyruvate is converted into lactate which in turn can be exported from the cell as a waste product. Under aerobic conditions pyruvate can be converted into Acetyl-CoA and enter the Krebs cycle to be further broken down. The Krebs cycle produces a single GTP per Acetyl-CoA molecule, but it also produces 3 NADH and 2 $FADH_2$ molecules which can enter the second major catabolic pathway: oxidative phosphorylation.

1.9.2 Oxidative phosphorylation

Oxidative phosphorylation (OxPhos) is the main energy-providing pathway in normal cells and takes place in the mitochondria (Cooper, 2000; Papa et al., 2012). In a series of redox reactions, it combines oxygen with electrons derived from NADH and $FADH_2$ (products of glycolysis, the Krebs cycle, and fatty acid beta-oxidation) to drive the phosphorylation of ADP into ATP. The transfer of electrons from NADH to O_2 is spread over a series of five protein complexes (Fig. 1.9). The first four complexes form the electron transport chain. Complex I receives the electrons from NADH, complex II receives electrons from succinate (an intermediate of the Krebs cycle) and transfers them to $FADH_2$. From complex I and $FADH_2$, electrons are transferred to coenzyme Q (also known as ubiquinone) and from there to complex III and complex IV through cytochrome c. The passage of electrons through complexes I, III, and IV generates energy that is used to create a proton gradient across the inner mitochondrial membrane. This proton gradient is used by complex V to drive the synthesis of ATP. In total, oxidative phosphorylation can produce an additional 36 ATP molecules from the 2 pyruvates produced by glycolysis.

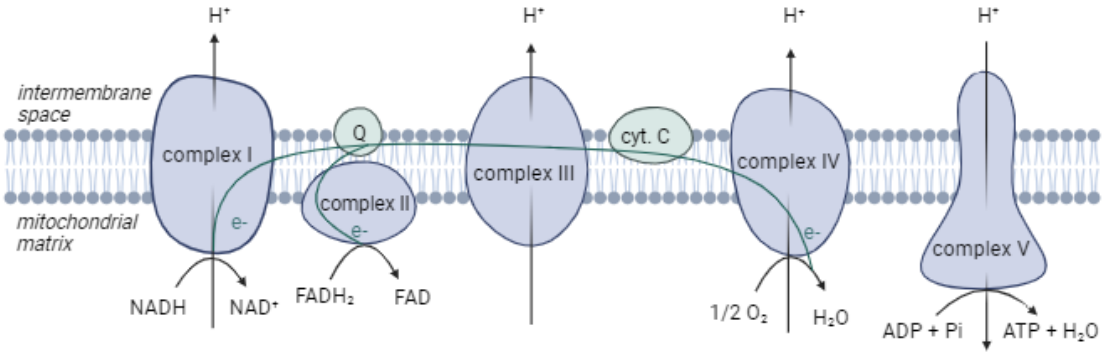

Figure 1.9. Electron transport chain. *Electrons are transported from complex I to IV to generate energy that creates a proton gradient across the mitochondrial membrane. This proton gradient is used to drive complex V which generates ATP from ADP and Pi. Created in BioRender.*

1.9.3 Metabolomic reprogramming

Cancer cells have an altered metabolomic profile compared to their healthy counterparts to fulfil their specific metabolic needs (DeBerardinis et al., 2008; Romero-Garcia et al., 2011). Intermediates of the glycolytic pathway, fatty acid catabolism, and the Krebs cycle can be used as input for multiple anabolic pathways that produce nucleotides, triglycerides, or amino acids. To generate the building blocks needed to support tumour cell growth and proliferation cancer cells tend to increase their uptake of glucose and decrease oxidative phosphorylation in favour of glycolysis. This metabolic shift is known as the Warburg effect and is caused by an upregulation of glycolytic genes and activation of the Akt pathway (Liberti & Locasale, 2016). Apart from supporting tumour growth, metabolic reprogramming can also affect cell migration and invasion, immune modulation, and drug sensitivity (Rahman et al., 2015; Zaal & Berkers, 2018).

One of the byproducts of OxPhos are reactive oxygen species (ROS) (Bhardwaj & He, 2020; Kim et al., 2016; Zhao et al., 2023). As the name suggests, ROS are highly reactive molecules that can react with and damage DNA, proteins, and lipids. While some level of DNA damage induction can be beneficial for cancer since mutagenesis can drive tumorigenesis, high levels of ROS are lethal. ROS are neutralised by the cells antioxidant system to maintain ROS homeostasis, but cancer cells can also modulate their metabolic profile to decrease the production of ROS by shifting their metabolic flux from OxPhos to glycolysis. Not only

does this protect the cells from endogenous ROS, but it also protects against ROS created by chemotherapy and is a known mechanism of resistance.

1.9.4 *In vitro* measurement of metabolism

Seahorse Agilent XF analysers can be used to perform real-time energy metabolism profiling of in vitro cell cultures (Romero et al., 2021). The machine measures the oxygen consumption rate (OCR) and extracellular acidification rate (ECAR) which are used to calculate the ATP production rate. The OCR can be used as a measure for oxidative phosphorylation since this process is the main consumer of oxygen in the cells, and the ECAR can be used as a measure for glycolysis since it produces 2 H^+ per glucose which are exported from the cells. However, the sequential addition of electron transport chain inhibitors makes it possible to differentiate ATP produced by glycolysis and by OxPhos more precisely. To do this, the OCR and ECAR are calculated under three conditions: baseline, after addition of oligomycin, and after addition of antimycin A. Oligomycin and antimycin A are inhibitors of complex V and III of the electron transport train, respectively. A set of calculations that take into account the ratio of ATP production to proton production in glycolysis; the ratio of proton production to oxygen consumption in OxPhos; the buffer factor and volume of the media are then used to determine the ATP production per pathway.

1.10 AIMS

1.10.1 Overall hypothesis

The DNA damage repair (DDR) pathway is an effective target for pancreatic ductal adenocarcinoma, both in DDR-deficient and DDR-proficient tumours.

1.10.2 Aims

The overall aim of this thesis is to identify weaknesses in PDAC with acquired and intrinsic resistance that can be used to target tumours by targeting the DDR pathway.

The aims that are discussed in chapter 3 – *Modelling Cancer Drug Screening* are two-fold. Firstly, to compare the effect of 2D and 3D cell culture methods as well as DDR status on sensitivity to drug treatment. Secondly, to develop and characterise patient-derived organoids from periampullary tumours.

The aim of chapter 4 – *Mechanisms of PARPi and Cisplatin Resistance in PDAC* is to identify mechanisms of resistance to platinum (cisplatin) and PARPi (olaparib and talazoparib) treatment in PDAC.

The aim of chapter 5 – *Targeting DNA Damage Repair Deficiency in PDAC* is to identify novel targets that sensitise to PARPi (olaparib and talazoparib), and which are mutated or can be inhibited in PDAC.

2 METHODS

2.1 LOCATION

All experiments were performed at the Life Science Research Facility (LSRF) part of the Life Science Institute, Dublin City University (LSI, DCU), except for the CRISPR screen and the Seahorse metabolism assays. The CRISPR experiments were performed in the lab of Prof. Christian Pilarsky, Üniversitätsklinikum Erlangen, Erlangen, Germany. The Seahorse assays were performed at Trinity Translational Medicine Institute, Trinity College Dublin (TTMI, TCD).

2.2 CELL CULTURE

2.2.1 Cell lines

Cell lines were propagated in a humidified atmosphere in 5% CO_2 at 37 °C. Media was replaced every 3 to 4 days and mycoplasma testing was performed every 6 months. The cell lines used are represented in Table 2.1.

According to LSRF SOP, cells were passaged when at approximately 80% confluency. After trypsinisation, cells were split in a 1:3-1:20 ratio depending on the cell line or frozen down in FBS with 10% DMSO. Cells were used for a maximum of 15 passages after thawing.

Table 2.1. Cell lines used in this project, media composition, and source.

Cell line	Media composition	Source
Capan-1	DMEM + 10% FBS + Glutamax	ATCC
MiaPaCa-2	DMEM + 10% FBS	ECACC
PT127	DMEM + 10% FBS + Glutamax	LSRF
Hek293	DMEM + 5% FBS + Glutamax	ATCC
Panc-1	DMEM + 10% FBS	ATCC
L-WRN	DMEM + 10% FBS + Glutamax + 1 mM sodium pyruvate	ATCC
PDM41	DMEM + 10% FBS + Glutamax	LSRF
VR096	adDMEM/F12 + 50% conditioned media	LSRF
VR100	adDMEM/F12 + 50% conditioned media	LSRF

DMEM (#41965-039, Gibco), FBS (#F7524-500ML, Sigma-Aldrich), Glutamax (#35050038, BioSciences), sodium pyruvate (#11360070, Gibco), adDMEM/F12 (#12634-010, Gibco). ATCC: American Type Culture Collection. ECACC: European Collection of Authenticated Cell Cultures.

2.2.2 Conditioned medium

L-WRN cells (containing a plasmid for Wnt3A, R-Spondin, and Noggin) at low passage number (passage <6) were thawed and seeded in a T175 cm^3 vented flask. 24 hours after seeding, the media was refreshed. When the cells were 90-95% confluent, 0.5 mg/mL selection agent G-418 and 0.5 mg/mL hygromycin were added to fresh media. Once the cells had reached confluency again, they were washed with trypsin and split into 10 T175 cm^3 flasks with 25 mL media per flask. The next four days the conditioned media was collected every day. The media was mixed well and centrifuged for 5 min at 200 RCFM to remove cell debris. The media was aliquoted and stored at -20 °C until use. Prior to use the conditioned media was filter-sterilised using a 0.45 µm PES filter (#15216869, Fisher Scientific).

2.2.3 PolyHEMA-coated plates

A 1X solution of poly-2-hydroxyethyl methacrylate (polyHEMA, #p3923, Merck) was made by mixing 10 g polyHEMA with 41.67 mL UHP and 791.67 mL 100% ethanol. The polyHEMA was dissolved by heating the mixture overnight at 60 °C under constant agitation. Plates were prepared by adding 75 µL, 300 µL, or 400 µL polyHEMA to each well of a 96-, 24-, or 6-well plate, respectively. The plates were incubated overnight in an oven at 60 °C. A second coat was added the following day, and the plates were incubated again. Double-coated plates were stored at room temperature until use.

2.2.4 Organoids

2.2.4.1 Media used for organoids

Table 2.2. Human Splitting Media (HSM+++). *Used as transport media for tissue samples and base media for organoids.*

Reagent	**Volume**	**Final concentration**
Advanced DMEM/F12 (#12634-028, Gibco)	500 ml	
Glutamax (#35050-061, Gibco)	5 ml	1x
HEPES (#15630-080, Gibco)	5 ml	1x
Anti-mycotic/antibiotic (#A5955-100ML, Sigma-Aldrich)	5 ml	1x

Table 2.3. Digestion media (DM). *Digestion media is to be made fresh shortly before use.*

Reagent	**Volume**	**Final concentration**
HSM+++	10 mL	
Collagenase II (#17101-015, Gibco)	50 mg	5 g/L
Dispase I (#17105041, Gibco)	10 mg	1 g/L
RhoKi (#Y0503, Sigma-Alrdich)	10 µL	10.5 µM

Table 2.4. Human complete feeding media (hCPLT) reagents. *Preparation reagents for hCPLT. All diluted reagents are stored at -20 °C.*

Reagent	**Weight**	**Diluent**	**Volume**	**Stock conc.**
N-Acetylcysteine (NAC) (#A9165, Sigma-Aldrich)	5 g	UHP	61.2 mL	500 mM
Nicotinamide (#N0636, Sigma-Aldrich)	4.88 g	PBS	40 mL	1 M
EGF (#PMG8043, Gibco)	1 mg	UHP	2 mL	50 µg/mL
A-83 (#2939, Tocris)	10 mg	DMSO	47.5 mL	0.5 mM
FGF10 (#100-26, Peprotech)	1 mg	PBS	1 mL	1 mg/mL
Gastrin (#3006, Tocris)	1 mg	PBS	4.8 mL	100 µM
RhoKi (#Y0503, Sigma-Aldrich)	5 mg	UHP	1480 µL	10.5 mM
B-27 (#17504-044, Gibco)				100x
Antibiotic/antimycotic (#A5955, Sigma-Aldrich)				100x

Table 2.5. hCPLT media. *To prepare hCPLT, combine the following reagents. hCPLT can be stored for 2 weeks at 4°C. Note: RhoKi is only added when establishing or passaging organoids. Reduced hCPLT (RhCPLT) is made without the addition of nicotinamide and A-83.*

Reagent	**Stock concentration**	**Volume**	**Final concentration**
HSM+++		9 mL	
Conditioned media		10 mL	
B-27	50x	400 µL	1x
NAC	500 mM	50 µL	1.25 mM
Nicotinamide	1 M	200 µL	10 mM
EGF	50 µg/mL	20 µL	50 ng/mL
FGF10	100 µg/mL	20 µL	50 ng/mL
A-83	0.5 mM	20 µL	500 nM
Gastrin	10 µM	20 µL	10 nM
Antibiotic/antimycotic	100x	200 µL	1x
RhoKi	10.5 mM	20 µL	10.5 µM

2.2.4.2 Establishment of patient-derived organoids

Patient samples were collected as part of a larger European wide study called PancREatic Cancer OrganoiDs rEsearch (PRECODE). The PRECODE project has received ethical approval to collect tissue and blood samples as well as medical data from the Research Ethics Committee of St. Vincent's University Hospital (reference RS20-052). Written informed consent was obtained from all patients prior to collection of samples and data. Tissue samples were donated by patients undergoing Whipple procedure at St. Vincent's University Hospital. Collection started in June 2022. After examination by the pathologist samples were placed in 10 mL HSM+++, if possible, a small section was also placed in AllProtect Tissue Reagent (#76405, Qiagen) for DNA and RNA extraction. Sample was stored at 4 °C and transported to LSRF within 18 hours post-surgery. Samples were collected from a total of 14 patients (of which 10 had tumour tissue and 14 normal tissue). Only tumour tissue samples were used for the establishment of organoids.

The AllProtect sample was stored at -80 °C upon arrival at LSRF. The remaining tissue sample was examined macroscopically and if the sample was large enough, part of it was snap-frozen in liquid nitrogen and stored at -80 °C. The remaining tissue was washed three times in 5% antibiotic/antimycotic for 2 minutes, and then minced into small fragments (<1 mm^3) using sterile scalpels (#11798343, FisherScientific). Tissue pieces were transferred into a 15 mL conical tube and 8 mL of pre-warmed DM was added to digest the tissue. The tube was placed on a shaker (220 RPM) at 37°C for an initial digestion. After 1 hour, a 20 µL sample was placed on a slide and examined for the presence of small cell clusters. If cell clusters were not visible, digestion was continued for up to 2 hours. To stop digestion, the tube was placed on ice for 2 minutes. Next, the tube was centrifuged at 1500 RPM, 4 °C for 5 minutes. All but 1.5 mL supernatant was removed, and the pellet was resuspended in 8.5 mL ice-cold HSM+++. The tube was centrifuged at the same settings and all the supernatant was removed. The pellet was resuspended in 1.5 mL TrypLE supplemented with 15 µL DNAse I (10 mg/mL) and incubated for 5-10 minutes at 37 °C. 10 mL of ice-cold HSM+++ was added to stop the trypsinisation process and the cell suspension was centrifuged as above. The supernatant was removed, the pellet was resuspended in 40-400 µL Matrigel, and 40 µL cell suspension was plated per well of a 24-well polyHEMA-coated plate. The plate was placed in an incubator at 37 °C for 15 minutes to let the Matrigel solidify. 500 µL hCPLT (with RhoKi) was added to each well. Organoids were propagated in a humidified atmosphere in 5% CO_2 at 37 °C, media was topped up or replaced every 3-4 days. Organoids were considered successfully established if they could be propagated for five or more passages and could be revived after freezing.

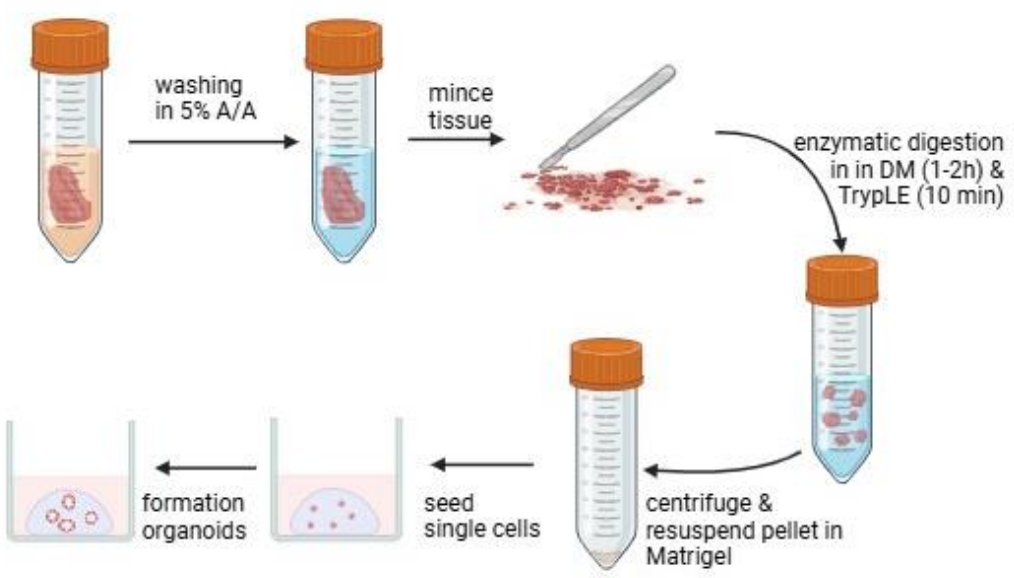

Figure 2.1. Establishment of patient-derived organoids. *Tissue samples were collected in HSM+++ and transported to LRSF within 18 hours. The tissue samples were washed in 5% antibiotic/antimycotic, minced using a sterile scalpel, and placed in digestion media (DM) for 1-2 hours. Once digestion was completed, cell clusters were placed in TrypLE to create a single cell suspension. The TrypLE was neutralised by adding HSM+++ and the suspension was centrifuged to remove the supernatant. The cell pellet was resuspended in Matrigel and plated in 40 µL droplets in a 24-well polyHEMA-coated plate. hCPLT media was added and cells were incubated to form organoids.*

2.2.4.3 *Passaging organoids*

Media and Matrigel were collected from each well and centrifuged at 1500 RPM 4 °C for 10 minutes. The supernatant was removed, and the cell pellet was washed with Cell Recovery Solution (#354253, Corning). Next, the cells were centrifuged at the same settings and the supernatant was removed. The pellet was resuspended in TrypLE (1 mL per 3 wells) and incubated at 37 °C for 5-15 minutes. To break up remaining organoids the suspension was pipetted up and down multiple times. An equal volume DMEM/F12 + 10% FBS to TrypLE was added to quench the enzymatic reaction. The cell suspension was centrifuged at 1500 RPM, 4 °C for 10 minutes, supernatant was removed, the cells were resuspended in Matrigel, and 40 µL was plated per well of a 24-well polyHEMA-coated plate. The plate was placed in an incubator at 37 °C for 15 minutes to let the Matrigel solidify. 500 µL hCPLT (with RhoKi) was added to each well.

2.2.4.4 Freezing organoids

Organoids were passaged at a high confluency as described above and allowed to grow for 3 days. Media and Matrigel were collected from each well and centrifuged at 1500 RPM, 4°C for 10 minutes. The supernatant was removed, and cells were resuspended in 1 mL Recovery Cell Culture Freezing media (#12648010, Thermo Fisher) at a concentration of 4 wells/cryovial. Cryovials were placed in a Mr. Frosty Freezing Container (#5100-0001, Thermo Fisher), and placed into a -80 °C for 48 hours before they were moved into liquid nitrogen for long-term storage.

2.3 MYCOPLASMA TESTING

Cells were regularly tested for mycoplasma contamination using the MycoStrip™ Mycoplasma detection kit. Cell culture media that had been on the cells for several days was collected. 1 mL of media was centrifuged at 16000 RPM for 5 minutes. The supernatant was discarded, and another 1 mL was added and centrifuged. The supernatant was discarded, and the pellet was resuspended in 500 µL sterile PBS. 15 µL Reaction Mix was combined with 5 µL Reaction Buffer and 5 µL sample. This mixture was incubated at 65 ˚C for 40 minutes. 200 µL Migration Buffer was added and mixed well. A detection strip was placed in the sample tube and incubated for 5 minutes. If after 5 minutes only the control band had appeared the sample, no mycoplasma was detected. The presence of a control and test band indicated the presence of mycoplasma.

2.4 VIABILITY ASSAYS

2.4.1 Cell lines – 2D culture

Cells were trypsinised and 100 µL of a single cell suspension of $1x10^4$-$5x10^4$ cells/mL (Table 2.6) was seeded into each well of a 96-well plate except for the blank. 24 hours after seeding 100 µL media (control) or 100 µL drug dissolved in media at 2X concentration was added. After 7 days of treatment, viability was measured by PrestoBlue (#P50201, Thermo Fisher). 20 µL PrestoBlue was added to each well, cells were incubated for 3 hours, and fluorescence was measured on a plate reader (Infinite 200, Tecan) using Gen4 software. Background fluorescence was subtracted from the measurements and viability was normalised to untreated control.

Table 2.6. Seeding density used for toxicity assays

Cell line	Seeding density (cells/mL)
Capan-1	50000
MiaPaCa-2	10000
Panc-1	10000
HPAC	25000
PDM41 organoid	50000
PDM41 cell line	50000
Patient-derived organoids	50000
VR096 cell line	20000
VR100 cell line	50000

2.4.2 Cell lines and organoids – 3D culture

Cells were trypsinised and a 100 µL of a single cell suspension of $1x10^4$-$5x10^4$ cells/mL was seeded into a well of a round-bottom polyHEMA-coated plate.

Organoids were split as described above (Chapter 2.2.4.3). Single cells were resuspended in Matrigel at a concentration of 5000 cells/20 µL Matrigel/well of a polyHEMA-coated 96-well plate. The plate was placed in the incubator for 15 minutes to let the Matrigel solidify and 80 µL hCPLT was added to each well.

The plates were incubated for 72 hours to allow the 3D structures to form. 100 µL media (control) or 100 µL drug dissolved at 2X concentration was added. After 7 days of treatment, viability was measured by CellTiter Glo 3D (#G9681, Promega). Both plate and reagent were allowed to come to room temperature. 20 µL reconstituted reagent was added to each well and the contents of the plate were mixed for 2 minutes using an orbital shaker. The plate was incubated for 10 minutes at room temperature to stabilize the signal before 100 µL media/reagent was transferred to a black, clear flat-bottomed 96-well plate. The luminescent signal was measured on a plate reader (Infinite 200, Tecan). Background luminescence was subtracted from the measurements and viability was normalised to untreated control. Black plates were washed twice with UHP and incubated with ethanol at 37 °C until the ethanol had evaporated and were then reused.

Table 2.7. Drugs used

Drug	Catalogue number, supplier
Cisplatin	#CAYM13119-50, VWR
Olaparib	#17281212, Fisher Scientific
Talazoparib	#S7048, Selleckchem
Gemcitabine	#S1714, Selleckchem
Oxaliplatin	#S1224, Selleckchem
SN38	#A12011, CliniSciences
5-fluoruracil	#S1209, Selleckcheck
AZD1390	AZD1390, AstraZeneca
Lynparza (olaparib)	AstraZeneca
Ceralasertib	AZD6738, AstraZeneca
Saruparib	AZD5305, AstraZeneca

2.5 DEVELOPMENT OF RESISTANT CELL LINES

Two methods were used to develop platinum (cisplatin) and PARP inhibitor (olaparib and talazoparib) resistant Capan-1 cells. For the first method, cells were continuously exposed to IC_{50} concentrations of each drug (230 nM cisplatin, 1346 nM olaparib, or 1352 nM talazoparib) for a period of 3.5 weeks. Since continuous exposure at these concentrations resulted in senescence an adjusted method was used to successfully generate the resistant cells. For this, Capan-1 cells were treated with the approximate IC_{50} concentraitons of cisplatin (75 nM), olaparib or talazoparib (450 nM) for 14 days, given a drug break of 45 days to recover, followed by an increasing concentration of drug (starting from IC_{10} for cisplatin and IC_5 for olaparib and talazoparib) over a period of 105 days with a 3-4 day drug break after passaging (used concentrations: 20 to 50 nM cisplatin, 50 to 75 nM olaparib, and 50 to from 50 to 87.5 nM talazoparib). After confirmation of resistance (defined as an ≥2-fold increase in IC_{50} concentration, see section 2.4.1) at day 165, cells were maintained in 50 nM cisplatin or 75 nM olaparib or talazoparib.

2.5.1 Doubling time

Cells were seeded at 10,000 cells/well in a 12-well plate, trypsinised and counted after 3, 5, and 7 days (n=3). The cell number was ln transformed to plot a linear growth curve and the doubling time was calculated by GraphPad Prism using nonlinear fit.

2.6 COLONY FORMATION ASSAY

Cells were seeded as single cells in a 12-well plate, at a concentration of 8000 cells/well for Capan-1 and 600 cells/well for Panc1. 24 hours after seeding, drug treatment was added. Capan-1 cells were incubated with drug for 7 days and then fixated. Panc-1 cells were incubated in with drug for 7 days, at day 7 half of the media was replaced, and the cells were incubated for another 3 days. The media was removed, and cells were gently washed with PBS. To fixate, 350 µL ice-cold methanol was added and the plates were incubated for 5 minutes at -20 ˚C. The methanol was removed, and the plates were allowed to air dry for at least 30 minutes. Once the plates were dry, the cells were stained with 0.25% crystal violet for 10 minutes. The crystal violet was removed, and the cells were washed twice with UHP water to remove excess dye. The plates were left to dry overnight. The next day, pictures were taken to visualise growth and colony formation. The dye was eluted with 300 µL 1% Triton-X by placing the plates on a plate shaker at 300 RPM for 1.5 hours. The absorbance was measured at 570 nm using a plate reader (Bio-Tek Synergy HG) with Gen4 software.

2.7 INVASION/MIGRATION ASSAY

Migration assays were carried out as the invasion assays without the coating with Matrigel. Plates for invasion assays were prepared by coating the insert of an 8.0 µm pore transwell plate (#3464, Corning) with 100 µL Matrigel diluted to 1 mg/mL in DMEM. The plate was incubated overnight at 4 ˚C, and 1 hour at 37 ˚C. Excess solution was removed, and wells were washed gently with PBS. $1x10^5$ cells in 200 µL DMEM were added to each insert. 500 µL complete media (DMEM + 10% FBS + 1% Glutamax) was added to each well. The cells were incubated for 24 hours. The media was removed, and the inside of the inserts was gently wiped with a cotton swab to remove non-migrated cells. The inserts were washed with PBS. Cells were fixated for 20 minutes with ice-cold methanol. Methanol was removed and the plates were airdried for 30 minutes. Lastly, the cells were stained with 0.25% crystal violet for 10 minutes and rinsed with UHP to remove excess stain. The number of invaded/migrated cells was quantified by counting the number of cells in 10 random fields within a grid at 20x microscope objective and graphed as the total number of invading/migrating cells at 200x magnification.

2.8 B-GALACTOSIDASE ASSAY

Senescence was detected using the Senescence β-Galactosidase Staining Kit (#9860, Cell Signaling Technology) according to the manufacturer's protocol. 10x fixative and 10x staining solution were diluted to 1x in distilled water. 20 mg X-gal was dissolved in 1 ml DMSO to prepare a 20 mg/mL stock solution. β-Galactosidase Staining Solution was prepared by combining 930 µL Staining Solution, 10 µL 100x Solution A, 10 µL 100x Solution B, and 50 µL X-gal stock solution per well of a 6-well plate. Cells were rinsed once with PBS and fixated with 1 mL Fixative Solution at room temperature for 15 minutes. The plate was rinsed twice with PBS. 1 mL β-Galactosidase Staining Solution was added to each well, the plate was sealed with parafilm and incubated overnight at 37 °C. Brightfield images were taken using a Canon EOS 550D camera (Canon GmbH, Krefeld, Germany) through a Leica DM IL LED inverted microscope (Leica Microsystems, Wetzlar, Germany).

2.9 WESTERN BLOTTING

Cells were collected and washed twice with ice-cold PBS. The cells were centrifuged, the PBS removed, and an appropriate amount of lysis buffer (RIPA buffer (#R0278, Sigma), 7.7% protease inhibitor (#US1539131-1VL, Calbiochem), 7.7% PMSF (#10837091001, Sigma), 7.7% NaOV (#5086050004, Sigma) was added to the pellet. After 20 minutes of incubation on ice, the cells were further lysed by passing through a syringe multiple times. The resulting lysate was centrifuged at 14000 RPM for 5 minutes at 4 °C and the supernatant was stored at -20 °C. Protein was quantified using the Pierce BCA Protein Assay Kit (#23225, Thermo Scientific) according to the manufacturer's protocol.

25 µL sample, consisting of 20 µg protein, loading buffer (4X, #NP0007, Invitrogen), reducing agent (10X, #NP0009, Invitrogen), and PBS, was boiled for 10 minutes at 95 ˚C, cooled on ice, and loaded onto a pre-cast Bolt 4-12% Bis-Tris Plus Gel (#NW04125, Bio-Sciences). Samples were run for 1-1.5 h at 230 V. Next, protein was transferred to a nitrocellulose membrane (#IB301001, Bio-Sciences). The membrane was blocked in 1X NET buffer (1.5 M NaCl, 0.05 M EDTA, 0.5 M Tris at pH 7.8, 0.5% Triton X-100, 0.25% w/v porcine gelatine) for 1 hour at room temperature. The membrane was then incubated with primary antibody (Table 2.8) made up in NET buffer for 1.5 hour at room temperature or overnight at 4 °C. The membrane was washed 3x for 10 minutes with NET buffer. Next, the membrane was incubated with a secondary antibody diluted in NET buffer for 1 hour. Again, the

membrane was washed 3x with NET buffer. Blots were developed using the Odyssey Imaging System (LI-COR Imaging Systems). Beta-actin was used as a loading control and densitometry analysis was performed using ImageJ.

Table 2.8. Antibodies used for Western blot analysis

Antibody	**Dilution**	**Catalogue no., supplier**
Beta-actin	1:7500	#A5441, Sigma
PARP1	1:1000	#ab6079, Abcam
GSK3β	1:1000	#610201, BD Transduction Laboratories
Cox4	1:1000	#sc376731, Santa-Cruz Biotechnology
E-cadherin	1:1000	#ab17021, Abcam
Beta-catenin	1:1000	#8480, Cell Signaling
ABCG2	1:1000	#801-029-C125, Enzo Life Sciences
goat anti-mouse, green secondary	1:10000	#926-32210, Licor
goat anti-rabbit, green secondary	1:10000	#926-32211, Licor

2.10 IMMUNOFLUORESCENCE MICROSCOPY

2.10.1 DNA damage in Capan-1 parental and resistant cells after drug treatment

Cells were seeded on sterile glass coverslips placed in a 24-well plate at a concentration of $5x10^5$ cells/well in 500 µL and grown overnight. Cells were treated with 500 µL 10 µM cisplatin, 50 µM olaparib, or 20 µM talazoparib. After 4 or 24 hours, the media was removed, and the cells were washed 3 times for 5 minutes with wash buffer (PBS + 0.1% Tween + 2% BSA). After each following step the cells were washed again. The cells were fixated in 300 µL 4% paraformaldehyde (#28908, ThermoScientific) in PBS for 20 minutes. To permeabilise the cells, they were incubated with 300 µL 0.5% Triton-X100 (#X100, Sigma-Aldrich) for 20 minutes. Next, the cells were blocked with 10% FBS in PBS for 1.5 hours, followed by overnight incubation at 4 °C with 150 µL primary antibody diluted in wash buffer. Cells were washed again and were incubated in the dark at room temperature with 150 µL secondary antibody diluted in wash buffer for 1 hour. To visualize the nucleus, cells were counterstained with DAPI (1.6 µg/mL in PBS) (#D1306, Invitrogen) for 3 minutes. Lastly, coverslips were placed on glass slides and mounted with DPX mounting media.

Table 2.9. Antibodies used for immunofluorescence of γH2AX and RAD51

Antibody	**host**	**dilution**
γH2AX (#613402, Biolegend)	mouse	1:250
RAD51 (#PA5-27195, Invitrogen)	mouse	1:300
anti-Mouse IgG (H+L), Alexa Fluor 488 (#PA5-27195, Invitrogen)	goat	1:200

2.10.2 Immunofluorescence of organoids

Formaldehyde-fixed parafilm-embedded (FFPE) tissue slides were obtained from SVUH. Slides with the corresponding organoids were made by Optimal Cutting Temperature compound (OCT, #KMA-0100-00A, CellPath) embedding. Full grown organoids were collected, washed with cold PBS, and centrifuged for 10 minutes at 1500 RPM, 4 ˚C to remove Matrigel. The supernatant was discarded, and the organoids were fixated in 2 mL 4% paraformaldehyde for 30 min. The paraformaldehyde was removed, and the organoids were washed with PBS for 3 minutes. After washing, the PBS was removed, and the organoids were placed in 10 mL 10% sucrose. After overnight incubation at 4 ˚C, 1 gram of sucrose was added to increase the concentration to 20%. The organoids were again incubated overnight at 4 ˚C. Another 1 gram of sucrose was added to increase the concentration to 30% followed by another overnight incubation. At this point the organoids had sunken to the bottom of the tube and the sucrose solution could be removed. The bottom of an embedding mould was covered with OCT, organoids were placed on top of this and were covered with another layer of OCT. OCT blocks were stored at -80 ˚C until use. Using a cryostat (CM1900, Leica) that was cooled to -20˚C prior to use, OCT blocks were mounted onto the freezing block and organoids were cut into 20 µm sections and placed onto SuperFrost Plus slides (#10149870, Thermo Fisher). Slides were stored at -20˚C until use. Slides were washed briefly with wash buffer to remove OCT and were stained as for the Capan-1 cell lines starting from the Triton-x permeabilisation step (Chapter 2.10.1) using the antibodies in Table 2.10.

2.10.3 Immunofluorescence of tissue slides

FFPE tissue slides were provided by the pathology department at SVUH. Slides were dewaxed and rehydrated prior to staining by incubating twice in 100% xylene for 10 minutes, twice with 100% ethanol for 2 minutes, twice with 90% ethanol for 2 minutes, and twice with 70% ethanol for 2 minutes. The slides were rinsed in UHP water and were

stained as for the Capan-1 cell lines starting from the Triton-x permeabilisation step (Chapter 2.10.1) using the antibodies in Table 2.10.

Table 2.10. Antibodies used for immunofluorescent staining of cancer markers

Antibody	**host**	**dilution**
ALDH1A1 (#ab5292, Abcam)	Rabbit	1:100
CXCR4 (#5224-100, Biovision)	Rabbit	1:100
HCAM (#sc-7297, Santa-Cruz)	Mouse	1:100
PDX1 (#PA5-14824, Thermo Fisher)	Rabbit	1:50
Ki-67 (#M7240, Dako)	Mouse	1:150
MUC1 (#4538S, Cell Signalling)	Mouse	1:100
anti-Mouse IgG (H+L), Alexa Fluor 488 (#PA5-27195, Invitrogen)	Goat	1:200
Anti-Rabbit IgG (H+L), Alexa Fluor 488 (#A-11008, Invitrogen)	Goat	1:200

2.10.4 Confocal imaging

Slides were imaged on a Nikon Eclipse Ti-E widefield fluorescence microscope with Andor Zyla sCMOS camera and Plan Fluor ELWD lenses. DAPI was excited at 370 nm with emission captured at 457.5 nm. Alexa Fluor was excited at 467.5 nm with emission captured at 535 nm. For the quantification of γH2AX and RAD51 foci formation images were processed in ImageJ using the following script:

```
setAutoThreshold("Default dark");
//run("Threshold...");  > adjust threshold to cover the nuclear DAPI stain completely
setOption("BlackBackground", false);
run("Convert to Mask");
run("Smooth");
run("Convert to Mask");
run("Fill Holes");
run("Watershed");
run("Analyze Particles...", "size=50-300 exclude clear include add");
selectImage("[…]"); // > select the Alexa Fluor image with the γH2AX/RAD51 stain
roiManager("Measure");
```

2.11 BRIGHTFIELD IMAGING

Brightfield imaging was performed using a Leica DM IL LED inverted microscope (Leica Microsystems, Wetzlar, Germany) equipped with a Canon EOS 550D camera (Canon GmbH, Krefeld, Germany). To evaluate Capan-1 cell proliferation during drug exposure images were taken 2, 4, and 7 days after seeding at 10x magnification. Confluence was calculated using ImageJ. Brightfield RGB images were transformed to 16-bit, the threshold was adjusted to cover all cells, and the confluence was calculated as the ratio of the covered area against the total area.

2.12 CRISPR

CRISPR libraries targeting DNA damage repair (DDR) and protein kinases (PK) were provided as viral stocks by Prof. Pilarsky. A full overview of the targets and sgRNAs of these libraries can be found in Supplemental Table 3 and 4. Prof. Pilarsky also provided the Panc-1 cell line with stable Cas9 expression (Panc-1Cas9).

2.12.1 Determination MOI library

Panc1-Cas9 cells were seeded at a density of $7.8x10^5$ cells/T25 cm^3 flask and incubated overnight. Lentivirus containing DDR library or PK library was thawed on ice. In a 15 ml tube, 5.7 mL medium was combined with 5.7 µL polybrene (10 mg/mL) and the following volumes of virus (Table 2.11).

Table 2.11. MOI determination

Library	**Volumes of virus (µL)**
DDR	400, 500, 600
PK	100, 200, 300
Negative control	0

All media was removed from the flasks and 5 mL medium containing virus was added to each flask. The cells were incubated for 24 hours. The media was replaced, and cells were allowed to grow for another 48 hours. Next, the cells with successful transduction were selected by changing the media for medium containing 5 µg/mL puromycin. After 72 hours, the media was removed, and the cells were gently washed with PBS to remove dead cells. The remaining cells were trypsinised and counted to calculate the fraction of survival compared to untreated control, which is a measure of the multiplicity of infection (MOI). The concentration of virus needed to result in a MOI of 0.3 was used for the full screen.

2.12.2 CRISPR screen

CRISPR screening was performed in Panc-1 Cas9-expressing cells. $1.2x10^7$ and $8x10^5$ cells were transduced at MOI=0.3 in triplicate with the PK and DDR sgRNA libraries, respectively. After overnight incubation, the media was replaced with fresh media without virus. Cells were allowed to grow for 48 hours before selection with 10 µg/ml puromycin for 4 days. Cells were washed with PBS to remove dead cells and debris, fresh media with or without drug (1.2 µM olaparib or 2.5 nM talazoparib) was added. After 72 hours, cells were passaged 1:2 and the remaining cells (>$1.1x10^7$ cells for kinase screen and >$2.5x10^6$ cells for DDR screen) were harvested, washed with PBS, and stored as cell pellet at -20˚C. The cells were allowed to settle overnight before new drug was added for another 72 hours. Again, the cells were passaged and harvested. This was repeated for a total of 5 cycles or 25 days. With every cycle the drug concentration was increased to a final concentration of 40 µM olaparib or 100 nM talazoparib.

DNA was extracted from samples at timepoint t=5 using the Qiagen DNA Blood & Tissue kit (#69504, Qiagen) according to the manufacturer's protocol. The extracted DNA was quantified using Nanodrop. For representative sequencing a 50-300x coverage for each sgRNA is required. Since 10^6 cells amounts to roughly 6 µg of DNA, 5 µg of DNA was used for the PCR to have a coverage of at least 119-fold (5 µg ~ $8.3x10^5$ cells. $8.3x10^5$ cells/7000 sgRNAs = 119x coverage). The DNA was combined with PCR master mix and primers according to Table 2.12 and amplified by PCR following the PCR cycling conditions in Table 2.13.

Table 2.12. PCR master mix

Reagent	**Volume**
Q5 Hot Start Mix (#M0494S, Biolabs)	50 uL
P5 (10pmol) (p5_Gecko_f1, #2209697, TIB MolBio)	3 uL
P7 (10 pmol)(p7_Gecko_r1, #45-1297, Eurofins)	3 uL
DNA	5 uL
ddH_2O	39 uL

Table 2.13. PCR cycling conditions

Temperature	Duration	
98	30s	
98	10s	25 cycles
66	30s	
72	30s	
72	2 min	
4	∞	

PCR product amplification was confirmed by agarose gel electrophoresis. A 1% agarose gel was made by dissolving 1 g agarose in 100 mL TAE buffer (#1140407, Serva). The solution was microwaved for 3 minutes at full power and left to cool down to approximately 50 ˚C. 10 µL GelRed Nucleic Acid Stain (10000x, #003, Biodium) was added and the gel was poured into a cast and left to solidify for 20-30 minutes. Once the gel had solidified, 10 µL DNA was mixed with 2 µL DNA Loading Dye (#R0611, Thermo Scientific) and 10 µL DNA sample and 3 µL ladder (100bp DNA ladder, #15628019, Invitrogen) was loaded onto the gel. The gel was run at 120V for 25 minutes. DNA was visualised using UV light. No product was detected. The process was repeated for the samples at t=1 which did work, so these samples were quantified by Qubit and used for sequencing. 20 ng PCR product in 20 µL water was sequenced on an Illumina HiSeq 2500 platform at the Deep Sequencing Facility of the TU Dresden. Sequencing analysis was performed using the Model-based Analysis of Genome-wide CRISPR-Cas9 Knockout (MAGeCK) pipeline at the recommended settings (Li et al., 2014).

2.13 siRNA KNOCKDOWN

Cells were transfected by reverse transfection using $1x10^5$ cells in a 12-well, at a concentration of 50 nM siRNA (Table 2.14). 50 µL Opti-MEM (#31985-062, Gibco) was combined with 3 µL Lipofectamine 3000 Reagent (#L3000001, Thermo Fisher). 50 µL Opti-MEM was combined with siRNA and mixed well. Both mixtures were combined and incubated for 10-15 minutes at room temperature. Cells were seed in 1 mL media per well, 100 µL transfection mix was added and mixed by gentle pipetting. Cells were incubated for 48 hours before extraction (RT-PCR). For viability assays, volumes were adjusted to 96-well plates and cells were treated the following day.

Table 2.14. siRNAs for gene knockdown

siRNA target gene	Catalog number, supplier
BRCC3	#EHU069041, Merck
NEIL1	#EHU081311, Merck
PTEN	#EHU106441, Merck
XRCC3	#EHU138141, Merck
Negative control	#4611G, Ambion

2.14 TRIZOL RNA EXTRACTION

1 mL Trizol (#15596026, Invitrogen) was added to approximately $2x10^5$ cells and incubated for 5 minutes at room temperature. 0.2 mL chloroform (#C2432, Sigma-Aldrich) was added and mixed thoroughly. The mixture was placed in an Eppendorf tube and incubated for 2-3 minutes at room temperature Next, the tubes were centrifuged for 15 minutes at 1200 RPM at 4 ˚C. The mixture separates into a lower red phenol-chloroform phase, an interphase, and an upper colourless aqueous phase. The aqueous phase containing the RNA was transferred into a new tube. 0.5 mL isopropanol (#19519, Sigma-Aldrich) was added and mixed in by inverting the tube 10 times. The mixture was incubated for 10 minutes at room temperature and was then centrifuged for 10 minutes at 1200 RPM at 4 ˚C. The RNA forms a pellet, and the supernatant was discarded. The pellet was resuspended in 1 mL of 75% ethanol. This was vortexed briefly and centrifuged for 5 minutes at 7500 RPM at 4 ˚C. The supernatant was discarded, and the pellet was allowed to air-dry for 20-30 minutes. The dry pellet was resuspended in 30 µL RNAse-free water and incubated at 60 ˚C for 10-15 minutes. Lastly, the RNA concentration was measured using Nanodrop. Samples were stored at -80 ˚C until use.

2.15 cDNA REVERSE TRANSCRIPTION

RNA was transcribed into cDNA using a High Capacity cDNA Reverse Transcription Kits (#4368814, Thermo Fisher). Briefly, 2x reverse transcription master mix was prepared according to Table 2.15. The master mix was placed on ice and mixed. 10 µL of master mix was combined with 10 µL RNA sample in a PCR tube. Tubes were centrifuged and placed on ice until use. Reverse transcription was performed in a thermo cycler according to the settings in Table 2.16 with the volume set to 20 µL.

Table 2.15. RT master mix

Component	Volume/reaction (µL)
10X RT buffer	2.0
25X dNTP Mix (100 mM)	0.8
10X RT random primers	2.0
MultiScribe reverse transcriptase	1.0
Nuclease-free water	4.2

Table 2.16. Thermo cycler conditions

Temperature (˚C)	25	37	85	4
Time (min)	10	120	5	∞

2.16 RT-PCR

Quantitative RT-PCR was performed using the TaqMan® Fast Advanced Master Mix (#4444556, Thermo Fisher) according to the manufacturer's protocol. Per reaction, PCR reaction mix was formed by combining 10 µL of TaqMan® Fast Advanced Master Mix, 1.0 µL TaqMan Assay, and 7.0 µL nuclease-free water. This mixture was vortexed briefly and centrifuged to collect the reaction mix at the bottom of the tube. 18 µL of reaction mix was placed into a PCR plate (#4346907, Thermo Fisher) and 2 µL cDNA template or nuclease-free water for negative control was added to each well. The plate was sealed and centrifuged briefly to collect the mixture at the bottom of the wells and remove air bubbles. The plate was run on an QuantStudio 5 System according to the settings in Table 2.17 with the volume set to 20 µL. mRNA expression levels were normalised against the housekeeping gene *GAPDH* and untreated control to calculate the fold change.

Table 2.17. RT-PCR cycling conditions

			40 cycles	
Temperature (˚C)	50	95	95	60
Time	2 min.	2 min.	1 sec.	20 sec.

Table 2.18. TaqMan RT-PCR probes

Target Gene	Assay ID	Catalog number, supplier
GAPDH	Hs02786624_g1	# 4351370, ThermoFisher
BRCC3	Hs02386484_g1	#4331182, ThermoFisher
XRCC3	Hs00193725_m1	#4331182, ThermoFisher
PTEN	Hs02621230_s1	#4331182, ThermoFisher
NEIL1	Hs00908563_m1	#4331182, ThermoFisher

2.17 SEAHORSE

ATP flux and mitochondrial stress were evaluated using the Seahorse Xfe24 analyser. Cells were seeded in quadruplicate in a 24-well Seahorse plate (Seahorse XFe24 FluxPak, #102340-100, Agilent Technologies) at $1.8x10^3$ cells/well in 250 µL media. After 48 hours, the media was removed and the cells were washed with Seahorse media (Seahorse XF DMEM assay medium pack (pH 7.4), 10 mM glucose, 1 mM sodium pyruvate, 2 mM L-glutamine) (#103680-100, Agilent Technologies). After washing, 500 µL Seahorse media was left in the wells and the cells were incubated at 37 ˚C in a non-CO_2 incubator for 1 hour. Oxygen consumption rates (OCR) and extracellular acidification rates (ECAR) were measured before and after treatment with 0.9 µM oligomycin, 2 µM FCCP, and 2 µM antimycin (XF Cell Mito Stress Kit; 103015-100, Agilent Technologies) according to the Seahorse ATP flux and MitoStress assay protocols. Measurements were normalised to cell number using a crystal violet assay. Cells were fixated in 1% glutaraldehyde (340855, Sigma-Aldrich) for 15 minutes at room temperature. The fixative was removed, and the cells were washed with PBS. The cells were stained with 50 µL crystal violet (1% in PBS) for 30 minutes at room temperature. The dye was removed, and the cells were washed with UHP water and allowed to air dry overnight. The dye was solubilised with Triton X (1% in PBS) (#X-100, Sigma-Aldrich) on a shaker at 400 RPM for 1 hour. Absorbance was read at 595 nm using the Promega Glomax explorer.

2.18 DNA AND RNA EXTRACTION AND SEQUENCING

DNA and RNA were extracted from Capan-1 parental and resistant cells using DNA/RNA AllPrep kit (#80204, Qiagen). DNA and RNA concentrations were quantified using Nanodrop and were sequenced using the Illumina NovaSeq platform (Novogene) at 100X coverage.

2.18.1 Whole exome sequencing analysis

DNA sequencing data was analysed using SomaSnake pipeline (v1.3)(Charlotte, 2023). In short, quality reports were generated using FastQC, reads were trimmed using Sickle and mapped by Burrows-Wheeler Aligner on human genome build 38. Genome Analysis Toolkit (GATK) was used to remove duplicates, recalibrate mapped reads, and apply base quality score recalibration. Evaluation and visualisation of coverage depth was performed by Mosdepth, Sambamba, and Samtools. Variant calling, estimation of contamination, and detection of false positive SNPs was performed using the GATK tools Mutects, CalculateContamination, and FilterMutectCalls, respectively. Bcftools and vcfintersect were used to filter and format output. Control-FREEC was used to detect copy number alterations (CNA), B-allele frequency (BAF), and loss of heterozygosity (LOH). Somatic variants were annotated using Variant Effect Predictor tool and intersectBed. Variant clustering was performed using PyClone and SciClone.

2.18.2 Transcriptomic analysis

Transcriptomic analysis was performed using the public server at usegalaxy.org (The Galaxy Community et al., 2022). Adapter sequences present in a fraction of the reads were removed using Cutadapt (sequence AGATCGGAAGAG, filter minimum length: 20, quality cutoff: 20) and trimmed reads were mapped onto the human reference genome (Hg38) using HISAT2. Count reads were mapped to genes with FeatureCounts. To determine enriched pathways, differential expression analysis was performed in Omicsbox using the NOISeq package with the parameters in Table 2.19 (Bioinformatics, 2019; Skuta C et al., 2014). KEGG pathway enrichment analysis was performed using ShinyGO Version 0.80 (Ge et al., 2020).

Table 2.19. Parameters differential expression analysis NOISeq

Parameter	**Value**
CPM Filter	0.5
Normalisation method	TMM (Trimmed mean of M values)
Number of simulated replicates	5
Size of simulated replicates	0.2
Variability	0.02

2.19 SYNERGY

Synergy between two drugs at a single concentration was determined using the combination index (CI) calculated according to the Bliss Independence approach:

$$CI = \frac{E_A + E_B - E_A E_B}{E_{AB}}$$

In which E_A is the effect of drug A (given as the viability ratio), E_B is the effect of drug B, and E_{AB} is the effect of the combination treatment. Combinations can be synergic (CI<1), additive (CI=1), or antagonistic (CI>1).

2.20 STATISTICAL ANALYSIS

Data were analysed using GraphPad Prism version 10.2.1 for Windows (GraphPad Software, Boston, Massachusetts USA). Student's T-test was performed to investigate differences in IC50 values in viability assays, colony formation, invasion and migration, protein expression, foci formation, and siRNA knockdown between either a parental and resistant cell line or a treated and a control sample. One-way ANOVA followed by Dunnett's multiple comparisons test with parental cells set as the control was used to analyse the Seahorse experiments. Differences were considered significant when $p<0.05$.

3 CANCER DRUG SCREENING IN HOMOLOGOUS RECOMBINATION DEFICIENT (HRD) AND PROFICIENT 2D AND 3D MODELS

3.1 INTRODUCTION

Over the last 25 years PDAC survival rates have barely improved despite the introduction of novel treatments and treatment combinations (Latenstein et al., 2020). One of the limitations in the development of effective treatments is the lack of representative *in vitro* models. Until very recently, established cell lines grown as monolayer in a culture flask or plate have been the main model for the validation and characterisation of drugs (van Staveren et al., 2009). They are cheap, easy to use, and highly scalable, which makes them an attractive model to work with. However, due to their simplicity established cell lines lack certain features (e.g. polarity, cell-matrix interaction) that are present in tumours which contributes to the high drug attrition rates for cancer (Hutchinson & Kirk, 2011).

3.1.1 2D versus 3D *in vitro* models

Recently, efforts have been made to develop 3D *in vitro* models that are more representative of the tissue morphology. The simplest model is the 3D spheroid culture method, in which cell lines are stimulated to form clusters. There are several methods to do this, the method used in this chapter was to seed the cells in low-attachment U-bottom plates and centrifuge the plates immediately after seeding to promote the formation of spheroids. Compared to 2D monolayer culture, 3D spheroids form a more realistic structure with cell-cell contacts, polarised cells, with medium and oxygen gradients that are lacking in monolayer cultures (Fennema et al., 2013). However, spheroids still miss a lot of the tissue architecture and heterogeneity that is observed in tumours.

3D organoids, on the other hand, are a much more sophisticated model that is characterised by the presence of a supporting extracellular matrix (ECM), organ-typical architecture, and varied cell cycle states. This makes them more similar to patient tumours, and several studies have shown that patient-derived PDAC organoids recapitulate patient response to treatment (Grossman et al., 2022; Romero-Calvo et al., 2019; Tiriac et al., 2018). Organoids are established by seeding primary cells in extracellular matrix and feeding the cells with media that is supplemented with growth factors that stimulate stem

cell maintenance and organ-specific differentiation. This model is self-organising, meaning that without any additional outside stimulus the cells will form 3D structures.

3.1.1.1 High-throughput screening (HTS)

High-throughput screening (HTS) plays an important role in drug discovery and repurposing in cancer. Due to their low cost, easy handling, and low heterogeneity (and thus high replicability) 2D cell lines are well-suited to HTS and have been used extensively. 3D spheroid and organoid cultures have been used for HTS as well, but large-scale implementation is hindered by their higher heterogeneity in composition and variability in drug response (Gündel et al., 2023; Gündel et al., 2021; Hirt et al., 2022; Kaur et al., 2021; Watanabe et al., 2022; Zhou et al., 2023) . More importantly, the need for specialised equipment and high material cost are highly restrictive in the case of HTS of 3D organoids (Hirt et al., 2022). This is mainly due to the use of ECM such as Matrigel or Basement Membrane Extract (BME) which are expensive and solidify above 4˚C, thus requiring the use of cooled liquid handlers. Until these issues are resolved cell lines remain the model of choice for large scale drug screening.

3.1.2 Homologous recombination deficiency (HRD) status

DNA damage repair deficiency (DDR), or more specifically homologous recombination deficiency (HRD), has been shown to sensitise to platinum and PARPi treatment. Most research on HRD has been done on models with *BRCA* mutations, but mutations in other HR genes such as *PALB2* have been studied as well (Javle et al., 2021; Principe, 2022). However, functional HRD status is not purely dependant on genetic alterations but may be influenced by cell intrinsic and extrinsic factors which in turn may be influenced by the cell culture model used.

For example, due to their size and high cell density spheroids may develop a hypoxic centre as they grow which is not seen in monolayer culture or organoids. Hypoxia has been shown to reprogram DDR and down-regulate *RAD51* and *BRCA1/2* expression (Begg & Tavassoli, 2020; Zihlif et al., 2023), which has been linked to chemotherapy and PARPi resistance (Lee et al., 2024; Mehibel et al., 2021). In contrast, organoids are characterised by a more heterogenous cell population which includes stem cells. Stem cells have an enhanced DDR capacity which is thought to contribute to intrinsic chemoresistance but may also result in

a vulnerability in cancer stem cells with DDR mutations that are more dependent on alternative repair pathways (Abad et al., 2020; Gillespie et al., 2023).

3.1.3 Development of novel cell culture models

There are two general approaches for the establishment of primary pancreatic cancer models: directly from primary tissue, or from tissue that has been propagated in patient-derived xenografts. While the latter model has a higher success rate due to the generally larger tumour volume and selection for more aggressive cells, it is also more time consuming and runs the risk of contamination with murine cells. A common method to establish novel cell lines is to finely mince freshly harvested tissue and perform enzymatic digestion to create a single cell suspension that is placed in a cell culture flask with appropriate media where the cells are allowed to attach and proliferate (Feldmann et al., 2009; Torres et al., 2013). Alternatively, cell lines can be established from organoids by creating a single cell suspension through enzymatic digestion and seeding this in a culture flask (Noorani et al., 2022). This is the method that was applied in this chapter.

The first steps for the development of organoids are similar, but instead of seeding cells in a culture flask the cells are plated in extracellular matrix such as Matrigel or BME and the media is supplemented with factors that promote stem cell maintenance and tissue-specific differentiation (Boj et al., 2015; Driehuis et al., 2020). While it is possible to establish cell lines and organoids from small tissue samples such as biopsies, larger tissue volumes tend to have better success rates. The location of the pancreas does not lend itself easily to the acquisition of biopsies so often the only tissue material available is that of tumours that were resected by Whipple surgery. Whipple surgery involves the removal of the pancreatic head, distal bile duct, gallbladder, and part of the duodenum (D'Cruz et al., 2024). While this surgery is predominantly used for PDAC it can also be applied for the resection of other periampullary cancers.

Because of their more life-like representation, research is more and more shifting towards the use of 3D models. However, little is known about how well drug sensitivity data of 2D models correlates with 3D models. Additionally, there is a need for the development of novel cell culture models, especially those with HR deficiency.

3.1.4 Aims and objectives

This chapter has two overarching aims: 1) compare the effect of 2D and 3D cell culture methods, as well as DDR status, on sensitivity to drug treatment; 2) develop and characterise patient-derived organoids from pancreatic tumours.

Objective 1: Development of 3D spheroid models from cell lines Capan-1, MiaPaCa-2, and PT127 and 2D cell lines from organoid lines PDM41, VR096, and VR100.

Objective 2: Comparison of the sensitivity to platinum agent (cisplatin) and two PARPi (olaparib and talazoparib) in 2D cell line, 3D spheroid, and 3D organoid models.

Objective 3: Development and characterisation of novel patient-derived organoids from resected periampullary tumour tissue.

3.2 Effect of 2D and 3D cell culture conditions on sensitivity to drugs

While 3D models more closely mimic the *in vivo* tumour morphology, 2D models are more suited for high-throughput drug screening, leaving a place for both model systems in drug development. However, there is a distinct lack of knowledge on how culture methods affect treatment sensitivity. Therefore, to assess the sensitivity of 2D and 3D culture models to platinum (cisplatin) and PARPi (olaparib, talazoparib) treatment, toxicity assays were performed on cells grown as 2D monolayer and 3D spheroid or 3D organoid (Fig. 3.3-3.5 and Table 3.1-3.3). For these comparisons, the established cell lines Capan-1 and MiaPaCa-2 and the primary cell line PT127 were grown as 2D cell line and 3D spheroid; the patient-derived organoids PDM41, VR096 and VR100 were grown as 2D organoid-derived cell lines and 3D organoids (Fig. 3.1).

3.2.1 Establishment of 2D and 3D models

Spheroids were grown by seeding the cell lines Capan-1, MiaPaCa-2, and PT127 in polyHEMA-coated U-bottom plates that were centrifuged after seeding to promote clustering and spheroid formation. Capan-1 is a well-differentiated epithelial cell line that formed dense spheroids with smaller, budding protrusions. MiaPaCa-2 has a more polymorphic morphology that includes epithelial, elongated, and non-adherent cells. Spheroids were very dense and relatively smooth. PT127 also has an epithelial morphology and formed clusters of smaller spheroids rather than a single big spheroid.

Cell lines were established from PDM41, VR096, and VR100 organoids by seeding single cell suspensions in tissue culture plates in advanced DMEM/F12 media supplemented with 50% L-WRN conditioned media to promote the presence of stem cells. The cell lines were cultivated over several passages to confirm viability and to establish a stable phenotype. PDM41 is a patient-derived organoid (PDO) line that forms large hollow organoids and formed large, elongated cells when grown as cell line. VR096 forms cystic organoids and had an epithelial morphology when grown as cell line. VR100 forms more dense organoids and had an epithelial morphology with different cell sizes when grown as a 2D cell line.

To investigate if cell culture methods modulate the effect of HR status on treatment sensitivity three HR-proficient and three HR-deficient models were used. PT127, PDM41, and VR096 are HR-proficient, whereas MiaPaCa-2, Capan-1, and VR100 have a mutation in HR genes (Fig. 3.2).

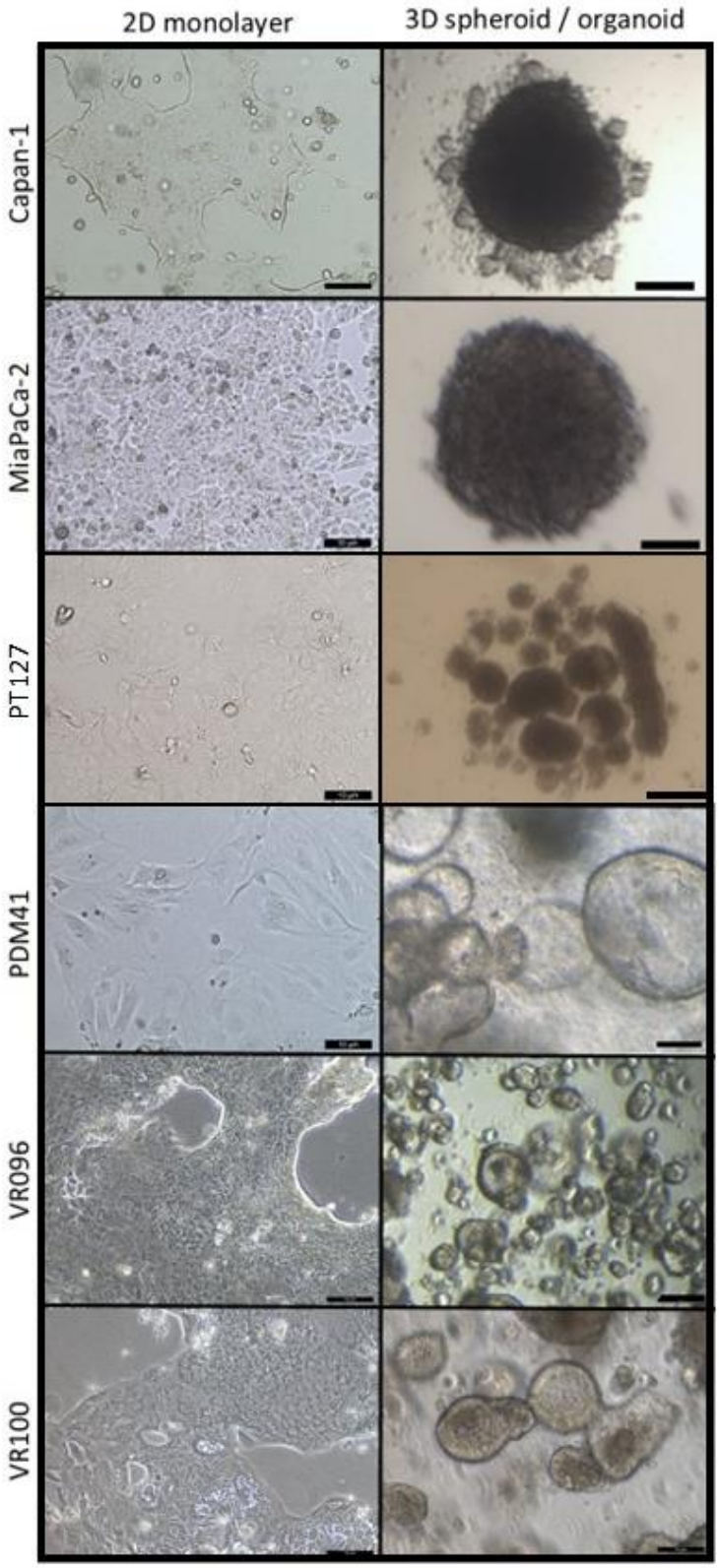

Figure 3.11. Brightfield imaging of 2D and 3D cell culture. *All models were grown as 2D monolayer. Capan-1, MiaPaCa-2, and PT127 were grown as 3D spheroids. PDM41, VR096, and VR100 were grown as 3D organoids. Scale bar monolayer and organoids, 10 µm (10x magnification), scale bar spheroids, 50 µm (4x magnification).*

Capan-1 has lost one *BRCA2* allele and has a frameshift mutation resulting in a premature stop codon in the remaining allele (p.1532V>Sfs*2) and VR100 has an in-frame insertion in *BRCA2* (p.308F>FSX). Both mutations are likely to impair *BRCA2* function. Additionally, VR100 has a deletion and resultant frame-shift mutation in *RAD50* (p.719L>X). MiaPaCa-2 has a missense mutation in *PALB2* (p.64S>L). This mutation has not been reported in literature and the effect on protein function is unknown. As the mutation is located in the DNA binding domain and constitutes the change of a polar and hydrophilic amino acid to a non-polar and hydrophobic amino acid which may affect DNA binding MiaPaCa-2 was tentatively classified as HR deficient.

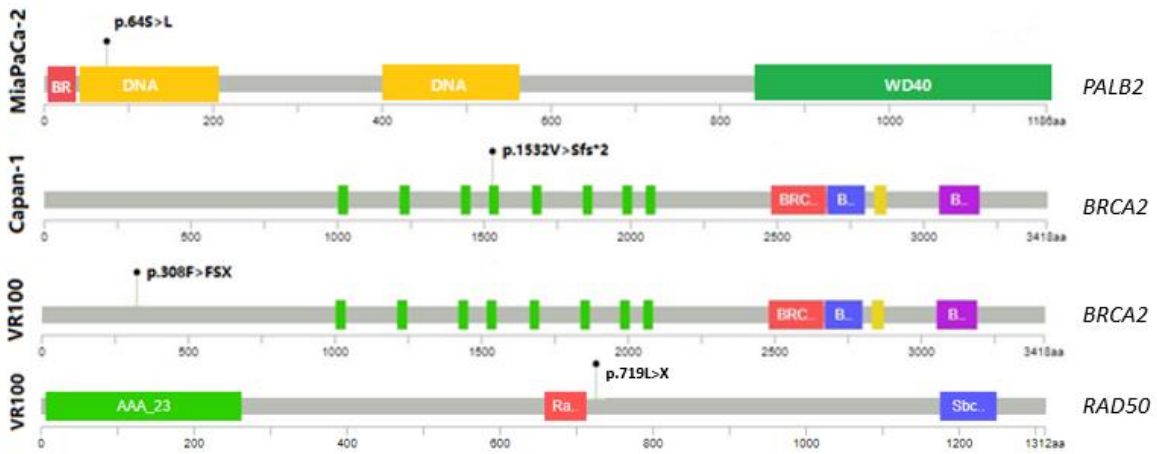

Figure 3.22. HR mutations in MiaPaCa-2, Capan-1, and VR100 cell culture models*. Lollipop plots were modified from cBioportal, sequencing data for VR100 was provided by PRECODE.*

3.2.2 Sensitivity to cisplatin

Sensitivity to drug treatment was evaluated by PrestoBlue reagent (a resazurin-based solution that becomes fluorescent due to the reducing power of living cells) for 2D and by CellTiter Glo (which generates a fluorescent signal by reacting with ATP) for 3D after seven days of treatment (Chapter 2.4). For the established cell line Capan-1 there is no significant difference in sensitivity between 2D monolayer and 3D spheroid culture (Fig. 3.3 and Table 3.1). Both models have an IC_{50} around 1 µM ($p=0.97$). For MiaPaCa-2, there also no significant difference in the IC_{50} between the 2D and 3D culture method ($p=0.36$). For the cell line model PT127, the 3D spheroid model is remarkably less sensitive to cisplatin with a 14.7-fold change (FC) in IC_{50} (16.4 µM vs 242.11 µM, $p<0.001$).

Similarly, the organoid model VR096 is also highly resistant to cisplatin. While the 2D monolayer model had an IC_{50} of 2.00 µM, this was 28.32-fold higher in the organoid model at 56.64 µM ($p<0.001$).

In contrast, for the organoid lines PDM41 and VR100 the 2D monolayer culture is less sensitive to treatment. For PDM41 the 2D monolayer had not reached the IC_{50} at the highest treatment concentration of 40 µM at which it had a viability of 87.2% compared to 20.8% in the organoid model (-4.19 FC, $p<0.001$). For VR100 the monolayer culture has an IC_{50} of 0.40 µM compared to 0.038 µM in the organoid model (-10.5 FC, $p=0.06$) although both show exquisite sensitivity to cisplatin.

Table 3.1. IC_{50} values of 2D and 3D in vitro models treated with cisplatin. *The IC_{50} values are interpolated from the graph in figure 3.1 and given in µM. Values in brackets are the standard deviation. FC: fold change in IC_{50} value of 3D models compared to 2D models.*

		HR-deficient			**HR-proficient**		
		Capan-1	**MiaPaCa-2**	**VR100**	**PT127**	**PDM41**	**VR096**
cisplatin	**2D**	1.04 (0.85)	3.44 (0.54)	0.4 (0.15)	16.4 (3.89)	>40	2.00 (1.58)
	3D	1.04 (0.46)	7.06 (9.21)	0.038 (0.015)	242.11 (20.38)	10.25 (0.40)	56.64 (7.67)
	FC	1.00	2.05	-10.5	14.76	<-3.9	28.32

When looking at the HR status in relation to cisplatin sensitivity, there is a clear separation in sensitivity between the HR-deficient and -proficient cell models (Table 3.1). The two mt*BRCA2* models, Capan-1 and VR100, are most sensitive to cisplatin treatment with an IC_{50} of less than 1.1 µM, for both the 2D and the 3D model. The MiaPaCa-2 model with the *PALB2* mutation is slightly less sensitive with an IC_{50} of 3.4 µM in 2D and 7.1 µM in 3D.

In contrast, for the HR-proficient models the IC_{50} ranges between 10.3 to 242.1 µM, with an exception for the 2D model of VR096 which is 28.3-fold more sensitive than its organoid-derived model with an IC_{50} of 2.0 µM. However, for all three HR-proficient cell lines either the 2D or the 3D model has an IC_{50} above 40 µM showing high levels of resistance.

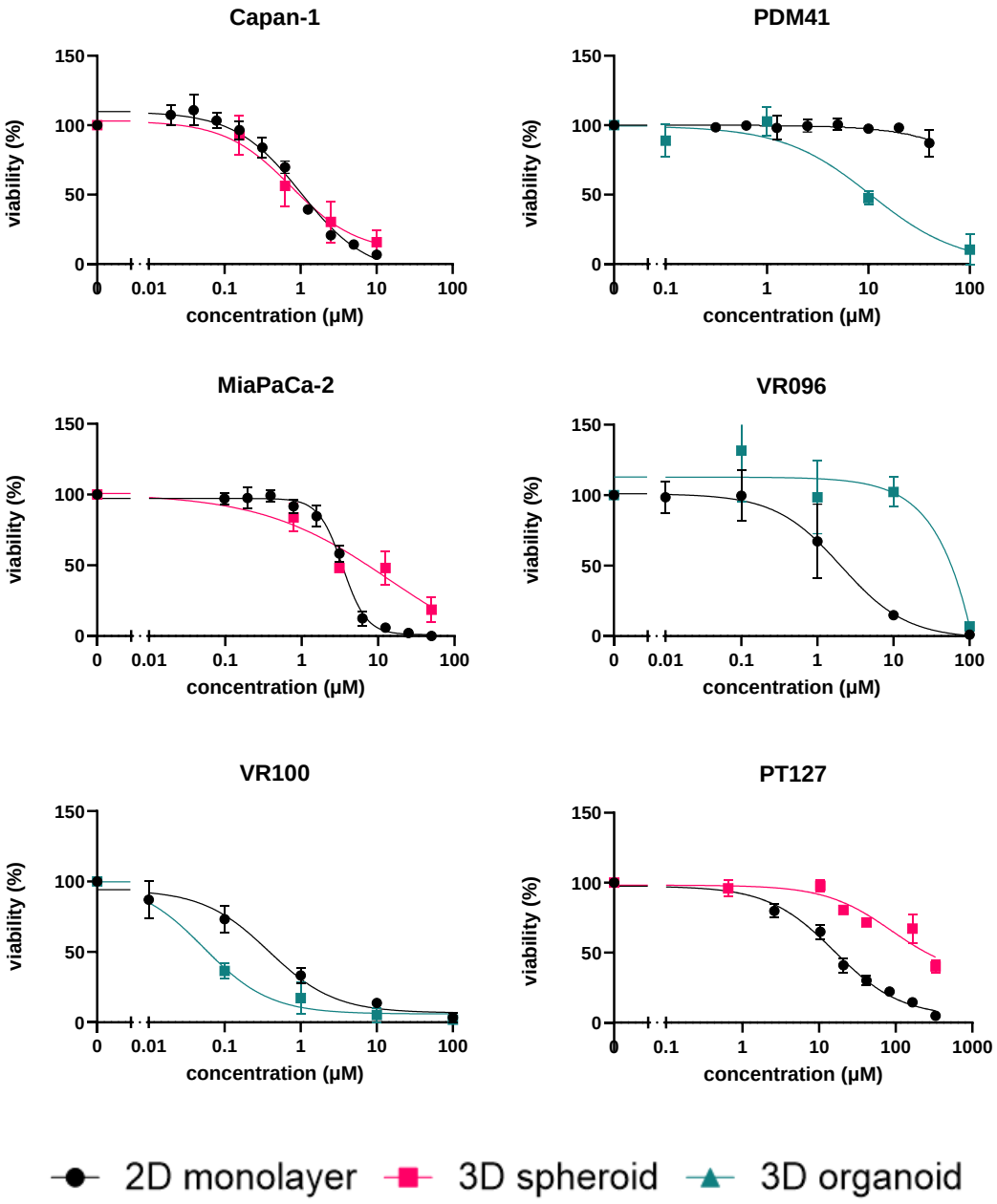

Figure 3.3. Effect of cell culture conditions on sensitivity to cisplatin. *Cells cultured in 2D (black circle), 3D spheroids (magenta square), or 3D organoids (turquoise square) and treated with cisplatin for 7 days. Viability was measured by PrestoBlue (2D) or CellTiter Glo (3D) and was normalised against untreated control. Error bars represent the standard deviation (n=3).*

3.2.3 Sensitivity to olaparib

Monolayer culture of Capan-1 had an IC_{50} of 23.2 μM, but the spheroid culture model was considerably less sensitive to treatment as the IC_{50} value was not reached at the maximum treatment concentration of 40 μM, which is at least a 2.04-fold increase in IC_{50} (Fig. 3.4 and Table 3.2). At this concentration the monolayer model had a viability of 47.2% compared

to 61.8% in the spheroid model (p=0.23). For MiaPaCa-2, the 2D model was more sensitive to olaparib at every concentration, but the difference in sensitivity increased at higher concentrations where the viability of the spheroids seemed to reach a plateau. At the highest treatment concentration of 40 µM, viability of the spheroids was 69.1% compared to 29.4% in the monolayer model (2.35 FC, p=0.02). This effect was even stronger in the PT127 models as an IC_{50} could not be reached highlighting the resistance to olaparib. At the highest tested concentration of 40 µM, the 3D spheroids had a 119.3% viability compared to 64% in the 2D monolayer, which is a 1.86 FC (p=0.003).

In contrast, the PDM41 organoid-derived cell line grown as 2D monolayer culture was remarkably resistant, with an 82.9% viability compared to 39.1% in the 3D organoid model (-2.12 FC, p=0.003).

For the remaining two organoid lines there is no significant difference in IC_{50}. For VR096, the monolayer model has an IC_{50} of 19.51 µM compared to 11.39 µM in the organoid model (-1.71 FC, p=0.64). For VR100, the monolayer model has an IC_{50} of 1.16 µM compared to 0.73 in the organoid model (-1.59 FC, p=0.32).

Table 3.2. IC_{50} values of 2D and 3D in vitro models treated with olaparib. *The IC_{50} values are interpolated from the graph in figure 3.2. Values in brackets are the standard deviation. FC: fold change in IC_{50} value of 3D models compared to 2D models.*

		HR-deficient			**HR-proficient**		
		Capan-1	**MiaPaCa-2**	**VR100**	**PT127**	**PDM41**	**VR096**
olaparib	**2D**	19.64 (15.31)	17.5 (10.5)	1.16 (1.62)	>40	>40	19.51 (1.00)
	3D	>40	>40	0.73 (1.05)	>40	26.51 (14.02)	11.39 (11.10)
	FC	>2.04	>2.28	-1.59	N/A	<-1.51	-1.71

Looking at the effect HR status has on sensitivity to olaparib treatment, no clear separation in sensitivity can be distinguished between the HR-deficient and HR-proficient cell lines, except for VR100 (Table 3.2). VR100 is over 18-fold more sensitive to olaparib than any of the other models. Although Capan-1 and MiaPaCa-2 show an at least 2-fold lower sensitivity compared to PT127 and PDM41 when grown as monolayer, the sensitivity is similar to VR096 and similar or higher when grown in 3D.

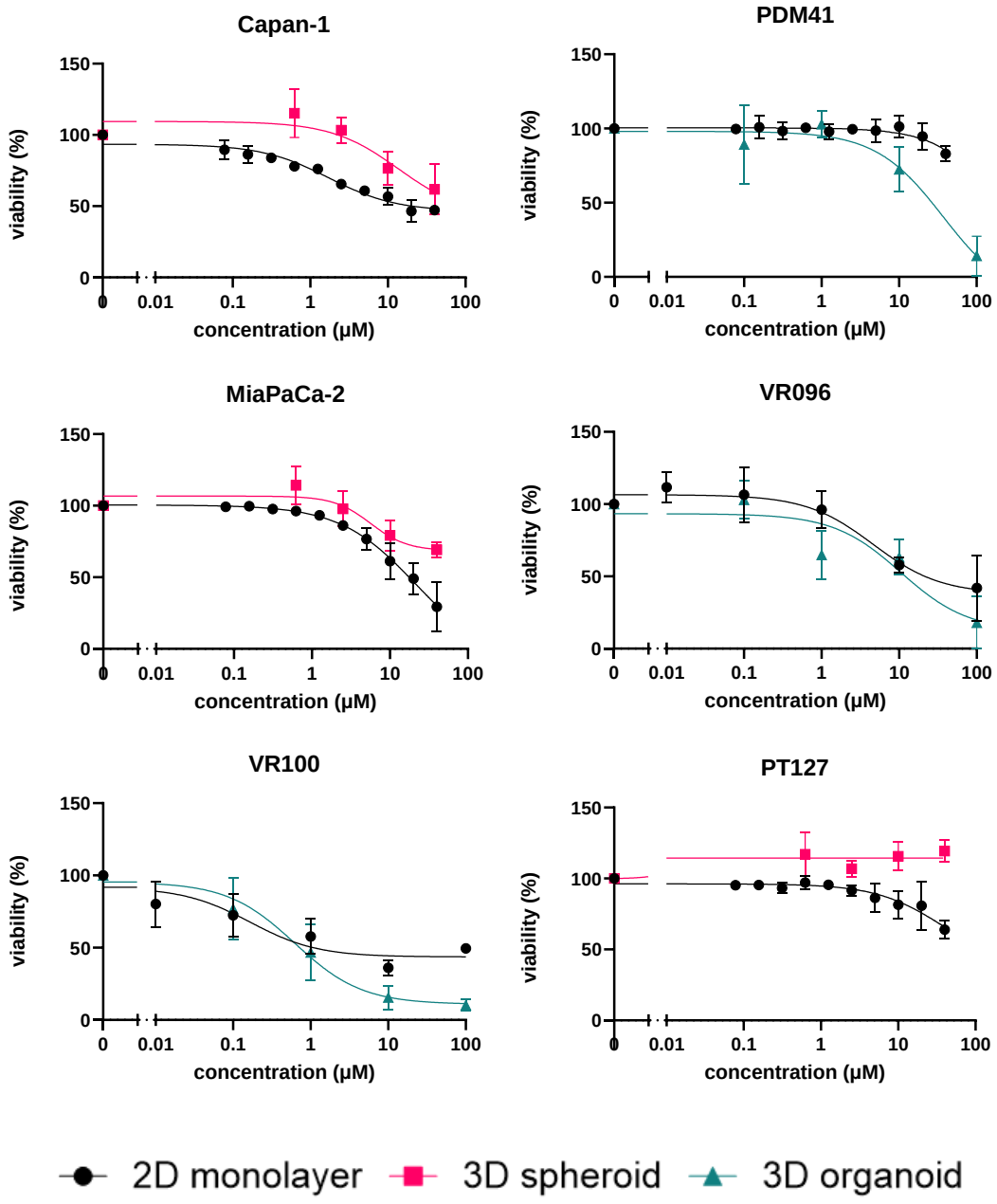

Figure 3.4. Effect of cell culture conditions on sensitivity to olaparib*. Cells cultured in 2D (black circle), 3D spheroids (magenta square), or 3D organoids (turquoise square) and treated with olaparib for 7 days. Viability was measured by PrestoBlue (2D) or CellTiter Glo (3D) and was normalised against untreated control. Error bars represent the standard deviation (n=3).*

3.2.4 Sensitivity to talazoparib

For Capan-1 there is no significant difference in response to talazoparib between 2D monolayer and the 3D spheroid culture models (p=0.66) (Fig. 3.5 and Table 3.3). MiaPaCa-2, in contrast, is considerably less sensitive in the spheroid model, with an IC_{50} of 0.25 μM in the monolayer model and 1.75 μM in the spheroid model which is a 7-fold change in IC_{50}

(p=0.0035). In the primary cell line model PT127, the 3D spheroid model does not respond to treatment at all. At the highest tested concentration of 2.5 µM the 2D monolayer model has a 44.5% viability compared to 113.2% in the spheroid model (p<0.001). The opposite effect is seen for PDM41, where the 2D monolayer is not sensitive to treatment. Viability is very variable between replicates but fluctuates around 80% for all tested talazoparib concentrations.

In the primary organoid lines VR100 and VR096 the culture methods have a similar effect in which the organoid models are significantly less sensitive at lower concentrations but have a steeper curve at higher concentrations, resulting in a significantly different IC_{50} but a similar IC_{70}. As such, VR096 has 16.25-fold increase in IC_{50} compared to the 2D model (p=0.022), but the graphs cross each other at 19 µM with a viability of 20%. Likewise, VR100 has a 59.6-fold increase in IC_{50} compared to the 2D model (4.17 nM vs 0.07 nM, p=0.044), the graphs cross each other at 7 nM with a viability of 35%.

Table 3.3. IC_{50} values of 2D and 3D in vitro models treated with olaparib. *The IC_{50} values are interpolated from the graph in figure 3.3. Concentrations are given in µM. Values in brackets are the standard deviation. FC: fold change in IC_{50} value of 3D models compared to 2D models.*

		HR-deficient			HR-proficient		
		Capan-1	**MiaPaCa-2**	**VR100**	**PT127**	**PDM41**	**VR096**
talazoparib	**2D**	0.25 (0.65)	0.25 (0.06)	0.00007 (0.016)	1.52 (1.25)	>2.5	0.12 (0.095)
	3D	0.25 (0.08)	1.75 (0.69)	0.00417 (3.48)	>2.5	0.84 (1.48)	1.95 (1.42)
	FC	1.00	7.00	59.57	>1.64	<-2.98	16.25

When looking at the effect HR status has on response to talazoparib no clear separation can be seen in IC_{50} values between HR-deficient and HR-proficient cell models, except for VR100 (Table 3.3). VR100 shows exceptional sensitivity with an IC_{50} of 0.07 nM in 2D and 4.17 nM in 3D, which is, respectively, at least 1714-fold and 60-fold lower than any of the other models.

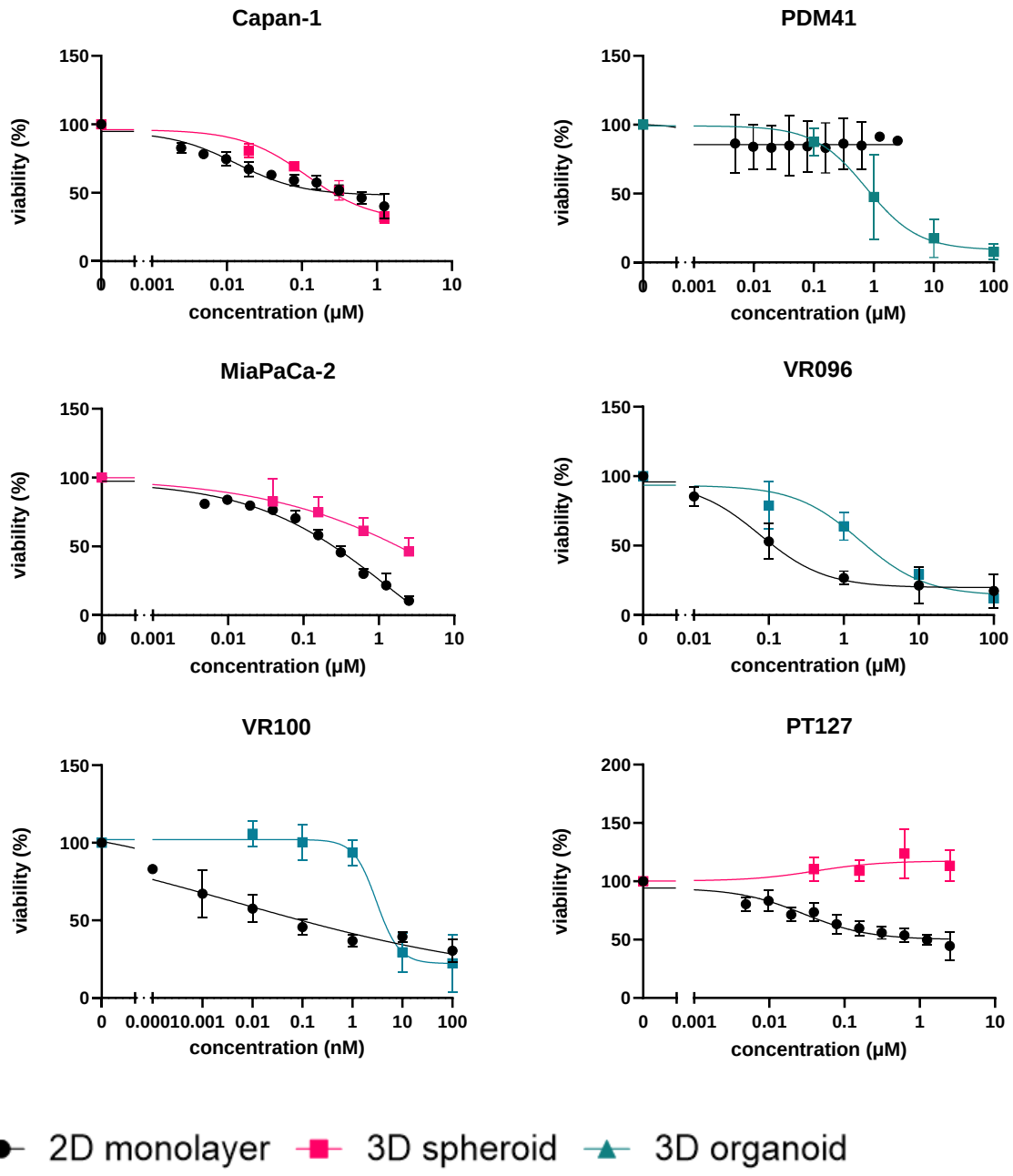

Figure 3.5. Effect of cell culture conditions on sensitivity to talazoparib. *Cells cultured in 2D (black circle), 3D spheroids (magenta square), or 3D organoids (turquoise square) and treated with talazoparib for 7 days. Viability was measured by PrestoBlue (2D) or CellTiter Glo (3D) and was normalised against untreated control. Error bars represent the standard deviation (n=3).*

3.3 Development of Patient-Derived Organoids (PDOs)

Over the course of 18 months, blood and tissue samples were collected from 14 patients undergoing Whipple surgery at St. Vincent's University Hospital (Table 3.4). Histopathological examination after resection identified a wide variety of periampullary tumours. For four patients a complete set of tumour, normal tissue, and blood was collected. In total, four PDO lines were successfully established (LCT01, LCT06, LCT10, LCT11).

Table 3.4. Clinical characteristics of patient samples used to establish patient-derived organoids. *Adjacent normal and tumour tissue were both collected when possible, but organoids were solely established from tumour tissue.*

ID	type	blood	sex	age	diagnosis	organoid culture
LC01	normal & tumour	Y	M	83	distal cholangiocarcinoma	successful
LC02	normal	Y	F	69	low grade biliary intraepithelial neoplasia	
LC03	normal & tumour	Y	F	67	extrahepatic cholangiocarcinoma	unsuccessful
LC04	normal & tumour	N	M	69	extrahepatic cholangiocarcinoma	unsuccessful
LC05	normal	Y	M	72	low grade pancreatic intraepithelial neoplasia	
LC06	normal & tumour	Y	M	82	intra-ampullary papillary-tubal neoplasm of duodenal origin	successful
LC07	normal & tumour	N	F	55	intraductal papillary neoplasm	unsuccessful
LC08	normal	N	M	72	intestinal adenocarcinoma	
LC09	normal	N	F	54	mucinous cystic neoplasm	
LC10	normal & tumour	N	M	75	duodenal adenocarcinoma, intestinal type	successful
LC11	normal & tumour	N	M	74	duodenal adenocarcinoma, intestinal type	successful
LC12	normal & tumour	Y	M	74.5	cystic carcinoma	unsuccessful
LC13	normal & tumour	N	F	80	extrahepatic cholangiocarcinoma	unsuccessful
LC14	normal & tumour	N	M	70	pancreatic adenocarcinoma	unsuccessful

LCT01 was established from a stage IV distal cholangio adenocarcinoma (pT3N2M1) found in an 82-year-old male patient. The main tumour was removed during the surgery and the patient received adjuvant chemotherapy, but passed away within 5 months. The established organoid line LCT01 formed a mixture of hollow and compact organoids (Fig. 3.6). Immunocyto and immunohistochemistry-mediated fluorescent profiling was performed for the organoids (Chapter 2.10). The organoids are positive for cancer stem cell markers ALDH1A1, CXCR4, and HCAM. Glandular epithelial marker Muc1 is expressed throughout the organoid. The organoids also express pancreatic lineage marker PDX1 and proliferation marker Ki67 (Fig. 3.6).

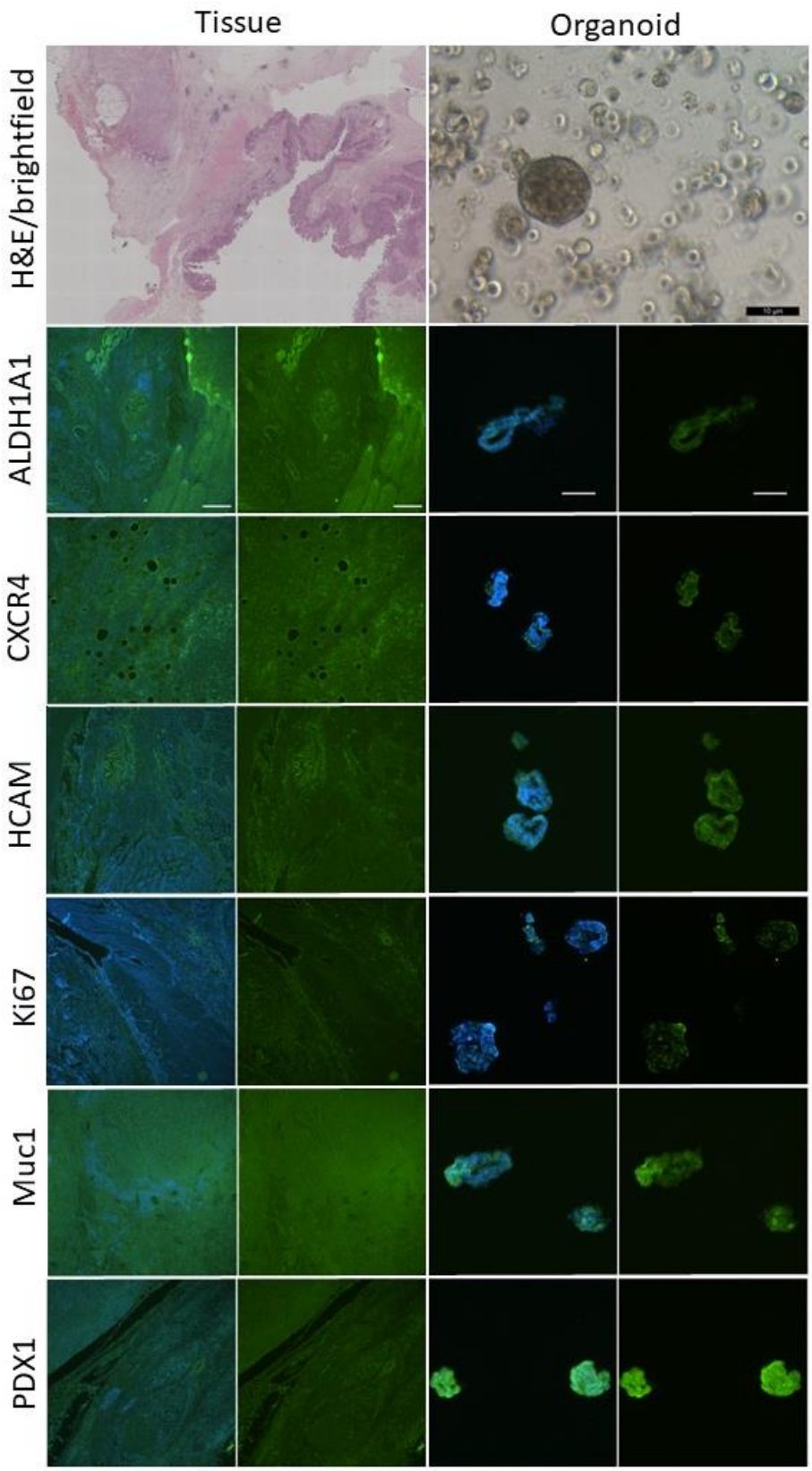

Figure 3.6. Immunocyto and immunohistochemistry-mediated characterisation of LCT01 tumour tissue and organoids. *Cells were stained for CSC markers (ALDH1A1, CXCR4, HCAM), proliferation (Ki67), epithelial differentiation (Muc1), and pancreatic differentiation (PDX1). Left panel: overlay DAPI and antibody. Right panel: antibody. Scale bar brightfield 10 µm, fluorescence tissue 500 µm, fluorescence organoids 100 µm.*

LCT06 was established from an Intra-ampullary Papillary-Tubular Neoplasm (IAPN) of duodenal origin found in a 78-year-old male patient. The tumour formed a 1.5 cm large ampullary adenoma without high grade dysplasia and was removed during the Whipple surgery, but the patient passed away within a month due to medical comorbidities. The established organoid line LCT06 formed mainly large hollow organoids (Fig. 3.7). Due to issues with revival of frozen stocks for preparation of immunofluorescent slides (most likely due to incorrect storage), immunofluorescent characterisation was not acquired.

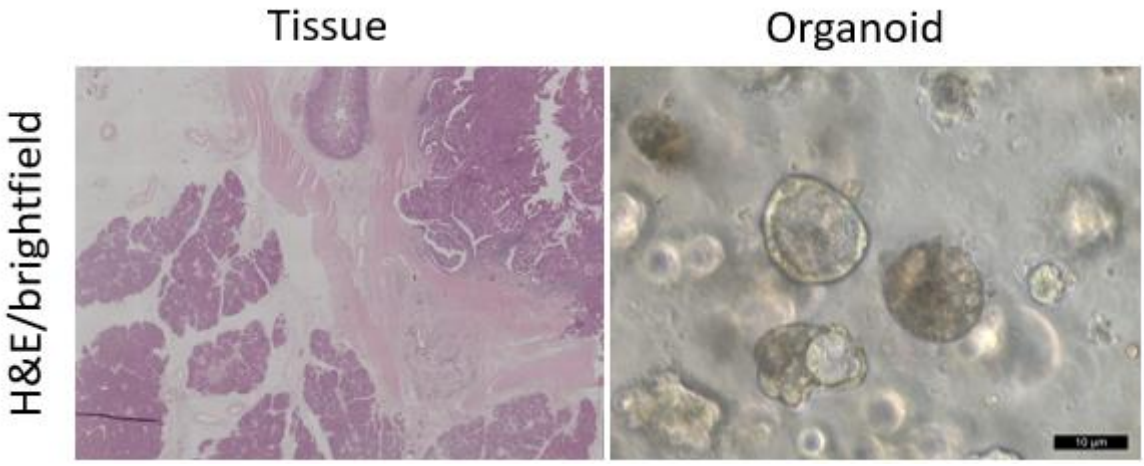

Figure 3.7. Morphology of LCT06 tissue and organoid. *Left: H&E staining of tissue. Right: brightfield imaging of organoid. Scale bar: 10 µm.*

LCT10 was established from a duodenal adenocarcinoma (pT2N1M0) with intestinal type lineage found in a 75-year-old male patient. The tumour was removed during surgery and the patient received adjuvant FOLFOX chemotherapy for 6 months. At 18 months after diagnosis the patient was disease-free. Additional genetic profiling found that the tumour was micro-satellite stable. The established organoid line formed large hollow organoids (Fig. 3.8). Immunocyto and immunohistochemistry-mediated fluorescent profiling was performed for the organoids (Chapter 2.10). The organoids are positive for CSC markers ALDH1A1 and HCAM, although expression of ALDH1A1 is lower than in the other organoids. LCT10 organoids are also positive for Ki67, Muc1, and PDX1.

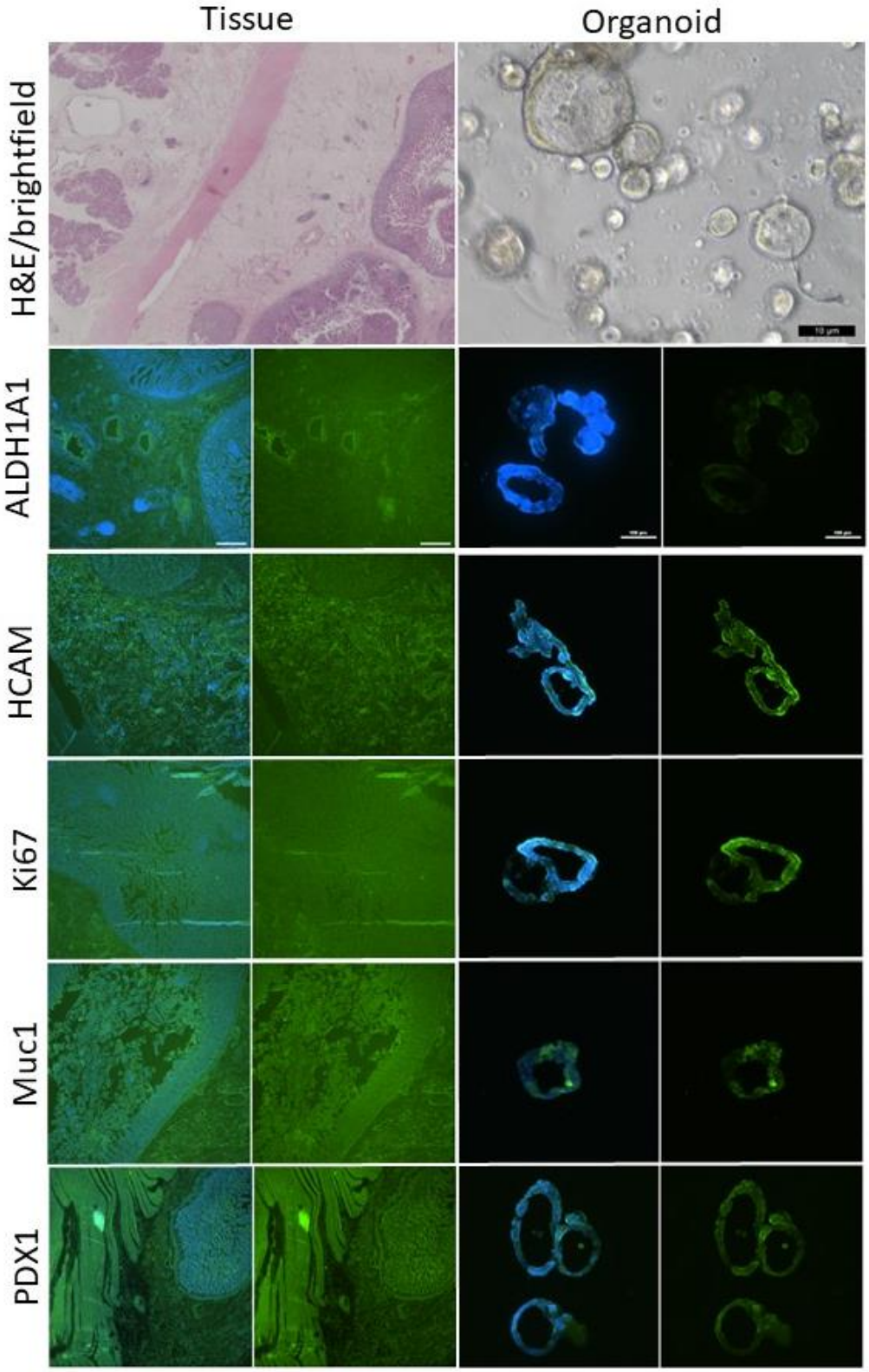

Figure 3.8. Immunocyto and immunohistochemistry-mediated characterisation of LCT10 tumour tissue and organoids. *Cells were stained for CSC markers (ALDH1A1, HCAM), proliferation (Ki67), epithelial differentiation (Muc1), and pancreatic differentiation (PDX1). Left panel: overlay DAPI and antibody. Right panel: antibody. Scale bar: brightfield 10 µm, fluorescence tissue 500 µm, fluorescence organoids 100 µm.*

LCT11 was established from a low-grade duodenal adenocarcinoma (pT1bN0M0) with intestinal type lineage, found in a 64-year-old female patient with a family history of colorectal cancer. The tumour was removed during surgery and no adjuvant therapy was given. At 18 months after diagnosis the patient was disease-free. Additional genetic profiling found that the tumour was micro-satellite stable. The established organoid line forms a mixture of hollow and compact organoids (Fig. 3.9). Immunocyto and immunohistochemistry-mediated fluorescent profiling was performed for the organoids (Chapter 2.10). The LCT11 organoids are positive for all six investigated markers.

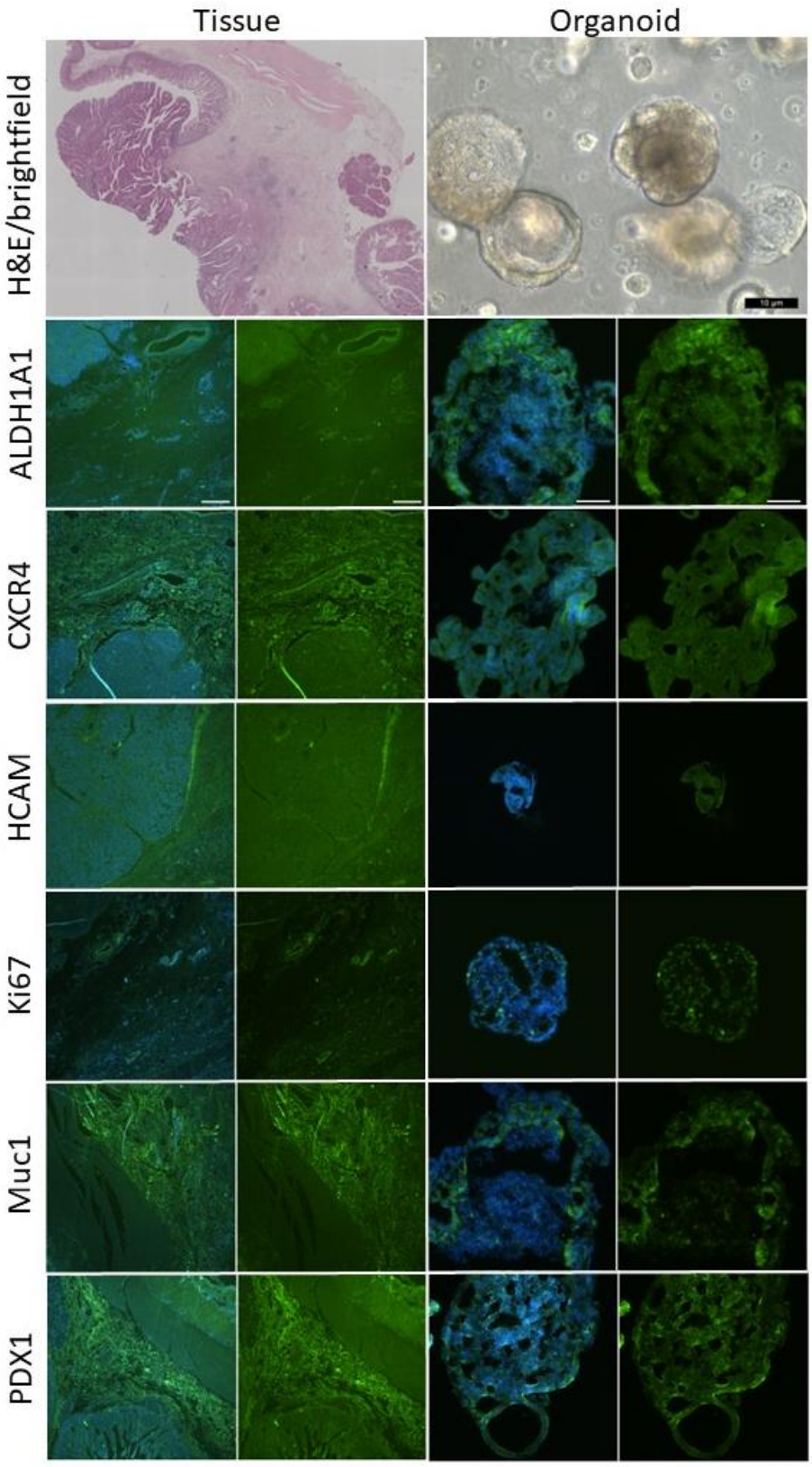

Figure 3.9. Immunocyto and immunohistochemistry-mediated characterisation of LCT11 tumour tissue and organoids*. Cells were stained for CSC markers (ALDH1A1, CXCR4, HCAM), proliferation (Ki67), epithelial differentiation (Muc1), and pancreatic differentiation (PDX1). Left panel: overlay DAPI and antibody. Right panel: antibody. Scale bar brightfield 10 µm, fluorescence tissue 500 µm, fluorescence organoids 100 µm.*

3.4 SENSITIVITY TO DRUG TREATMENT OF PRIMARY PDOS

To assess the sensitivity of these newly established primary PDOs to PARPi (olaparib, talazoparib) and chemotherapy (cisplatin, FOLFIRINOX, gemcitabine, nab-paclitaxel) treatment toxicity assays (Chapter 2.4.2) were performed on LCT01, LCT10, and LCT11 (Fig. 3.10 and Table 3.5). LCT10 is considerably more sensitive to PARPi compared to LCT01 and LCT11. For olaparib, LCT10 has an IC_{50} of 1.66 µM versus 65.08 and 43.51 µM for LCT01 and LCT11, respectively. For talazoparib, the IC_{50} was not reached for LCT01 and LCT11, but at a concentration of 3.13 µM LCT10 had a viability of 22% versus 87% and 77% for LCT01 and LCT11, respectively.

LCT10 also showed the greatest sensitivity to chemotherapeutic agents. For cisplatin, LCT10 and LCT11 had a similar IC_{50} value of 4.71 µM and 4.90 µM, respectively, while LCT01 was slightly less sensitive with an IC_{50} value of 19.41 µM. IC_{50} values for gemcitabine were 2.34, 2.71, and 4.54 ng/mL for LCT10, LCT11, and LCT01, respectively. LCT01 and LCT11 also showed a considerably lower sensitivity to nab-paclitaxel with a viability of 73.6% and 76.2% at a maximum concentration of 1000 ng/ml compared to 13.2% for LCT10. In contrast, LCT11 was least sensitive to FOLFORINOX treatment with an IC_{50} of 1.69% of the maximum concentration compared to 0.19% for LCT01 and 0.15% for LCT10. However, since these concentrations are well below the maximum plasma concentration (which is approximately 10x of the maximum treatment concentration) all three organoids are still very sensitive to the treatment.

Table 3.5. IC_{50} concentrations of primary PDOs treated with PARPi or chemotherapy.

	LCT01	**LCT10**	**LCT11**
Olaparib (µM)	65.08 (2.84)	1.66 (1.92)	43.51 (15.98)
Talazoparib (µM)	>6.25	0.45 (0.25)	>12.50
Cisplatin (µM)	19.41 (14.09)	4.71 (0.50)	4.90 (3.72)
FOLFIRINOX (%)	0.19 (0.12)	0.15 (0.07)	1.69 (0.86)
Gemcitabine (ng/mL)	4.54 (1.48)	2.34 (3.02)	2.71 (1.95)
nab-paclitaxel (ng/mL)	>1000	433.61 (259.89)	>1000

IC_{50} values (with SD) were interpolated from the graphs in figure 3.10, with the curves plotted as non-linear fit.

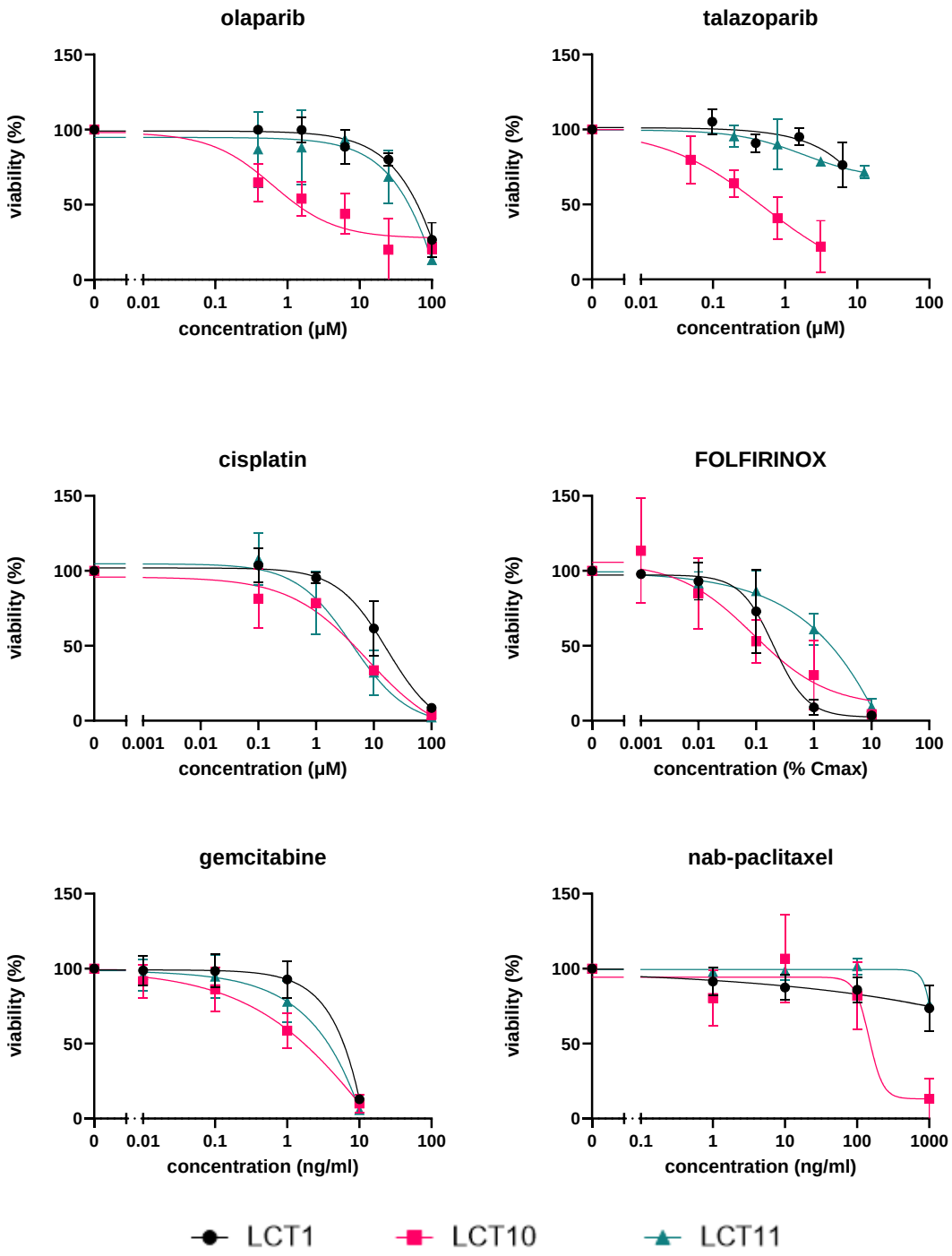

Figure 3.10. Percentage viability of primary PDOs after drug treatment for 7 days. *Organoids were seeded as single cells three days in advance of treatment to allow for the formation of organoids before treating. Viability was measured after 7 days of treatment using CellTiter Glo and normalised against untreated control. Error bars represent the standard deviation (n=3). *FOLFIRINOX is a combination treatment consisting of folinic acid, 5-fluorouracil, irinotecan (active compound is SN-38), and oxaliplatin. For easier interpretation, the maximum concentration is set at 100%. This equals to 0.428 μM folinic acid, 34.4 μM 5-fluorouracil, 0.4 μM SN-38, and 0.32 μM oxaliplatin.*

3.5 DISCUSSION

3.5.1 2D versus 3D cell culture models

Cell lines have long been the primary *in vitro* model for the study of cancer and contributed hugely to our understanding and treatment of cancer (Masters, 2002). Established cell lines are easy and cheap to use, can grow indefinitely, and are homogenous enough to produce highly replicable results. However, the simplicity and homogeneity of this model is both its main advantage and disadvantage as it fails to mimic many of the *in vivo* characteristics of a tumour that are inherent to its 3D structure and interaction with the microenvironment. Recently, efforts have been made to develop novel 3D models such as spheroids and organoids that better reflect the *in vivo* situation.

Characterisation of PDAC organoids developed from mouse and human tumour tissue has shown that they reflect many characteristics of the primary tumour. PDOs recapitulate tumour morphology and histopathological subtypes, mutation status, and RNA expression profiles (Boj et al., 2015; Hirt et al., 2022; Krieger et al., 2021). Additionally, cytotoxicity studies have shown that drug sensitivity of organoids correlates with therapeutic response in patients (Demyan et al., 2022; Driehuis et al., 2019; Grossman et al., 2022).

Comparison of 2D monolayer and 3D spheroid culture in three established breast cancer cell lines has shown that monolayer culture is more sensitive to paclitaxel and doxorubicin than spheroid culture and related this to spheroid density and expression of proliferation marker Ki67 (Imamura et al., 2015). Similarly, a screen of 12 drugs in a panel of four established PDAC cell lines (AsPC1, BxPc3, Capan-1, and Panc-1) and the mouse KPC cell line grown as monolayer and spheroid found that the spheroids were consistently more resistant to treatment (Longati et al., 2013). Zeeberg et al. compared three 3D spheroid culture methods (ultralow adhesion, Matrigel inclusion/hanging drop, organotypic on top of Matrigel) to 2D monolayer culture and murine orthotopic transplants for four established PDAC cell lines (Panc-1, BxPc3, MiaPaCa-2, Capan-2) and saw that cell morphology was affected with the organotypic model being most representative of the orthotopic mice model (Zeeberg et al., 2016). They observed considerable differences in sensitivity to erlotinib with the organotypic model having a ~9-fold higher IC_{50} value compared to the monolayer model. These studies suggest that 3D culture is a more realistic *in vitro* model that has increased chemoresistance compared to monolayer culture which

may contribute to the high attrition rates of drugs that have traditionally been developed in monolayer culture (Hutchinson & Kirk, 2011). However, these studies are all based on a small set of established cell lines, some of which have been established nearly 50 years ago, and do not reflect the heterogeneity that is found in primary cell lines. Additionally, none of these studies include a comparison with organoids which have a considerably different morphology compared to spheroids and may therefore react differently to treatment.

3.5.2 Morphology of 2D and 3D *in vitro* models

To investigate the effect of cell culture method on sensitivity to platinum agent cisplatin and PARPi olaparib and talazoparib, toxicity assays were performed on cells grown as 2D monolayer, 3D spheroid, or 3D organoid. The established cell lines Capan-1 and MiaPaCa-2 and primary cell line PT127 were grown as 2D monolayer and 3D spheroid; the patient derived organoid lines PDM41, VR096 and VR100 were grown as 2D monolayer and 3D organoid. VR096 and VR100 were kindly gifted by PRECODE partner Prof. Corbo, Italy.

Capan-1 is a well-differentiated cell line of epithelial origin that formed dense budding spheroids with a diameter of approximately 200 µm. Previous studies that cultivated Capan-1 as spheroid using ultra-low attachment plates with or without the addition of adhesion-promoting matrix methylcellulose found that Capan-1 forms loose aggregates rather than the true spheroids that we observed (Feng et al., 2017; Longati et al., 2013).

MiaPaCa-2 is also of epithelial origin but has a polymorphic morphology that includes spindle-like cells. Under the used culture conditions, it formed very dense and smooth spheroids with a diameter of approximately 200 µm. This in contrast to previous studies that were either unable to establish spheroids (Longati et al., 2013), or found that MiaPaCa-2 formed very loose spheroids (Kaur et al., 2021; Minami et al., 2021; Shichi et al., 2022).

PT127 is a primary PDAC cell line derived from a PDX-model with an epithelial morphology (Nelson et al., 2020) that formed clusters of small spheroids with a diameter of less than 50 µm. PDM41 is a patient-derived PDAC organoid line that forms large hollow organoids and forms elongated cells when grown as monolayer as previously reported (Noorani et al., 2022). VR096 is a primary PDAC organoid line that forms hollow organoids and has an epithelial morphology when grown as monolayer. VR100 is another primary PDAC organoid line that forms more dense organoids and also has an epithelial morphology when grown as monolayer.

3.5.3 Effect of culture method on drug sensitivity

In contrast to previous publications, 3D culture did not always reduce sensitivity to treatment in the models tested in this chapter. As expected, the established cell line MiaPaCa-2 had a consistently higher IC_{50} when grown in 3D, as did the primary cell line PT127 (IC_{50} could not be determined for olaparib, but since there was no response to treatment at the highest concentration in the spheroid compared to 64% viability in the monolayer culture it is safe to assume that the IC_{50} is higher in the spheroid). In contrast, PDM41 was consistently less sensitive when grown in 2D. While the effect of cell culture method on proliferation rate was not examined, we did notice that PDM41 was very slow growing as cell line which may have contributed to the lack of sensitivity. For the remaining models no correlation was observed between culture method and drug sensitivity.

These findings highlight the importance of not only using multiple cell models to account for tumour heterogeneity when performing drug screening, but also using multiple cell culture methods.

3.5.4 Effect of method on drug sensitivity in relation to HR status

Apart from the cell culture method, one of the cell characteristics that is known to affect drug sensitivity is the DDR or HR status of the model. DDR deficiency, and especially HR deficiency, sensitises to platinum agents and PARPi.

Some of the characteristics that are affected by the cell culture method may also affect HR proficiency. For example, oxygen gradients which are observed in spheroids may contribute to hypoxia which has been linked to the alteration of DDR gene expression and genome instability (Debruyne et al., 2023; Glicklis et al., 2004; Kaplan & Glazer, 2020; Tang et al., 2021). Alternatively, organoid media is supplemented with factors that stimulate stem cells which are necessary for the development of the organoids and cancer stem cells in turn have been linked to increased DDR (Choi et al., 2021; Noorani et al., 2022; Schulz et al., 2019).

HR proficient and deficient models were included in the comparison of the cell culture methods to investigate if culture methods have a different effect dependent on HR status. Since the number of HRD models that were available was too low to perform any statistical analysis, these comparisons are explorative.

Three HR proficient and three HR deficient cell models were used in this study. Capan-1 is HRD due to loss of one *BRCA2* allele and a frameshift mutation leading an early stop codon in the remaining allele. VR100 also has a mutation in *BRCA2*: an in-frame insertion that results in the addition of two amino acids. MiaPaCa-2 has a missense mutation in *PALB2* that is located in the *BRCA2*-binding domain. Of these three models, only Capan-1 has complete loss of gene function and would therefore be expected to have the strongest HRD and be most sensitive to drug treatment. However, for each of the three tested drugs VR100 was considerably more sensitive, especially to the PARPi. Interestingly, no clear distinction could be made between the HR deficient and proficient models in terms of treatment sensitivity. This was especially unexpected for Capan-1 with its complete loss of *BRCA2* function which suggests that this cell line may have some level of intrinsic resistance to the used drugs.

3.5.5 Development of PDOs

Development of successful novel treatments is crucial to improve PDAC survival and very little progress has been made in the last decade. Well over 90% of novel drugs fail in the first clinical or preclinical trials highlighting the need for improved preclinical models (Dowden & Munro, 2019; Wong et al., 2019). One of the few novel drugs that have been approved in a clinical setting is olaparib but while it has been shown to improve PFS and the application of PARPi in PDAC is promising there is still a lot to be gained in the prevention and overcoming of resistance. However, there are very few HRD *in vitro* models available to study PARPi which compromises effective research. To our knowledge, the only commercially available 2D cell line with *BRCA* deficiency is Capan-1. The Human Cancer Model Initiative (HCMI) offers four PDAC organoids with *BRCA* mutations, but none with complete loss like Capan-1.

As was shown above, cell culture method does affect drug sensitivity, but due to a lack of patient data (and since a single patient would not have received all three drugs) it remains unclear how this correlates to the patient treatment response. It is therefore crucial to develop and characterise novel PDAC models. In this chapter, patient-derived organoids were developed from tissue samples that were obtained during surgical removal of periampullary tumours. Periampullary cancer is a collective name for cancers that arise within 2 cm of the papilla of Vater (also known as the major duodenal papilla) (Chandrasegaram et al., 2017; Kamarajah, 2018; Sarmiento et al., 2001; Washington et al.,

2021). The papilla of Vater is the point where the pancreatic duct and the distal bile duct, merged as the ampulla of Vater or hepatopancreatic ampulla, join the duodenum. Periampullary cancers can be of ampullary, biliary, pancreatic, or duodenal origin, although sometimes a distinction is made between periampullary and ampullary cancers due to their slightly different location. Additionally, a distinction can be made between intestinal or pancreatobiliary type of differentiation. Although these cancers have different characteristics and prognoses, the similar morphology and complex topography can make it hard to distinguish specific cancers. Treatment consists of surgical resection by Whipple procedure when possible and chemotherapy.

Patient-derived organoids were successfully developed from distal bile duct carcinoma (cholangiocarcinoma, LCT01), intra-ampullary papillary-tubular neoplasm (LCT06), and intestinal adenocarcinoma (LCT10 and LCT11).

3.5.5.1 Cholangiocarcinoma PDO

Cholangiocarcinoma, also known as bile duct carcinoma, is a rare form of cancer with an incidence of 0.3-6 cases per 100,000 yearly and accounts for approximately 3% of gastrointestinal malignancies (Banales et al., 2020). Cholangiocarcinoma can be divided into intrahepatic (iCCA) and extrahepatic (eCCA) disease with a subclassification of phildar CCA (pCCA) and distal CCA (dCCA) (Chun et al., 2017). Approximately 20-30% of the eCCA tumours are distal and located in the pancreas where they account for approximately 13% of the periampullary cancers (Jong et al., 2022). Disease outcome is poor, with a 5-year overall survival of 24% in localised disease and 2% in distant metastases (Surveillance Research Program, 2024). Standard of care for resectable tumours is surgery, followed by adjuvant chemotherapy with capecitabine, and for non-resectable tumours generally combination therapy of gemcitabine with cisplatin (Cho et al., 2022; Valle et al., 2010; Zhang et al., 2022). Additionally, tumours with high microsatellite instability or MMR deficiency may be treated with pembrolizumab. HRD due to *BRCA* mutation occurs in 3.4% of the patients (Esmail et al., 2024).

Histologically, dCCA is similar to PDAC in that both are adenocarcinomas that consist of infiltrating glands with varying levels of differentiation (reviewed in (Gkountakos et al., 2023)). Both cancers are characterised by atypical tumour cells with enlarged nuclei and similar expression of immunohistochemistry markers such as cytokeratin (CK) 8, 18, 19, 20

and Muc1. Due to these similarities, differential diagnosis is predominantly based on the location of the tumour; dCCA is located around the common bile duct whereas PDAC is more centred on the parenchyma.

The number of available preclinical CCA models is limited and the majority of preclinical research has been performed in just two cell lines. Recently, several groups have attempted to establish CCA PDOs to expand and improve the number of available models. Maier et al. attempted to establish PDOs from 29 tissue samples (Maier et al., 2021). While they were able to cultivate all samples for several days, only 7 organoids could be cultivated for more than two months. Of the three dCCA samples none survived for more than two weeks. The two non-distal CCA organoids that could be cultivated more than 36 weeks were characterised. Both organoids formed hollow cysts that clustered together like a grape and expressed several cancer markers including Muc1. Kinoshita et al. were able to establish 60 PDOs from samples which included 30 dCCAs (Kinoshita et al., 2023). Although the majority of the organoids had a large, hollow cystic morphology, solid, grape-like, and multilayer cystic organoids were also seen.

The dCCA organoid that was established in this chapter (LCT01) formed a mixture of hollow and compact organoids that expressed CSC markers ALDH1A1, CXCR4, and HCAM. The organoids were also positive for pancreatic lineage marker PDX1 which is also frequently expressed in CCA and whose expression is associated with increased proliferation (Igarashi et al., 2012). In concordance with this, the organoids were also positive for proliferation marker Ki67. LCT01 was not sensitive to PARPi (olaparib or talazoparib), cisplatin, or nab-paclitaxel, but did respond to FOLFIRINOX and gemcitabine. Toxicity assays have been reported for gemcitabine and cisplatin in two CCA organoid lines established by Maier et al. (Maier et al., 2021). They reported a similar response to gemcitabine with IC_{50} of approximately 5 nM (1.3 ng/mL) and 10 nM (2.6 ng/mL) which is comparable to the IC_{50} of 4.5 ng/mL observed in LCT01. In contrast, their organoids did not respond to cisplatin at all with complete viability at 100 µM compared to an IC_{50} of 19.4 µM in LCT01.

3.5.5.2 Intra-ampullary papillary-tubular neoplasm PDO

Intra-ampullary papillary-tubular neoplasm (IAPN) is a precursor lesion of intra-ampullary adenocarcinoma that arises from the ampulla of Vater (Ohike et al., 2010). IAPN is a rare form of neoplasm with a yearly incidence of 0.025 per 100,000 inhabitants in the US and

accounts for approximately 0.5% of all gastrointestinal tumours (Ren et al., 2019). The majority of the patients are diagnosed with grade I (31%) or grade II (33%) disease. With a 33.1% five-year overall survival, the prognosis is considerably better than for PDAC.

The lesions are characterised by outward growth protruding from the epithelium within dilated intra-ampullary ducts which can cause obstruction of the ducts (Ohike et al., 2010). Microscopically, the lesions are well-characterised with a tubular or papillary morphology and do not invade the surrounding tissue. IAPNs can have a pancreatic-biliary (44.4%) or intestinal cell lineage morphology (55.6%) (Tarcan et al., 2024). Intestinal-type cases have a morphology that is comparable to conventional intestinal tubular adenomas with villous or tubular glandular units that are lines by columnar cells (Ohike et al., 2010). Pancreatic-biliary cases have a papillary or tubulopapillary morphology. Expression of Muc1 is seen in approximately 90% of pancreatic-biliary and 20% of intestinal cases.

Due to the rarity of this lesion, research is severely limited and mostly pertains to case reports and population-based statistics. There have been a few preclinical ampullary adenocarcinomas published in literature (Frazier et al., 1992; Lai et al., 2016), but to our knowledge, LCT06 is the first preclinical IAPN model. The model formed large hollow organoids that could be passaged and cultivated over multiple months. This makes it possible to use this model for preclinical characterisation and drug screening. The development of preclinical models from normal or precursor lesions has always been more difficult than for tumour samples due to their lack of uncontrolled proliferation. That makes this model extra valuable as it can be used to model tumorigenesis and disease progression.

3.5.5.3 Periampullary duodenal adenocarcinoma PDOs

Periampullary duodenal adenocarcinoma accounts for approximately 7% of all periampullary cancers (Jong et al., 2022). Approximately half of the patients are diagnosed with stage III or IV disease and the three-year survival rates are 34%. Tumours generally have a moderate differentiation and form plaque-like or ulcerating lesions (Dhakhwa & Kafle, 2016). One study found that 13% of patients had mutations in mismatch repair proteins which is an option for targeted therapy (Xue et al., 2016).

In this chapter, two periampullary duodenal adenocarcinomas of the intestinal type were successfully established (LCT10 and LCT11). Like IAPNs, duodenal adenocarcinomas can have an intestinal or pancreatic-biliary lineage morphology. LCT10 formed large, hollow

organoids and LCT11 formed a mixture of hollow and solid organoids. Both organoids were positive for the CSC markers ALDH1A1, CXCR4, and HCAM. The organoids were also positive for pancreatic and duodenal lineage marker PDX1, proliferation marker Ki67. Additionally, the organoids were positive for Muc1 as has been reported previously (Xue et al., 2016). LCT10 was markedly more sensitive to PARPi compared to the other PDOs. Clinical evaluation of microsatellite stability found that LCT10 and LCT11 were both microsatellite stable, ruling out the possibility that mismatch repair deficiency caused PARPi sensitivity.

There have been three other groups that have also established duodenal organoids, although two of these studies established organoids from rat tissue rather than human tissue (Hedrich et al., 2020; Tanaka et al., 2023; Yamashita et al., 2021). Yamashita et al. established a single human duodenal organoid that, after several passages, formed large hollow organoids as observed for LCT10. To our knowledge, LCT10 and LCT11 are the first human duodenal organoids that have been used for evaluation of drug sensitivity.

3.6 CONCLUSIONS AND FUTURE WORK

In this chapter, the effect of 2D and 3D cell culture methods on cisplatin, olaparib, and talazoparib treatment sensitivity was investigated. To do this, 3D spheroid models were developed from established cell lines Capan-1 and MiaPaCa-2 and from patient-derived cell line PT127. Novel 2D cell lines were established from patient-derived organoids PDM41, VR096 and VR100. The effect of cell culture method on drug sensitivity was drug and model dependent and did not affect HR-mediated treatment sensitivity. The variability between *in vitro* models as well as the lack of HRD models highlights the importance of using both 2D and 3D cell culture methods when performing drug screening or toxicity assays, as well as the need for the establishment and characterisation of novel isogeneic matched 2D and 3D models.

We therefore established and characterised patient-derived organoids from resection samples of periampullary tumours. Four organoids were successfully established: LCT01, (cholangiocarcinoma), LCT06 (intra-ampullary papillary-tubular neoplasm), and LCT10 and LTC11 (both duodenal adenocarcinoma). Periampullary tumours are rare and not well investigated, partly due to a lack of preclinical models which makes these four organoid models very valuable, especially LCT06 which is the first reported IAPN organoid and as a neoplastic rather than cancerous organoid can provide valuable information about tumorigenesis and disease progression.

3.6.1 Future work

1. Characterisation of the HR status of the novel patient-derived organoids, in particular for LCT10, to determine if HRD contributes to the observed PARPi sensitivity.
2. Expansion of the immunofluorescent characterisation and viability assays to include LCT06.
3. Establishment of 2D monolayer cultures of the novel patient-derived organoids to expand the comparison of the effect of culture method on drug sensitivity.

4 MECHANISMS OF ACQUIRED PARPI AND CISPLATIN RESISTANCE IN PDAC

4.1 INTRODUCTION

Pancreatic cancer is associated with a high mortality rate, often due to its rapid metastasis and the ineffectiveness of conventional therapy regimens. In recent years, the development of novel therapies has shifted from chemotherapeutic agents such as FOLFIRINOX, gemcitabine, and nab-paclitaxel to the development of targeted agents (Hosein et al., 2022).

Approximately 3% of sporadic and 5-10% of familial PDAC patients have mutations in the double-strand break repair genes *BRCA1* or *BRCA2* resulting in homologous recombination deficiency (HRD) (Pilarski, 2019). HR is crucial for the effective and accurate repair of DSBs, which can be caused by natural processes such as ionising radiation and reactive oxygen species produced by oxidative phosphorylation as well as chemotherapeutic agents. HRD has been shown to be synthetic lethal with inhibition of single-strand break (SSB) repair through inhibition of PARP (Golan et al., 2021).

4.1.1 HRD sensitises to PARPi and cisplatin

The PARPi olaparib has recently received FDA and EMA approval for maintenance therapy of platinum-sensitive stage IV *BRCA*-associated pancreatic cancer, after the POLO trial found significant improvement in PFS (Golan et al., 2021). Despite these promising results in PFS, OS was not changed between cohorts. Furthermore, patients with germline *BRCA1/2* mutations display variable responses to platinum-based and/or PARPi treatment; a subset of patients are inherently resistant to first-line platinum-based therapy. However, most patients display an initial response to treatment but eventually develop resistance, while for a few a complete response or stable disease for over 36 months is achieved (Golan et al., 2021). One of the platinum agents that has shown increased efficacy in *BRCA*-associated pancreatic cancer is cisplatin (O'Reilly et al., 2020). However, the mechanisms that underlie these differing responses between patients are unknown. Therefore, this chapter investigates the mechanisms of acquired PARPi and cisplatin resistance.

At the moment, the only clinically approved PARPi for PDAC is olaparib although additional PARPi, such as talazoparib and veliparib, have been approved for other cancers. Talazoparib is a second-generation PARPi that has an increased potency, which has been attributed to its increased PARP-trapping ability rather than protein inhibition (Rudolph et al., 2022). Both olaparib and talazoparib are used in this chapter to investigate mechanisms of PARPi resistance.

4.1.2 Known resistance mechanisms

One of the key mechanisms of resistance to PARPi and platinum agents in HRD tumours that have been observed in both cells lines and patients is the restoration of HR through reversion mutations of BRCA1/2 (Darabi et al., 2022; Tobalina et al., 2021). Reversion mutations generally do not fully restore the complete gene sequence but do, at least partially, restore protein function. Two other mechanisms that have been described to contribute to PARPi resistance *in vitro* are increased drug clearance (due to increased expression of drug efflux pumps) and alteration of target expression in targeted therapies. Molecular alteration of PARP1 and drug efflux pump ABCG2 proteins were previously found to be associated with acquired resistance to PARPi (Pettitt et al., 2018; Teng et al., 2024) but do not account for resistance in all models (Sasaki et al., 2024). Overexpression of ABCG2 protein, as well as other drug efflux pumps, can also contribute to cisplatin resistance (Shruthi & Shenoy, 2024). Additional mechanisms of resistance to cisplatin include reduced drug uptake and alteration of apoptotic pathways.

4.1.3 Development and characterisation of resistance models

Preclinical models that can recapitulate clinical responses in terms of the genetic heterogeneity, pathological and molecular profile of PDAC are important to model treatment response and emergence of resistance. To mirror the clinical setting of acquired resistance in PARPi after platinum therapy, and to compare resistance development between two different PARPi (olaparib and talazoparib) as well as platinum agent cisplatin, the *BRCA2* mutant Capan-1 PDAC cell line was semi-continuously exposed to PARPi and cisplatin. The resultant models were evaluated for resistance and cross-resistance to commonly used chemotherapies, and the mechanism of resistance was investigated by evaluation of DNA damage recognition as well as transcriptomic, genomic, and metabolomic profiling.

4.1.4 Aims and objectives

The overarching aim of this chapter is to identify mechanisms of resistance to platinum (cisplatin) and PARPi (olaparib and talazoparib) treatment in PDAC.

Objective 1: Develop cisplatin, olaparib, and talazoparib-resistant *BRCA2* mutant Capan-1 cell lines.

Objective 2: Investigate the mechanisms of acquired resistance in PDAC to gain more insight into the functional mechanisms of the resistance.

I. Evaluation of induced resistance and cross-resistance by toxicity assays.
II. Analyse doubling time, migration and invasion capability, and γH2AX and RAD51 foci formation.
III. Perform RNA sequencing, whole exome sequencing, and metabolomic profiling.

4.2 RESULTS

4.2.1 Development of resistance

4.2.1.1 Optimisation of drug selection concentrations

To generate platinum and PARP inhibitor resistant cell lines, *BRCA2*-mutated Capan-1 cells were treated with low dose cisplatin (platinum), olaparib (PARPi), or talazoparib (PARPi). The starting dose was determined by treating cells with the IC_{10}, IC_{25}, and IC_{50} concentrations (as determined in Chapter 3.4) and analysing the confluency and cell morphology over a week (Fig. 4.1-4.6). For each drug treatment, the cells were still proliferating at the IC_{50} treatment and cell morphology was unchanged, therefore this concentration was chosen as starting concentration for long-term drug exposure. After 3.5 weeks of treatment the cells stopped proliferating and cell morphology became flattened and enlarged, indicative of senescence. β-galactosidase staining (Chapter 2.8) confirmed senescence in the majority of the treated cells but not in the untreated parental cells (Fig. 4.7).

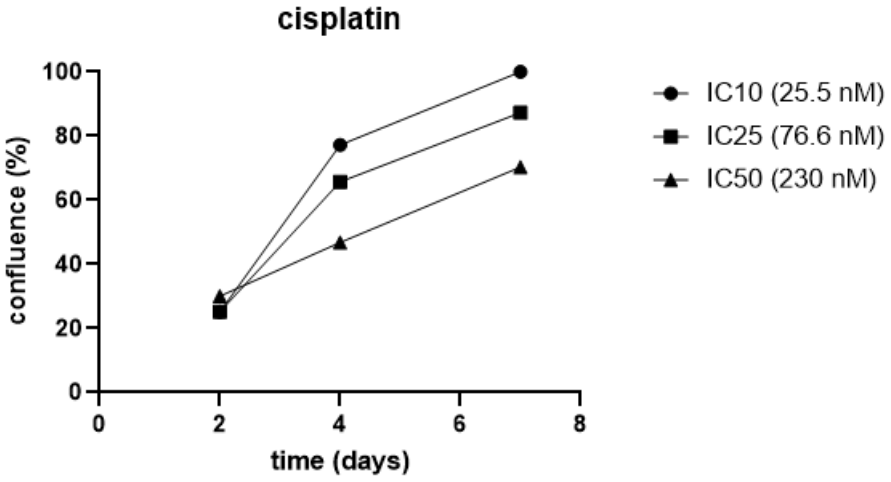

Figure 4.1. Confluence of Capan-1 during treatment with IC_{10}, IC_{25}, and IC_{50} concentrations of cisplatin over a period of 7 days*. ImageJ software was used to calculate confluence (n=1).*

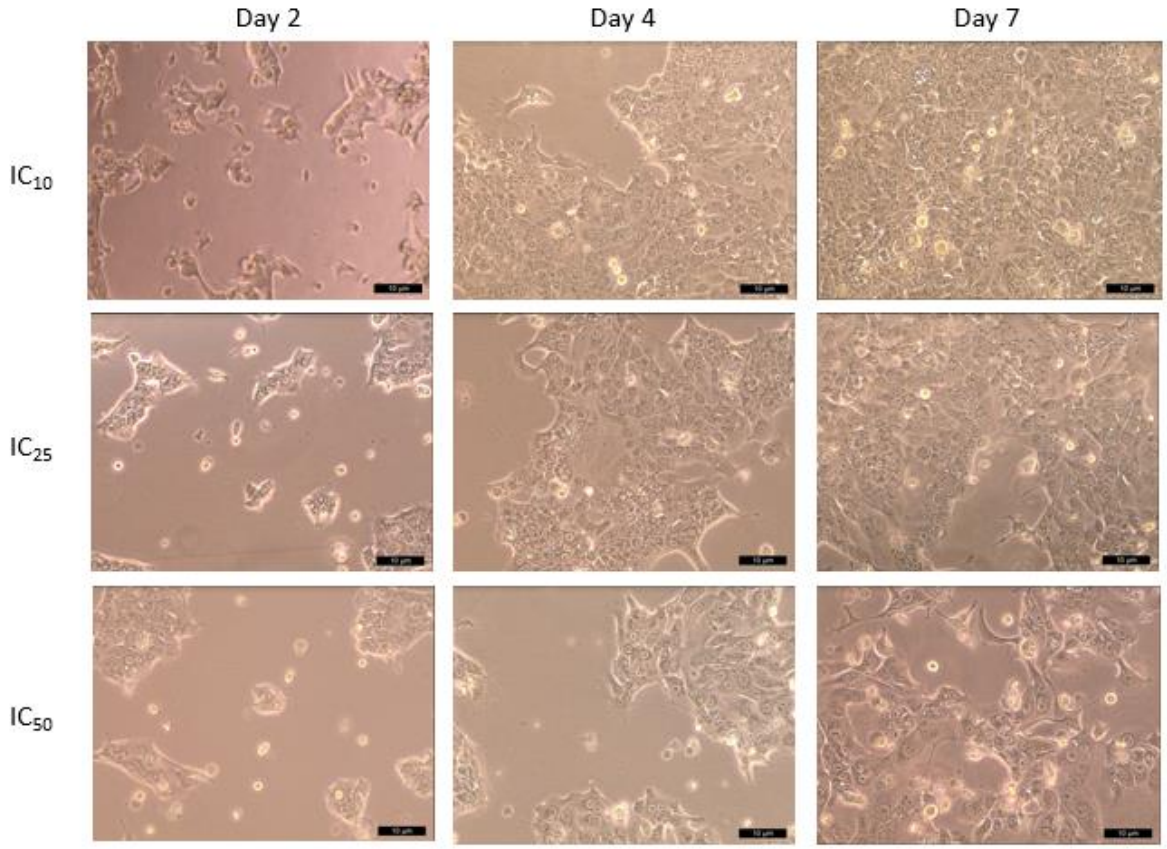

Figure 4.2. Brightfield images taken of Capan-1 during treatment with IC_{10}, IC_{25}, and IC_{50} concentrations of cisplatin over a period of 7 days. *Images taken at 10X magnification, scale bar 10 µm.*

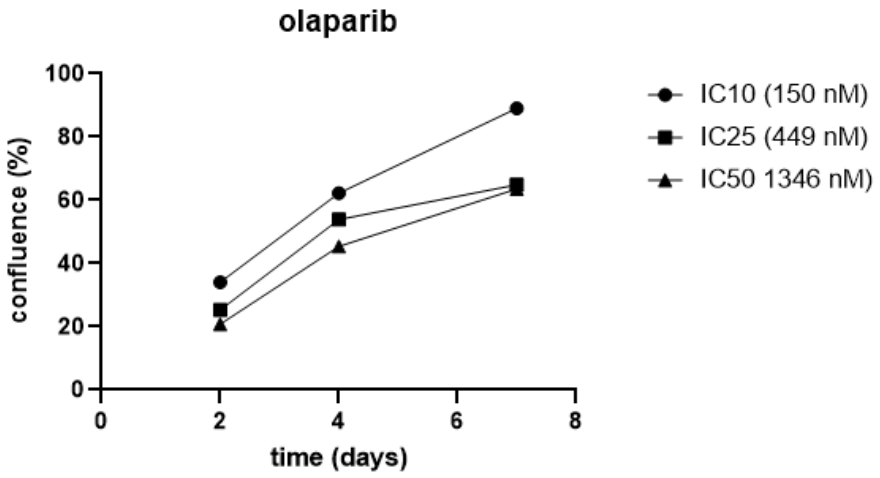

Figure 4.3. Confluence of Capan-1 during treatment with IC_{10}, IC_{25}, and IC_{50} concentrations of olaparib over a period of 7 days. *ImageJ software was used to calculate the confluence (n=1).*

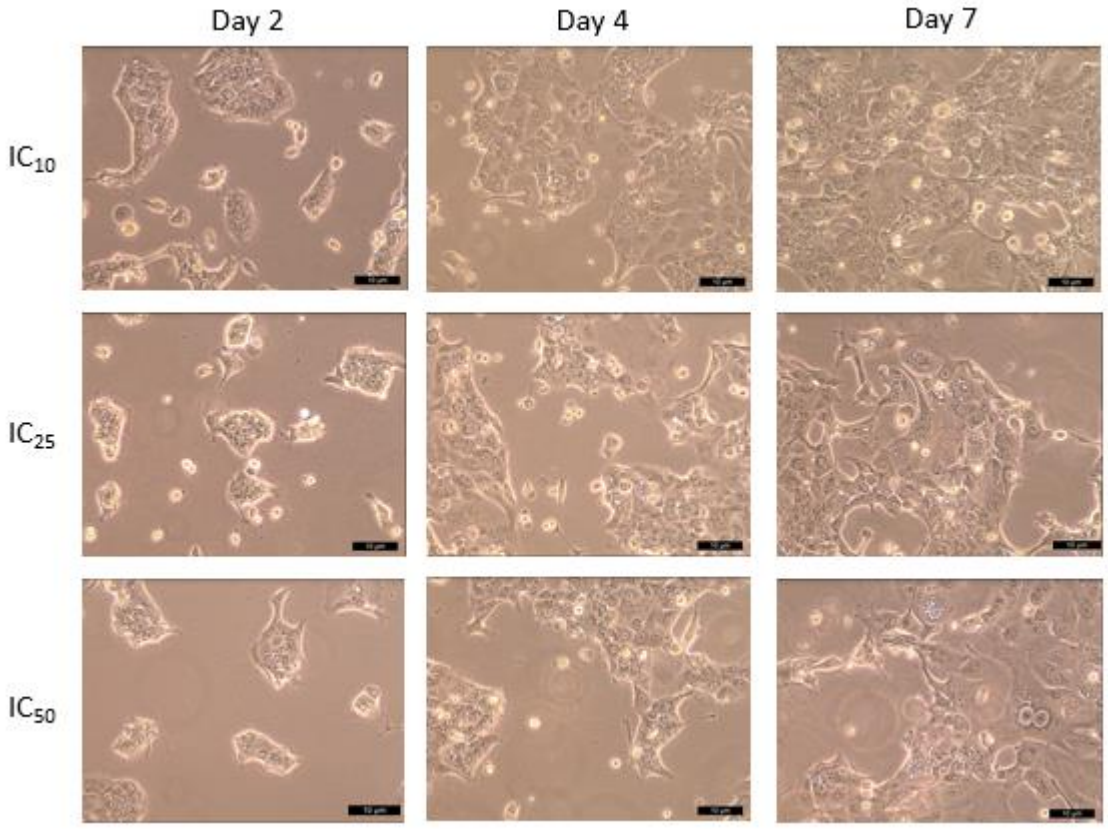

Figure 4.4. Brightfield images taken of Capan-1 during treatment with IC_{10}, IC_{25}, and IC_{50} concentrations of olaparib over a period of 7 days. *Images taken at 10X magnification, scale bar 10 µm.*

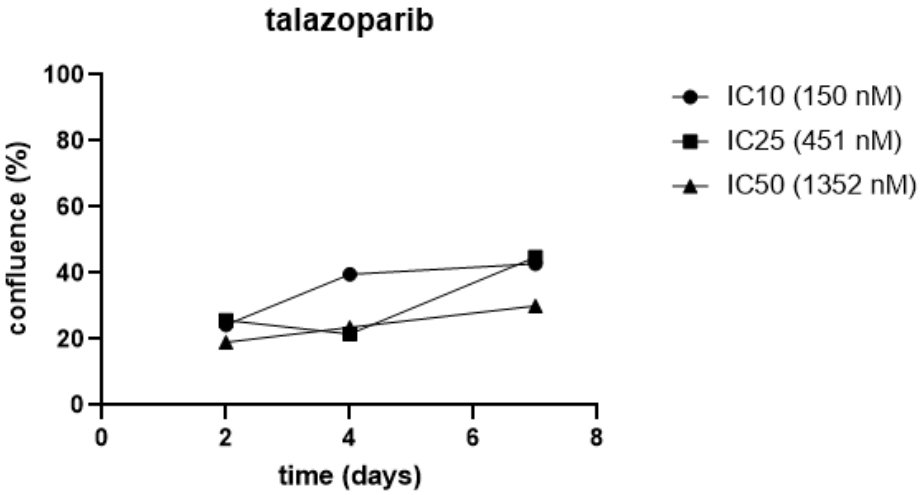

Figure 4.5. Confluence of Capan-1 during treatment with IC_{10}, IC_{25}, and IC_{50} concentrations of talazoparib over a period of 7 days. *ImageJ software was used to calculate the confluence (n=1).*

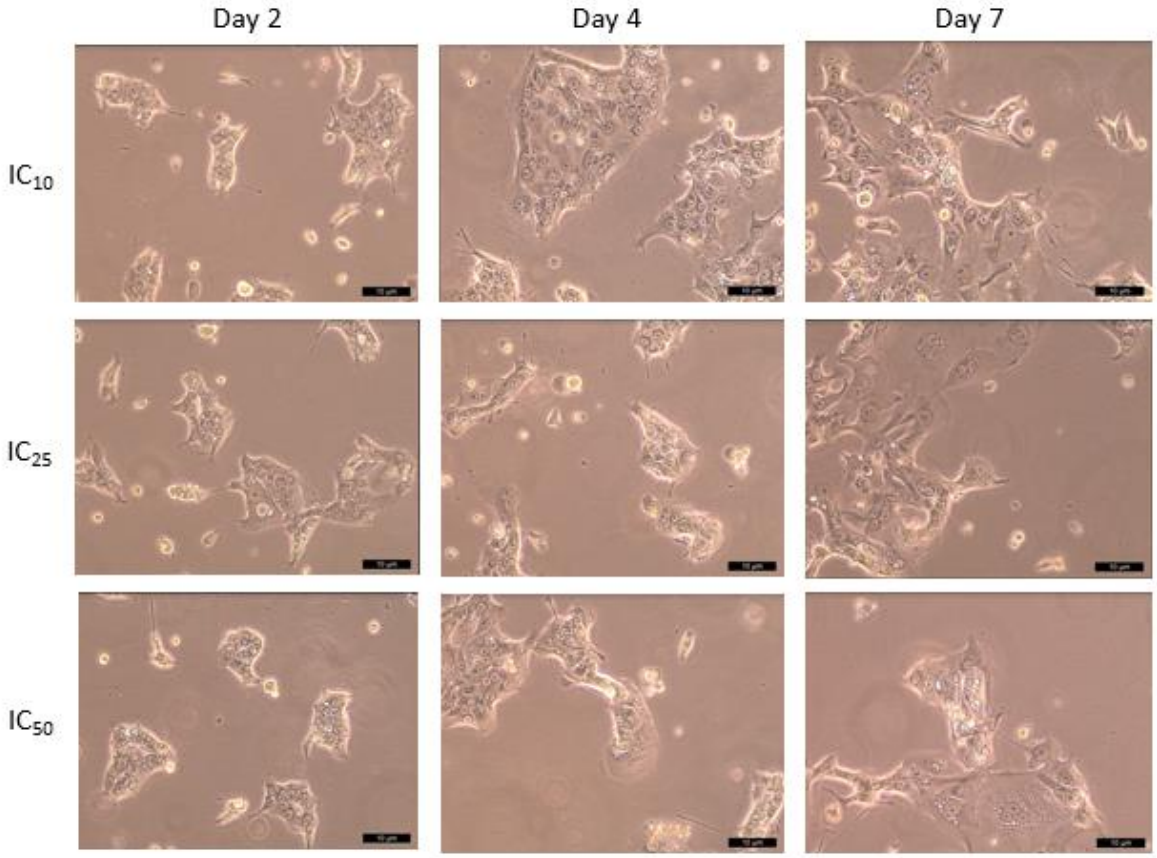

Figure 4.6. Brightfield images taken of Capan-1 during treatment with IC_{10}, IC_{25}, and IC_{50} concentrations of talazoparib over a period of 7 days*. Images taken at 10X magnification, scale bar 10 µm.*

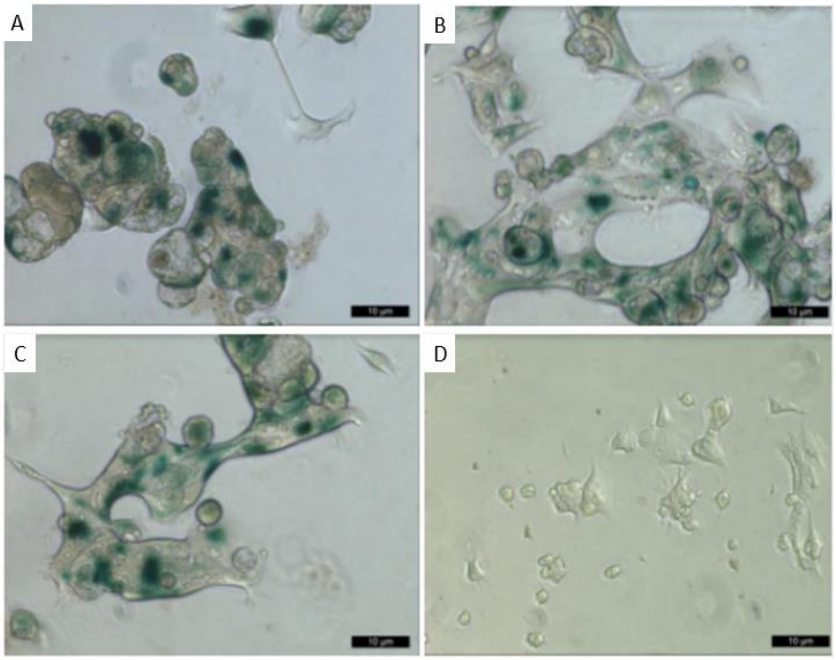

Figure 4.7. Brightfield images of β-galactosidase staining of Capan-1 cells. *A) cisplatin-treated, B) olaparib-treated, C) talazoparib-treated, D) parental. Images taken at 10x magnification, scale bar 10 µm.*

4.2.1.2 Development of resistance

For the second attempt, the cells were treated with the approximate IC_{10} concentrations ofcisplatin (75 nM), olaparib or talazoparib (450 nM) for 14 days, given a drug break of 45 days to recover, followed by treatment with an increasing concentration of drug over a period of 105 days with a 3-4 day drug break after passaging (used concentrations: 20 to 50 nM cisplatin, 50 to 75 nM olaparib, and 50 to 87.5 nM talazoparib)(Fig. 4.8). After confirmation of resistance on day 165, cells were maintained in 50 nM cisplatin or 75 nM olaparib or talazoparib.

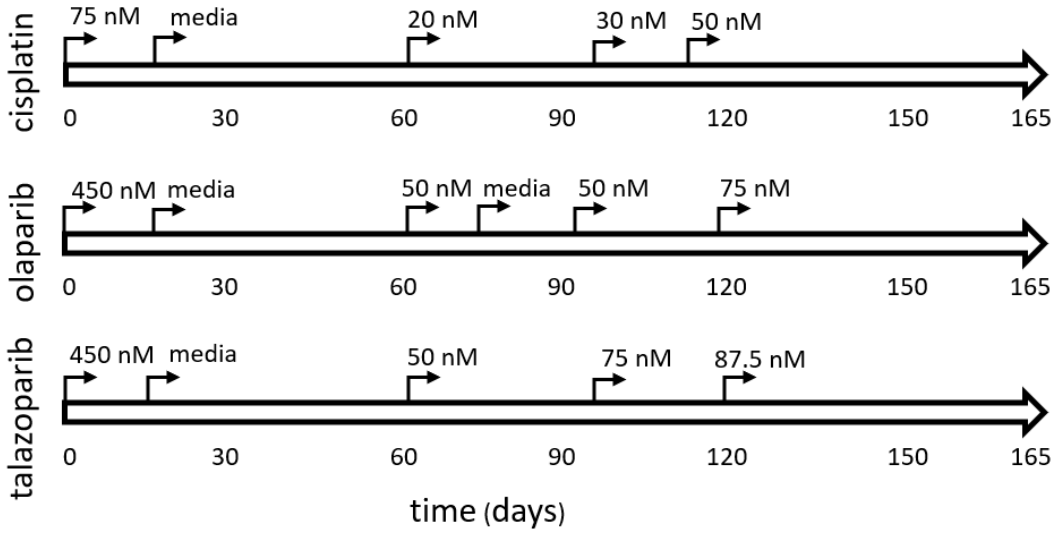

Figure 4.8. Treatment schedule used to generate cisplatin, olaparib, and talazoparib-resistant Capan -1 cells. *Capan-1 cells were treated with 75 nM cisplatin, 450 nM olaparib or talazoparib for 14 days, given a drug break of 45 days to recover, followed by an increasing concentration of drug over a period of 105 days with a 3-4 day drug break after passaging After confirmation of resistance at day 165, cells were maintained in 50 nM cisplatin, 75 nM olaparib, or 75 nM talazoparib.*

4.2.1.3 Confirmation of acquired drug resistance

The response of parental and resistant cells to drug treatment was evaluated by viability assay (Chapter 2.4.2). The IC_{50} value of cisplatin-resistant Capan-1 cells (Capan-1CisR) increased 4.8-fold compared to parental cells (5.3 µM vs. 1.1 µM) (Fig. 4.9). For olaparib-resistant Capan-1 cells (Capan-1OlaR), the IC_{50} value was not reached, but it was at least 3.1-fold higher compared to parental cells (>100 µM vs. 32 µM) (Fig. 4.10). Similarly, the IC_{50} value was not reached for talazoparib-resistant Capan-1 cells (Capan-1TalR), resulting in a fold change of >18 (>20 µM vs. 1.1 µM) (Fig. 4.11).

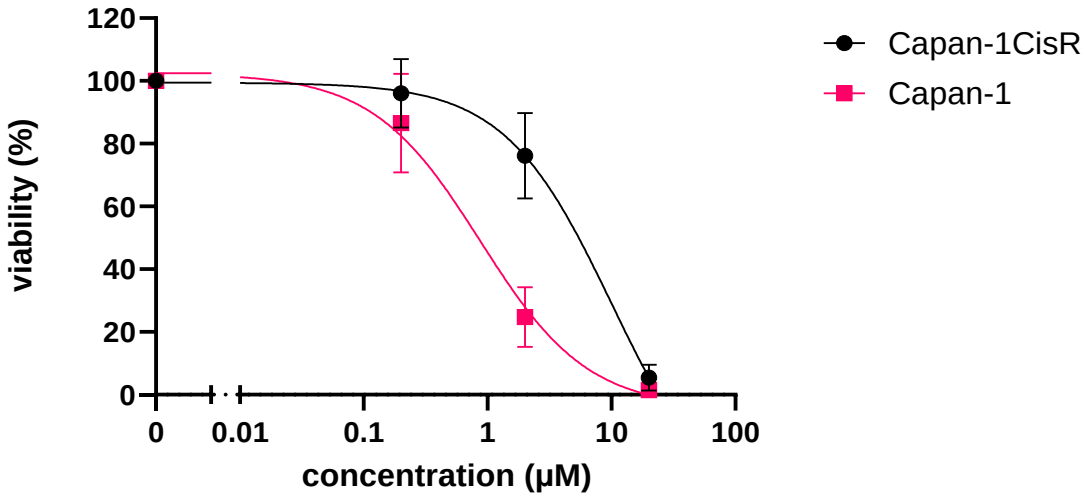

Figure 4.9. Percentage viability of parental and cisplatin-resistant Capan-1 cell lines after treatment with cisplatin for 7 days. *Cell viability was measured by fluorescent intensity of PrestoBlue staining and normalised against untreated control. Error bars represent the standard deviation of the mean for 3 biological replicates.*

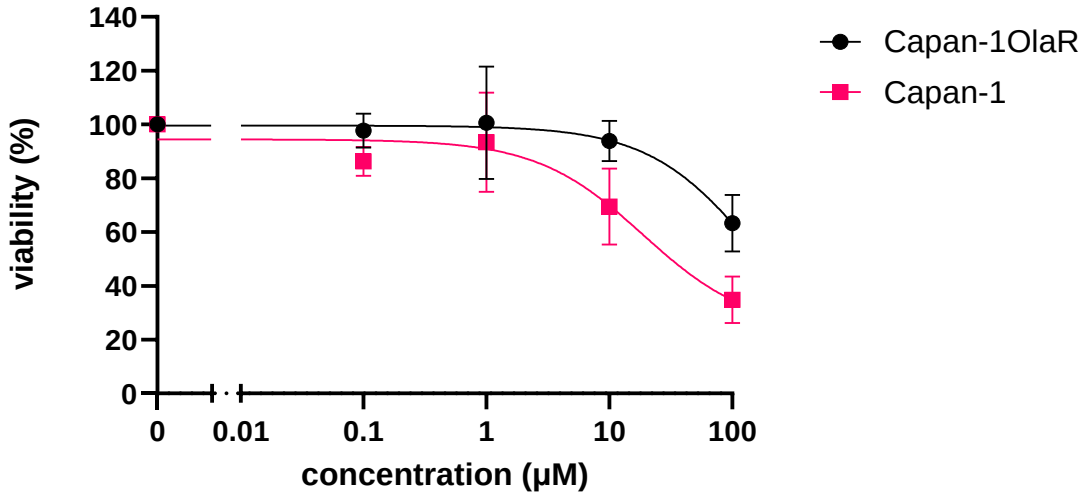

Figure 4.10. Percentage viability of parental and olaparib-resistant Capan-1 cell lines after treatment with olaparib for 7 days. *Cell viability was measured by fluorescent intensity of PrestoBlue staining and normalised against untreated control. Error bars represent the standard deviation of the mean for 3 biological replicates.*

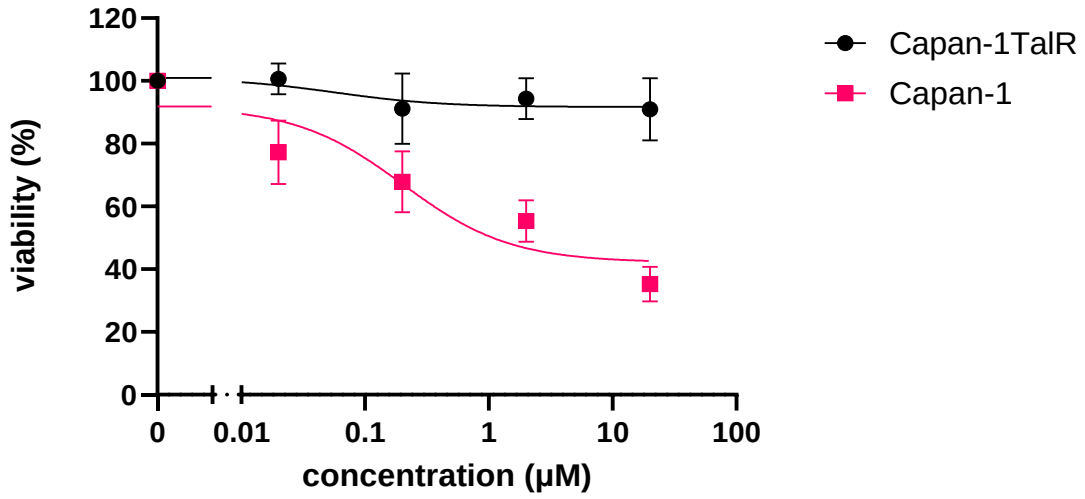

Figure 4.11. Percentage viability of parental and talazoparib-resistant Capan-1 cell lines after treatment with talazoparib for 7 days. *Cell viability was measured by fluorescent intensity of PrestoBlue staining and normalised against untreated control. Error bars represent the standard deviation of the mean for 3 biological replicates.*

4.2.1.4 Doubling time

To determine whether the development of resistance affected the proliferation rate of the Capan-1 cells, the doubling time was measured for each of the cell lines (Fig. 4.12, section 2.5.1). The parental line had a doubling time of 2.0 days (95% CI 1.74-2.36), the Capan-1CisR cells had a considerably shorter doubling time of 1.31 days (95% CI 1.15-1.51). The PARP inhibitor resistant lines also had slightly shorter doubling times compared to the parental cells at 1.90 days (95% CI 1.61-2.32) for Capan-1OlaR, and 1.62 days (95% CI 1.37-1.97) for Capan-1TalR.

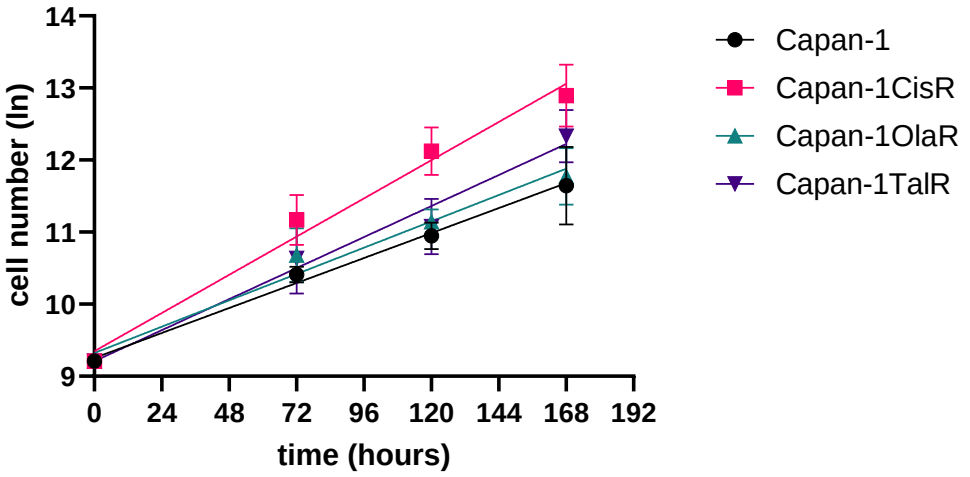

Figure 4.12. Doubling time of parental and resistant Capan-1 cells. *Cells were seeded at 10000 cells/well in a 12-well plate, trypsinised and counted after 3, 5, and 7 days (n=3). The cell number was ln transformed to plot a linear growth curve. The doubling time was calculated by GraphPad Prism using nonlinear fit.*

4.2.2 Cross-resistance to PARPi and standard-of-care treatments

Viability assays were used to assess cross-resistance to common systemic treatments used to treat PDAC (PARP inhibitors olaparib and talazoparib, platinum agents cisplatin and oxaliplatin, antimetabolic agents gemcitabine and 5-fluorouracil, and the combination FOLFIRINOX) (Fig. 4.13). Cells were treated for 7 days, and viability was normalised to untreated control.

Capan-1TalR displayed the highest level of resistance to cisplatin (Fig. 4.13A), with an 8.3-fold change (FC) in IC_{50} compared to the parental cells (6.6 µM vs. 0.8 µM, p=0.002), which is higher than the Capan-1CisR cells (IC_{50} 5.3 µM, 6.6 FC, p=0.05). There was no significant cross-resistance in Capan-1OlaR (IC_{50} 1.3 µM, p=0.1).

High levels of cross-resistance were also seen for olaparib (Fig. 4.13B), where none of the resistant cells reached the IC_{50} at the highest tested concentration of 100 µM. At this concentration, Capan-1CisR, Capan-1OlaR, and Capan-1TalR have a viability of 92.7%, 63.3%, and 67.7%, respectively, compared to 34.8% in the parental cells (1.8-2.7 FC, p<0.002).

Similarly, the IC_{50} values for talazoparib could not be determined in the resistant cells due to high levels of cross-resistance (Fig. 4.13C). At the highest tested concentration of 20 µM, Capan-1CisR has a very similar viability as Capan-1TalR at 85.2% compared to 90.9%,

respectively. Capan-1OlaR has a slightly lower viability at 71.5%. Viability in the parental cells is 35.2% at this concentration, which resulted in a 2-2.5 FC for the resistant cells ($p<0.005$).

Capan-1CisR and Capan-1TalR showed a slight, but non-significantdecrease in sensitivity to gemcitabine (Fig. 4.13D), with an IC_{50} of 0.15 and 0.12 ng/mL, respectively, compared to 0.07 ng/mL in the parental cells (2.1 and 1.7 FC). In contrast, the Capan-OlaR cells were slightly, but not significantly, more sensitive to gemcitabine compared to the parental cells with an IC_{50} of 0.05 ng/mL (-1.4 FC).

For 5-FU, no change in sensitivity was observed for Capan-1TalR (Fig. 4.13E), where the IC_{50} remained at 0.09 µM. Capan-1CisR and Capan-1OlaR also showed no significant cross-resistance to 5-FU, although the IC_{50} was slightly higher (0.23 and 0.17 µM, respectively). At higher concentrations, the viability seems to stabilise at approximately 15% for the parental cells and Capan-1OlaR and at approximately 30% for Capan-1CisR and Capan-1TalR, suggesting that there is a subpopulation of highly resistant cells in each of the cell lines.

For oxaliplatin, significant cross-resistance was observed across all three resistant cell lines (Fig. 4.13F), with IC_{50} values of 2.2 ($p=0.003$), 2.9 ($p=0.05$), and 4.7 ($p=0.002$) µM, for Capan-1CisR, Capan-1TalR, and Capan-1OlaR, respectively. Compared to the IC_{50} of 0.51 µM in the parental cells, this is a 2.2 to 4.7 FC in IC_{50}.

Lastly, Capan-1TalR showed strong cross-resistance to the combination treatment FOLFIRINOX (Fig. 4.13G), with an IC_{50} of 0.35%, compared to 0.045% in the parental cells (7.8 FC, $p=0.003$). In contrast, the Capan-1CisR and Capan-1OlaR cells showed no significant change in sensitivity with an IC_{50} of 0.032% and 0.17%, respectively.

When comparing these viability curves to maximum plasma (C_{max}) values that have been reported in literature (Table 4.1), it becomes clear that both the parental and resistant cells have an innate resistance to olaparib, talazoparib, and oxaliplatin, with more than 25% viability at the $C_{max.}$ For cisplatin and FOLFIRINOX less than 10% viability was seen at the highest tested concentrations which were both under the $C_{max.}$ In contrast, all cells remained highly sensitive to gemcitabine. The lowest reported C_{max} for gemcitabine is still over 450-fold higher than the maximum concentration used in this assay at which the viability was less than 15%.

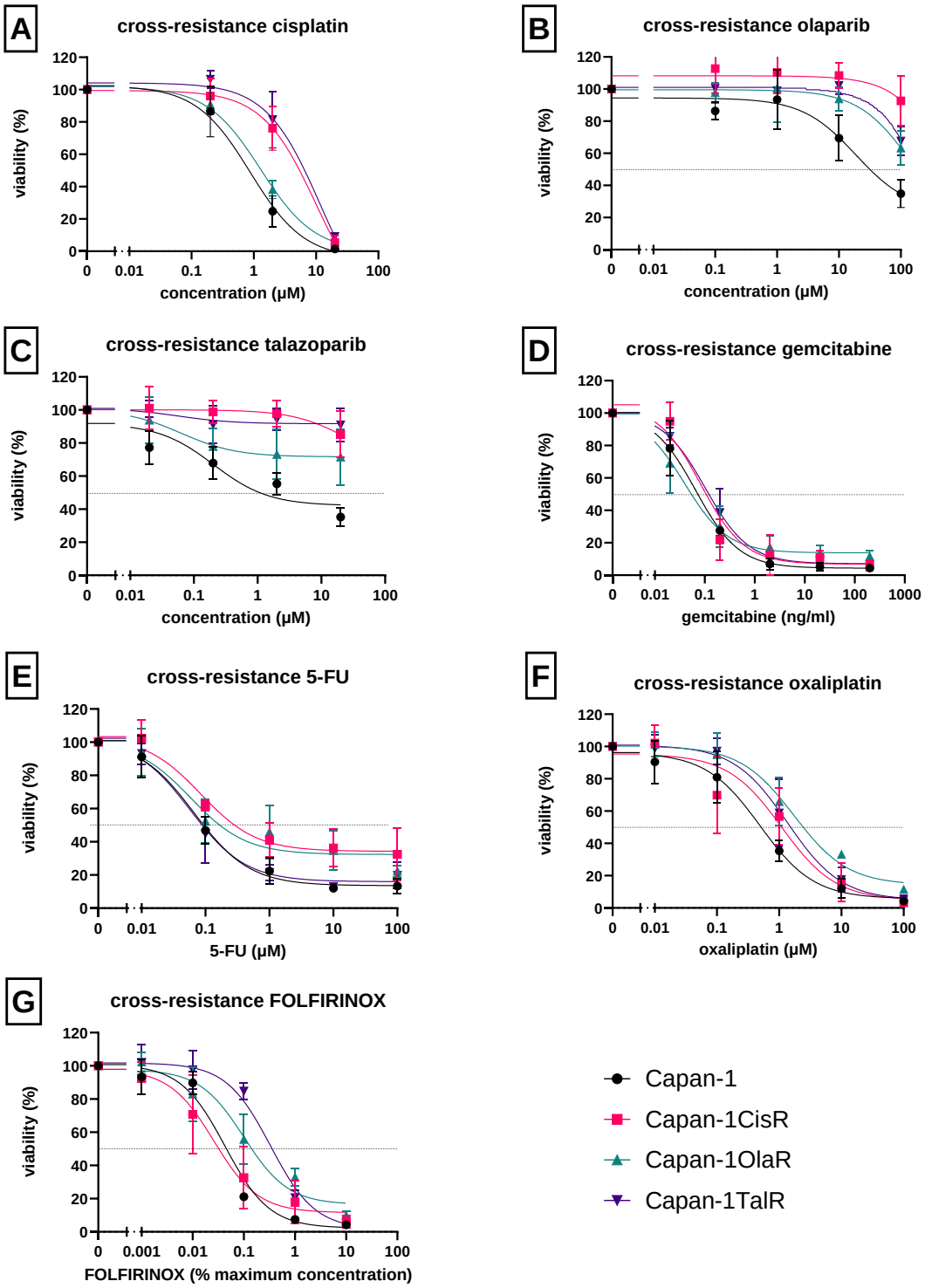

Figure 4.13. Percentage viability of Capan-1CisR, Capan-1OlaR, Capan-1TalR, and parental Capan-1 after treatment for 7 days. *A) cisplatin, B) olaparib, C) talazoparib, D) gemcitabine, E) 5-FU, F) oxaliplatin, G) FOLFIRINOX. Cell viability was measured by PrestoBlue staining and normalised against untreated control. The horizontal dotted line indicates the IC_{50}, the vertical dotted line indicates the maximum plasma concentration (C_{max}) as reported in literature. Where no C_{max} is indicated it is above the maximum tested concentration. Error bars represent the standard deviation of the mean (n=3).*

Table 4.1. Sensitivity of Capan-1 parental and resistant cells to common systemic treatments for PDAC

Drug	**C_{max}**		**IC_{50}**			
			Capan-1	**Capan-1CisR**	**Capan-1OlaR**	**Capan-TalR**
Cisplatin	30 µM	(Rajkumar et al., 2016)	0.8 µM	5.3 µM†	1.3 µM	6.6 µM†
Olaparib	30.1 µM	(AstraZeneca, 2014, 2017)	32 µM	>100 µM	>100 µM	>100 µM
Talazoparib	28.9-86.3 nM	(Y. Luo et al., 2023; Naito et al., 2021; Pfizer Europe, 2019)	1.1 µM	>20 µM	>20 µM	>20 µM
Gemcitabine	9.1-15.6 µg/ml	(Caffo et al., 2010; Masumori et al., 2008)	0.06 ng/ml	0.24 ng/ml	0.05 ng/ml	0.12 ng/ml
5-FU	168-423 µM	(Casale, 2004; Di Paolo et al., 2008)	0.09 µM	0.23 µM	0.17 µM	0.09 µM
Oxaliplatin	1.8-9 µM	(Ehrsson et al., 2002; Lévi et al., 2012; Takimoto et al., 2007)	0.51 µM	1.1 µM†	2.4 µM†	1.5 µM†
FOLFIRINOX	1000%*	(Conroy et al., 2018; Porter et al., 2019)	0.045%	0.032%	0.14%	0.35%†

*IC_{50} values were interpolated from the graphs, with the curves plotted as non-linear fit. *FOLFIRINOX is a combination treatment consisting of folinic acid, 5-fluorouracil, irinotecan, and oxaliplatin. Irinotecan is a precursor to the active compound SN-38 and is processed in the liver by carboxylesterase enzymes. Since this is not possible in vitro the active compound SN-38 was used. For easier interpretation, the maximum concentration is set at 100% which is approximately 1/10th of the maximum plasma concentration for 5-FU and oxaliplatin (423 µM and 3.62 µM, respectively) and in a ratio similar to what is given to patients. This equals to 0.428 µM folinic acid, 34.4 µM 5-fluorouracil, 0.4 µM SN-38, and 0.32 µM oxaliplatin. The C_{max} is the average maximum plasma concentration as reported in literature. † indicates a significantly altered IC_{50} compared to the parental cells as determined by Student's T-test.*

4.2.3 Invasion and migration

Changes in aggressiveness and invasive capability are known to contribute to drug resistance. To test if this is also the case in the resistant Capan-1 cells, migration and invasion capabilities of the cells were evaluated using transwell plates (Chapter 2.7). A 1.57-fold increase (p=0.035) in migration was found in Capan-1CisR compared to parental cells (Fig. 4.14). No significant changes in migration or invasion were observed for the PARPi resistant cells (Fig. 4.14 and 4.15).

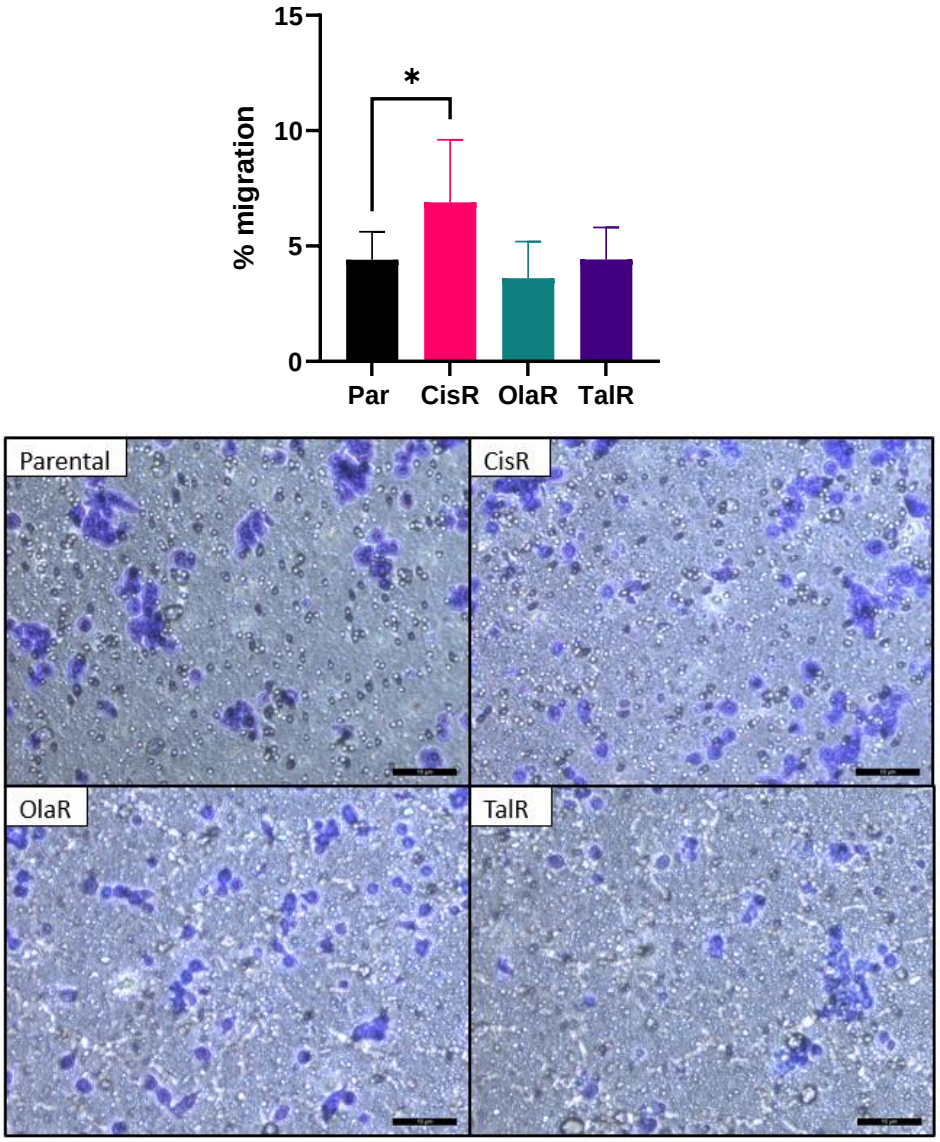

Figure 4.14. Migration of Capan-1 parental and resistant cells. *Cells were seeded in the top chamber of a transwell plate, incubated for 24 hours, fixated, and stained with crystal violet. Top: percentage migration relative to the total number of cells seeded (n=3). Statistical comparison of resistant cells versus parental cells by Student's T-test (*: p<0.05). Bottom: representative images showing the migrated cells. Magnification 10x, scale bar 10 µm.*

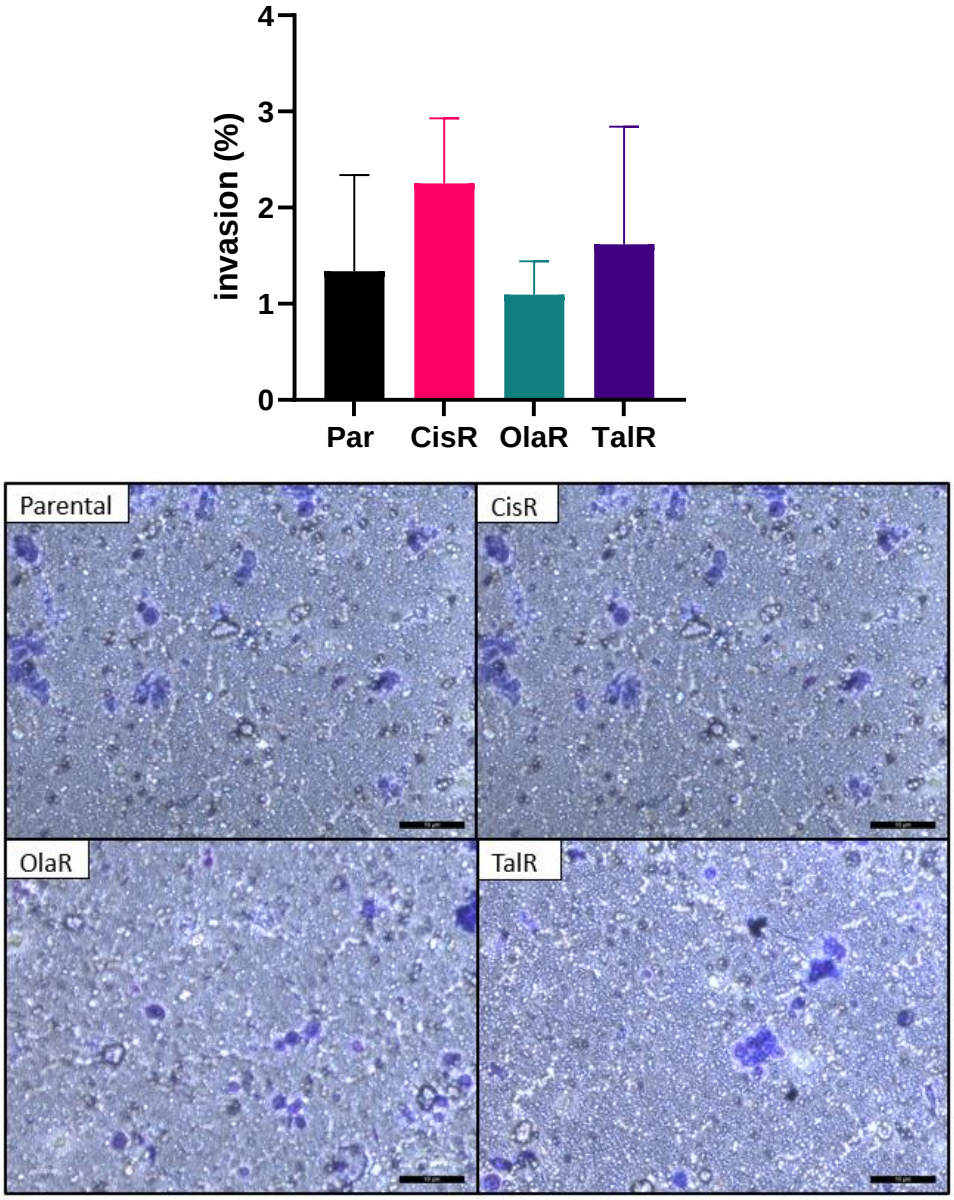

Figure 4.15. Invasion of Capan-1 parental and resistant cells. *Cells were seeded in the top chamber of a Matrigel-coated transwell plate, incubated for 24 hours, fixated, and stained with crystal violet. Top: percentage invasion relative to the total number of cells seeded (n=3). Statistical comparison of resistant cells versus parental cells by Student's T-test (*: p<0.05). Bottom: representative images showing the invading cells. Magnification 10x, scale bar 10 µm.*

4.2.4 Immunofluorescent evaluation of DNA damage recognition in resistant cells

Immunofluorescent imaging of γH2AX and RAD51 after 24 hours of drug treatment was performed to investigate if induction of DNA damage recognition and repair differs between resistant and parental cells (Chapter 2.10.1). H2AX is a histone protein that is rapidly phosphorylated at Ser-139 in response to DSBs, this modified form is referred to as γH2AX (Mah et al., 2010; Prabhu et al., 2024). Neighbouring H2AX proteins are also phosphorylated, resulting in the formation of a γH2AX focus at the location of a DSB. γH2AX is involved in signalling and initiating the repair of DSBs through chromatin modification and recruitment of DDR proteins.

Another protein that forms foci at DSBs is RAD51. Recruitment of RAD51 to DSBs is essential for HR and is mediated through direct interaction with BRCA2, except for during the S phase where RAD51 foci can form independent of BRCA2 (Tarsounas et al., 2004; Z. Wang et al., 2022). In Capan-1 cells, the truncation of the BRCA2 protein has been shown to impair RAD51 foci formation in response to irradiation-induced DSBs (Tarsounas et al., 2003). The formation of RAD51 foci in response to treatment has been suggested as a measure of functional HR proficiency (Blanc-Durand et al., 2023).

No significant differences were found in the average fluorescent intensity per nucleus between resistant and parental cells for either of the two proteins (Fig. 4.16). RAD51 was mainly detected in the cytoplasm (Fig. 4.17), whereas γH2AX foci were found in the majority of the cells (Fig. 4.18), with a trend of higher expression (based on mean fluorescent intensity in the nucleus) in all three resistant cell lines. Interestingly, different subpopulations could be distinguished: some cells were negative for γH2AX or only had one or two foci, others had high levels of foci (Fig. 4.19).

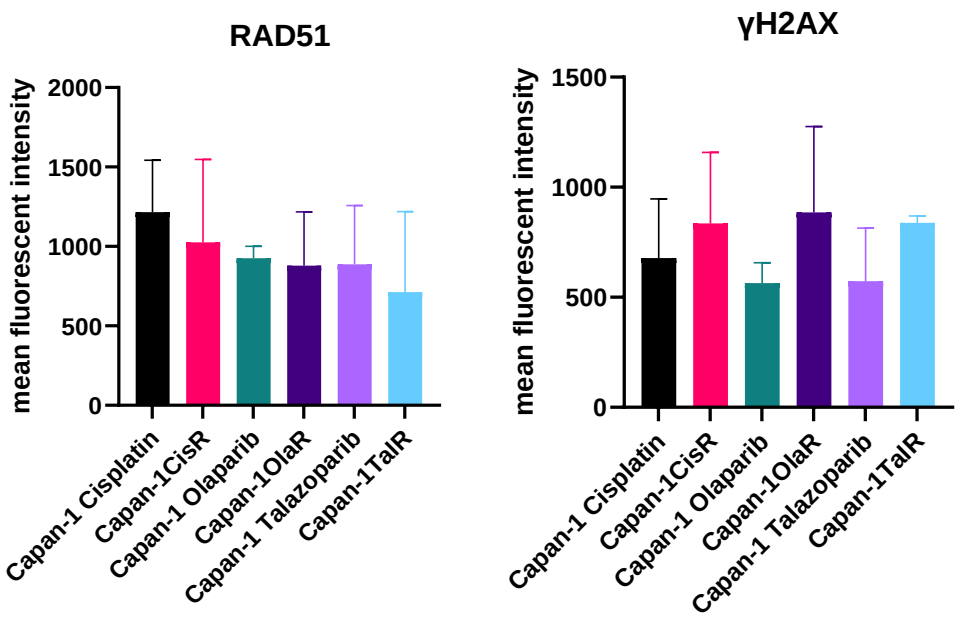

Figure 4.16. Mean fluorescent intensity per nucleus for RAD51 and γH2AX 24 hours after treatment. *Cells were treated with 500 µL 10 µM cisplatin, 50 µM olaparib, or 20 µM talazoparib, fixated, and stained with antibodies against RAD51 and γH2AX. Slides were imaged at 60x magnification and mean fluorescent intensity per nucleus was measured using ImageJ. Error bars represent the standard deviation of the mean for 3 biological replicates. Statistical comparison of resistant cell line to parental cell line treated with the same drug using Student's T-test.*

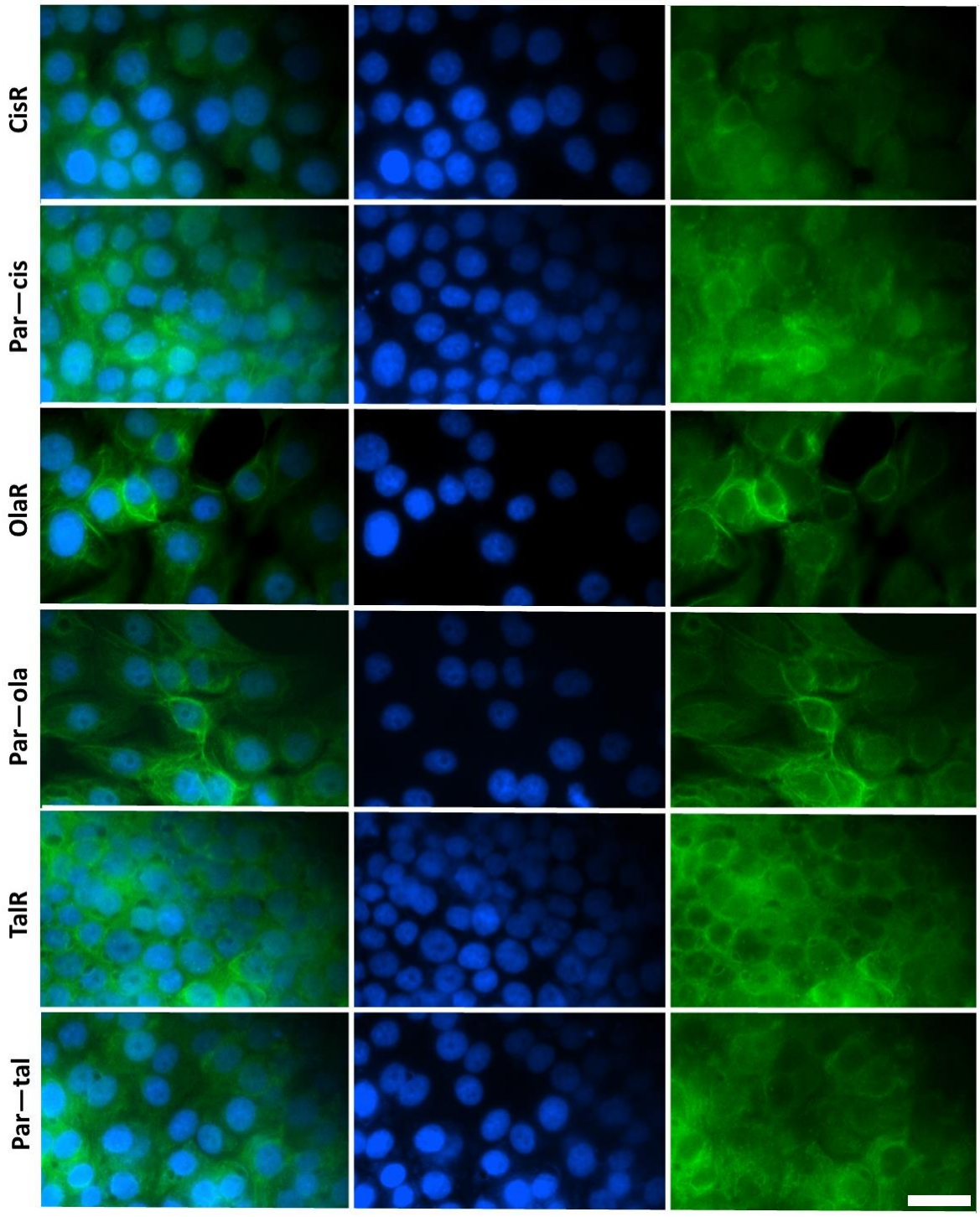

Figure 4.17. Immunofluorescent imaging of RAD51 after 24-hour treatment with cisplatin, olaparib, or talazoparib*. Cells were treated with 500 µL 10 µM cisplatin, 50 µM olaparib, or 20 µM talazoparib, fixated, and stained with antibodies against RAD51 and γH2AX. Blue: DAPI, green: γH2AX. Magnification 60x, scale bar 20 µm. Representative images of three biological replicates.*

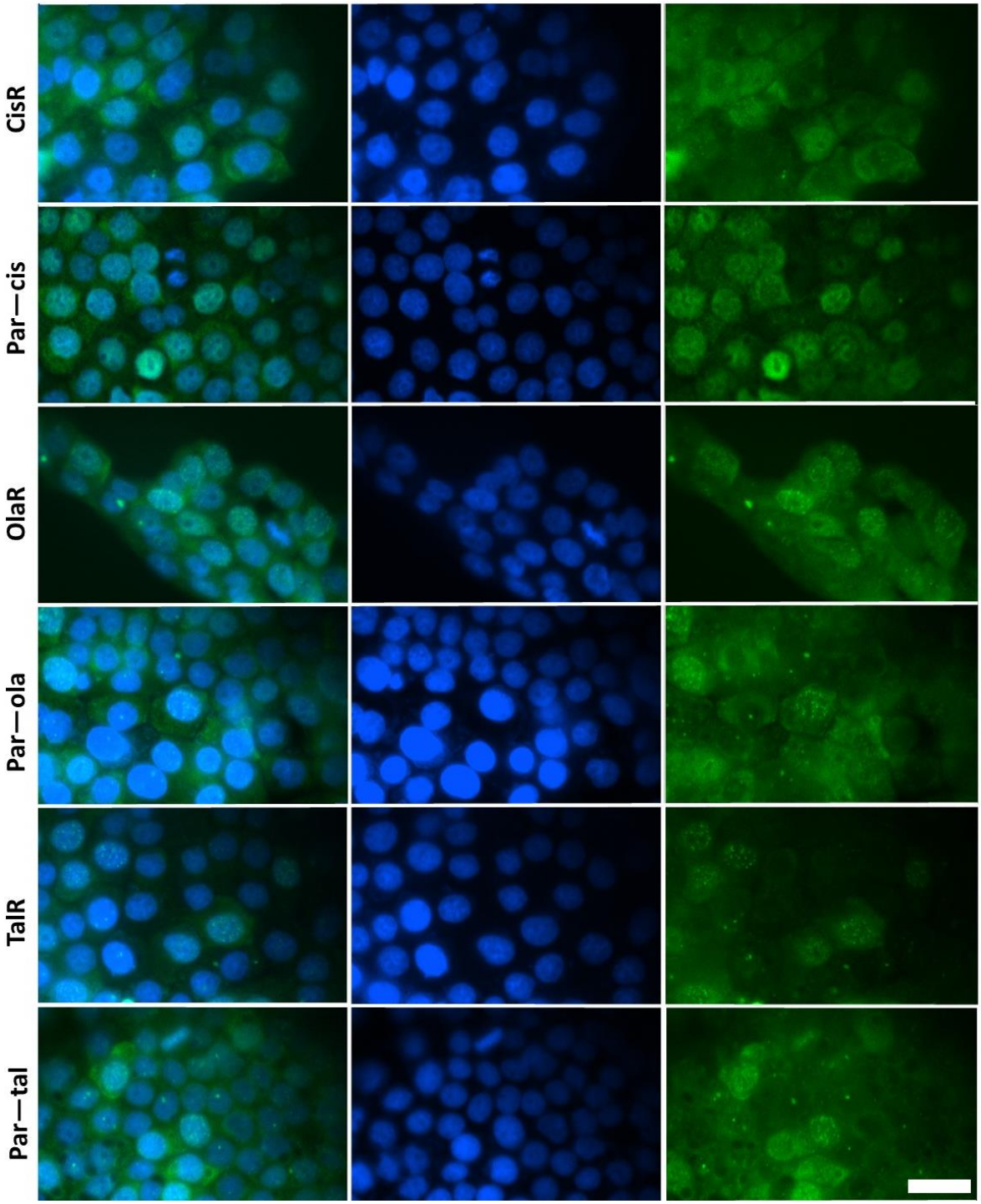

Figure 4.18. Immunofluorescent imaging of γH2AX after 24-hour treatment with cisplatin, olaparib, or talazoparib. *Cells were treated with 500 µL 10 µM cisplatin, 50 µM olaparib, or 20 µM talazoparib, fixated, and stained with antibodies against RAD51 and γH2AX. Blue: DAPI, green: γH2AX. Magnification 60x, scale bar 20 µm. Representative images of three biological replicates.*

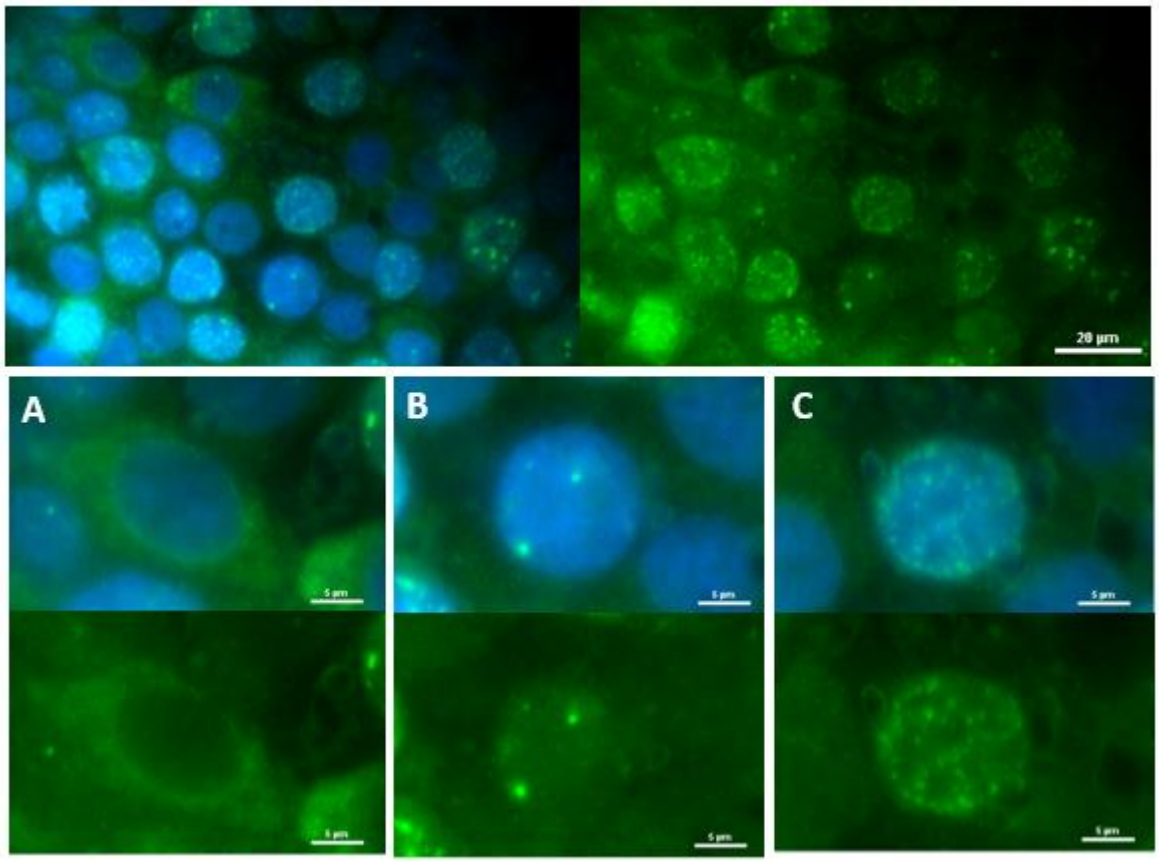

Figure 4.19. γH2AX foci formation is heterogeneous in Capan-1 cells. *Representative image of talazoparib-treated Capan-1TalR, the presence of foci ranges from none (insert A) to few (insert B) to high (insert C). Blue: DAPI, green: γH2AX Magnification of main figure 60x, addition 3x zoom on inserts.*

4.2.5 Validation of known resistance mechanisms

Molecular alterations of PARP1 and drug efflux pump ABCG2 proteins were previously found to be associated with acquired resistance to PARPi (Pettitt et al., 2018; Teng et al., 2024). To validate if these known proteins were mediators of resistance in our resistant cells the expression of PARP1 and ABCG2 was examined by Western blotting (Fig. 4.20, section 2.9).

Expression of the PARPi target PARP1 was significantly reduced in Capan-1CisR ($p=0.003$) and Capan-1TalR cells ($p<0.005$) by 53% and 34%, respectively. PARP1 expression in Capan-1OlaR was not significantly affected ($p=0.65$). Expression of the drug efflux pump ABCG2 was significantly altered in all three resistant cell lines. In Capan-1CisR, expression was decreased by 58% ($p=0.0002$), in Capan-1OlaR expression was decreased by 41% ($p=0.03$), and in Capan-1TalR expression was decreased by 71% ($p=0.003$).

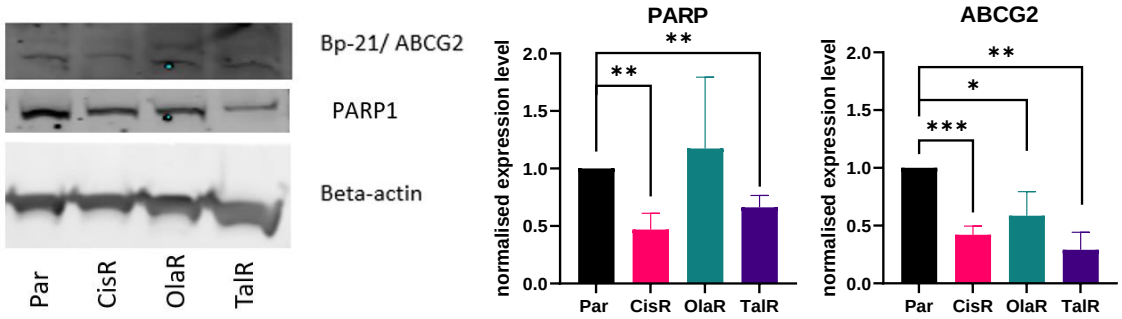

Figure 4.20. Expression of PARP1 and ABCG2 in Capan-1 by Western blot. *Expression was quantified using ImageJ and corrected against the loading control beta-actin and then normalised against the parental cells. Student's T-test was used to identify statistical differences between each resistant cell line and the parental cell line. Error bars show the standard deviation of the mean (n=3). *:p<0.05, **:p<0.005, ***:p<0.001.*

4.2.6 Identification of novel resistance mechanisms

To elucidate the mechanism of resistance to cisplatin, olaparib, and talazoparib in these *BRCA2*-mutant cells, RNA-sequencing analysis was performed in the resistant and parental cells (Chapter 2.18). Differential Gene Expression analysis was performed using NoiSeq with the parental line set as reference. Compared with the parental cells, a total of 543 differentially expressed genes (DEG, probability >0.9) were detected in the Capan-1CisR cells, with 31 genes upregulated and 512 genes downregulated. Analysis of the Capan-1OlaR cells, detected 2029 DEGs (probability >0.9), of which 523 were upregulated and 1506 genes were downregulated. Lastly, analysis of the Capan-1TalR cells detected 1981 DEGs (probability >0.9) of which 740 were upregulated and 1241 were downregulated.

A multidimensional scaling (MDS) plot (Fig. 4.21A) was generated to visualise the similarity and dissimilarity between the four cell lines. The parental and Capan-1CisR lines cluster relatively closely together, indicating a high similarity between these samples. The Capan-1OlaR and Capan-1TalR samples do not cluster with the other samples, indicating a larger dissimilarity.

To visualise the dissimilarity of the resistant lines compared to the parental line at the gene level a mean-difference (MD) plot was generated (Fig. 4.21B-D). For each gene, the plot compares the logFC between a resistant and parental line (difference, D+1) to the log expression of that gene across all the samples (mean, M). Genes with the same expression level across all samples are plotted at (0,1), genes with a large difference in expression

compared to the parental cell line have a large D+1. Additional labelling with the probability visualises the likelihood that genes truly are differentially expressed.

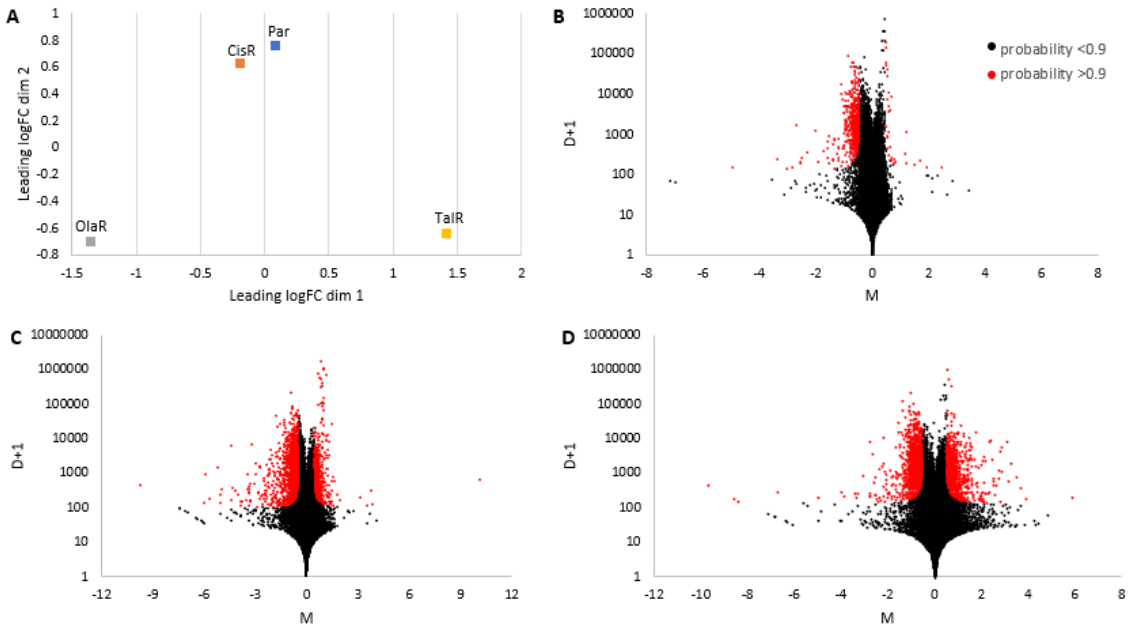

Figure 4.21. Similarities in gene expression between Capan-1 parental and resistant lines. Based on RNA sequencing data. *A) Multidimensional scaling plot. B) Mean-difference plot for CisR. C) Mean-difference plot for OlaR. D) Mean-difference plot for TalR. (n=1).*

Subsequent KEGG pathway analysis and clustering of all DEGs (with probability >0.9) showed multiple significantly affected pathways in each resistant cell line (Fig. 4.22). The metabolic and oxidative phosphorylation pathways were affected in all three lines and were therefore selected for further investigation.

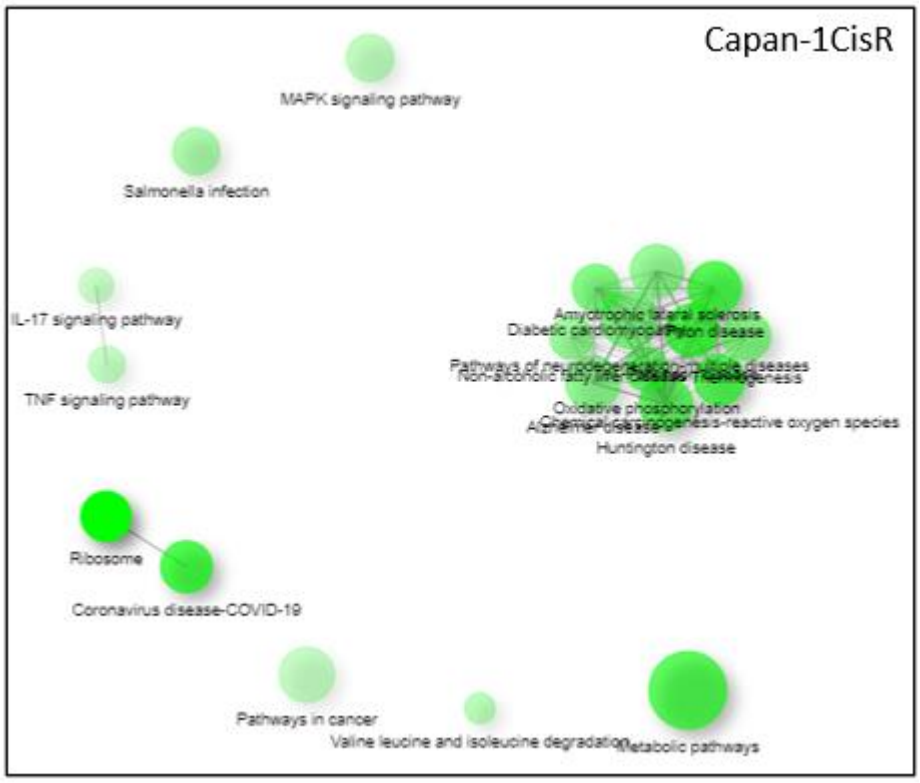
Capan-1CisR
MAPK signaling pathway
Salmonella infection
IL-17 signaling pathway
TNF signaling pathway
Amyotrophic lateral sclerosis
Diabetic cardiomyopathy
Prion disease
Oxidative phosphorylation
Huntington disease
Ribosome
Coronavirus disease-COVID-19
Pathways in cancer
Valine leucine and isoleucine degradation
Metabolic pathways

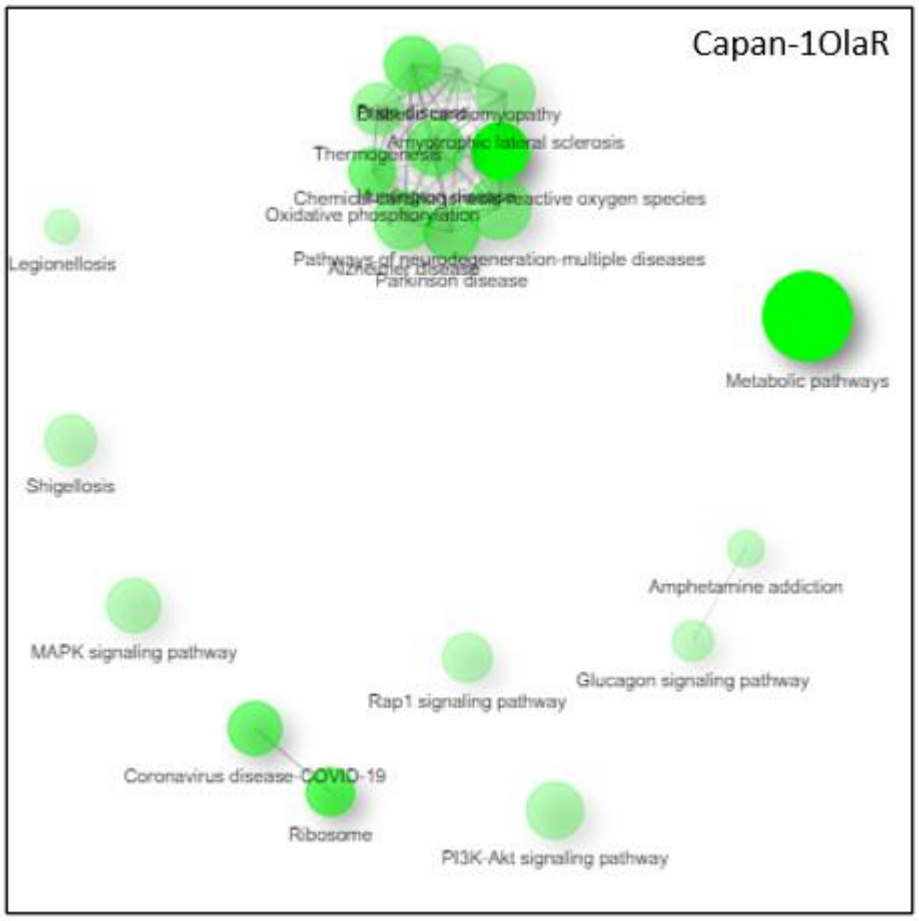
Capan-1OlaR
Amyotrophic lateral sclerosis
Thermogenesis
Oxidative phosphorylation
Parkinson disease
Legionellosis
Metabolic pathways
Shigellosis
Amphetamine addiction
MAPK signaling pathway
Glucagon signaling pathway
Rap1 signaling pathway
Coronavirus disease-COVID-19
Ribosome
PI3K-Akt signaling pathway

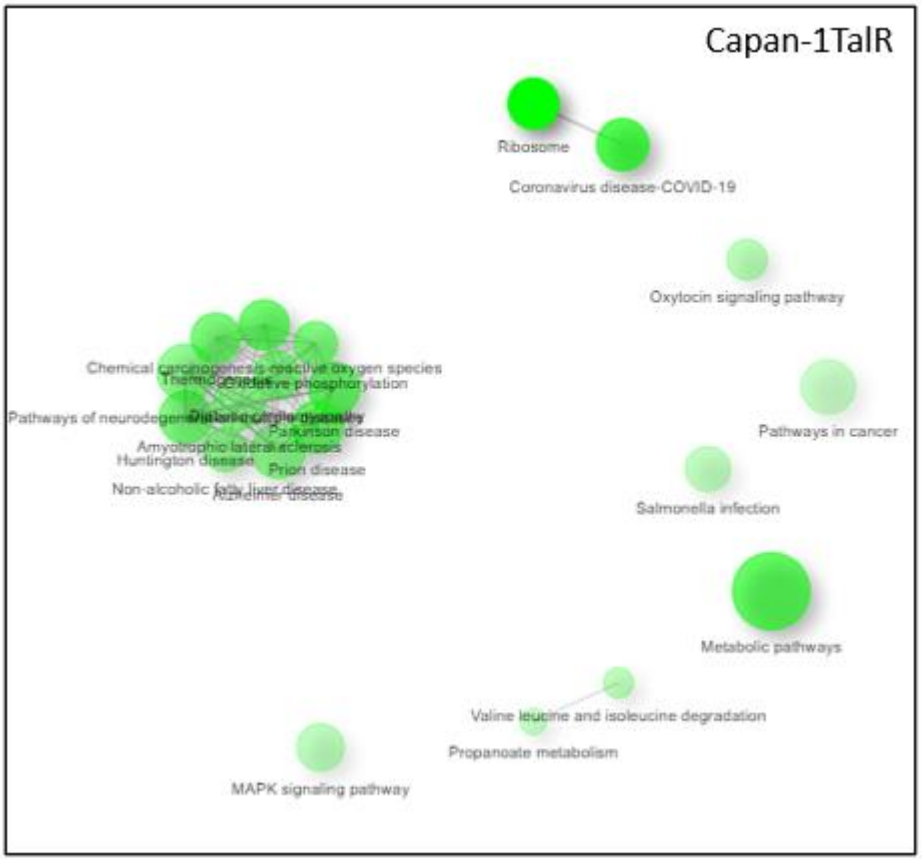

Figure 4.22. KEGG pathway analysis and clustering of all differentially expressed genes in resistant Capan-1 cells compared to parental Capan-1 cells. *Clustering was performed using ShinyGO. From top to bottom: Capan-1CisR, Capan-1OlaR, Capan-1TalR. The size of each node indicates the number of genes in each pathway. The darker the node, the more significantly enriched the pathway is. Nodes or pathways that share more than 20% of their genes are connected by an edge.*

4.2.7 Metabolomic analysis

To investigate the alterations in metabolism as indicated by the transcriptomic analysis, real-time ATP rate and metabolic flux assays were performed (Chapter 2.17). Both assays measure the extracellular acidification rate (ECAR) and oxygen consumption rate (OCR) at baseline and after inhibition of components of the electron transport chain in the mitochondria. At baseline, the ECAR and OCR are representative of glycolysis and oxidative phosphorylation, respectively. Capan-1OlaR had a significantly higher ECAR ($p=0.0064$) and Capan-1TalR had a significantly higher OCR ($p=0.0001$) compared to the parental cells (Fig. 4.23). When plotted as the ECAR:OCR ratio, significant differences were found for all resistant cell lines compared to the parental line ($p<0.001$). Capan-1CisR and Capan-1TalR

both have a decreased ratio indicating a shift towards oxidative phosphorylation, whereas Capan-1OlaR has an increased ratio indicating a shift towards glycolysis.

Evaluation of the mitochondrial respiration under stress conditions found that Capan-1CisR have a significantly increased maximal respiration (133%, p=0.0021, Fig. 4.24) compared to parental cells, meaning that the cells can produce more energy than their parental counterparts. Capan-1OlaR and Capan-1TalR both have significantly decreased spare respiratory capacity (46%, p=0.0001 and 61%, p=0.0027, respectively).

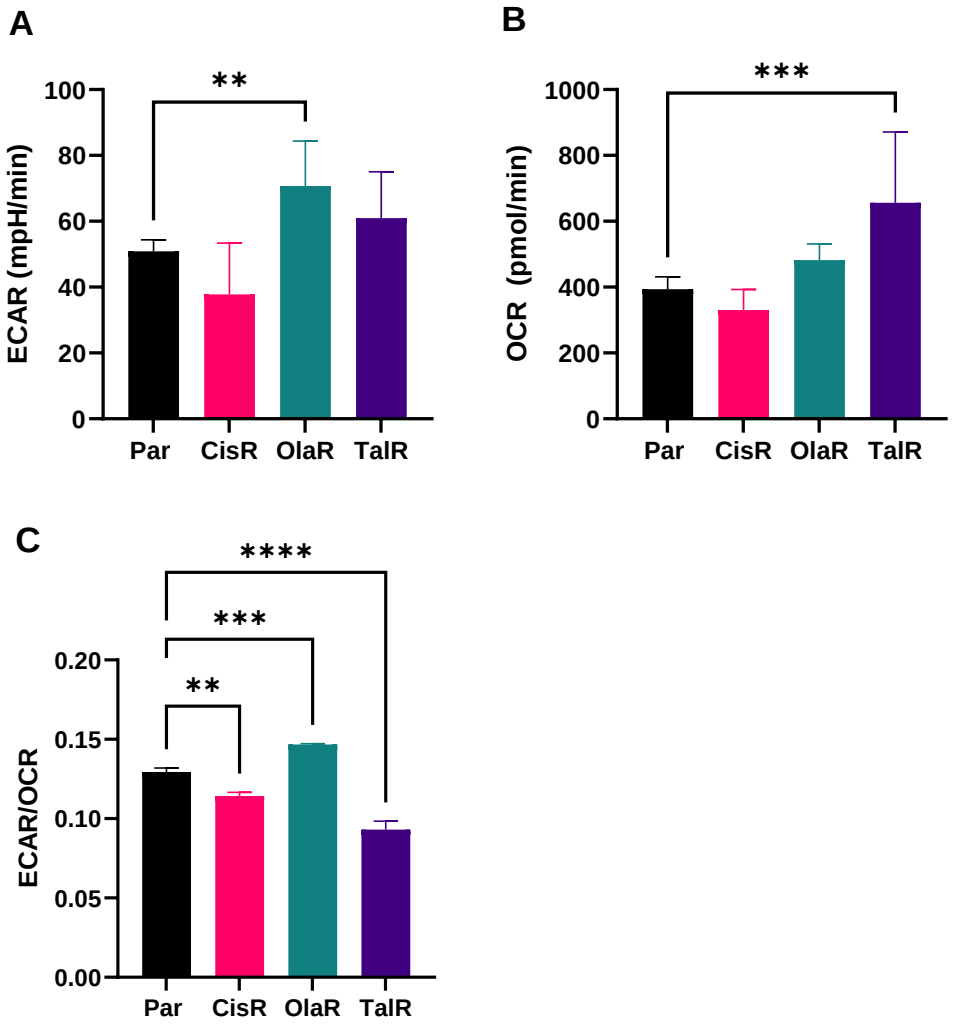

Figure 4.23. Metabolomic profiling of Capan-1 parental and resistant cells. *A) Extracellular acidification rate as a measure of glycolysis. B) Oxygen consumption rate as a measure of oxidative phosphorylation. C) ratio between ECAR and OCR. Stars indicate statistical significance based on one-way ANOVA followed by Dunnett's multiple comparisons test with parental cells set as the control to compare to (*: p<0.05, **: p<0.01, ***: p<0.001, ****: p<0.0001)(n=3).*

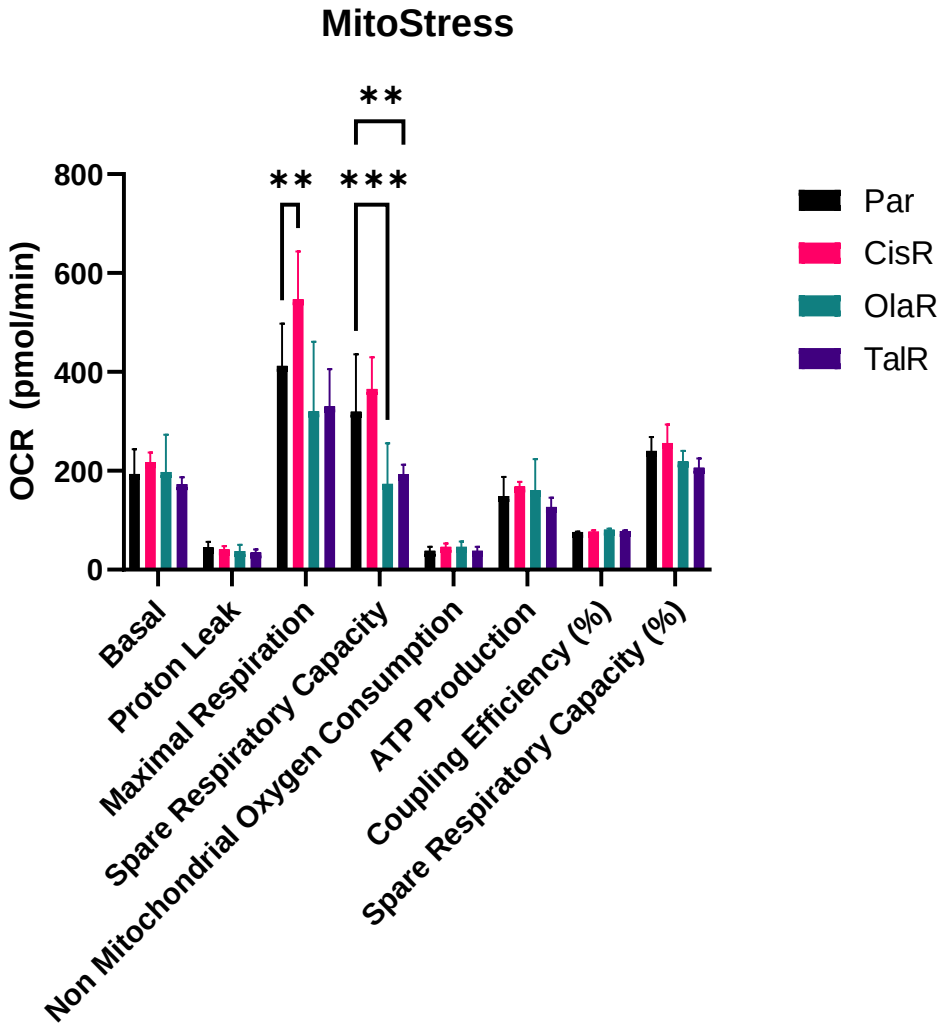

Figure 4.24. Metabolomic profiling of adaptability to mitochondrial stress in Capan-1 parental and resistant cells. *Stars indicate statistical significance based on one-way ANOVA followed by Dunnett's multiple comparisons test with parental cells set as the control (*: p<0.05, **: p<0.01, ***: p<0.001, ****: p<0.0001)(n=3).*

4.2.8 DNA sequencing

To elucidate further the mechanisms of acquired resistance and alterations in metabolism, whole exome sequencing analysis was performed (Chapter 2.18). The parental genome was set as control to select only those changes that were acquired during the development of resistance.

The majority of the variants were single nucleotide polymorphisms (SNPs) that caused missense mutations, followed by deletions (Fig. 4.25). No additional mutations were found in *BRCA2*, although Capan-1OlaR and Capan-1TalR both had one additional copy, and Capan-1CisR two additional copies of the remaining allele.

Capan-1CisR gained 63 alterations, Capan-1OlaR gained 62 alterations, and Capan-1TalR gained 53 alterations. Of these alterations, only the *CROCC* gene was altered in all three resistant lines. This alteration is a synonymous point mutation (c.1660A>T) and has an allele frequency of 22-25% in the resistant lines compared to 3.7% in the parental cells. Alterations with an allele frequency of more than 20% and with modifying, moderate, or high predicted impact were selected for further analysis.

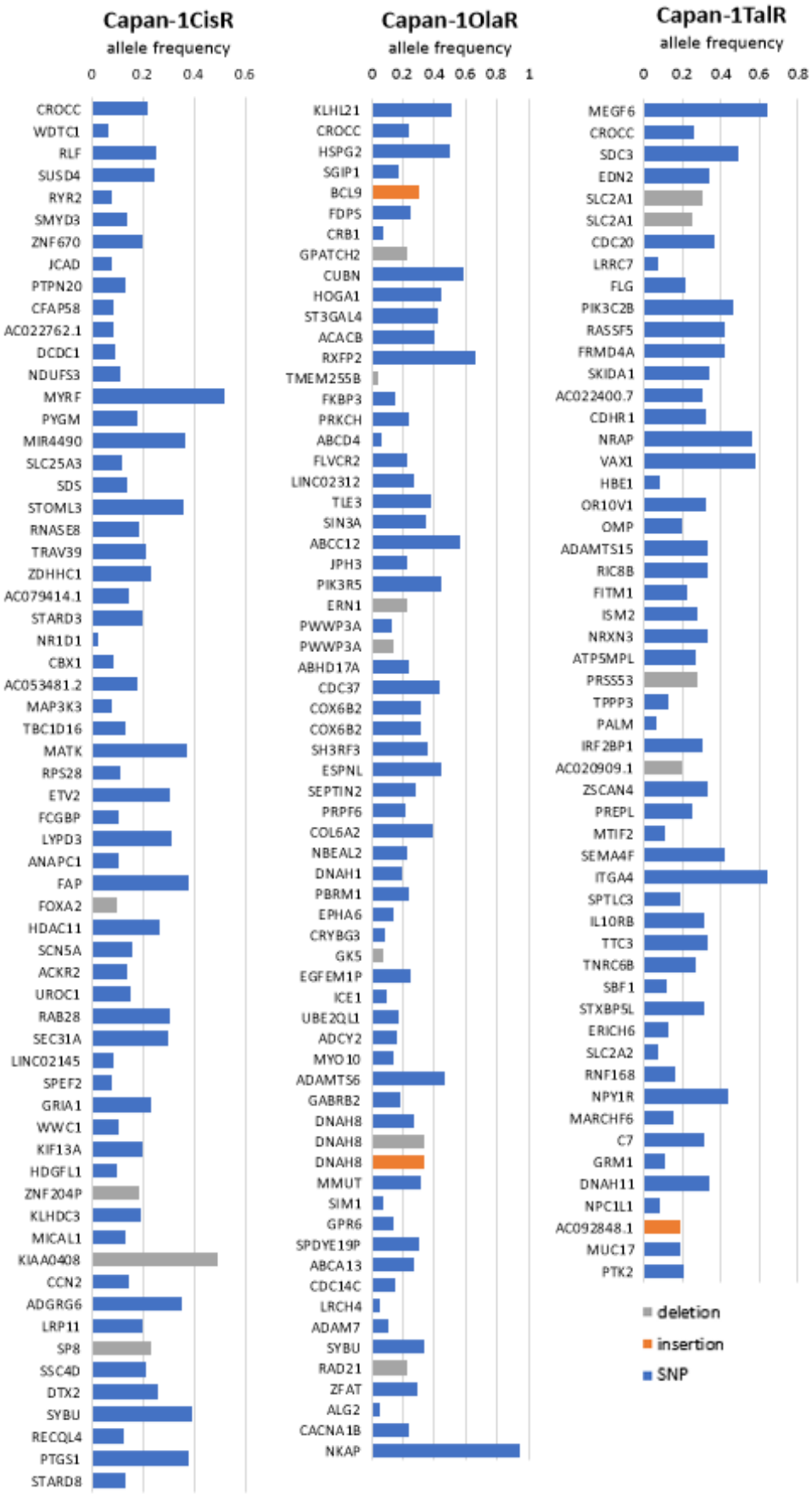

Figure 4.25. Allele frequencies of mutated genes in Capan-1 resistant cell lines. The genome of the Capan-1 parental cells was set as control to select alterations specific to the resistant cells. *(n=1).*

The Capan-1CisR cell line gained 63 coding alterations in comparison to the parental cells of which 18 were selected for further analysis. Mutations were found in four genes that are related to metabolism (*FAP, HDAC11, STARD3, LYPD3). FAP* is a metabolic regulator (Sánchez-Garrido et al., 2016); *LYPD3* and *HDAC11* are both involved in glucose metabolism (Bi et al., 2021; Sun et al., 2018); and *STARD3* is involved in cholesterol metabolism (Asif et al., 2021; Zhou et al., 2018). Additionally, Capan-1CisR had a mutation in *SP8* which is involved in Wnt signalling (Kennedy et al., 2016).

The Capan-1OlaR cell line gained 62 coding alterations in comparison to the parental cells, of which 34 were selected for further analysis. Mutations were found in six genes involved in metabolism (*HOGA1, ACACB, ERN1, COX6B2, SEPTIN2, ABCA13*). *HOGA1* catalyses the final step in hydroxyproline metabolism (Belostotsky et al., 2012; Tong et al., 2022); *ACACB* plays a central role in fatty acid metabolism (Bhattacharjee et al., 2020); *ERN1* and *SEPTIN2* are metabolic regulators (Huang et al., 2019; James et al., 2019); *COX6B2* is part of complex IV of the electron transport chain in oxidative phosphorylation (Nie et al., 2020); and *ABCA13* is involved in lipid transport as well as drug resistance (Pasello et al., 2020). Additionally, mutations were also found in the Wnt signalling pathway (*BCL9, TLE3*). *BCL9* is a core component of the nuclear β-catenin complex and regulates Wnt target gene transcription (Makena et al., 2019). *TLE3* is a Wnt transcriptional repressor (Gessler et al., 2024; Kalita et al., 2024).

The Capan-1TalR cell line gained 53 coding alterations in comparison to the parental cells, of which 30 were selected for further analysis. Again, mutations were found in four genes involved in metabolism (*SLC2A1, FITM1, ATP5MPL*, and *PRSS53*). *FITM1* is involved in fat storage (G. Wang et al., 2022); *ATP5MPL* is a component of ATP synthase complex V (He et al., 2018; Makoto et al., 2014); *PRSS53* is a serine protease whose expression affects Glut2 expression (Noriko et al., 2022); and *SLC2A1* is a glucose transporter that is also affected by Wnt signalling (Liu et al., 2016; Ooi & Gomperts, 2015). Additional mutations were also found in the Wnt pathway (*SDC3, RASSF5, VAX1*). *SDC3* integrates multiple pathways, including Wnt (Hillemeyer et al., 2022). *RASSF5* and *VAX1* inhibit canonical Wnt signalling (Murphy et al., 2022; Schmidt et al., 2014).

4.2.9 Validation of altered pathways by Western blot

Based on the transcriptomic and metabolomic profiling, the expression of several possible resistance markers was evaluated by Western blotting (Fig. 4.26). No changes in expression were observed for cytochrome c oxidase subunit 4 (Cox4) or glycogen synthase kinase 3 beta (GSK3β). In contrast, a significant decreased expression was observed for full-length β-catenin in Capan-1CisR and Capan-1TalR ($p<0.0001$) which corresponded with increased expression of its 85 and 65 kDa cleavage products. In addition, an increase in expression of E-cadherin was observed in the Capan-1CisR ($p=0.003$) and Capan-1TalR ($p=0.07$), which corresponded with a decrease in its 65 and 45 kDa cleavage products.

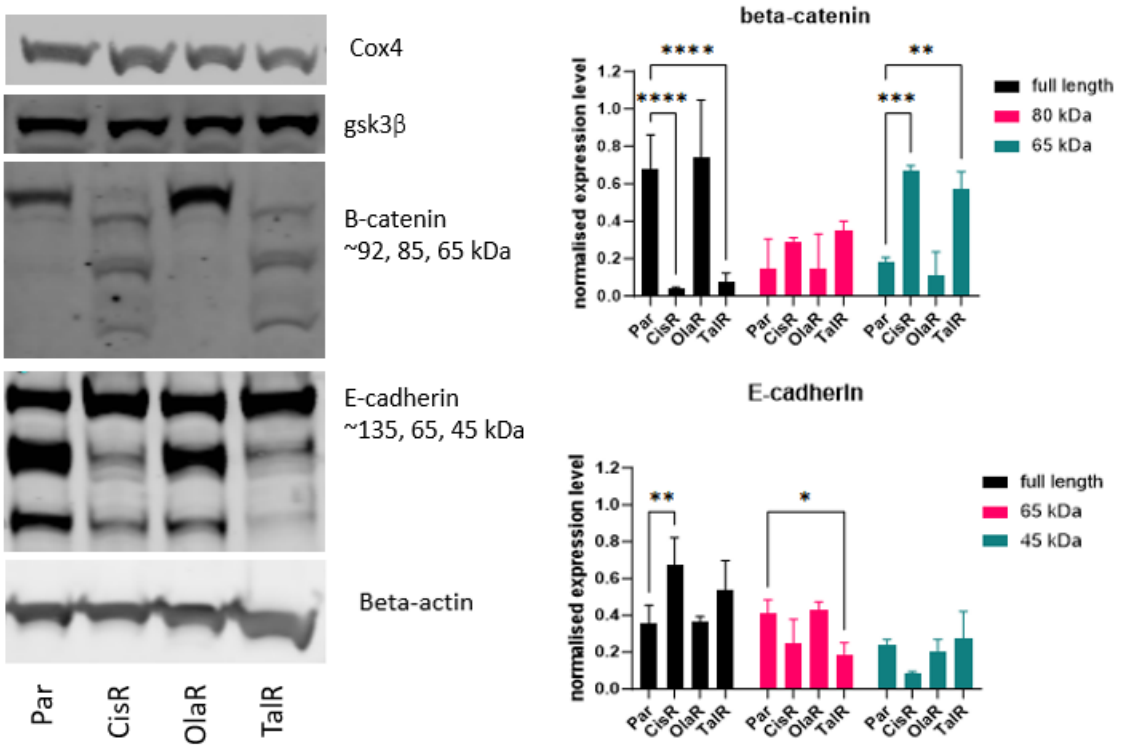

Figure 4.26. Protein expression levels of COX4, GSK3β, β-catenin and E-cadherin as possible resistance markers*. Protein separation and detection was performed by Western blotting, protein band intensity as a measure of protein quantity was performed in ImageJ. Statistical comparison of resistant cells versus parental cells for beta-catenin and E-cadherin by ANOVA followed by Dunnett's multiple comparisons test (*: $p<0.05$, **: $p<0.005$, ***: $p<0.0005$, ****: $p<0.0001$)(n=3).*

4.3 DISCUSSION

4.3.1 Establishment of resistant cell lines

Drug resistance in advanced and metastatic pancreatic cancer is one of the leading causes of treatment failure and cancer-related death. While targeted therapies such as PARP inhibitors have improved PFS, these therapies are also especially susceptible to acquired resistance because of their targeted nature. Additionally, cancer cells may develop resistance mechanisms that cause cross-resistance to other drugs thus further decreasing the possibility of successful treatment.

In this thesis, the *BRCA2* mutant PDAC cell line Capan-1 was used to establish platinum and PARPi resistant cells to study the mechanisms of resistance. The cells were treated semi-continuously with cisplatin, olaparib, and talazoparib to develop polyclonal resistant cell line pools that mimic the heterogeneity of the tumour. Resistance mechanisms were investigated using genomic, transcriptomic, and functional assays.

4.3.1.1 Cisplatin

Cisplatin is one of the oldest chemotherapeutic agents and has been used in the clinic since the 1970s to treat a variety of cancers. It belongs to the class of platinum agents and functions by creating DNA damage and thereby inducing apoptosis. The drug is activated intracellularly where its chloride atoms are replaced by water molecules. This creates a highly reactive electrophile that can react with purine residues in the DNA causing 1,2-intrastrand cross-links and other DNA adducts (Dasari & Tchounwou, 2014). Induction of DNA damage is especially lethal in tumour cells with impaired DDR, especially HR deficiency, since these cells are unable to repair cross-links effectively.

In a recent phase II trial patients with previously untreated stage III or IV and pathogenic germline *BRCA* or *PALB2* mutated PDAC were treated with a combination of cisplatin and gemcitabine (O'Reilly et al., 2020). Treatment was administered in 21-day cycles, where patients received 25 mg/m^2 cisplatin and 600 mg/m^2 gemcitabine on day 3 and 10. The trial had a 65.2% response rate, with a median PFS and OS of 9.7 months and 16.4 months, respectively. As a result the combination of cisplatin with gemcitabine has been approved for PDAC patients with germline *BRCA* mutations (Conroy et al., 2023). However, this trial also highlights the issues with both intrinsic and acquired drug resistance.

To investigate the mechanisms of cisplatin resistance the Capan-1CisR cell line was generated by semi-continuous treatment of Capan-1 cells with cisplatin. The Capan-1CisR cells exhibited a 4.8-fold increase in IC_{50} value compared to the parental cells. The resistant cells also had a considerably shorter doubling time (1.31 vs. 2.0 days).

4.3.1.2 PARP inhibitors

Olaparib and talazoparib are both PARP inhibitors. Olaparib has been approved for clinical use in patients with germline *BRCA* mutated metastatic PDAC based on the POLO trial (Golan et al., 2021). Talazoparib is a novel agent and is currently under evaluation in multiple clinical trials.

PARPi have a dual mechanism of action. PARPi were originally developed to inhibit PARP1/2 protein function and thereby impair SSB repair resulting in the accumulation of SSBs and progression into DSBs. In combination with HR deficiency, the DSBs cannot be repaired leading to cell cycle arrest and apoptosis. However, PARPi also trap PARP1/2 protein at the DNA which blocks the progression of the replication fork machinery during DNA synthesis and causes replication fork stalling and collapse. This means that PARPi not only hinder SSB repair but also create DNA damage. The PARP trapping potency differs between PARPi, with talazoparib having a 100 to 1000-fold higher trapping potency than olaparib (Rudolph et al., 2022). In line with this, the *in vitro* cytotoxicity of several PARP inhibitors has been correlated to their PARP trapping potency rather than their catalytic inhibition (Murai et al., 2012; Murai et al., 2014; Rudolph et al., 2021). Differences in PARP protein inhibition and PARP trapping potency between PARPi may lead to differences in mechanism of resistance. To study the mechanism of resistance to two major PARPi used in PDAC olaparib and talazoparib resistant Capan-1 cells were generated.

Capan-1OlaR was generated by semi-continuous treatment of Capan-1 cells with olaparib over a period of 165 days. The Capan-1OlaR cell line exhibited an over 3.1-fold increase in IC_{50} concentration (>100 µM vs. 32 µM) and the Capan-1TalR cell line exhibited an over 18-fold increase in IC_{50} concentration (>20 µM vs. 1.1 µM). The doubling time of both resistant cell lines was slightly, but not significantly, shorter compared to the parental cells.

There have been several other studies on olaparib and talazoparib resistance in Capan-1. Guo et al. established olaparib-resistant cells by treating Capan-1 cells with increasing concentrations of olaparib, ranging from 0.125 to 8 µM (Guo et al., 2022). Cells were

treated for 35 days, were allowed to recover in drug-free media, and were then treated at a higher concentration for another 35 days. In total, cells were exposed to six treatment cycles. The resultant resistant cells, termed Capan-1OP, had a 77.5-fold change in IC_{50}, from 2 µM in the parental to over 100 µM in Capan-1OP. In addition, Capan-1OP showed a significant cross-resistance to talazoparib (1 µM versus 6 nM, $p<0.005$). Similarly, Chen et al. established olaparib- and talazoparib-resistant Capan-1 cells by exposing cells to increasing concentrations of drug ranging from 1 to 60 µM for olaparib, and 25 to 500 nM talazoparib over a period of 246 and 169 days, after which they subcloned the population to establish Capan-1/OP and Capan-1/TP (Chen et al., 2020). The olaparib-resistant Capan-1/OP had a 46-fold increase in IC_{50}, from approximately 0.55 µM in the parental cells to 60 µM in Capan-1/OP. The talazoparib-resistant Capan-1/TP had a 70-fold increase in IC_{50}, from approximately 0.07 µM to 1.5 µM.

There are a couple of interesting similarities and differences between these two studies and the work in this thesis. Firstly, the IC_{50} values for both PARP inhibitors in the parental cells differ between studies. The IC_{50} value for olaparib in this thesis is markedly higher. The IC_{50} value for talazoparib, however, is in the same range as the value found by Chen et al.

Secondly, both studies expose the cells to concentrations of olaparib that are more than 100-fold higher than what we used and for a longer period of time. These concentrations are also well above the maximum plasma concentration, raising questions regarding how well these models represent the *in vivo* situation. Additionally, the starting concentration used by Chen et al. was higher than the concentration that induced senescence in our cells, despite our cells having a higher initial IC_{50} concentration. While the researchers did not mention the presence of senescence during the development of resistance, prolonged drug exposure may have selected for a small subpopulation of cells that escaped or avoided senescence.

Despite the differences in development of PARPi resistance between this thesis and these two studies that would suggest the cell lines developed by Guo and Chen would have a higher resistance due to their prolonged and more intense drug exposure, the sensitivity of all three resistant olaparib models is in a similar range.

In contrast, our Capan-1TalR model is substantially more resistant than the Capan-1/TP developed by Chen et al., despite the parental cells having a similar drug sensitivity and our cells being exposed to lower drug concentrations.

These findings imply that how resistant cells are generated affects their level of resistance, and exposure to high concentrations of drug do not necessarily lead to more resistance. We therefore suggest that using concentrations that are more representative of the concentrations seen *in vivo* is preferred as it may avoid the development of resistance mechanisms that are only seen at these unrealistically high concentrations.

4.3.2 Cross-resistance to chemotherapy

Cross-resistance profiling showed a significant increase in resistance in all three resistant cell lines for oxaliplatin, with fold changes ranging between 2.2 and 4.7. Additionally, Capan-1TalR, but not Capan-1OlaR, showed significant cross-resistance to cisplatin (8.3 FC) and FOLFIRINOX (7.8 FC). However, none of the resistant cell lines showed significant cross-resistance to gemcitabine or 5-FU.

The cross-resistance profile for olaparib in literature is varied. Gajan et al. established a *BRCA1* wild-type and *BRCA1* mutant olaparib-resistant triple negative breast cancer cell line (Gajan et al., 2021). Both cell lines retained their original sensitivity to cisplatin. In contrast, Kim et al. developed four gastric cancer olaparib-resistant cell lines of which three showed significant cross-resistance to cisplatin (Kim;, Min, et al., 2020). Similarly, an olaparib-resistant *BRCA1* knock-out clone of PDAC cell line MiaPaCa-2 established by Sasaki et al. acquired a 2.7-fold increase in IC_{50} to cisplatin as well as an over 30-fold increase in IC_{50} to talazoparib (Sasaki et al., 2024) which is line with the cross-resistance observed between our two PARPi-resistant Capan-1 cell lines.

4.3.2.1 PARPi to chemotherapy cross-resistance in patients

Clinical studies of cross-resistance between PARPi and chemotherapy are limited but suggest that PARPi may cause cross-resistance to chemotherapy. Frenel et al. performed post-hoc analysis of the efficacy of chemotherapy after progression on olaparib or placebo in patients with *BRCA1/2* mutated platinum-sensitive recurrent epithelial ovarian cancer that participated in the SOLO2 trial (Frenel et al., 2020). They found that patients who had progressed on olaparib treatment had a significantly shorter PFS on their second-line chemotherapy compared to patients who had received a placebo (7 months vs. 11.1

months, respectively. HR 1.93; 95% CI [1.35-2.76]). This difference was even stronger in the patients receiving platinum-based chemotherapy with a PFS of 7 months in the olaparib group and 14.3 months in the placebo group. For non-platinum therapy this difference was 5.5 and 8.3 months, respectively. However, the difference in PFS on second-line chemotherapy did not affect the OS. These findings were corroborated by Park et al. who collected data of 197 epithelial ovarian cancer patients with *BRCA* mutation who received platinum treatment, 105 of whom received olaparib as maintenance treatment and 92 who did not (Park et al., 2022). Patients receiving olaparib had a longer PFS than those who did not, but the time from progression on olaparib to progression on second-line treatment was significantly shorter (7.9 months versus 13.6 months, p=0.0005). Over 67% of the patients received platinum treatment and less than 20% received non-platinum treatment but the PFS of these subgroups was not analysed.

The cross-resistance found in the PARPi-resistant Capan-1 cell lines to platinum but not non-platinum treatments confirms the difference in cross-resistance seen in the SOLO2 trial. These results indicate that patients who have progressed on PARPi may respond better to non-platinum chemotherapies.

4.3.3 Invasion and migration in resistant cells

Acquired resistance after systemic therapy is often encountered in the clinic and may result in more aggressive disease including metastasis. To study the relationship between cisplatin/PARPi resistance and invasion/migration the invasion and migration status of the parental and resistant Capan-1 cells was investigated. A significant 1.57-fold increase in migration was found for Capan-1CisR (p=0.035) but not for Capan-1OlaR or TalR. Additionally, no significant differences were found in invasion in any of the three resistant cell lines. Multiple studies have reported increased migration and invasion in cell lines with acquired cisplatin resistance (Bahar et al., 2020; Hou et al., 2019; Liu et al., 2017). Similarly, Guo et al. found that their olaparib-resistant Capan-1 cells had a 1.7-fold increase in both invasion and metastasis.

4.3.4 Validation of existing resistance mechanisms

Molecular alterations of PARPi target PARP1, drug efflux pump ABCG2, and HR protein BRCA2 have previously been associated with acquired resistance to PARPi. To validate if these proteins are mediators of resistance in our resistant cells the expression of PARP1

and ABCG2 was investigated by Western blotting. The mutation status of all three genes was investigated using whole exome sequencing, but no additional mutations were detected. Expression of PARP1 was significantly reduced in Capan-1CisR and Capan-1TalR but not in Capan-1OlaR. Loss of PARP1 expression has been associated with acquired resistance and is hypothesised to protect the cell from the formation of cytotoxic PARP-DNA complexes (Murai et al., 2012; Pettitt et al., 2018). Decreased PARP1 protein expression in the Capan-1CisR cells was unexpected as PARP1 overexpression has previously been associated with cisplatin resistance (Michels et al., 2013), although this could explain the observed cross-resistance to olaparib and talazoparib.

Downregulation of ABCG2 protein expression was observed in all three resistant cell lines. ABCG2 is a multidrug transporter and is commonly upregulated in resistant cancers (Mo & Zhang, 2012; Tang et al., 2014; Teng et al., 2024). The effect of downregulation on acquired cisplatin or PARPi resistance is unclear and warrants further investigation.

Genomic reversal of *BRCA2* mutation to restore protein function is a common mechanism of acquired PARPi resistance and has also been reported in acquired cisplatin resistance (Dhillon et al., 2011; Fu et al., 2024; Sakai et al., 2008). While no additional mutations were observed in the resistant cells compared to the parental Capan-1 cells, Capan-1OlaR and Capan-1TalR had gained one copy and Capan-1CisR had gained two copies. Amplification of the truncated *BRCA2* allele has been reported before in Capan-1 cells that had acquired resistance to PARPi olaparib and rucaparib (Park; et al., 2020). Amplification resulted in increased protein expression and the truncated protein was observed to interact with DDR protein RAD51 and DOT1L suggesting that BRCA2 may have retained some functionality.

4.3.4.1 Multi-drug transporter ABCG2

Intrinsic and acquired drug resistance is one of the main causes for cancer treatment failure and cancer-associated death. Multi-drug resistance (MDR) is generally caused by increased drug clearance or inactivation and can confer cross-resistance to molecularly diverse drugs. One of the mechanisms of resistance to cisplatin that has previously been reported is overexpression of multi-drug transporter *ABCG2* (Marin et al., 2022; Mo & Zhang, 2012; Xu et al., 2007). *ABCG2* is a transmembrane transporter that has a wide range of biological and chemical compounds as its substrates. Overexpression of *ABCG2* expression as a result of acquired cisplatin resistance has been reported in the NSCLC cell lines H460 and A549 (Tang

et al., 2014). However, no change in expression of *ABCG2* was seen in the ovarian cancer cell line with acquired cisplatin resistance OVCAR8 (Patel et al., 2021). Induction of *ABCG2* can also be transient in response to cytotoxic treatment and may be associated with cancer stem cells in PDAC (Kuo et al., 2023; Yin et al., 2011). Additionally, overexpression of *ABCG2* has also been associated with acquired talazoparib resistance in the ovarian cancer cell line A2780/T4 (Teng et al., 2024) and acquired olaparib resistance in the ovarian cancer cell line UWB1.289 (Klotz et al., 2023-07-25). Interestingly, UWB1.289 is *BRCA1*-deficient and expression of *ABCG2* was reduced in a UWB1.289 model with restored *BRCA1* expression and acquired olaparib resistance. Similarly, in this chapter, a significant 41% to 71% decrease in *ABCG2* expression was observed in all three resistant Capan-1 cell lines. These studies suggest that the role of *ABCG2* in mediating acquired resistance might not be as clear cut as it was thought to be, and more research is necessary to elucidate this.

4.3.4.2 PARP1 protein expression

One of the mechanisms of resistance to PARPi that have previously been described is the loss of functional *PARP1* expression. As mentioned previously, part of PARPi toxicity stems from PARP-trapping on the DNA which interferes with DNA replication. Knockout and knockdown of *PARP1* in the DT40 chicken lymphoma cell line has been shown to strongly induce olaparib resistance (Murai et al., 2014) and loss of *PARP1* expression was observed in the HCT116 colon cancer cell line with acquired temozolomide/veliparib resistance (Liu et al., 2009). In addition, several mutagenesis screens in mouse embryonic stem cells have identified mutation and subsequent loss of function of *PARP1* to be the main cause for PARPi resistance (Herzog et al., 2018; Pettitt et al., 2018; Pettitt et al., 2013). In depth evaluation of the mutation sites revealed that most mutations were located in the DNA-interacting regions. One of the mutations discovered in the screen was also identified in an ovarian cancer patient with *de novo* olaparib resistance.

In line with these findings, a significant decrease of PARP1 protein levels was observed in Capan-1TalR. However, no significant change in PARP1 protein levels was observed in Capan-1OlaR suggesting that a different resistance mechanism might be involved in these cells. A significant decrease in PARP1 protein level was also observed in the Capan-1CisR cells. This is in contrast with previous studies that have reported increased PARP1 expression in cisplatin resistant cells (Michels et al., 2013; Singh et al., 2019; Wang et al., 2017) and points to the presence of alternative resistance mechanisms.

4.3.5 γH2AX and RAD51 foci formation

γH2AX and RAD51 foci are both well-established markers of DNA damage recognition and homologous recombination mediated repair, respectively (Valdiglesias et al., 2013; Wijk et al., 2022). Phosphorylation of histone H2AX at Ser-139 to form γH2AX occurs at the site of DSBs and this modification spreads to neighbouring H2AX histones which can be detected as the formation of γH2AX foci. While γH2AX foci formation is a commonly used marker for DSB detection, γH2AX is also generated at damaged or stalled replication forks caused by replicative stress (Alexander & Orr-Weaver, 2016; Fragkos et al., 2023; Mah et al., 2010). In both instances γH2AX foci formation results in the recruitment and activation of DDR proteins, including BRCA1/2. During the S/G2 phase of the cell cycle, HR repair is initiated through recruitment of RAD51 by BRCA2 (Merighi et al., 2021; Summers et al., 2011). The *BRCA2* mutation found in Capan-1 results in a truncated protein that has no nuclear localisation signal, remains sequestered in the cytoplasm, and is unable to recruit RAD51 (Dréan et al., 2017; Tarsounas et al., 2003). However, γH2AX formation is unaffected because it is upstream of BRCA2 (Dréan et al., 2017). As expected, no RAD51 formation upon treatment was observed in either the parental or resistant cells. This indicates that recruitment by BRCA2 is still impaired in the resistant cells (which is in accordance with the lack of secondary mutation in *BRCA2* as observed by WES) and that the resistant cells have not developed a way to bypass the impaired recruitment to improve DDR.

A small but not significant increase in γH2AX foci was observed in the resistant cells. The foci formation that was seen was highly heterogeneous between cells ranging from no or few foci to so many foci that individual foci could no longer be distinguished. This possibly indicates that there are subpopulations of sensitive and resistant cells in the parental line and that cells with intrinsic resistance have expanded in the resistant lines.

4.3.6 Metabolomic alterations contribute to resistance

To identify novel mechanisms of resistance to cisplatin and PARPi transcriptomic profiling of the parental and resistant cells was performed. A total of 543 DEGs in Capan-1CisR, 2029 DEGs in Capan-1OlaR, and 1981 DEGs in Capan-1TalR were found. The majority of the DEGs were downregulated compared to the parental cells. Multidimensional scaling showed that the Capan-1CisR cells were most similar to the parental cells and that the PARPi resistant cells were more dissimilar from each other than from the parental cells which suggests that these cell lines have different resistance mechanisms. KEGG pathway analysis found

significant enrichment of the metabolomic and oxidative phosphorylation pathways in all three resistant cell lines. Because both of these pathways are associated with energy production and metabolism, *in vitro* metabolomic profiling was performed.

PDAC is a highly heterogeneous disease, and this is reflected in the metabolomic profile of cancer cells. Masoud et al. performed metabolomic characterisation of six established PDAC cell lines and 21 primary PDAC PDX cell lines and found considerable differences between the OCR and ECAR of these cells, leading the researchers to make a distinction between high and low OxPhos cells. In their experiments Capan-1 was characterised as having a less metabolic status, meaning that it had both low OCR (OxPhos) and ECAR (glycolysis) compared to the other cell lines. Interestingly, they also concluded that there was no correlation between the proliferation rate and the metabolomic status. Similarly, the three resistant cell lines developed in this chapter had different metabolomic profiles despite all having a higher proliferation rate.

Metabolomic characterisation of the parental and resistant Capan-1 cell lines was performed using a Seahorse assay to measure OCR and ECAR as measures of OxPhos and glycolysis, respectively. No significant alterations were observed in either the ECAR or OCR for Capan-1CisR, although a small but significant decrease was found in the ratio between the two. This suggests that the overall energy production in the Capan-1CisR cells is slightly lower than in the parental cells and that they are more dependent on OxPhos. In addition, the Capan-1CisR cells also had a significantly higher maximal respiration, which is indicative of a good mitochondrial status (Jang et al., 2017). A significantly increased ECAR and a small but significantly increased ECAR/OCR was observed in the Capan-1OlaR cell line, indicating that the cells have increased glycolysis. In contrast, a significantly increased OCR and ECAR/OCR was observed in the Capan-1TalR cell line, indicating an increased OxPhos. Since the change in ECAR/OCR in Capan-1OlaR and TalR was caused by an increase in either ECAR or OCR, this suggests that the overall energy production was higher compared to the parental cells, which is in accordance with the increased proliferation rate.

While metabolomic reprogramming favouring glycolysis is generally associated with cancer, metabolic reprogramming favouring oxidative phosphorylation, like that observed in the Capan-1CisR and TalR cells, has also been described to contribute to cisplatin resistance. Metabolism is a complex network of interacting pathways and so a variety of alterations can contribute to metabolic shift. The next section will discuss several

previously reported alterations and how these may relate to the observations in the cisplatin and PARPi resistant cell lines.

4.3.6.1 Glucose consumption

Reduction in glucose consumption due to the downregulation of glucose transporter GLUT-1 has been shown to decrease proliferation and protect against chemotherapies that target rapidly proliferating cells. In this case, downregulation of glycolysis is due to a decrease in available substrate (glucose) and prevents the cells from creating the building blocks necessary for proliferation. However, as mentioned before, all three of the resistant Capan-1 cell lines had an increased proliferation compared to the parental cells, suggesting that the observed metabolic shift is not directly associated with proliferation. This is in accordance with the Masoud et al., who performed metabolomic characterisation of six established PDAC cell lines and 21 primary PDX cell lines (Masoud et al., 2020). They found considerable differences in the OCR and ECAR between samples, leading them to make a distinction between less metabolic, energetic, high OxPhos, and high glycolysis cell lines. However, they found no correlation between the proliferation rate and the metabolomic status.

4.3.6.2 Interaction between metabolism and DNA repair

Metabolism and DNA repair are connected and influence each other. Metabolism produces the nucleotides and NAD+ that are necessary for DNA repair but also produces ROS which can induce DNA damage. Lahiguera et al. showed that HRD tumours rely on OxPhos for the production of NAD+ (Lahiguera et al., 2020). While NAD+ is a relatively common substrate for a variety of enzymes it is predominantly used by PARP proteins in DNA repair. Studies in ovarian and breast HRD preclinical models showed that HRD models have enhanced OxPhos and decreased glycolysis. Enhanced OxPhos contributed to PARPi resistance whereas induction of glycolysis sensitised to PARPi.

In line with this, olaparib has been shown to increase TCA cycle activity which, together with increased OxPhos, resulted in olaparib resistance in triple-negative breast cancer cell lines (Furusawa et al., 2024). High OxPhos and low glycolysis create glutamine dependency in order to obtain the carbon and nitrogen that are needed for nucleic acid synthesis and that under normal glycolysis conditions would have been derived from glycolysis intermediates (Wangpaichitr et al., 2021). As a result, glutamine depletion can resensitise

cisplatin-resistant NSCLC cells (Obrist et al., 2018). However, PARPi by PJ-34, talazoparib, or veliparib did not reverse starvation-induced death suggesting increased OxPhos is not solely induced to improve DDR through PARP. Indeed, the Capan-1CisR and TalR cells developed in this chapter had decreased PARP1 protein levels in conjuction with increased OxPhos indicating that there is not necessarily a correlation between OxPhos and PARP-mediated DDR.

In contrast, OxPhos produces reactive oxygen species that can induce DNA damage and metabolic reprogramming in favour of glycolysis to protect from endogenous DNA damage, while at the same time also producing intermediates for DNA replication and repair without becoming dependent on glutamine. Wang et al. observed that olaparib-resistant ovarian cancer cells were more dependent on glycolysis and had increased expression levels of multiple glycolytic proteins including glucose transporters Glut1/2 and glycogen synthase kinase 3 Gsk3β (Wang et al., 2017). While increased glycolysis was observed in Capan-1OlaR no changes in protein expression of Gsk3β were observed in any of our resistant Capan-1 cell lines.

The question remains why the Capan-1OlaR cells have a different change in metabolism than the Capan-1CisR and TalR cells, especially since olaparib and talazoparib both target PARP. Recently, Zampieri et al. found that olaparib, but not talazoparib, is also a mitochondrial complex I inhibitor (Zampieri et al., 2021). In a parental and temozolomide-resistant glioblastoma cell line, olaparib fully reverted temozolomide resistance and decreased mitochondrial OCR whereas talazoparib had no effect on mitochondrial OCR. Enzymatic evaluation of mitochondrial complex activity found that olaparib significantly inhibits complex I activity but did not affect the other complexes.

4.3.6.3 Mutations in metabolism-associated genes

To elucidate further the mechanisms of acquired resistance and alterations in metabolism, whole exome sequencing analysis was performed. Mutation of histone deacetylase *HDAC11* was found in Capan-1CisR. Mutation and expression of *HDAC11* have been associated with prognosis is many cancer types. In a pan-cancer analysis, *HDAC11* was found to have both positive and negative correlations with OS and PFS in multiple cancer types although no significant difference was found in PDAC (Li et al., 2022). Additionally, in the same paper, *HDAC11* expression was negatively correlated with sensitivity to multiple

chemotherapies including oxaliplatin. In a hepatocellular carcinoma mouse model, depletion of *HDAC11* reduced tumorigenesis by inhibition of glycolysis which in turn led to the suppression of cancer stem cells (Bi et al., 2021). The induction of resistance to oxaliplatin and the inhibition of glycolysis are both observed in the Capan-1CisR cells.

Cytochrome c oxidase subunit 6B2 (*COX6B2*) was observed to have acquired an upstream gene variant with a modifying function in Capan-1OlaR. *COX6B2* mRNA expression is increased in PDAC and is associated with poor prognosis (Nie et al., 2020). However, *COX6B2* knockdown in three PDAC cell lines did not affect cell growth but did decrease mitochondrial complex IV and inhibited OxPhos. Additionally, knockdown decreased invasion and migration ability. Decreased oxidative phosphorylation was also observed in our Capan-1OlaR cells although there was no significant change in expression of COX4 which is another member of mitochondrial complex IV. Additionally, we also did not observe significant changes in invasion or migration ability in Capan-1OlaR.

SLC2A1, also known as *GLUT1*, was found to have acquired an insertion leading to a frameshift variant. *SLC2A1* mRNA expression is aberrated in most cancers and is significantly upregulated in PDAC which correlates with poor prognosis (Wang et al., 2023). Metabolomic profiling of 28 PDOs found that *SLC2A1* was upregulated in organoids with high glucose metabolism and knockdown decreased ECAR (Li et al., 2023). Additionally, shRNA-mediated knockdown of *SLC2A1* increased sensitivity to 5-FU and gemcitabine. While a shift towards OxPhos was observed in our Capan-1TalR cells, no significant changes were observed in the ECAR. The Capan-1TalR cells also did not have increased sensitivity to 5-FU or gemcitabine.

4.3.6.4 Targeting metabolism in the clinic

Metabolism is a burgeoning field in PDAC research and while targeted therapies against metabolism are still a long way from routine treatment there a numerous clinical trials running that investigate a variety of metabolomic pathways (Stine et al., 2021; Wu et al., 2024). One of the treatments that is receiving a considerable amount of attention is the metabolic regulator metformin (Zamanian et al., 2024). Metformin has been shown to increase the production of reactive oxygen species and decrease the mitochondrial membrane potential through release of cytochrome C and increased olaparib sensitivity in ovarian cancer cell lines (Gralewska et al., 2021). Additionally, metformin was shown to

reverse epithelial to mesenchymal transition (EMT) upon olaparib treatment in triple-negative breast cancer cells (Han & Li, 2019). While the Capan-1OlaR cells did not show a significant change in EMT proteins β-catenin or E-cadherin, a significant loss of β-catenin and increase in E-cadherin protein expression was observed in Capan-1CisR and Capan-1TalR. As these two cell lines had an increase in OxPhos, which is likely to increase the production of ROS, this might pose a vulnerability that can be targeted by metformin.

4.4 CONCLUSION

In this chapter we successfully established cisplatin, olaparib, and talazoparib-resistant *BRCA2*-mutant Capan-1 cells. The cell lines showed significant cross-resistance to cisplatin, PARPi, and oxaliplatin, but not to 5-FU or gemcitabine. 5-FU and gemcitabine may therefore be more suitable second-line treatment agents rather than oxaliplatin or FOLFIRINOX.

Investigation of resistance mechanisms found similar alterations in cisplatin and talazoparib-resistant cells that were not found in olaparib-resistant cells. The difference between the two PARPi may be explained by their difference in PARP-trapping potency. Talazoparib has a considerably higher PARP-trapping potency which is more likely to cause replication fork collapse and DNA damage thus conferring a more genotoxic effect similar to chemotherapy and could explain the similarities with Capan-1CisR. Transcriptomic, genomic, and metabolomic profiling found significant alterations in metabolism. Capan-1CisR and Capan-1TalR favoured oxidative phosphorylation whereas Capan-1OlaR favoured glycolysis. Several mutations were found that may contribute to this metabolomic shift but more research is needed to validate and target these alterations.

4.4.1 Future work

1. Further evaluation of the observed metabolomic shift in the resistant cells by serum starvation assays to determine substrate dependency. This will also provide information on how to target resistant cells.
2. Investigation of the contribution of the genetic alterations identified here to resistance by gene knockdown in sensitive cells and gene transfection in resistant cells.

5 TARGETING DNA DAMAGE REPAIR DEFICIENCY IN PDAC

5.1 INTRODUCTION

The PARPi olaparib is approved for treatment of patients with germline *BRCA1/2* mutant advanced PDAC which is stable following treatment with platinum-based chemotherapy. The *gBRCA* PDAC population only accounts for approximately 3-17% of familial PDAC patients and 5-7% of the general patient population (Lai et al., 2021). However, mutations in DDR genes are common in PDAC and can be found in up to 43% of the patient population, suggesting that there is potential to expand therapy to other patients. Additionally, combination treatment of two DDR inhibitors may be synergic and could be used to either prevent development of resistance or be applied in DDR proficient patients.

In other cancers, CRISPR/Cas9 knockout screens have been used to investigate synthetic lethality with olaparib for larger gene panels but to our knowledge this has not been applied to PDAC or talazoparib (Ipsen et al., 2022; Jamal et al., 2022; Zimmermann et al., 2018).

CRISPR/Cas9 knockout screening is a powerful tool to identify possible synthetic lethal interactions between a drug and a large number of genes (He et al., 2021; Shalem et al., 2015). By using an sgRNA library that targets the genes of interest, a mixed population of cells with a different gene knocked out in each cell can be created. This mixed population is treated with drug or a media control and the presence of each sgRNA after treatment is quantified by NGS. Loss of an sgRNA, or gene depletion, indicates that the gene is synthetic lethal with the treatment whereas an increase in sgRNA, or gene enrichment indicates that the gene confers resistance to treatment.

In this chapter, two sgRNA libraries are used, one which targets 100 major DDR genes and another which targets 1052 protein kinase (PK) genes. The DDR library was selected because loss of DDR genes is most likely to confer synthetic lethality with PARPi based on the known synthetic lethality of *BRCA1/2* and *PALB2*. The PK library was selected because protein kinases are relatively easy to inhibit pharmacologically and may therefore be used to identify synergic drug combinations. Both screens were treated with media (control), olaparib, or talazoparib. From the top fifteen most significantly depleted sgRNAs four genes (*NEIL1, PTEN, XRCC3,* and *BRCC3*) were selected for further validation by siRNA. siRNA

knockdown was achieved for *PTEN, XRCC3,* and *BRCC3*, but not *NEIL1.* Viability and colony formation assays showed that knockdown of *PTEN, XRCC3,* or *BRCC3* significantly sensitises to olaparib and talazoparib treatment.

There are currently no targeted inhibitors available for BRCC3 or XRCC3 in clinical trials. We therefore investigated whether alternative DDR inhibitors can also overcome PARPi resistance in *BRCA2*-deficiant cells. Two targeted therapies that are promising are ATM and ATR inhibitors. Both proteins are major regulators in double-strand break repair and signalling (Wagh et al., 2020). ATM deficiency as well as ATR inhibition have been shown to sensitise to chemotherapy in pancreatic cancer (Höfer et al., 2024; Wallez et al., 2018). Additionally, the combination of olaparib and ATR inhibition sensitises to radiotherapy in HR proficient PDAC (Parsels et al., 2021). Combination of PARPi and ATRi in ATM deficient PDAC has also been shown to be synergic (Jette et al., 2020; Lloyd et al., 2020). At the time of writing several clinical trials are ongoing to evaluate the safety and efficacy of the combination of ATR inhibitor AZD6738 and olaparib in solid tumours (NCT03682289, NCT03787680, NCT03878095). In this section we investigate whether experimental ATMi (AZD1390) or ATRi (AZD6738) alone or in combination with PARPi (Lynparza, talazoparib, AZD5305) can overcome treatment resistance in our *BRCA2*-mutated Capan-1 cell lines. Additionally, we investigate possible mechanisms of action by looking at the expression of various proteins, γH2AX and RAD51 foci formation, and cell cycle status.

5.1.1 Aims

The overarching aim of this chapter is to identify novel targets that sensitise to PARPi (olaparib and talazoparib), and which are mutated or can be inhibited in PDAC.

Objective 1: Perform a CRISPR knockout screen in the Panc-1 cell line to discover novel protein kinase or DDR genes that act as a synthetic lethal partner for PARP inhibitors.

- Validate selected targets in viability and colony formation assays using siRNA.

Objective 2: Combine novel ATM/ATR and PARP inhibitors in the previously developed resistant Capan-1 cell lines to overcome resistance.

- Evaluate the efficacy of the combination by viability and colony formation assay.
- Study the effect on DNA damage by immunofluorescent imaging of RAD51 and yH2AX foci formation.
- Study the mechanisms of action by analysing protein expression.

5.2 RESULTS

5.2.1 CRISPR screen analysis

The DDR proficient cell line Panc-1 was selected for CRISPR screening (Chapter 2.12). The cells were infected with lentivirus containing a DDR or PK sgRNA library and treated for 3 days with the approximate IC_{10} concentration of each PARPi (1.2 µM olaparib or 2.5 nM talazoparib (Fig. 5.1)). The cells were harvested, the DNA was extracted and amplified by PCR with sgRNA-specific primers.

While each sample contained an equal amount of cDNA for sequencing, the resulting sequence counts and coverage varied (Fig. 5.2). The DDR screen had 9.3-18.3 million counts, with library coverage ranging from 19,400-383,000x. The PK library had a slightly lower coverage, with 1.3-14.1 million counts and a 183-1,989x coverage. Despite one of the control samples for the PK library having considerably lower coverage than other samples, its coverage of 183x remained acceptable for analysis.

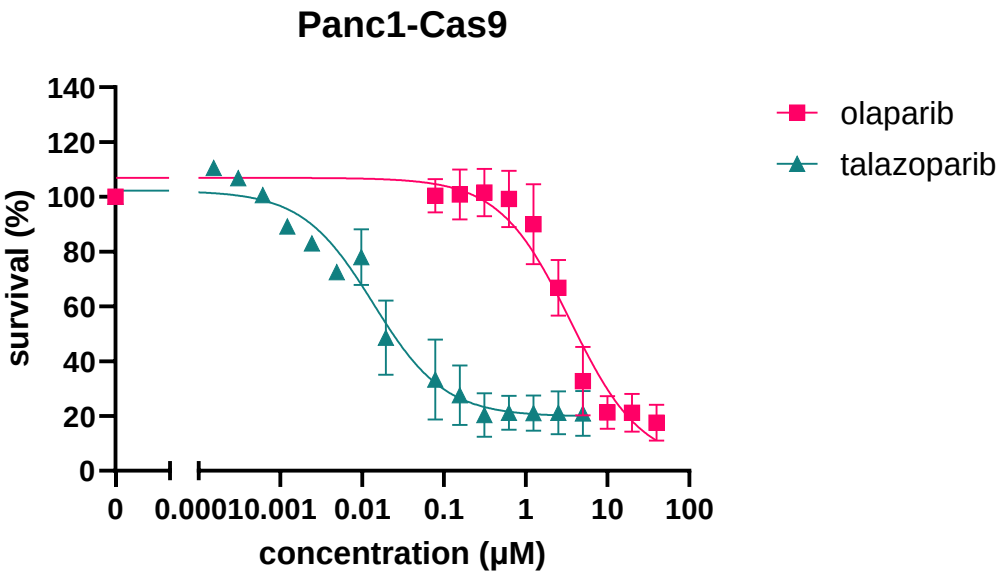

Figure 5.1. Viability assay for Panc-1 expressing Cas9 to determine the treatment concentrations for the CRISPR screen. *Cells were treated for 7 days. Viability was measured using CellTiter Glo and normalised against untreated control (n=3).*

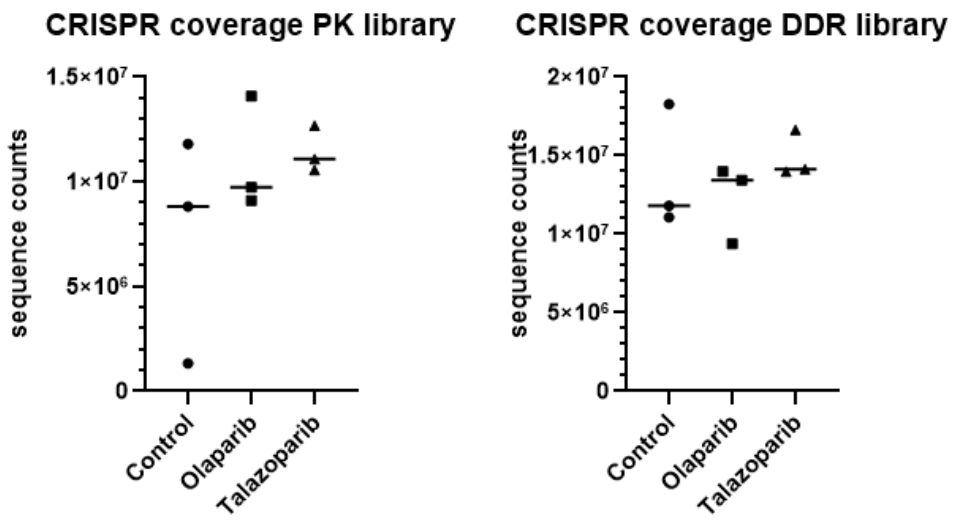

Figure 5.2. Sequence counts as a measure of coverage of the CRISPR libraries. *(n=3)*

After adapter trimming, the remaining sequences were 28-30 base pairs long. MaGeCK count was used to calculate the number of sgRNA counts and counts per gene for the DDR library (Table 5.1). Approximately 94% of the reads could be mapped to the library file. However, just over one hundred sgRNAs had zero reads. Further investigation revealed these were mostly non-treatment control (NTC) sgRNAs. After conferring with the group in Erlangen that prepared the viral DDR library, it was discovered that the NTCs had not been included in library preparation. These sgRNAs were therefore removed from further analysis. Read count distributions were similar between samples, with outliers having higher counts. Although principal component analysis and hierarchical clustering showed some clustering of biological replicates, there was no clear separation between the different treatment conditions (Fig. 5.3).

Table 5.1. Mapping of reads in the DDR library

Label	Reads	Mapped	Percentage	Zero counts	Gini Index
ContA1	18277736	17156953	0.9387	106	0.2592
ContA2	11082309	10398066	0.9383	110	0.263
ContB	11810412	11052272	0.9358	109	0.2617
OlaA1	9387779	8778120	0.9351	102	0.259
OlaA2	13434909	12599589	0.9378	107	0.2611
OlaB	13994267	13092577	0.9356	102	0.2578
TalA1	13968695	13086957	0.9369	109	0.261
TalA2	16641779	15591005	0.9369	108	0.2594
TalB	14148533	13257131	0.937	106	0.2568

Reads is the number of reads sequenced, mapped is the number of reads that could be mapped to the library file, and percentage is the fraction of mapped reads. Zero counts are the number of reads in the library file that had no counts in the sequencing file. The Gini index is a measure of inequality, an index of 0 indicates that every sgRNA is present in the same quantity, whereas an index of 1 means that there is only one sgRNA with read counts.

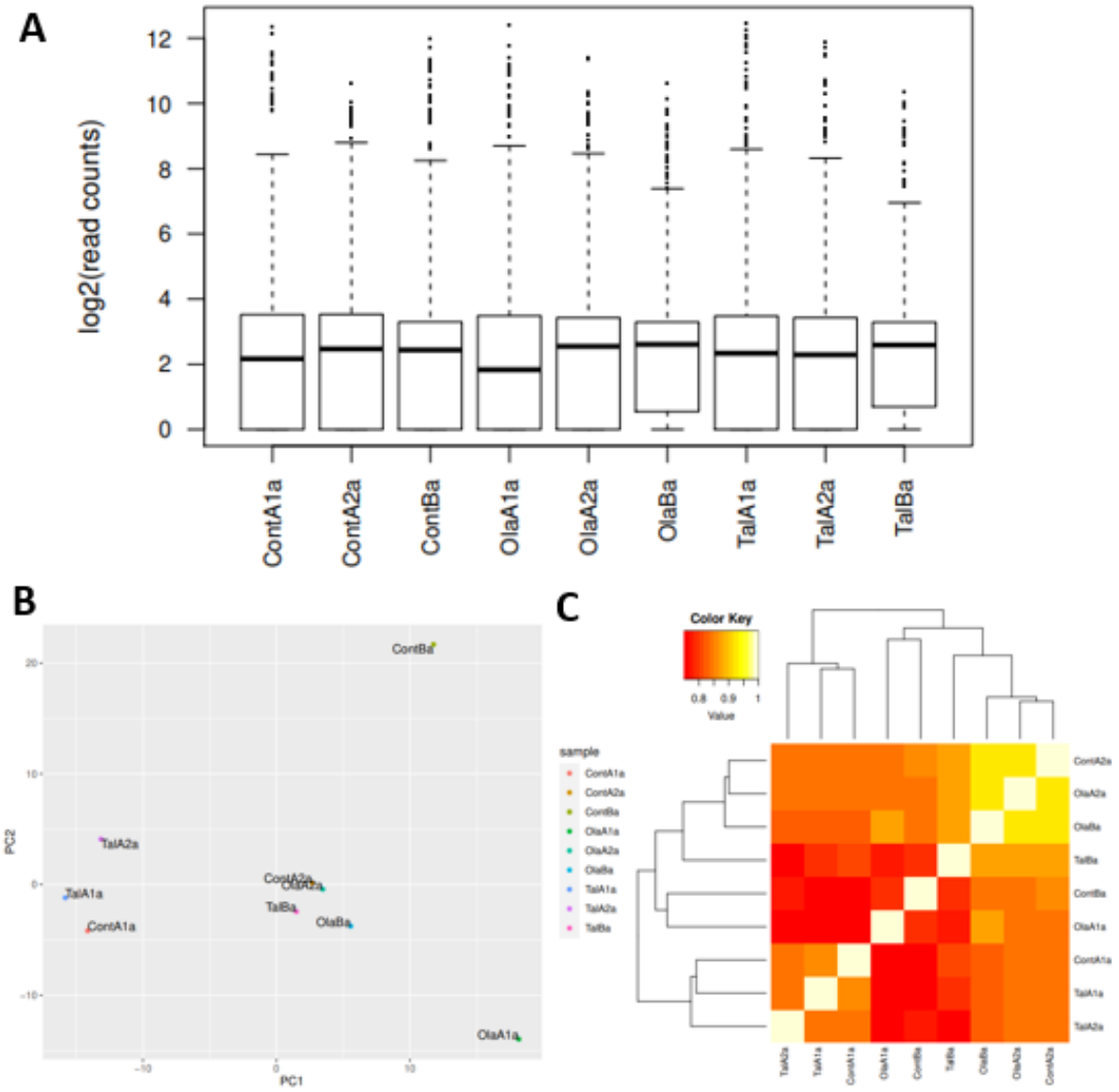

Figure 5.3. Read distribution and sample similarity within the DDR library*. A) read distribution shows similar distribution of read counts between samples with outliers to the higher counts. B) principal component analysis and C) hierarchical clustering.*

For the PK library, approximately 68% of the reads could be mapped onto the provided library file (Table 5.2). Even with the loss of some reads the coverage was still >130x. Unfortunately, the number of sgRNAs that had no reads was quite high (191-1166 sgRNAs, or 6-20%; <1% is recommended). However, the Gini Index, measuring the inequality of count distribution, was still within the recommended range (0.11-0.25, recommended <0.3) indicating an equal infection efficacy across counts. The box plots also showed a similar distribution of counts between samples, with more low-count outliers (Fig. 5.4). This suggests lower transduction efficacy for a subset of sgRNAs, unrelated to treatment since control and treated samples showed similar distributions. Principal component analysis

and hierarchical clustering revealed high sample similarity with no distinct replicate clustering, irrespective of treatment (Fig. 5.4).

Table 5.2. MaGeCK count results for PK library.

Label	Reads	Mapped	Percentage	Zero counts	Gini Index
ContA1	8817487	5994046	0.6798	267	0.1191
ContA2	1328429	904374	0.6808	606	0.1756
ContB	11800833	8040318	0.6813	507	0.1543
OlaA1	14098045	9599731	0.6809	340	0.1264
OlaA2	9743048	6633803	0.6809	505	0.1518
OlaB	9100984	6219737	0.6834	651	0.1751
TalA1	11080108	7566960	0.6829	191	0.09833
TalA2	12681305	8635934	0.681	267	0.1154
TalB	10570234	7180555	0.6793	1166	0.2458

Reads is the number of reads sequenced, mapped is the number of reads that could be mapped to the library file, and percentage is the fraction of mapped reads. Zero counts are the number of reads in the library file that had no counts in the sequencing file. The Gini index is a measure of inequality, an index of 0 indicates that every sgRNA is present in the same quantity, whereas an index of 1 means that there is only one sgRNA with read counts.

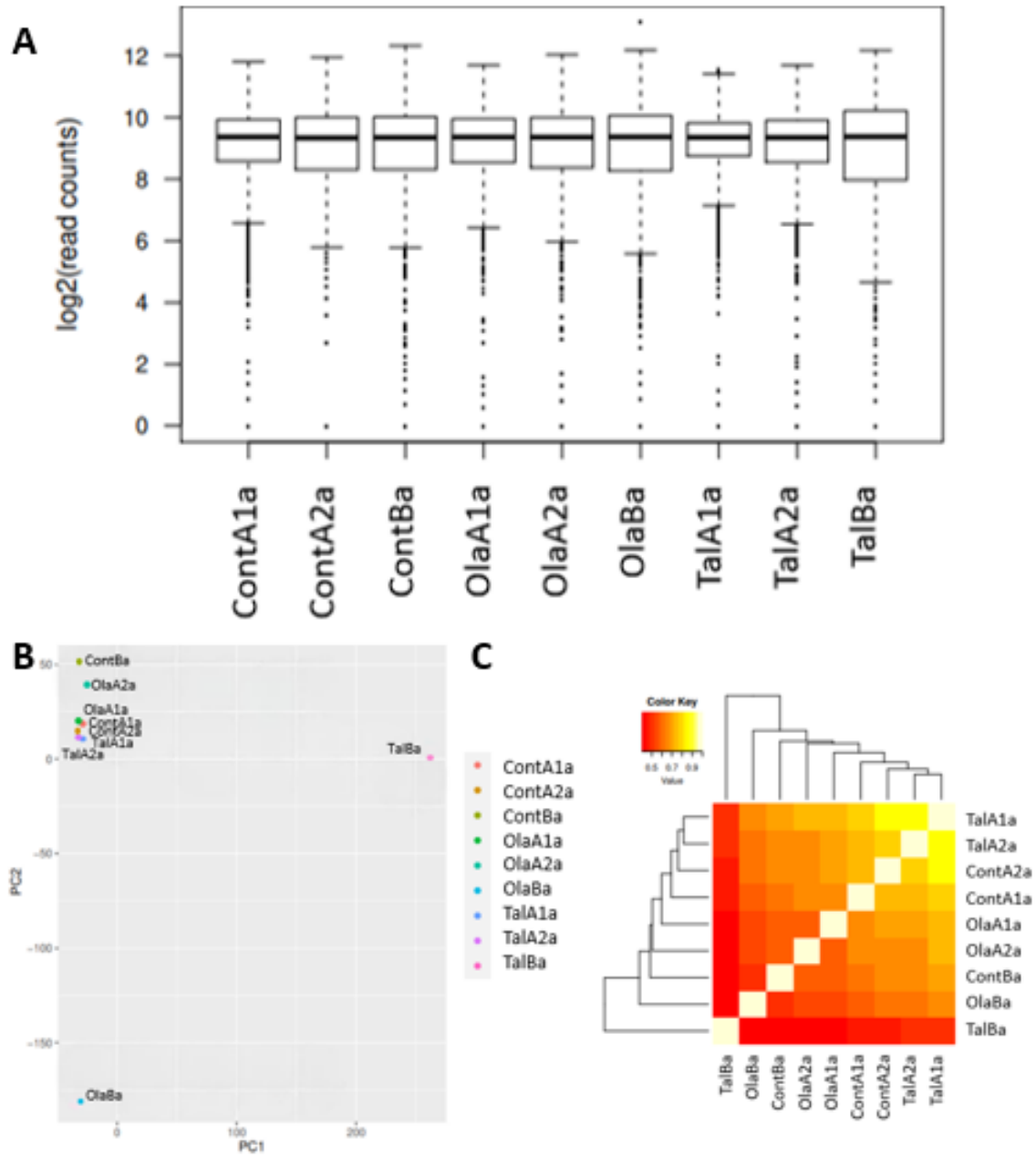

Figure 5.4. Read distribution and sample similarity within the PK library. *A) read distribution shows similar distribution of read counts between samples with outliers to the higher counts. B) principal component analysis and C) hierarchical clustering.*

5.2.2 CRISPR screen: gene enrichment and depletion

MaGeCK test was used to identify enriched and depleted sgRNAs using a robust ranking aggregation (RRA) algorithm. The outcome of the test is a ranked list of genes with scores for their negative and positive selection, statistical significance, and false discovery rate. The average log-fold change (logFC) for each gene in the treated screen compared to the untreated screen is plotted as a volcano plot with the logFC on the x-axis and the -log(p-value) on the y-axis (Fig. 5.5A, B). Cells containing sgRNAs that target genes which protect

against treatment are killed during treatment and these sgRNAs are therefore depleted compared to the untreated sample. In contrast, cells containing sgRNAs that target genes which inhibit survival or proliferation are more likely to be enriched in the treated sample compared to the untreated sample. The logFC is relatively small at less than 0.4 for all sgRNAs but tends to be larger in the sgRNAs with a significant change.

For the comparison between olaparib-control in the DDR screen, six genes were found to be significantly ($p<0.05$) depleted (*BRCA1, XRCC3, BRCA2, DNMT3A, PNKP,* and *BARD1*) (Fig. 5.5E). Another six genes were found to be significantly ($p<0.05$) enriched (*POLR2F, ERCC3, INO80D, GTF2H1, CDK7,* and *RPA1*) (Fig. 5.5C). For the comparison between talazoparib-control in the same screen, seven genes were found to be significantly depleted and four genes were significantly enriched ($p<0.5$; depleted: *BRCA2, BRCC3, SMARCA2, CLK2, NEIL1, TENT4A, PTEN*; enriched: *ERCC3, SSRP1, UBA1, USP7*) (Fig. 5.5 D, F).

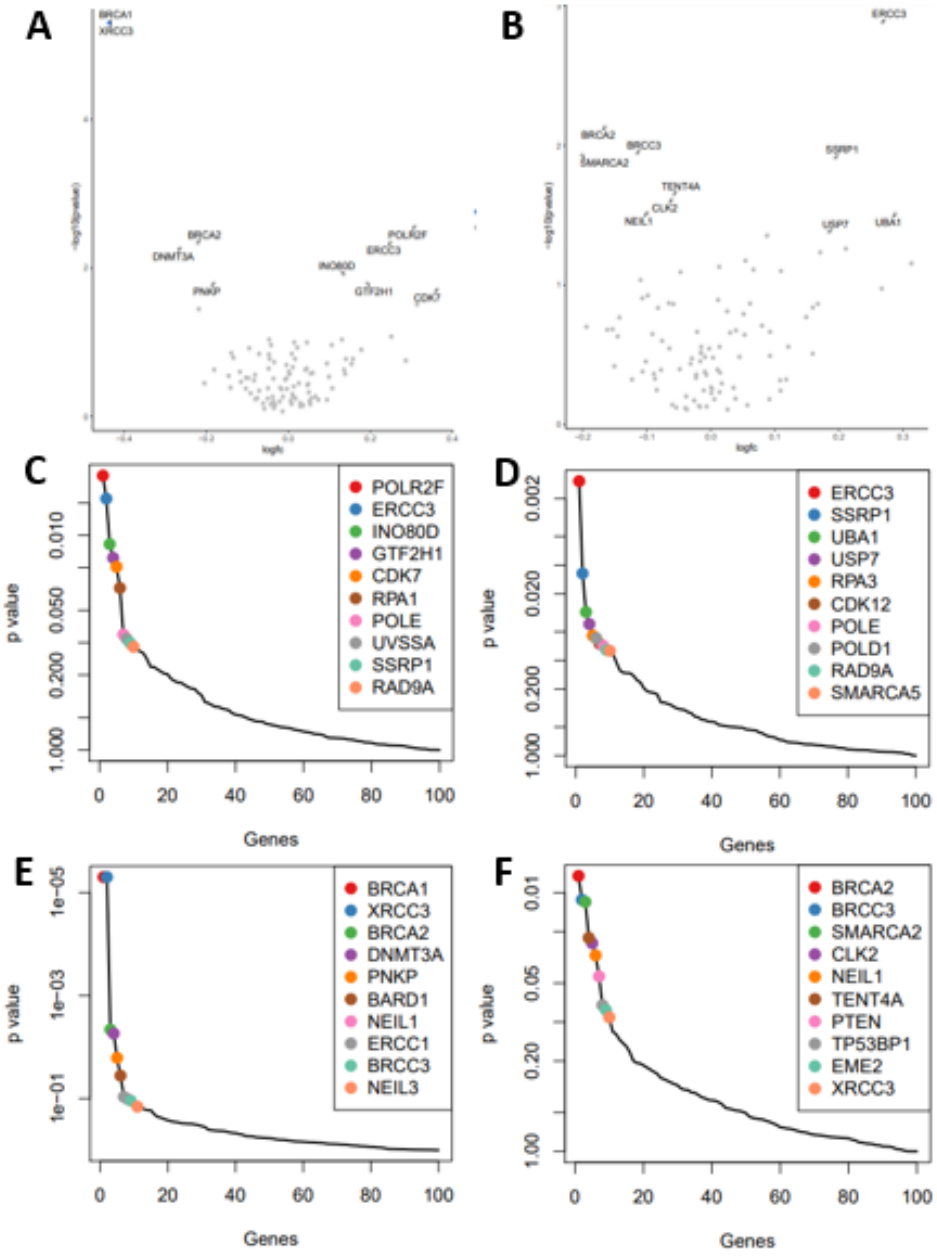

Figure 5.5. Distribution of p-values for enriched and depleted genes in the DDR screen. *The top 10 most significant genes are highlighted in the insert. A) volcano plot for olaparib-control comparison. B) volcano plot for talazoparib-control comparison. C) enriched genes in the olaparib-control comparison. D) enriched genes in the talazoparib-control comparison E) depleted genes in the olaparib-control comparison. F) depleted genes in the talazoparib-control comparison.*

For the comparison between olaparib-control in the PK screen, 72 genes were significantly depleted, and 63 genes were significantly enriched ($p<0.05$) (Fig. 5.6 A,C,E). The top three depleted genes were *NCK1, INO80D*, and *HLTF* ($p<0.00013$). The top three enriched genes were *MST1, BCKDK*, and *KGK2* ($p<0.0012$). For the comparison between talazoparib-control

in the PK screen, 85 genes were significantly depleted, and 58 genes were significantly enriched (p<0.05) (Fig. 5.6 B, D, F). Top three depleted genes were *NEIL1, SMAD4,* and *IFNGR1* (p<0.0001). The top three enriched genes were *BCKDK, ANLN,* and *MST1* (p<0.0024).

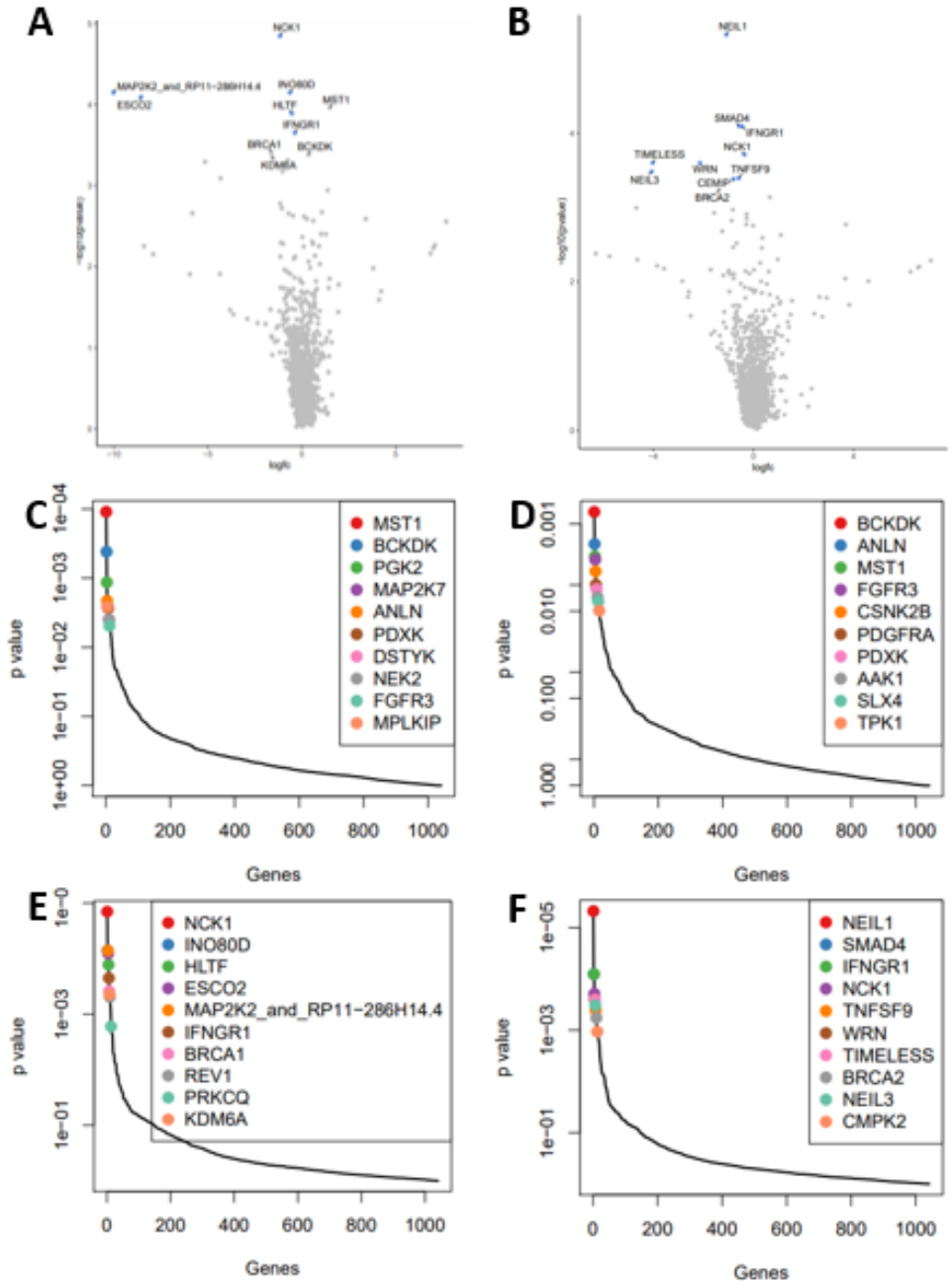

Figure 5.6. Distribution of p-values for enriched and depleted genes in the PK screen*. The top 10 most significant genes are highlighted in the insert. A) volcano plot for olaparib-control comparison. B) volcano plot for talazoparib-control comparison. C) enriched genes in the olaparib-control comparison. D) enriched genes in the talazoparib-control comparison E) depleted genes in the olaparib-control comparison. F) depleted genes in the talazoparib-control comparison.*

5.2.3 CRISPR screen target selection

The genes *BRCC3, XRCC3, NEIL1*, and *PTEN* were selected for further validation by siRNA knockdown. Because the prevalence of mutations in these four genes in PDAC is low (approximately 1%, TCGA), mRNA expression levels were investigated to see if low mRNA expression could contribute to gene deficiency. Expression levels of <0.5 fragments Per Kilobase of transcript per Million mapped reads (FPKM) are generally considered not expressed, expression levels between 0.5 and 10 FPKM are considered low, and 10 to 1000 FPKM is considered medium. mRNA expression levels ranged between 0.1 and 12.1 FPKM for *NEIL1;* 2.6 and 26.7 FPKM for *PTEN;* 2.3 and 16 FPKM for *BRCC3;* and 0.4 and 6.3 FPKM for *XRCC3* pointing to a relatively low mRNA expression for each of these genes.

Additionally, mRNA expression levels in patients are associated with prognosis (Fig. 5.7). High expression of *BRCC3* is significantly associated with a poorer prognosis (cut-off: 8.0, p=0.0014), whereas high expression of *XRCC3* and *NEIL1* is significantly associated with better prognosis (cut-off: 1.3, p=0.05 and cut-off: 1.7, p=0.00021, respectively). No significant association was found for *PTEN* (cut-off: 9.0, p=.098), although there is a trend for poorer prognosis in patients with high expression.

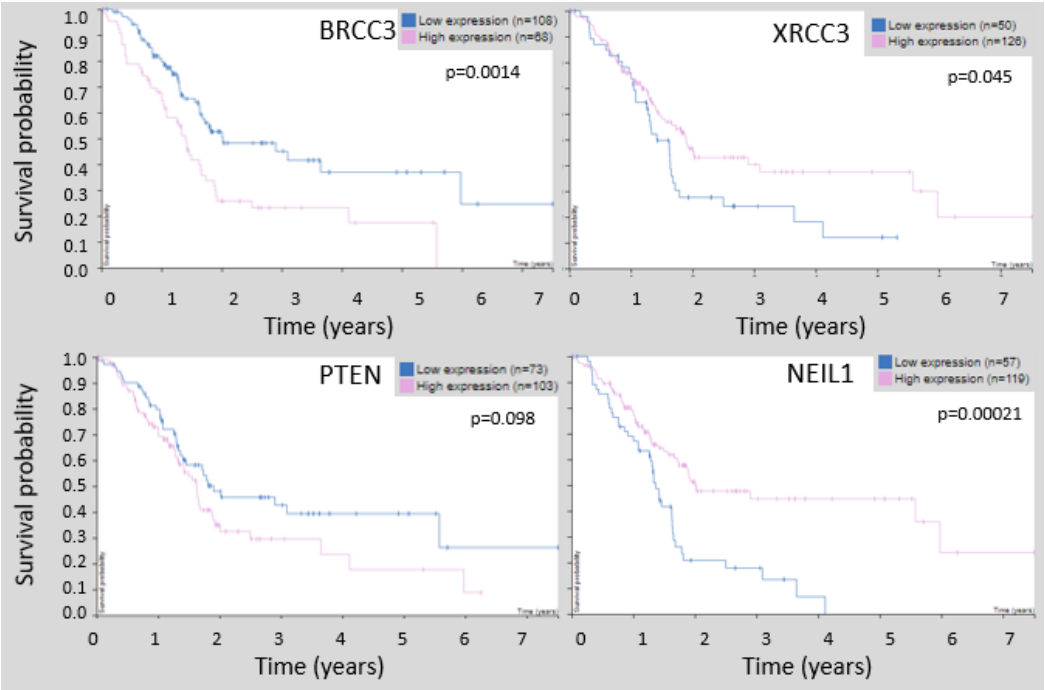

Figure 5.7. Correlation between mRNA expression levels of BRCC3, XRCC3, PTEN, and NEIL1 to survival. *Cut-off BRCC3: 8.0 FPKM, cut-off XRCC3: 1.3 FPKM, cut-off PTEN: 9.0 FPKM, cut-off NEIL1: 1.7 FPKM. Kaplan-Meier curves were obtained from The Cancer Genome Atlas (TCGA) data of PAAD from The Human Protein Atlas (Uhlén et al., 2015).*

5.2.4 siRNA knockdown of PTEN, BRCC3, XRCC3, and NEIL1

To validate the selected targets, siRNA knockdown was performed (Chapter 2.13). SiRNA knockdown efficacy was assessed by RT-qPCR 48 hours after transfection. Effective knockdown was achieved for *PTEN, BRCC3,* and *XRCC3* with a decrease of 65-77% in mRNA expression compared to an untreated control, and with a significant decrease ($p<0.05$) compared to a scrambled control (Fig. 5.8). For *NEIL1*, a considerable increase in mRNA expression was observed instead of the expected decrease and therefore this gene was excluded from further experiments.

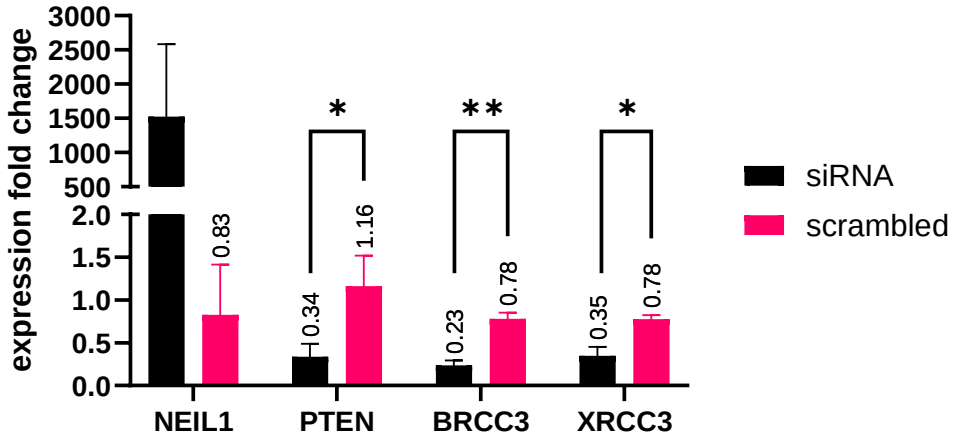

Figure 5.8. Validation of siRNA knockdown by RT-qPCR*. NEIL1, PTEN, BRCC3, and XRCC3 were knocked down in the Panc-1 cell line by siRNA. 48 hours after siRNA transfection, RNA was extracted, and gene expression was normalised by RT-qPCR. Expression fold change was normalized to untreated control. Statistical comparison was performed by Student's t-test for each individual gene. *: p>0.05, **: p>0.01*

5.2.5 Effect of siRNA knockdown of *BRCC3, XRCC3*, and *PTEN* on sensitivity to PARPi and cisplatin

To analyse the effect of gene knockdown on sensitivity to olaparib and talazoparib, viability and colony formation assays were performed. For the viability assay, transfected cells were treated for 72 hours with 3.5 µM olaparib or talazoparib (Fig. 5.9). Significant decreases in viability were found for all three siRNAs when treated with olaparib and for the *BRCC3* and *XRCC3* siRNAs when treated with talazoparib compared to the scrambled control ($p<0.05$).

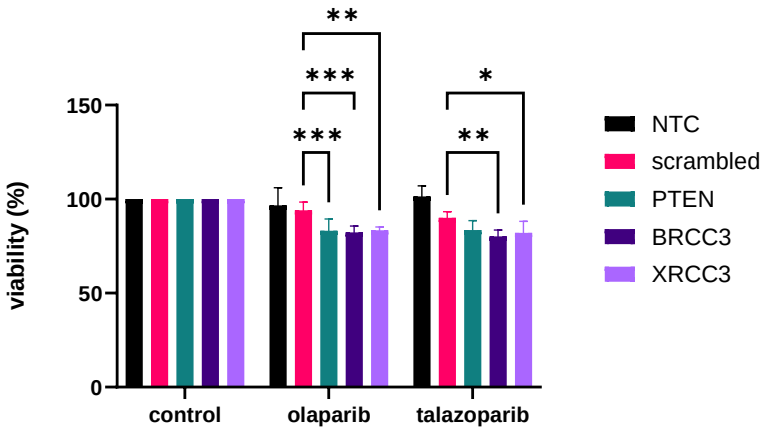

Figure 5.9. Effect of PTEN, BRCC3, and XRCC3 knockdown on sensitisation to PARPi as measured by viability assay. *PTEN, BRCC3, and XRCC3 were knocked down by siRNA, 24 hours after transfection, cells were treated with 3.5 µM olaparib or talazoparib.Viability was measured after 72 hours using PrestoBlue. Data shown is mean ± SD (n=3) *:p<0.05, **:p<0.01, ***:p<0.001 (two-way ANOVA).*

For the colony formation assay, transfected cells were treated with 200 nM cisplatin or 200 nM olaparib and were left to form colonies for 10 days (chapter 2.6). No significant differences were found in the percentage of colonies formed (Fig. 5.10 and 5.11).

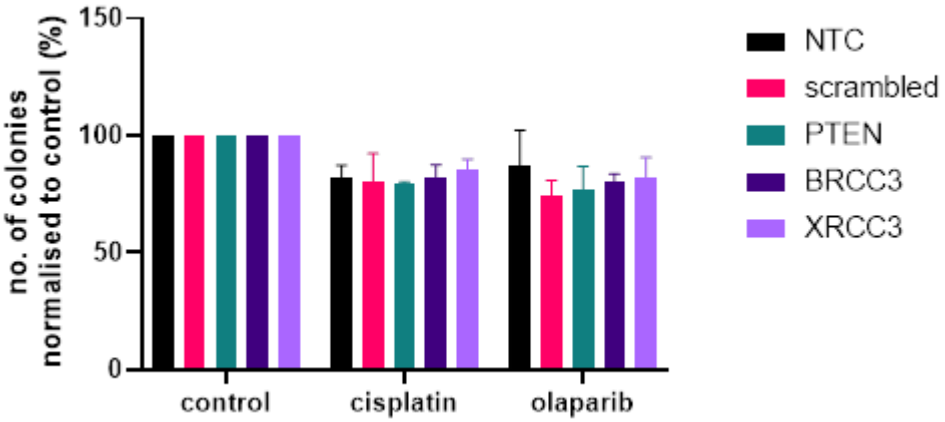

Figure 5.10. Effect of PTEN, BRCC3, and XRCC3 knockdown on sensitisation to PARPi as measured by colony formation assay. *PTEN, BRCC3, and XRCC3 were knocked down by siRNA, 24 hours after transfection cells were seeded at 600 cells/well, treated with 200 nM cisplatin or 200 nM olaparib and were left to form colonies for 10 days. Cells were fixated and stained with crystal violet. Colonies with more than 50 cells were counted. Data shown is mean ± SD (n=3).*

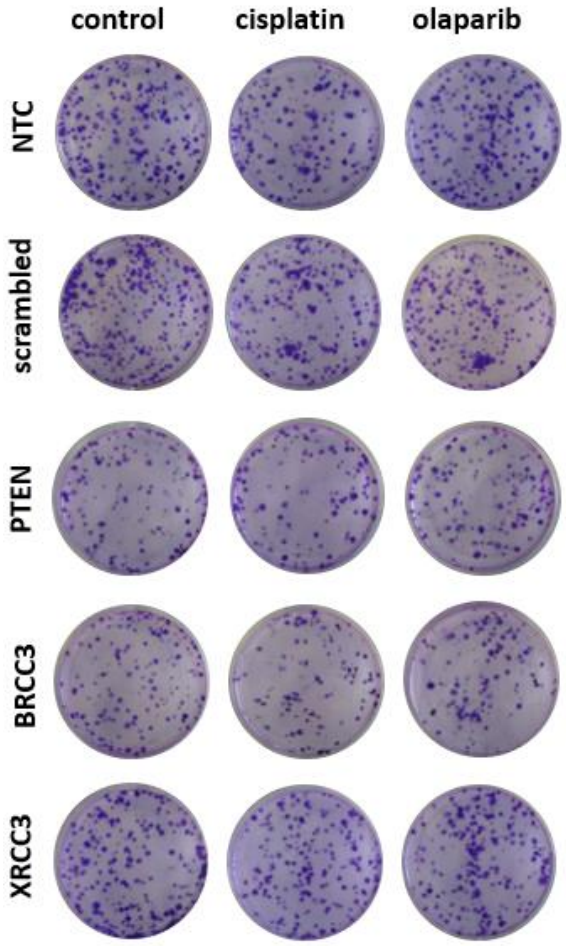

Figure 5.11. Visualisation of colony formation after siRNA knockdown and treatment with cisplatin or olaparib. *PTEN, BRCC3, and XRCC3 were knocked down by siRNA, 24 hours after transfection, cells were seeded at 600 cells/well, treated with 200 nM cisplatin or 200 nM olaparib and were left to form colonies for 10 days. Cells were fixated and stained with crystal violet. Colonies with more than 50 cells were counted. Representative images (n=3).*

5.2.6 Overcoming resistance using combination therapy with targeted agents

Lynparza (olaparib, PARPi), Saruparib (AZD5305, PARPi), AZD1390 (ATMi), and Ceralasertib (AZD6738, ATRi) were supplied by AstraZeneca. The resistant Capan-1 cells developed in Chapter 3 all show a reduced sensitivity to both Lynparza and Saruparib PARPi (Fig. 5.12 A, B). All four cell lines show a dose-response to the ATMi and ATRi (Fig 5.12 C, D). IC_{50} values for AZD1390 (ATMi) range from 13.14 to 20.50 µM with no significant difference compared to the parental cells (Table 5.3). IC_{50} values of Ceralasertib (ATRi) range from 0.44 to 4.33 µM, with a significant 2.4-fold increase in the Capan-1CisR cells (p=0.011) and a significant 4.11-fold decrease in the Capan-1OlaR cells (p=0.006) compared to the parental cell line. Pretreatment with 0.23 µM cisplatin (IC_{20} Capan-1) did not sensitise the cells to any of the inhibitors (Suppl. Fig. 1)

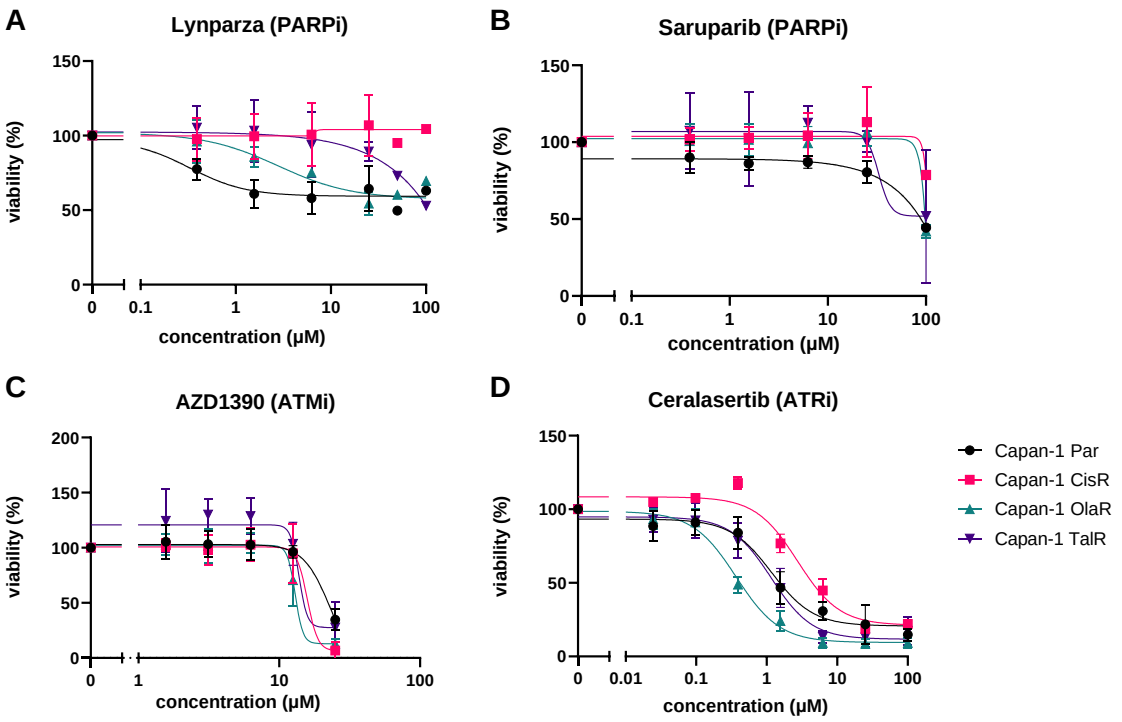

Figure 5.12. Sensitivity of resistant Capan-1 cells to PARP, ATM, and ATR inhibitors. *A) PARPi Lynparza, B) PARPi Saruparib, C) ATMi AZD1390, D) ATRi Ceralasertib. Cells were treated for 7 days with multiple concentrations of each drug. Viability was evaluated by PrestoBlue staining. Error bars show the standard deviation (n=3).*

Table 5.3. Sensitivity of Capan-1 parental and resistant cells to Lynparza, Ceralasertib, and AZD1390. *IC_{20} (Lynparza) and IC_{50} (Ceralasertib and AZD1390) determined from figure 5.13 with standard deviation. Statistical comparison to parental cells by Student's T-test.*

	Lynparza		Ceralasertib		AZD1390	
	IC_{20} (SD)	**p-value**	**IC_{50} (SD)**	**p-value**	**IC_{50} (SD)**	**p-value**
Par	0.27 (0.22)		1.81 (0.63)		18.19 (5.27)	
CisR	>100	n/a	4.33 (0.70)	0.01	20.50 (4.59)	0.60
OlaR	2.53 (1.53)	0.064	0.44 (0.14)	0.006	13.14 (0.97)	0.18
TalR	38.91(6.03)	0.0004	1.39 (0.67)	0.4	14.44 (0.83)	0.29

Next, the cells were treated with a combination of PARPi and ATM/ATRi to evaluate possible synergism. Cells were treated with the approximate IC_{25} for each drug in the parental line and synergism was calculated using the Bliss Independence approach. Response to each drug was variable across the cell lines, with in general lower viability in the combination treatments (Fig. 5.13). The combination of PARPi with ATRi seemed to be

more effective than the combination with ATMi, so these combinations were selected for further statistical analysis. Statistically significant synergism (Combination Index, CI<1) was observed for the combination of ATRi Ceralasertib with Saruparib in the parental (CI 0.47±0.26), Capan-OlaR (CI 0.78±0.03), and Capan-1TalR (CI 0.43±0.08) cells (Table 5.4). Significant synergism was also observed for the combination of Ceralasertib with Lynparza in the parental cells (0.70±0.09).

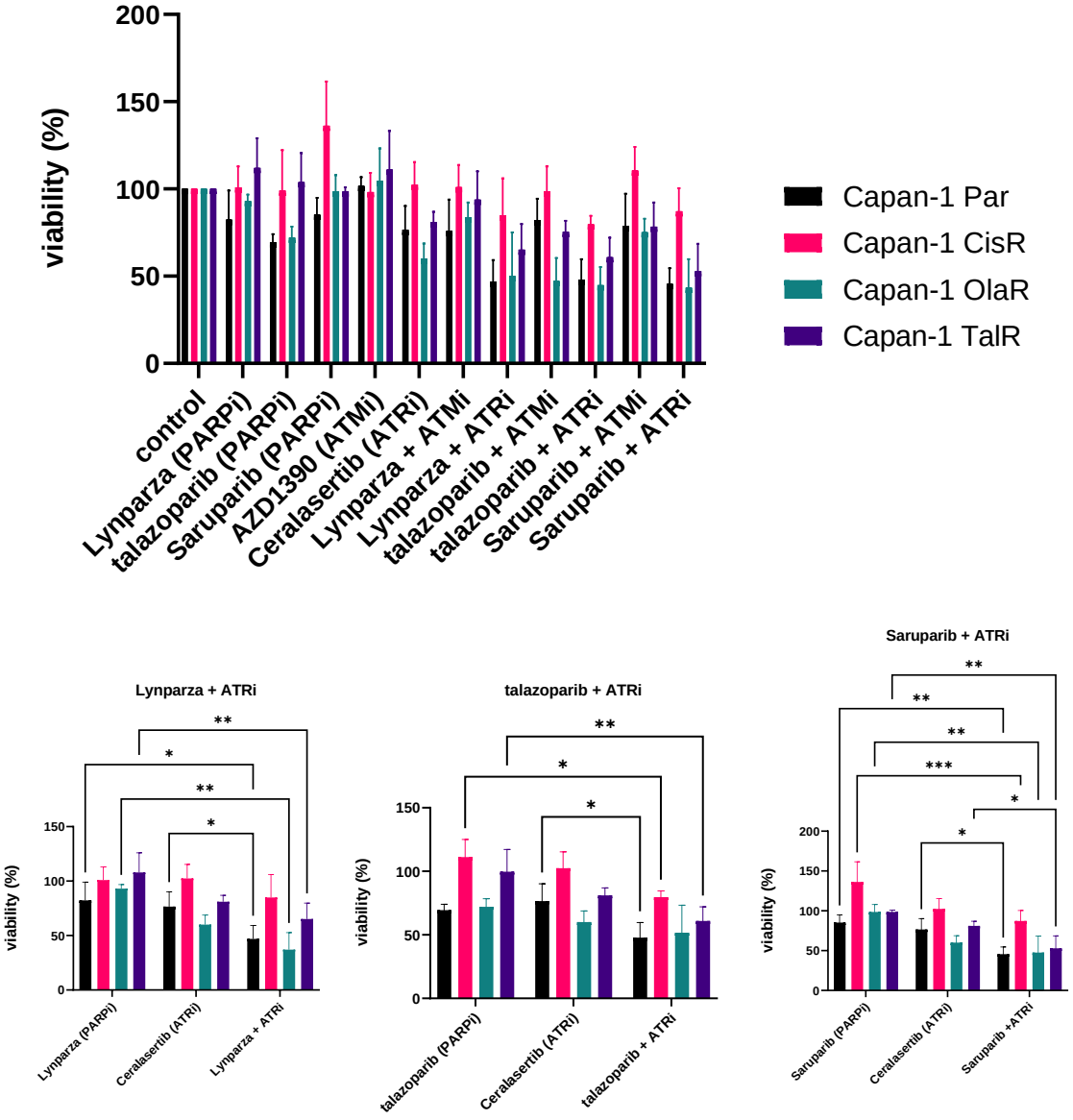

Figure 5.13. Combination treatment of PARPi and ATM/ATRi in Capan-1 resistant cells. *Cells were treated for 7 days with 0.4 µM Lynparza, 0.1 µM talazoparib, 37 µM Saruparib, 1.9 µM AZD1390, or 0.4 µM Ceralasertib. Top: overview of viability in all combinations. Bottom: selected combinations with statistical comparison. Error bars show the standard deviation of each measurement (n=3). Statistical analysis is two-way ANOVA with multiple comparisons limited within each cell line. *:p<0.05, **:P<0.01, ***:p<0.001.*

Table 5.4. Combination index for PARPi with ATRi as measured in viability assays.

	Lynparza	Talazoparib	Saruparib
Capan-1	0.70 (0.09)	0.92 (0.10)	0.47 (0.26)
Capan-1CisR	0.86 (1.62)	N/A	N/A
Capan-1OlaR	0.74 (0.35)	0.96 (0.21)	0.78 (0.03)
Capan-1TalR	0.42 (0.49)	0.46 (0.40)	0.43 (0.08)

Combination index (CI) was calculated according to Bliss Independence approach. Combination can be synergic (CI<1), additive (CI=1), or antagonistic (CI>1). N/A indicates that CI could not be calculated because viability was greater than 100% in two or more replicates. CI (with SD) was calculated based on 3 replicates.

5.2.6.1 Evaluation of combination treatment by colony formation assay

Cytotoxicity was also evaluated using colony formation assays. Cells were treated with the same concentration of drugs as for the combination assay and were allowed to form colonies over a period of seven days. Capan-1 cells have a low viability when seeded as single cells, so the cells were seeded at a relatively high concentration for a colony formation assay (5000 cells/well in a 12-well plate). Despite being seeded as single cells, it was observed that cells tended to migrate and form clusters within 24 hours. Because of this, counting of colonies was not a reliable measurement so after staining with crystal violet and imaging, crystal violet was eluted, and absorbance was measured as a measure of cell confluency (Fig. 5.14 and 5.15). Overall, Capan-1CisR cells were least sensitive to treatment whereas Capan-1OlaR cells were most sensitive to treatment.

Significant synergism for the combination of ATRi Ceralasertib with Lynparza was observed in the parental (CI 0.35±0.45) and Capan-1CisR (0.75±0.14) cells, for the combination with talazoparib in the parental cells (CI 0.21±0.38), and for the combination with Saruparib in the Capan-1TalR cells (CI 0.76±0.20) (Table 5.4).

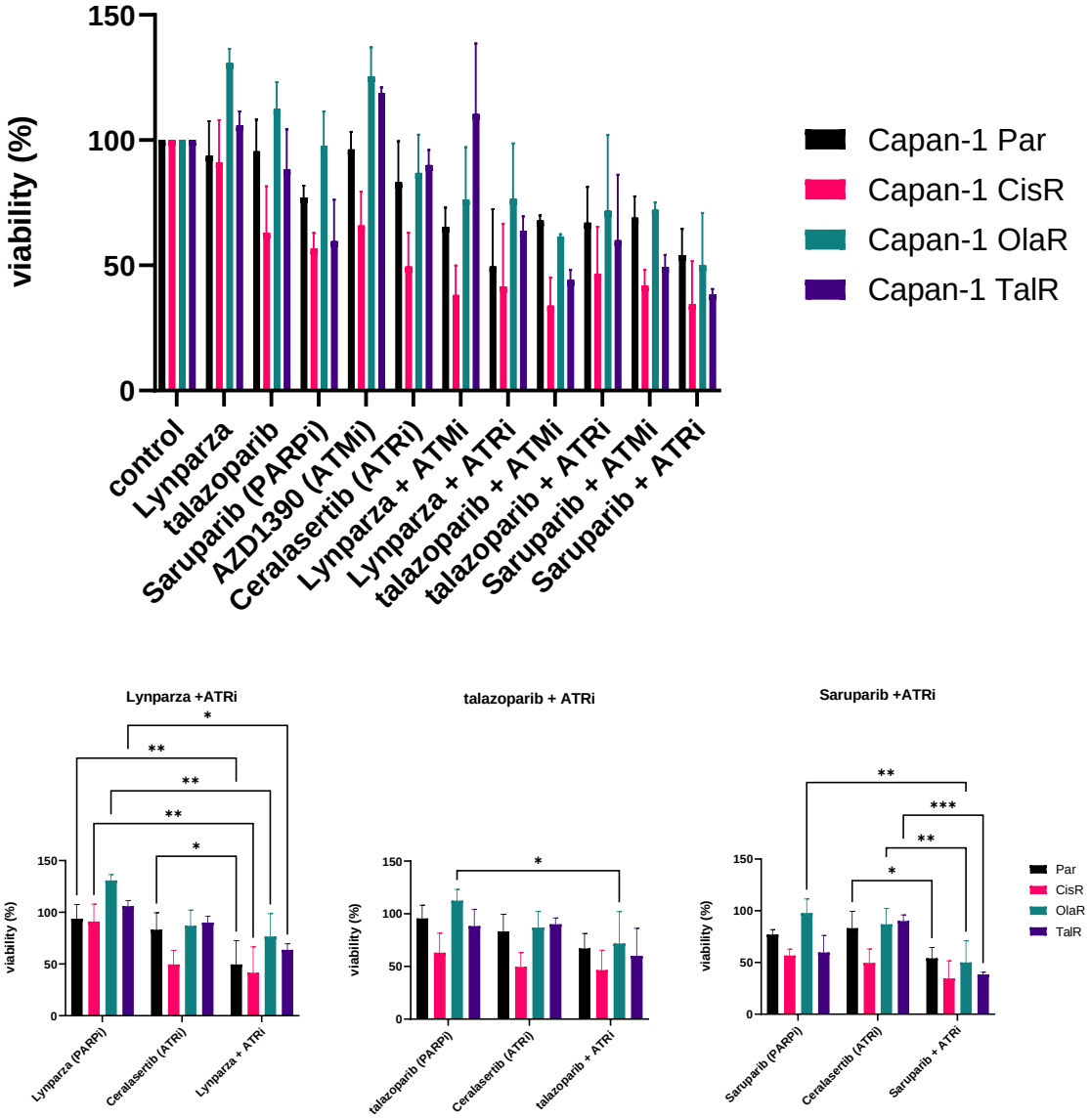

Figure 5.14. Colony formation assay. Response of Capan-1 resistant cells to PARPi, ATMi, and ATRi. *Cells were seeded at 5000 cells/well in a twelve-well plate, incubated for 24 hours, and treated with drug for 7 days (0.4 µM Lynparza, 0.1 µM talazoparib, 37 µM Saruparib, 1.9 µM AZD1390, or 0.4 µM Ceralasertib). Viability was measured as absorbance of eluted crystal violet normalised to the untreated control cells. Bars show the viability, with error bars displaying the standard deviation (n=3). Top: overview of all treatments. Bottom: selected combinations with statistical comparison. Error bars show the standard deviation of each measurement (n=3). Statistical analysis is two-way ANOVA with multiple comparisons limited within each cell line. *:p<0.05, **:P<0.01, ***:p<0.001.*

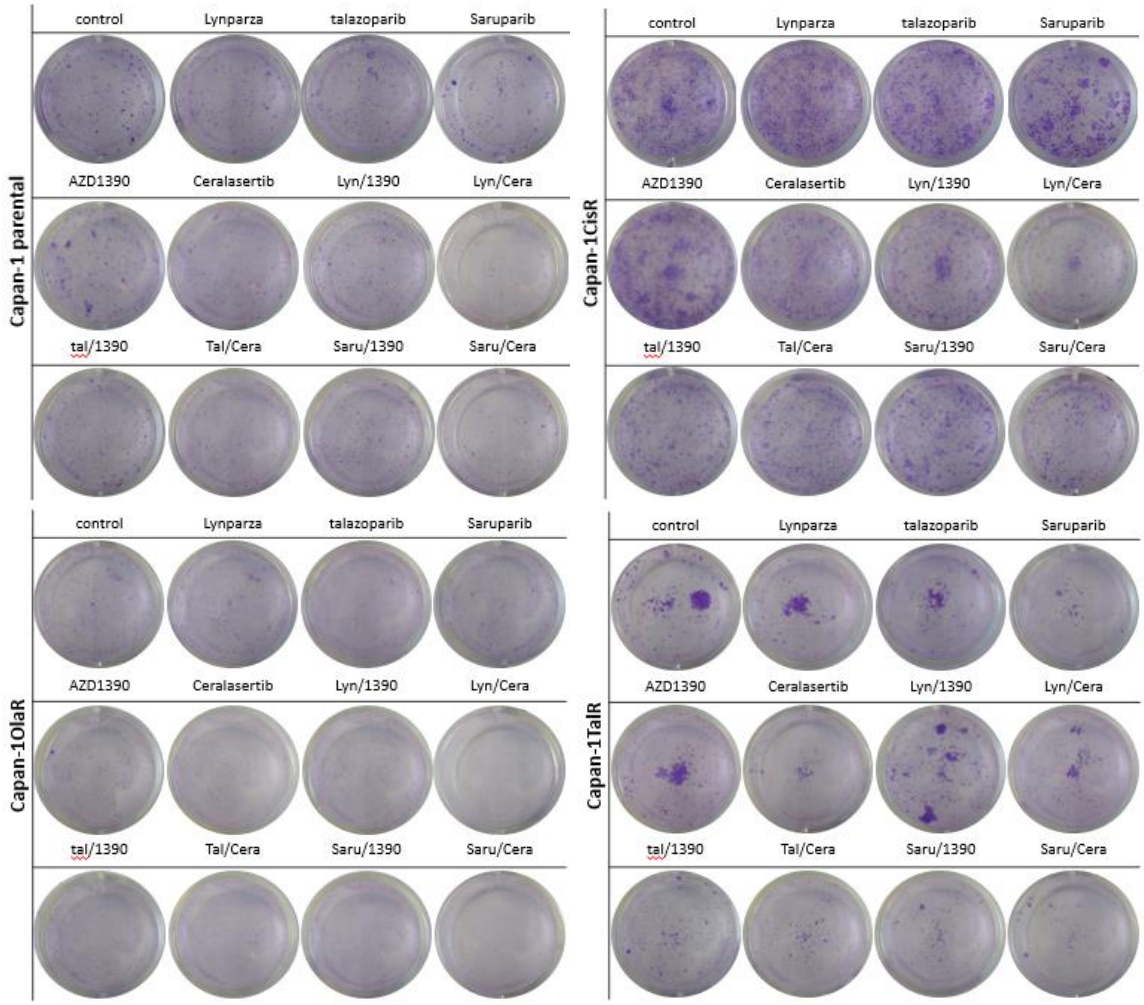

Figure 5.15. Visualisation of colony formation after treatment with PARPi, ATMi, and ATRi, alone or in combination. *Cells were seeded at 5000 cells/well and were treated with 0.4 µM Lynparza, 0.1 µM talazoparib, 37 µM Saruparib, 1.9 µM AZD1390, or 0.4 µM Ceralasertib. After seven days of treatment, cells were fixed and stained with crystal violet. Representative images of three biological replicates are shown.*

Table 5.5. Combination index for PARPi with Ceralasertib found by colony formation assays.

	Lynparza	**Talazoparib**	**Saruparib**
Capan-1	0.35 (0.45)	0.21 (0.38)	0.72 (0.29)
Capan-1CisR	0.75 (0.14)	1.09 (0.10)	1.16 (0.27)
Capan-1OlaR	N/A	N/A	N/A
Capan-1TalR	N/A	1.85 (1.80)	0.76 (0.20)

Combination index (CI) was calculated according to Bliss Independence approach. Combination can be synergic (CI<1), additive (CI=1), or antagonistic (CI>1). N/A indicates that CI could not be calculated because colony formation was greater than 100% in two or more replicates. CI (with SD) was calculated based on 3 replicates.

5.2.7 γH2AX and RAD51 foci formation upon PARPi and ATRi (Ceralasertib) treatment

Immunofluorescent imaging of γH2AX and RAD51 after 4 hours of drug treatment was performed to investigate the effect of treatment on DNA damage recognition and repair (Chapter 2.10). No significant differences were observed for either γH2AX or RAD51 in any of the cell lines (Fig 5.16-5.17). As was observed in section 4.2.4, foci formation was heterogenous within cell lines and treatment conditions with staining ranging from completely negative to fully confluent which complicated comparison of samples (Fig. 5.18 and Suppl. Fig. 2).

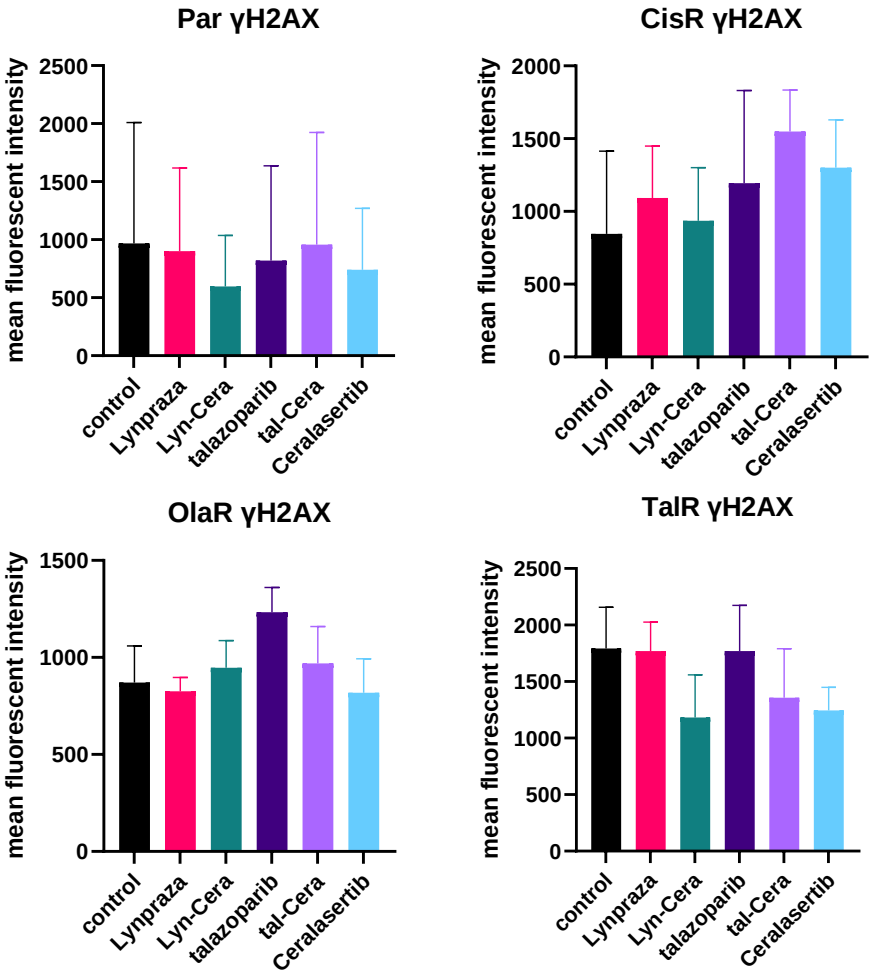

Figure 5.16. γH2AX foci formation upon treatment with PARP and ATR inhibitor in Capan-1 parental and resistant cells*. Cells were treated with 25 μM Lynpraza, 1 μM talazoparib, or 1.6 μM Ceralasertib for 4 hours before fixation. Error bars represent the standard deviation of the mean for 3 biological replicates. Statistical comparison of treated cells against untreated cells by one-way ANOVA.*

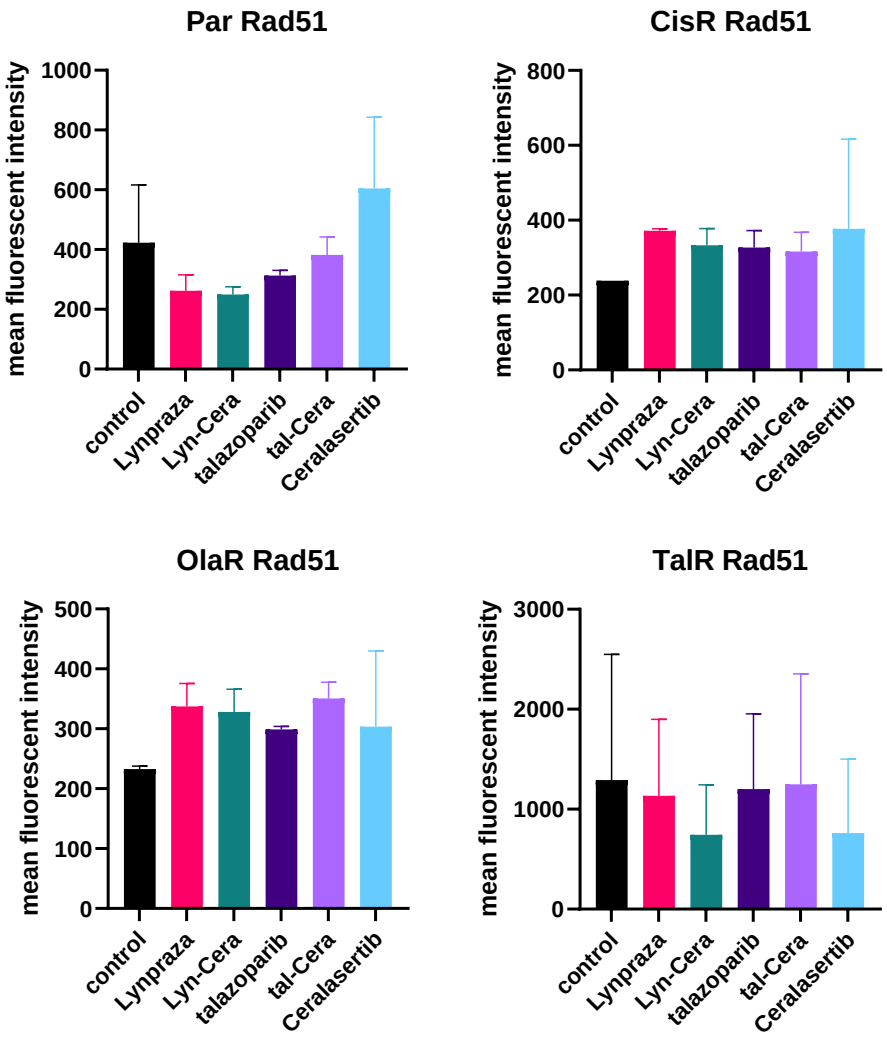

Figure 5.17. Rad51 foci formation upon treatment with PARP and ATR inhibitor in Capan-1 parental and resistant cells*. Cells were treated with 25 µM Lynpraza, 1 µM talazoparib, or 1.6 µM Ceralasertib for 4 hours before fixation. Error bars represent the standard deviation of the mean for 2 biological replicates. Statistical comparison of treated cells against untreated cells by one-way ANOVA.*

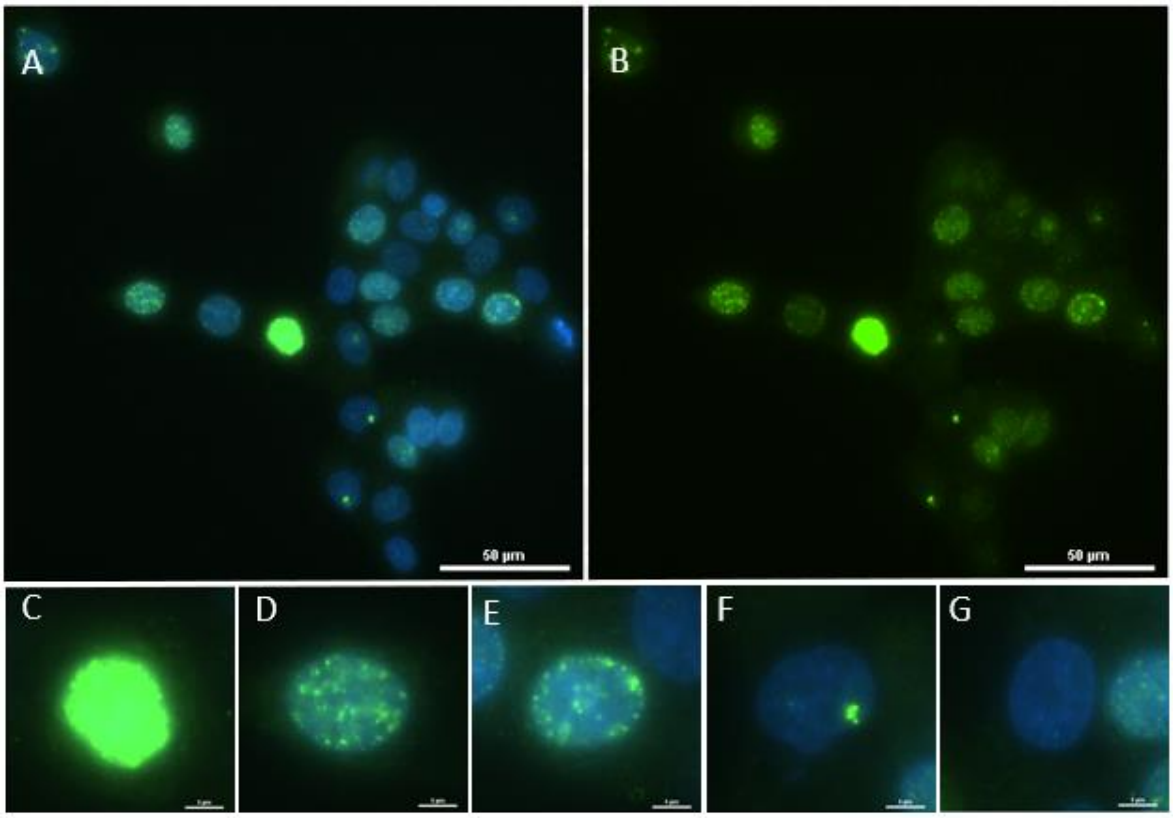

Figure 5.18. Heterogeneity of foci formation in Capan-1 cells after treatment with ATRi Ceralasertib*. Images were taken at 60x magnification. A) overlay of DAPI and FITC (RAD51). B) RAD51. C-G) 10x zoom of nuclei with differences in RAD51 foci formation.*

5.2.8 Expression of PARP1 and BRCC3 upon PARPi and ATRi (Ceralasertib) treatment

To investigate the mechanism of action of the single agent and combination treatment of PARPi and ATRi in the Capan-1 parental and resistant cells expression of PARP1 and BRCC3 was evaluated by Western blotting (Chapter 2.9). BRCC3 is a subunit of the BRCC complex and is necessary for the formation of BRCA1 foci at DSBs (Chen et al., 2006). No changes in expression in either of the proteins was observed (Fig. 5.19).

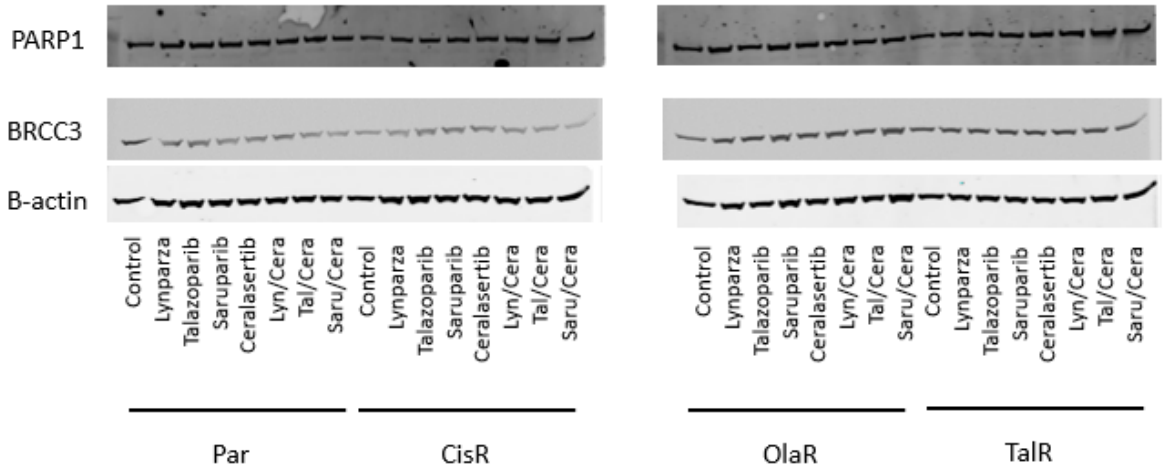

Figure 5.19. PARP1 and BRCC3 protein expression after 24h treatment with PARPi and/or ATRi (Ceralasertib). *Capan-1 parental and resistant cells were treated with 25 µM Lynpraza, 1 µM talazoparib, 74 µM Saruparib, or 1.6 µM Ceralasertib. Representative images of three biological replicates.*

5.3 DISCUSSION

5.3.1 Identification of synthetic lethal targets with PARPi

To identify potential genes that contribute to PARPi sensitivity and resistance in *BRCA2* wild-type PDAC, two CRISPR screens were performed in Panc-1 cells. The first screen targeted 100 DDR genes, while the second screen targeted 1052 protein kinase (PK) genes. The DDR screen was selected based on the principle that if DDR deficiency caused by *BRCA* mutation is synthetic lethal with PARPi, loss of other DDR genes may also be synthetic lethal. The PK screen was selected because protein kinases are relatively easy to target pharmacologically which makes potential clinical translation easier.

Cells were infected with lentivirus containing the sgRNA libraries and were exposed to 1.2 µM olaparib, 2.5 nM talazoparib, or left untreated. After 72 hours of treatment, cells were collected, and the DNA was sequenced to determine the level of each sgRNA compared to the untreated control. A decrease in sgRNA, or gene depletion, indicates that the gene is synthetic lethal with PARPi, whereas an increase in sgRNA, or gene enrichment, indicates that loss of the gene confers resistance to PARPi. We focused on the depleted genes as these may be potential drug targets or selection markers for PARPi treatment. Genes were selected based on the significance levels of their depletion rather than their log fold change (LFC) in expression level to account for the short expansion time of the cells. The doubling time of Panc-1 cells is relatively short at about 21 to 25 hours (McCluskey et al., 2011; Miura et al., 2016; Wang et al., 2015) meaning that in the 72 hours that the cells were exposed to treatment approximately three doubling steps could have taken place. While this does allow for the loss of cells with a synthetic lethal knockout and expansion of cells without, the resultant fold changes are expected to be rather subtle.

BRCA2 was significantly depleted in all four CRISPR screens, and *BRCA1* was significantly depleted in the olaparib-treated DDR and PK screens. Since *BRCA* is known to be synthetic lethal with PARPi these findings serve as a positive control and confirmed that the screen worked successfully.

5.3.2 Selection of targets for validation

Four genes (*PTEN, NEIL1, XRCC3, BRCC3*) were selected for further validation. Each of these genes was significantly depleted in at least one DDR and one PK screen and has a clear association with DDR. To validate the synthetic lethality of these genes with PARPi, siRNA

knockdown was performed in the Panc-1 cell line. Approximately 70% knockdown was achieved for *PTEN, BRCC3,* and *XRCC3* as measured by RT-qPCR, but knockdown was not achieved for *NEIL1* which was therefore excluded from further experiments. To analyse the effect of gene knockdown on sensitivity to PARPi olaparib and talazoparib viability and colony formation assays were performed.

5.3.2.1 PTEN

Phosphatase And Tensin Homolog (*PTEN*) was significantly depleted in the talazoparib DDR screen (p=0.04, LFC=-0.09) and olaparib PK screen (p=0.03, LFC=-0.5). *PTEN* is a multifunctional tumour suppressor gene whose expression is commonly lost in multiple cancers, including a small fraction of PDAC (Keniry & Parsons, 2008; Ying et al., 2011). *PTEN* affects a wide variety of cell processes, including cell cycle and DDR through the PI3K/Akt pathway although several studies have suggested a more direct involvement in DSB repair via RAD51 as well (Ho et al., 2020; Ming & He, 2012; Mukherjee et al., 2018).

Knockdown of *PTEN* in Panc-1 in combination with olaparib significantly reduced viability compared to scrambled control (83% vs. 97%, p=0.001), combination with talazoparib also decreased viability, but not significantly (84% vs. 101%, p=0.08). However, no significant difference in viability was observed between *PTEN* knockdown and scrambled control after treatment with olaparib in the colony formation assay (77% vs. 74.2%).

Similarly, several studies have reported synthetic lethality of *PTEN* deficiency with olaparib in other cancer cell lines. Mendes-Pereira et al. observed synthetic lethality between *PTEN* and olaparib in colon cancer cell line HCT116 where null cells were up to 25-fold more sensitive to olaparib than the wildtype cells (Mendes-Pereira et al., 2009). And in a panel with eight cell lines from different cancer types, the cells with *PTEN* deficiency were markedly more sensitive to olaparib. Additionally, knockout of *PTEN* was found to be synthetic lethal with olaparib in primary mouse astrocytes (McEllin et al., 2010). Mukherjee et al. overexpressed wildtype *PTEN* in endometrial carcinoma cell line Ishikawa which does not express endogenous *PTEN*. Overexpression of PTEN reduced the efficacy of olaparib but did not affect the efficacy of talazoparib (Mukherjee et al., 2018). In contrast, Fraser et al. compared the correlation of *PTEN* expression in three prostate cancer cell lines (22RV1 ($PTEN^{+/+}$), DU145 ($PTEN^{+/-}$), and PC3 ($PTEN^{-/-}$)) with clonogenic survival following olaparib treatment and found no correlation (Fraser et al., 2012). Lastly, combination of *PTEN*

inhibitor VO-OHpic with PARPi olaparib, veliparib, or rucaparib was synergic in ovarian cancer cell line ES2 (Qiu et al., 2024). This suggests that *PTEN* may be a suitable target for combination with olaparib in PDAC.

5.3.2.2 BRCC3

BRCA1/BRCA2-Containing Complex Subunit 3 (*BRCC3*) was significantly depleted in the talazoparib DDR screen (p=0.01, LFC=-0.1) and talazoparib PK screen (p=0.003, LFC=-0.8). *BRCC3* is a Lysine 63-specific deubiquitinating enzyme that is part of the BRCA1-A complex. This complex is recruited to the site of DNA breaks where it regulates the ubiquitination of chromatin and inhibits DNA end resection which may prevent overactive recombination and steer DSB repair towards NHEJ (Meyer et al., 2019; Rabl, 2020). The mutation frequency of *BRCC3* in PDAC is low at around 1% but differences in *BRCC3* mRNA expression levels have been observed in patients and low expression levels have been associated with better prognosis, possibly indicating that these patients are more sensitive to treatment as is the case for *BRCA2* (The Cancer Genome Atlas, TCGA-PAAD).

Knockdown of *BRCC3* in Panc-1 cells in combination with olaparib or talazoparib significantly reduced viability compared to scrambled control (82% vs 97%, p=0.0009 and 80% vs 101%, p=0.005, respectively). However, no significant difference in viability was observed between *BRCC3* knockdown and scrambled control after treatment with olaparib in the colony formation assay (80% vs. 74%).

In accordance with our findings, low expression of *BRCC3* has been associated with sensitivity to PARPi rucaparib in a panel of 39 ovarian cancer cell lines (Ihnen et al., 2013). Additionally, *BRCC3* expression was found to be significantly increased in three prostate cancer cell lines (LNCaP, C4-2B and DU145) with acquired olaparib resistance compared to their parental cells (Cahuzac et al., 2022). These results, in combination with our findings suggest that combination of PARPi and BRCC3 inhibition is effective in PDAC and may prevent development of resistance, although more research is needed to confirm this.

5.3.2.3 XRCC3

X-Ray Repair Cross Complementing 3 (*XRCC3*) was significantly depleted in the olaparib DDR screen (p=5.0e-06, LFC=-0.4) as well as the olaparib (p=0.007, LFC=-7.9) and talazoparib (p=0.007, LFC=-3.6) PK screens. Together with RAD51C, XRCC3 forms a complex (CX3) that acts downstream of RAD51 recruitment to DNA damage foci (Chun et al., 2013).

XRCC3 is essential for efficient repair of DSBs by HR (Brenneman et al., 2000). The mutation frequency of *XRCC3* is low at approximately 1% but differences in mRNA expression level have been observed in patients and are associated with survival (The Cancer Genome Atlas, TCGA-PAAD). Low *XRCC3* mRNA expression is significantly correlated to poorer survival so novel therapies are especially needed in this subgroup.

Knockdown of X*RCC3* in Panc-1 cells in combination with olaparib or talazoparib significantly reduced viability compared to scrambled control (84% vs 97%, p=0.003 and 82% vs 101%, p=0.03, respectively). However, no significant difference in viability was observed between *BRCC3* knockdown and scrambled control after treatment with olaparib in the colony formation assay (82% vs. 74%).

Similarly, Jamal et al. performed a genome-wide CRISPR/Cas9 KO screen in six tumour cell lines (breast, colon, bone) to identify genes whose inactivation sensitise to olaparib and combined their results with the results of previously published CRISPR screens in eight other cell lines (Jamal et al., 2022). Across these 14 screens they identified 1147 significantly depleted genes, of which 110 were found in more than one screen. Of these, *XRCC3* was found to be most frequently altered in PARPi-approved settings based on TCGA data and loss of *XRCC3* was mutually exclusive with *BRCA*. In prostate cancer, loss of function was predominantly caused by promoter methylation rather than mutation. To validate that loss of *XRCC3* indeed sensitises to olaparib they developed a DU145 *XRCC3* knockout cell line and confirmed that knockout indeed increases the sensitivity to olaparib compared to the wildtype DU145 by colony formation assay. This study confirms our finding that *XRCC3* loss sensitises to PARPi and makes a case to include *XRCC3* deficiency as clinical marker for olaparib sensitivity.

5.3.3 Overcoming resistance using ATM/ATRi with PARPi combination treatment

The genes identified in the CRISPR screen show promise for synthetic lethality interactions with PARPi. However, currently there are no BRCC3 or XRCC3 pharmacological inhibitors available and there have been no clinical trials using PTEN inhibitors registered on clinicaltrials.gov yet. Therefore, we investigated if FDA approved DDR targets ATM and ATR could overcome PARPi resistance using preclinical compounds obtained under MTA from AstraZeneca.

Both ATM and ATR proteins are major regulators in DSB repair and signalling (Wagh et al., 2020) and inhibition or deficiency of these proteins have shown promising results in several studies (Höfer et al., 2024; Jette et al., 2020; Lloyd et al., 2020; Parsels et al., 2021; Wallez et al., 2018). However, to our knowledge no one has investigated the combination of ATM/ATRi with PARPi in cisplatin or PARPi resistant PDAC.

We collaborated with AstraZeneca through their Open Innovation program, and they provided us with Lynparza (PARPi, branded olaparib), Saruparib (PARPi, AZD5305), AZD1390 (ATMi), and Ceralasertib (ATRi, AZD6738) to evaluate in our previously established resistant Capan-1 cells.

Neither the parental nor the cisplatin, olaparib, or talazoparib resistant Capan-1 cells were sensitive to PARPi Lynparza or Saruparib as IC_{50} values were not reached at a maximum treatment concentration of 100 µM. Interestingly, in a previously published Capan-1 PDX model treatment with 10 mg/kg or 1 mg/kg, corresponding to a maximum plasma concentration of approximately 15 µM and 1 µM respectively, was able to induce tumour stasis (Illuzzi et al., 2022).

Capan-1 cells were more sensitive to ATMi AZD1390 with IC_{50} values ranging from 13.1 to 20.5 µM, with no significant differences between the parental and the resistant cell lines. However, these concentrations are most likely not achievable in a clinical setting which suggests that none of these three agents are suitable as single agent therapies in this particular setting.

The response to ATRi Ceralasertib varied between the Capan-1 cell lines with IC_{50} values ranging between 0.4 and 4.3 µM. Capan-1CisR had a significantly higher IC_{50} value compared to the parental cells (4.3 vs. 1.8 µM, p=0.01), whereas Capan-1OlaR had a significantly lower IC_{50} value compared to the parental cells (0.4 vs. 1.8 µM, p=0.006). Combination of Ceralasertib with PARPi Saruparib was significantly synergic in Capan-1, Capan-1OlaR, and Capan-1TalR as measured by viability assay and in Capan-1TalR as measured by colony formation assay. Combination of Ceralasertib with PARPi Lynparza was significantly synergic in Capan-1 as measured by viability assay and in Capan-1 and Capan-1CisR as measured by colony formation assay. While further validation is required these experiments suggest that combination of ATRi and PARPi may be effective in preventing or overcoming PARPi resistance.

5.3.4 γH2AX and RAD51 foci formation upon ATRi and PARPi treatment

As discussed in the previous chapter, γH2AX and RAD51 are DSB markers and RAD51 recruitment is dependent on functional *BRCA2* expression. However, several studies have also suggested a BRCA2-independent role for RAD51 in the repair of stalled replication forks during the S-phase of the cell cycle (Sears et al., 2016; Tarsounas et al., 2004; Ward & Chen, 2001). These RAD51 foci overlap with PCNA, γH2AX, BRCA1, and 53BP1, and can be induced by hydroxyurea-induced fork stalling and replication block (Ward & Chen, 2001). ATR is known to be involved in replication stress and also forms foci at stalled replication forks that overlap with BRCA1 (Tibbetts et al., 2000). We therefore questioned whether treatment with ATRi or PARPi alone or in combination could affect γH2AX and RAD51 foci formation. We observed no differences in the formation of RAD51 foci for any treatment or cell line. A subpopulation of proliferating cells with stalled replication forks was observed.

We also observed no differences in the formation of γH2AX foci. Previous work by Ward et al., showed that γH2AX foci formation in response to replication stress induced by hydroxyurea required ATR (Ward & Chen, 2001). If PARPi causes replication fork stress due to PARP trapping an increase in γH2AX foci in the single agent PARPi treatment, but not (or to a lesser extent) in the PARP/ATRi combination treatment would be expected at least in the parental cells. This suggests that the γH2AX foci that were observed are not (purely) caused by stalled replication forks. Sears et al. showed that ATRi VE-821 does not affect γH2AX foci formation in irradiated cells but does decrease early γH2AX foci in cisplatin treated cells (30 min)(Sears et al., 2016). However, they did not observe a difference in late γH2AX foci in cisplatin-treated cells (24 hours). It is therefore likely that the γH2AX foci formation in our experiment also would not be affected.

5.3.5 PARP1 and BRCC3 protein expression after ATRi and PARPi treatment

Lastly, we investigated whether PARPi and ATRi alone or in combination affected PARP1 or BRCC3 protein expression. As the main target of PARPi, we wondered if inhibition affected PARP1 expression as well, but no changes were observed. Evaluation of literature found contradicting results. Xu et al. treated two HRD ovarian cancer cell lines with 25 μM olaparib and also saw no changes in expression (Xu et al., 2022). Ma et al. treated breast cancer cell lines MCF-7 and ZR-75-1 with 5 μM olaparib an saw a significant 40-60% decrease in PARP1 protein and mRNA expression (Ma et al., 2019). In contrast, Prasod and

Biegała both reported an increase in PARP1 expression upon olaparib treatment. Prasod et al. treated two cervical carcinoma cell line with 5 and 10 µM olaparib and showed an increase in PARP1 (not quantified) (Prasad et al., 2017). Biegała et al. treated ovarian cancer cell lines PEO1 and PEO4, and olaparib-resistant PEO1-OR with 5 µM olaparib and Ceralasertib alone or in combination (Biegała et al., 2023). Olaparib and the combination olaparib/Ceralasertib significantly increased full length PARP1 expression in all three cell lines, olaparib alone increased cleaved PARP1 in PEO1, and the combination increased cleaved PARP1 in PEO1 and PEO4 but not in PEO1-OR. Kim et al. saw an increase in chromatin-bound PARP1 after treatment with 10 µM talazoparib in HeLa cells (Kim;, Xu, et al., 2020). And lastly, Eskiler et al. saw no change in PARP1 expression after treatment with talazoparib in breast cancer cell line HCC1937 and BMN673-resistant HCC1937, and a decrease in expression in MCF-10A (Eskiler et al., 2018). Based on these varying results we suggest that changes in PARP1 expression after PARPi treatment are cell line dependent and are not necessarily correlated with resistance.

BRCC3 is a subunit of the BRCC complex and is necessary for the formation of BRCA1 foci at DSBs (Chen et al., 2006). Since it was unclear from the formation of RAD51 foci after treatment if damage was caused by replication fork stalling or DSBs the expression of DSB-specific repair protein BRCC3 was investigated under the assumption that increased expression is linked to increased presence of DSBs. No changes were observed in BRCC3 protein expression in any of the cell lines or treatments, which means that it cannot be excluded that the RAD51 foci are caused by stalled replication forks.

5.4 CONCLUSION

In summary, in this chapter we have identified three genes (*PTEN, BRCC3*, and *XRCC3*) whose depletion or loss sensitises to olaparib and talazoparib treatment. Tumours with deficiency of these genes due to mutation, loss, or inactivation may be more sensitive to PARPi. While further investigation is necessary, these findings suggest that more patients could be eligible for PARPi treatment. Additionally, these genes are promising targets for development of targeted inhibitors in combination with PARPi and may be used to expand treatment to DDR proficient patients.

We also evaluated the efficacy of novel ATM (AZD1390) and ATR inhibitors (Ceralasertib) alone or in combination with PARPi (Lynparza, talazoparib, Saruparib) in our Capan-1 parental and resistant models. We found that Ceralasertib is a very promising agent in an olaparib-treatment setting as olaparib-resistant cells have an increased sensitivity to this drug compared to parental cells and the drug was synergic in combination with Lynparza. Additionally, Ceralasertib was also synergic with Saruparib in the parental, olaparib, and talazoparib-resistant Capan-1 cells. Treatment did not affect the induction or accumulation of DNA damage as measured by γH2AX or RAD51 foci formation, or the expression of PARP1 and BRCC3, suggesting that the cytotoxic effect of these inhibitors is further downstream of these signalling pathways.

5.4.1 Future work

1. Many of the most significantly depleted genes in the DDR and PK CRISPR screens are involved in either replication fork regulation or DSB repair. So far, most research on synthetic lethality or synergism with PARPis has been focused on HR deficiency. However, these screens suggest that targeting the replication fork may also be a possible strategy. Further research is needed to validate these additional targets by siRNA knockdown or CRISPR knockout. DNA fiber assays could be used to investigate the effect of knockdown and PARPi treatment on replication fork dynamics.
2. Addition of colony formation assay for the combination of *PTEN, BRCC3,* or *XRCC3* knockdown in combination with talazoparib treatment to complement the results for the olaparib treatment.
3. Lynparza is AstraZeneca's branded version of olaparib. We noticed that the Capan-1 cells were less sensitive to Lynparza than to olaparib. Differences in sensitivity

may be caused by differences in drug formulation or biological differences in the used cells. Comparative viability assays with the same biological replicates should be performed to elucidate the cause for the observed difference.

4. The mechanism of action of the combination of PARPi and ATRi remains unclear. Evaluation of cell cycle status by flow cytometry and DNA fiber assays may provide more insight in the role of DNA damage signalling and cell cycle inhibition.

6 CONCLUSION

In this thesis, it was shown that cell culture method affects drug sensitivity in a model-specific manner. It is therefore important that drug sensitivity assays are performed in a variety of models and culture methods to provide a better scope of treatment responses. Therefore, four novel, rare periampullary adenocarcinoma organoids were established, characterised, and used for viability assays.

Homologous recombination repair deficiency has been used to target pancreatic ductal adenocarcinoma in the clinic using cisplatin and PARP inhibitors, but both intrinsic and rapidly acquired resistance prevent a curative response. Investigation of cisplatin, olaparib, and talazoparib resistance in *BRCA2*-deficient cell line Capan-1 showed that resistance is caused by a combination of multiple mechanisms, including alteration of PARP1 protein expression and metabolomic reprogramming. Interestingly, resistance mechanisms were similar between the cisplatin and talazoparib-resistant cells which both had loss of PARP1 expression and metabolomic shift in favour of oxidative phosphorylation, whereas the olaparib-resistant cells had no significant change in PARP1 expression and had a metabolomic shift in favour of glycolysis. These findings highlight the differences between the mechanism of action of the PARP inhibitors and suggest that the high PARP-trapping potential of talazoparib may make it act more like a genotoxic agent rather than a targeted inhibitor.

Deficiency of DNA damage repair genes *PTEN, BRCC3* and *XRCC3* was shown to be synthetic lethal with PARP inhibitors olaparib and talazoparib in the homologous recombination repair proficient cell line Panc-1. This suggests that PARP inhibitor treatment can be extended to patients with deficiency of these genes. Additionally, combination of ATR inhibitor Ceralasertib and PARP inhibitor Lynparza (olaparib) or Saruparib was synergic in the parental and olaparib-resistant Capan-1 cell lines, suggesting that addition of Ceralasertib to PARP inhibition may help to prevent or overcome PARP inhibitor resistance.

In conclusion, this thesis shows that targeting DNA damage repair deficiency is promising in pancreatic ductal adenocarcinoma and can be extended beyond *BRCA1/2* deficiency.

7 SUPPLEMENTAL FIGURES AND TABLES

Supplemental Table 1. Mutation frequency of DDR genes in PDAC patients and their associated pathways. Abbreviations: HR: homologous recombination, NHEJ: non-homologous end-joining, BER: base-excision repair, NER: nucleotide-excision repair, ICL repair: interstrand crosslink repair, MMR: mismatch repair.

Gene	Freq (%)	Pathways
TP53	68.90	NER
BRCA2	4.40	HR, NER
ATM	4.00	NHEJ
PRKDC	3.90	NHEJ
MCM4	3.50	HR
NIPBL	3.20	HR
POLQ	3.20	HR, NHEJ, BER
RIF1	3.10	HR, NHEJ
WRN	2.40	HR, BER
FAAP100	2.40	ICL repair
FANCD2	2.40	ICL repair
ERCC6	2.20	HR, NHEJ, BER, NER
EP300	2.10	NER
RECQL4	2.00	HR
HELQ	1.90	HR
CUL4A	1.80	NER
ARID2	1.80	HR
FANCM	1.80	HR, ICL repair
FANCA	1.80	ICL repair
PAXIP1	1.70	NHEJ
FAN1	1.60	HR, NER, ICL repair
BRCA1	1.60	HR, NHEJ
MUS81	1.60	HR, ICL repair
SETD2	1.60	HR, MMR
ATR	1.60	ICL repair
SLX4	1.40	HR, NER, ICL repair
RAD54B	1.40	HR
BRCC3	1.40	NHEJ

Gene	Freq (%)	Pathways
MSH6	1.40	ICL repair, MMR
POLE	1.30	BER, NER
GEN1	1.30	HR
PALB2	1.30	HR
XRCC3	1.30	HR, ICL repair
UIMC1	1.30	NHEJ
XPC	1.20	NER, MMR
MCM8	1.20	HR, ICL repair
RBBP8	1.20	HR
TP53BP1	1.20	HR, NHEJ
NEIL3	1.20	BER, ICL repair
XRCC1	1.10	HR, NHEJ, BER, NER
BLM	1.10	HR
POLD1	1.00	BER, NER, MMR
AXIN2	1.00	MMR
DCLRE1C	1.00	NHEJ, ICL repair
FANCI	1.00	ICL repair
NEIL2	1.00	BER
ERCC5	0.90	HR, BER, NER
LIG4	0.90	NHEJ, NER
CDC7	0.90	HR
MCM5	0.90	HR
RAD50	0.90	HR, NHEJ
ABL1	0.90	MMR
BARD1	0.90	NHEJ
EME1	0.90	ICL repair
MBD4	0.90	BER

MLH3	0.90	MMR
MSH2	0.90	MMR
BRIP1	0.80	NER
ERCC2	0.80	NER
FUS	0.80	HR
NBN	0.80	HR, NHEJ
MDC1	0.80	NHEJ
XPA	0.70	BER, NER, ICL repair
FANCL	0.70	ICL repair
MLH1	0.70	NHEJ, MMR
NEIL1	0.70	BER
NSD2	0.70	NHEJ
TDG	0.70	BER, MMR
XRCC6 (Ku70)	0.70	NHEJ
ERCC4	0.60	HR, NHEJ, NER, ICL repair
ERCC1	0.60	NHEJ, NER, ICL repair, MMR
FANCC	0.60	NER, ICL repair
WAS	0.60	HR
FANCE	0.60	ICL repair
FANCG	0.60	ICL repair
MUTYH	0.60	BER, MMR
PARP3	0.60	NHEJ
PMS2	0.60	MMR
DDB2	0.50	NER
OGG1	0.50	BER, NER
RAD21	0.50	HR
EXO1	0.50	MMR
FANCF	0.50	ICL repair
MSH3	0.50	MMR
POLB	0.50	NHEJ, BER
RNF8	0.50	NHEJ, ICL repair
UBE2T	0.50	ICL repair
XRCC4	0.50	NHEJ
XRCC5 (Ku80)	0.50	NHEJ
PARP1	0.40	HR, BER, NER
RPA1	0.40	HR, BER, NER, ICL repair, MMR
ERCC3	0.40	NER
CHEK1	0.40	HR
FANCB	0.40	HR, ICL repair
ABRAXAS1	0.40	NHEJ
PMS1	0.40	MMR
POT1	0.40	NHEJ, BER
RAD52	0.30	HR, NER
NTHL1	0.30	BER, NER
PNKP	0.30	NHEJ, BER, NER
DMC1	0.30	HR
RAD51C	0.30	HR
RAD54L	0.30	HR
SLX1A	0.30	HR, ICL repair
BABAM2	0.30	NHEJ
FAAP24	0.30	ICL repair
DDB1	0.20	NER
MRE11	0.20	HR, NHEJ
RAD51	0.20	HR, ICL repair
RECQL	0.20	HR
RTEL1	0.20	HR
BABAM1	0.20	NHEJ
FAAP20	0.20	ICL repair
XRCC2	0.10	HR
PPP4R2	0.09	HR
RAD51B	0.09	HR
RAD51D	0.09	HR, ICL repair

Supplemental table 2. Overview of clinical trials in PDAC that use DDR targeting therapies (clinicaltrials.gov). Abbreviations: OS: overall survival, ORR: overall response rate, OR: odds ratio, HR: hazard ratio, AE: adverse event, SAE: serious adverse event, DL: dose level, CBR: clinical benefit rate, DCO: data cut-off

NCT ID (publication)	Phase	Drug	Condition	Intervention	Status	Results (months, CI)
ATR						
NCT01337765	1	Dactolisib	advanced or unresectable solid tumours	Dactolisib, MEK162	completed	
NCT04514497	1	Elimusertib	metastatic or unresectable SCLC, PDNEC, PDAC	Arm A: limusertib, irinotecan liposome Arm B: elimusertib, topotecan	active, not recruiting	
NCT04616534	1	Elimusertib	uncurable solid tumour	Gemcitabine, elimusertib	active, not recruiting	
NCT04657068	1/2	ART0380	advanced or metastatic solid tumours	Part A1: intermittent vs. continuous ART0380 Part A2: intermittent ART0380, gemcitabine Part B1: ART0380 in patients without *ATM* mutations Part B2: ART0380, gemcitabine vs. gemcitabine in patients with advanced ovarian cancer	recruiting	
NCT02595931	1	M6620/ Berzosertib	Metastatic/unresectable tumour with DDR deficiency	Berzosertib, irinotecan HCl	active, not recruiting	
DNA-PK						
NCT02981342	2	LY3023414	metastatic PDAC	Arm A: abemaciclib Arm B: abemaciclib, LY3023414 Arm C: SOC (gemcitabine/capecitabine)	completed	PFS abemaciclib: 1.68 (1.35 to 1.84) abemaciclib+LY3023414: 1.81 (1.28 to 1.91) SOC: 3.25 (1.05 to 5.65)
NCT04172532	1/2	Peposertib	locally advanced PDAC	Phase 1: hypofractionated radiation, M3814	suspended	

				Phase 2, arm A: hypofractionated radiation, M3814 Phase 2, arm B: hypofractionated radiation, placebo		
PARP						
NCT02184195 (Golan et al., 2019)	3	Olaparib	PDAC (*BRCA*-mut)	Arm A: olaparib Arm B: placebo	active, not recruiting	PFS olaparib: 7.4 (4.14 to 11.01) vs. placebo: 3.8 (3.52 to 4.86), p=0.004 mOS Olaparib: 18.9 (14.85-26.15) vs. placebo 18.1 (12.62-26.12), p=0.6833
NCT03205176	1	Olaparib	solid tumours	Arm A: AZD5153 (BRD4/BETi) Arm B: AZD5153, olaparib	completed	Preliminary safety data: 50% AEs, 25% SAEs, 25%≥G3 AEs
NCT02677038	2	Olaparib	metastatic PDAC post ≥ first-line of prior therapy	Olaparib	completed	mPFS 24.7 weeks (3.9 to 41.1)
NCT03140670	2	Rucaparib	locally advanced or metastatic PDAC with *BRCA1/2* or *PALB2* mut that has not progressed on platinum-based therapy	Maintenance rucaparib	terminated	ORR: 41.7 (25.5 to 59.2) mOS: 23.5 (20 to 27)
NCT02890355 (Chiorean et al., 2019)	2	Veliparib	metastatic PDAC	Arm A: veliparib, mFOLFIRI Arm B: FOLFIRI	active, not recruiting	mOS veliparib+mFOLFIRI: 5.4 (3.7 to 7.2) mFOLFIRI: 6.5 (5.6 to 7.8), p=0.28
NCT01489865 (Pishvaian et al., 2020)	1/2	Veliparib	PDAC (BRCAness)	Veliparib, mFOLFOX-6	unknown	mOS all patients: 8.5, mOS platinum-naïve (DDR mut): 11.8 ORR entire cohort: 26% ORR in platinum-naïve (DDR mut): 57%
NCT01585805	1	Veliparib	advanced/metastatic PDAC (*BRCA/PALB2* mut)	Arm A: veliparib, gemcitabine HCl, cisplatin Arm B: gemcitabine HCl, cisplatin Arm C: veliparib	active, not recruiting	phase I result (n=17) OR: BRCA+ 7/9, BRCA- 0/7. OS: BRCA+ 23.3, BRCA- 11

NCT01296763	1/2	Olaparib	PDAC	Irinotecan, cisplatin, olaparib (mitomycin C)	completed	severe toxicity, further study not planned. SAEs 71.4% at DL1, 80% at DL2, 66,7% at DL3
NCT00515866 (Bendell et al., 2015)	1	Olaparib	Locally advanced or metastatic unresectable PDAC	Dose escalation phase: olaparib, gemcitabine Dose expansion: olaparib, gemcitabine vs. gemcitabine	completed	ORR expansion phase: olaparib + gemcitabine: 27% gemcitabine:14%, p=ns (no sign. difference OS or PFS)
NCT02042378	2	Rucaparib	PDAC (*BRCA* mut, germline or somatic)	Rucaparib	completed	ORR: 15.8%, DCR: 31.6
NCT01286987	1	Talazoparib	unresectable, locally advanced or metastatic solid tumour	Talazoparib	completed	PaCa PFS: 5.3 weeks (2.4 to 21.3)
NCT02286687	2	Talazoparib	Metastatic or inoperable locally advanced or recurrent cancer with somatic mutations or deletions in *BRCA1/2,* mutations or homozygous deletions in other *BRCA* pathway genes, or germline *BRCA1/2* mutations with cancers other than breast or ovarian	Talazoparib	active, not recruiting	
NCT00892736	1	Veliparib	malignant solid tumours with *BRCA1/2* mutations, platinum refractory ovarian, fallopian tube or primary peritoneal cancer, or progressive basal-like breast cancer	Veliparib	completed	*BRCA* mut: ORR 23%, CBR of 58% *BRCA* wt: ORR 3%, CBR of 38%
NCT01908478 (Tuli et al., 2019)	1	Veliparib	advanced unresectable or borderline resectable PDAC	Veliparib, gemcitabine, radiation	completed	mOS entire cohort: 14.6 (11.6-21.8) mOS DDR gene altered cohort: 19 (6.2-27.2)
NCT04673448	1	Niraparib	uresectable or metastatic breast, pancreas, ovary, fallopian tube or primary peritoneal cancer with *BRCA* mut	Niraparib, dostarlimab	recruiting	
NCT04764084	1	Niraparib	HER2- breast cancer, cholangiocarcinoma, gastric adenocarcinoma, pancreatic cancer with deleterious HRR mutations	Niraparib, anlotinib	unknown	
NCT04753879	2	Olaparib	stable or progressive PDAC post six cycles of GAX-CI	Nab-paclitaxel, gemcitabine, cisplatin, irinotecan, capecitabine (GAX-CI), pembrolizumab, olaparib	recruiting	

NCT04584008	N/A	?	metastatic gastrointestinal tumours	Arm A: matched targeted agent Arm B: unmatched therapy	recruiting	goal of the study is to see if targeted therapies improve response
NCT04503265	1/2	AMXI-5001	advanced or metastatic tumours	AMXI-500	recruiting	
NCT04644068	1/2a	AZD5305	advanced solid tumours	Arm A: AZD5305 Arm B: AZD5305, paclitaxel Arm C: AZD5305, carboplatin, +/-paclitaxel	recruiting	
NCT04425876	1	Fluzoparib	resectable or borderline resectable PDAC	Fluzoparib, mFOLFIRINOX → maintenance fluzoparib	unknown	
NCT04228601	1/2	Fluzoparib	local advanced/metastatic PDAC (g*BRCA1/2, gPALB2* mut)	Arm A: fluzoparib, mFOLFIRINOX → maintenance fluzoparib Arm B: placebo, mFOLFIRINOX → maintenance placebo	unknown	
NCT04300114	3	Fluzoparib	metastatic PDAC that has not progressed on first-line platinum-based therapy (*gBRCA1/2, gPALB2* mut)	Arm A: maintenance fluzoparib Arm B: placebo	unknown	
NCT03404960	1/2	Niraparib	locally advanced or metastatic PDAC	Arm A: niraparib, nivolumab Arm B: niraparib, ipilimumab	active, not recruiting	PFS at 6 months Arm A:20.6% (8.3% to 32.9%) Arm B: 59.6% (44.3% to 74.9%)
NCT03553004	2	Niraparib	metastatic pancreatic cancer with germline or somatic mutations in DDR	Niraparib	active, not recruiting	
NCT03601923	2	Niraparib	unresectable or metastatic pancreatic cancer (with *BRCA1, BRCA2, PALB2, CHEK2* or *ATM* mut – either germline or somatic)	Niraparib	active, not recruiting	
NCT04409002	2	Niraparib	metastatic PDAC	Niraparib, dostarlimab, radiation	completed	mPFS: 1.6 (1.1 to 2.7) mOS: 3.1 (1.5 to 7.7)
NCT04493060	2	Niraparib	metastatic PDAC with *BRCA1/2, PALB2, BARD1, RAD51c,* or *RAD51d* mut	Niraparib, dostarlimab	active, not recruiting	
NCT05442749	2	Niraparib	Advanced/metastatic PDAC with *BARD1, BRCA1, BRCA2, BRIP1, FANCA, FANCD2, FANCL, MRE11, NBN, PALB2, PPP2R2A, RAD51B, RAD51C, RAD51D,* or *RAD54L* mut	Niraparib	recruiting	.

NCT04779151	2	Niraparib	Advanced/metastatic solid tumour with bi-allelic LOF of A*RID1A, ARID2, ATM, BARD1, BRCA1, BRCA2, BRIP1, CDK12, CHEK2, FANCA, IDH1, IDH2, NBN, PALB2, PBRM1, RAD51C, RAD51D, FANCA, NBN, RAD51, RAD54L,* or *SMARCA4.*	Dostarlimab and niraparib	recruiting	.
NCT03221400	1/2	Niraparib	Locally recurrent/metastatic solid tumour (incl. PDAC)	Phase 1a: PEN-866 Sodium Phase 1b: PEN-866 Sodium, fluoruracil, folinic acid Phase 2a: PEN-866 Sodium Phase 2b: PEN-866 Sodium, niraparib	recruiting	.
NCT05238831	1	Niraparib Olaparib	Advanced sarcoma/prostate/breast/ovarian/pancreatic cancer	Alectinib, alpelisib, anastrozole, atezolizumab, bevacizumab, capecitabine, carboplatin, cobimetinib, entrectinib, eribulin, fulvestrant, trastuzumab, irinotecan, letrozole, nab-paclitaxel, niraparib, olaparib, paclitaxel, Palbociclib, pertuzumab, trastuzumab, vermurafenib, vinorelbine, vismodegib alone or in combination	not yet recruiting	.
NCT04182516	1	NMS-03305293	locally advanced/metastatic HER2- breast cancer, epithelial ovarian cancer, castration-resistant prostate cancer, pancreatic cancer (*BRCA1/2* not required for dose escalation phase, but enrichment will later be attempted in dose expansion phase)	NMS-03305293	recruiting	
NCT03878524	1	Olaparib	56 hematological and solid malignancies	selection of 2 targeted drugs	active, not recruiting	
NCT04005690	1	Olaparib	PDAC	Arm A: cobimetinib (MEK/ERKi) Arm B: olaparib	recruiting	
NCT02498613	2	Olaparib	NSCLC, SCLC, PDAC, TNBC	Cediranib maleate, olaparib	active, not recruiting	
NCT04548752	2	Olaparib	metastatic PDAC with g*BRCA*-mut	Arm A: olaparib, pembrolizumab Arm B: olaparib	recruiting	

NCT03337087	1/2	Rucaparib	Metastatic pancreatic, colorectal, gastro-esophageal and bilary cancer	Liposomal irinotecan, leucovorin, fluorouracil, rucaparib	active not recruiting	
NCT04171700	2	Rucaparib	Unresectable, locally advanced or metastatic solid tumour with deleterious mutation in *BRCA1, BRCA2, PALB2, RAD51C, or RAD51D (Arm A) or BARD1, BRIP1, FANCA, NBN, RAD51* or *RAD51B (ARM B)*	Rucaparib	terminated	mPFS arm A: 3.7 (1.9 to 5.4) mPFS arm B: 3.6 (1.6 to 6.3) mOS arm A: 13.3 (10.6 to NA) mOS arm B: 8.0 (4.8 to 16.6)
NCT04550494	2	Talazoparib	advanced tumours with DDR mutations	Talazoparib	recruiting	
NCT03637491	1/2	Talazoparib	metastatic solid tumours	Arm A: avelumab (PD-L1i), binimetinib (MEKi) Arm B: avelumab, binimetinib, talazoparib Arm C: binimetinib, talazoparib	terminated	Available clinical data has shown limited anti-tumour activity and reaching target study drug dose levels may not be feasible
NCT01233505	1	Veliparib	advanced solid tumours with *BRCA1/2* mutations	Veliparib, capecitabine, oxaliplatin	terminated	
NCT01282333	1	Veliparib	metastatic or unresectable advanced biliary/pancreatic cancer, urothelial cancer, or non-small cell lung cancer	Veliparib, gemcitabine hydrochloride, cisplatin	terminated	
NCT02511223	2	Olaparib	metastatic PDAC (no g*BRCA*, but somatic mut are allowed)	Olaparib	completed	mPFS 14 weeks (5.7-40)
NCT04666740	2	Olaparib	Metastatic PDAC on platinum maintenance with HRD (*BRCA1/2, PALB2, ATM, BAP1, BARD1, BLM, BRIP1, CHEK2, FAM175A, FANCA, FANCC, MUTYH, NBN, RAD50, RAD51, RAD51C, RTEL1)*	Pembrolizumab and olaparib	recruiting	
NCT05257993	1	JPI-547	Locally advanced/metastatic PDAC	Arm A: mFOLFIRINOX and JPI-547 Arm B: GemAbraxan and JPI-547	not yet recruiting	
NCT05093231	2	Olaparib	Metastatic PDAC with high tumour mutation burden	Pembrolizumab and olaparib	not yet recruiting	
NCT01078662	2	Olaparib	Solid tumour with BRCA mutation	Olaparib	active, not recruiting	mPFS PaCa: 4.55 (1.81 to 8.21) mOS PaCa: 9.81 (3.84 to 16.62)
NCT05659914	2	Olaparib	Metastatic PDAC with alterations in DDR genes	Olaparib and durvalumab	recruiting	

NCT06078787	2	Olaparib	Advanced/metastatic PDAC with PALB2 mutation	Olaparib	recruiting	
NCT06130254	1	Olaparib	Advanced solid tumours with KRAS-G12C mutation	Adagrasib and olaparib	not yet recruiting	
NCT05252390	1/2	Olaparib	Advanced solid tumours	Phase 1: NUV-868 Phase 1b, arm a: NUV-868 and olaparib Phase 1b, arm b: NUV-868 and enzalutamide Phase 2, arm A: NUV-868 and olaparib Phase 2, arm B: NUV-868 and enzalutamide Phase 2, arm C: NUV-868 Phase 2, arm D: enzalutamide	recruiting	
NCT04753879	2	Olaparib	Metastatic PDAC	Nab-paclitaxel, gemcitabine, cisplatin, irinotecan, capecitabine, pembrolizumab, and olaparib	recruiting	
NCT06065059	1/2	Olaparib	Advanced/metastatic solid tumour with BRCA1/2 mutation or other HRD	Arm A: TNG348 Arm B: TNG348, olaparib	recruiting	
NCT03851614	2	Olaparib	Advanced/metastatic MMRp-CRC, PDAC, leiomyosarcoma	Arm A: durvalumab, olaparib Arm B: durvalumab, cediranib	active, not recruiting	
NCT04666740	2	Olaparib	Metastatic PDAC with HRD (*BRCA1/2, PALB2, ATM, BAP1, BARD1, BLM, BRIP1, CHEK2, FAM175A, FANCA, FANCC, MUTYH, NBN, RAD50, RAD51, RAD51C, RTEL1*) or exceptional response to platinum-based therapy	Pembrolizumab and olaparib	recruiting	
NCT04858334	2	Olaparib	Curatively resected pancreatic cancer	Arm A: olaparib Arm B: placebo	recruiting	
NCT04348045	2	Olaparib	Stable or responsive metastatic PDAC	Arm A: olaparib Arm B: durvalumab and selumetinib Arm C: FOLFIRI	active, not recruiting	
WEE1						
NCT02194829	1/2	Adavosertib	metastatic or unresectable locally advanced PDAC	Arm A/B (phase 1): nab-paclitaxel, gemcitabine HCl, adavosertib	completed	Terminated at phase 1 due to severe dose limiting toxicities

				Arm C (phase 2): nab-paclitaxel, gemcitabine HCl, placebo Arm D (phase 2): nab-paclitaxel, gemcitabine HCl, adavosertib		
NCT02037230 (Cuneo et al., 2019)	1/2	MK-1775	Unresectable PDAC	MK-1777, gemcitabine, and radiation	completed	mOS: 21.7 (16.7 to 24.8)
NCT04768868	1	IMP7068	advanced solid tumour	IMP7068	recruiting	
NCT05212025	2	Adavosertib	Platinum-resistant advanced pancreatic cancer	Adavosertib and gemcitabine	withdrawn	
NCT06015659	2	ZN-c3/Zentalis	Advanced PDAC	ZN-c3 and gemcitabine HCl	recruiting	
Other						
NCT03682289	2	Olaparib / AZD6738	locally advanced or metastatic solid tumour	Arm A: AZD6738 (ATRi) Arm B: AZD6738, olaparib	recruiting	
NCT00839332 (Laquente et al., 2017)	1/2	Rabusertib	phase 1: metastatic cancers, phase 2: PDAC	Arm A: rabusertib, gemcitabine Arm B: gemcitabine	completed	OS rabusertib + gemcitabine: 7.8 (5.0 to 11.1) gemcitabine: 8.3 (5.1 to 14.1)
NCT03997968	1/2	CYT-0851 (RAD51 inhibitor)	B-cell malignancies, metastatic breast cancer, recurrent head and neck cancer, ovarian cancer, soft tissue sarcoma, recurrent metastatic or locally advanced pancreatic cancer, advanced SCLC	CYT-0851	active, not recruiting	10 patients response evaluable by DCO. 1 PaCa patient stable disease for 111 days.

Supplemental Table 3: Genes in the protein kinase screen

AAK1, AATK, ABCC1, ABL1, ABL2, ACTA2, ACTR2, ACVR1, ACVR1B, ACVR1C, ACVR2A, ACVR2B, ACVRL1, ADAM9, ADCK1, ADCK2, ADCK3, ADCK4, ADCK5, ADK, ADPGK, ADRBK1, ADRBK2, AGK, AJUBA, AK1, AK2, AK3, AK4, AK5, AK7, AK8, AK9, AKR1B1, AKT1, AKT2, AKT3, ALDH18A1, ALDH1A1, ALDH1A3, ALK, ALPK1, ALPK2, ALPK3, AMHR2, ANKK1, ANLN, APTX, ARAF, ARG1, ARHGAP11B, ARHGAP11B_and_ARHGAP11A, ARHGAP18, ARID1A, ARNTL2, ARSG, ASCC1, ATAD5, ATG7, ATL3, ATM, ATMIN, ATP23_former_XRCC6BP1, ATP2C1, ATR, AURKA, AURKB, AURKC, AXL, BAP1, BARD1, BAZ1B, BCKDK, BCL2L1, BCL2L11, BCORL1, BCR, BFAR, BIRC5, BLK, BMP2K, BMPR1A, BMPR1B, BMPR2, BMX, BRAF, BRCA1, BRCA2, BRCC3, BRD2, BRD3, BRD4, BRDT, BRSK1, BRSK2, BTK, BUB1, BUB1B, C17orf75, C1orf106, C1orf86, C8orf44-SGK3, CAD, CALM1, CALM3, CAMK1, CAMK1D, CAMK1G, CAMK2A, CAMK2B, CAMK2D, CAMK2G, CAMK4, CAMKK1, CAMKK2, CAMKV, CARD11,CASK, CAV2, CCL2, CCND2, CCNH, CD155, CD160, CD2, CD274, CD276, CD2AP, CD40, CD40LG, CD80, CD86, CDC14B, CDC42BPA, CDC42BPB, CDC42BPG, CDC7, CDK1, CDK10, CDK11A, CDK11A_and_CDK11B, CDK11B, CDK12, CDK13, CDK14, CDK15, CDK16, CDK17, CDK18, CDK19, CDK2, CDK20, CDK3, CDK4, CDK5, CDK5R1, CDK6, CDK7, CDK9, CDKL1, CDKL2, CDKL3, CDKL4, CDKL5, CDKN2A, Cemip, CERK, CERKL, CFLAR, CHEK1, CHEK2, CHKA, CHKB, CHUK, CIB1, CIB4, CIT, CKB, CKM, CKMT1A_and_CKMT1B, CKMT2, CKS1B, CKS2, CLK1, CLK2, CLK3, CLK4, CLP1, CMPK1, CMPK2, COASY, COL4A3BP, CPNE3, CPNE9, CRKL, CROT, CSF1R, CSK, CSNK1A1, CSNK1A1L, CSNK1D, CSNK1E, CSNK1G1, CSNK1G2, CSNK1G2_and_CSNK1D, CSNK1G3, CSNK2A1, CSNK2A1_and_CSNK2A3, CSNK2A2, CSNK2B, CTLA4, CUX2, CXCR4, DAPK1, DAPK2, DAPK3, DCAKD, DCK, DCLK1, DCLK2, DCLK3, DCLRE1B, DDB1, DDR1, DDR2, DEPTOR, DGKA, DGKB, DGKD, DGKE, DGKG, DGKH, DGKI, DGKK, DGKQ, DGKZ, DGUOK, DLG1, DLG3, DLG3_and_DLG2, DMPK, DNMBP, DNMT3A, DOLK, DSTYK, DTYMK, DYRK1A, DYRK1B, DYRK2, DYRK3, DYRK4, ECT2, EEF2K, EGFR, EIF2AK1, EIF2AK2, EIF2AK3, EIF2AK4, ELF3, EME2, EML6, ENDOV, ENGASE, EPHA1, EPHA10, EPHA2, EPHA3, EPHA4, EPHA5, EPHA6, EPHA7, EPHA8, EPHB1, EPHB2, EPHB3, EPHB3_and_EPHB2, EPHB4, EPHB6, ERBB2, ERBB3, ERBB4, ERCC1, ERCC2, ERCC3, ERCC8, ERN1, ERN2, ESCO2, ETNK1, ETNK2, ETS1, EXOSC10, EYA4, FAM63B, FANCA, FANCB, FANCC, FANCD2, FANCE, FANCM, FASTK, FASTKD1, FASTKD2, FASTKD3, FASTKD5, FER, FES, FGD6, FGFR1, FGFR2, FGFR3, FGFR4, FGFRL1, FGGY, FGR, FLNB, FLT1, FLT3, FLT4, FN3K, FN3KRP, FOSL1_ex1, FOSL1_ex2, FOXM1, FPGT-TNNI3K, FRK, FUK, FXN, FYN, G2E3, G3BP1, GAK, GALK1, GALK2, GALNT10,

GATA6, GCK, GEN1, GK, GK2, GK5, GLI1, GLI2, GLI3, GLYCTK, GNE, GNG12, GPRC5A, GRK4, GRK5, GRK6, GRK7, GSAP, GSG2, GSK3A, GSK3B, GSPT1, GTF2H1, GUCY2C, GUCY2D, GUCY2F, GUK1, HAVCR2, HCFC1, HCK, HELLS, HIPK1, HIPK2, HIPK3, HIPK4, HK1, HK2, HK3, HKDC1, HLTF, HNF1A, HNF4A, HSPB8, HUNK, HUS1, ICK, IDNK, IFNGR1, IGF1R, IGFN1, IKBKB, IKBKE, IKZF1, IKZF3, ILK, INO80D, INSR, INSRR, INTS3, IP6K1, IP6K2, IP6K3, IPMK, IPPK, IRAK1, IRAK2, IRAK3, IRAK4, ITGA5, ITGB1, ITK, ITPK1, ITPKA, ITPKB, ITPKC, JAG1, JAK1, JAK2, JAK3, KALRN, KDM3A, KDM6A, KDM6B, KDR, KHK, KIF20B, KIT, KLHL22, KMT2C, KMT2D, KRAS_G12D, KRBA2, KSR1, KSR2, LAG3, LAMTOR3, LATS1, LATS2, LCK, LGALS3, LGALS3BP, LIG4, LIMK1, LIMK2, LMO7, LMTK2, LMTK3, LOXL2, LRGUK, LRPPRC, LRRC1, LRRK1, LRRK2, LTK, LYN, MACF1, MAD2L2, MAGED4B_and_MAGED4, MAGI1, MAGI3, MAK, MAML2, MAP2K1, MAP2K2, MAP2K2_and_RP11-286H14.4, MAP2K3, MAP2K4, MAP2K5, MAP2K6, MAP2K7, MAP3K1, MAP3K10, MAP3K11, MAP3K12, MAP3K13, MAP3K14, MAP3K15, MAP3K19, MAP3K2, MAP3K21, MAP3K3, MAP3K4, MAP3K5, MAP3K6, MAP3K7, MAP3K8, MAP3K9, MAP4K1, MAP4K2, MAP4K3, MAP4K4, MAP4K5, MAPK1, MAPK10, MAPK11, MAPK12, MAPK13, MAPK14, MAPK15, MAPK3, MAPK4, MAPK6, MAPK7, MAPK8, MAPK9, MAPKAPK2, MAPKAPK2_and_MAPKAPK3, MAPKAPK3, MAPKAPK5, MARK1, MARK2, MARK3, MARK3_and_MARK1, MARK4, MAST1, MAST2, MAST3, MAST4, MASTL, MATK, MBOAT2, MCL1, MDC1, MELK, MERTK, MET, MEX3B, MINK1, MKNK1, MKNK2, MLH1, MLH3, MLKL, MLKL_and_INTS6L, MMS22L, MOK, MORN1, MORN2, MOS, MPLKIP, MPP1, MPP2, MPP3, MPP4, MPP5, MPP6, MPP7, MS4A1, MSH2, MSH6, MSLN, MST1, MST1R, MTOR, MUC16, MUM1, MUSK, MVK, MYC, MYCBP2, MYLK, MYLK2, MYLK3, MYLK4, MYO3A, MYO3B, MYT1, N4BP2, NADK, NADK2, NAGK, NBEA, NBN, NCK1, NEIL1, NEIL3, NEK1, NEK10, NEK11, NEK2, NEK3, NEK4, NEK5, NEK6, NEK7, NEK8, NEK9, NF2, NIM1K, NLK, NME1, NME1-NME2, NME2, NME2_NME3, NME3, NME4, NME5, NME6, NME7, NME8, NME9, NMRK1, NMRK2, NOL9, NOTCH1, NOV, NPR1, NPR2, NR5A2, NRBP1, NRBP2, NRK, NRP1, NRP2, NT5E, NTC, NTPCR, NTRK1, NTRK2, NTRK3, NUAK1, NUAK2, NUP62, OBSCN, ONECUT1, ORC5, OSBP, OSR1, OXSR1, PACSIN1, PAK1, PAK2, PAK3, PAK4, PAK6, PAK7, PALB2, PAN3, PANK1, PANK2, PANK3, PANK4, PAPD7, PAPSS1, PAPSS2, PARP1, PASK, PATJ, PBK, PCDH1, PCDH7, PCK1, PCK2, PDCD1, PDCD1LG2, PDGFRA, PDGFRB, PDGFRL, PDIK1L, PDK1, PDK2, PDK3, PDK4, PDPK1, PDXK, PEAK1, PF4, PF4_and_PF4V1, PFKFB1, PFKFB2, PFKFB3, PFKFB4, PFKL, PFKM, PFKP, PGK1, PGK2, PGM2L1, PHKA1, PHKA2, PHKB, PHKG1, PHKG2,

PHLDB3, PI4K2A, PI4K2B, PI4KA, PI4KB, PIK3C2A, PIK3C2B, PIK3C2G, PIK3C3, PIK3CA, PIK3CB, PIK3CD, PIK3CG, PIK3R1, PIK3R3, PIK3R4, PIK3R5, PIKFYVE, PIM1, PIM2, PIM3, PINK1, PIP4K2A, PIP4K2B, PIP4K2C, PIP5K1A, PIP5K1B, PIP5K1C, PIP5KL1, PITPNA, PKD1, PKD2, PKDCC, PKLR, PKM, PKMYT1, PKN1, PKN2, PKN3, PLAU, PLK1, PLK2, PLK3, PLK4, PLK5, PLXNA3, PLXNA4, PMS1, PMS2, PMVK, PNCK, PNKP, POLD1, POLE, POLN, POLQ, POLR2F, POMK, POSTN, PPARG, PPFIBP1, PPIP5K2, PRKAA1, PRKAA2, PRKAB1, PRKAB2, PRKACA, PRKACB, PRKACG, PRKAG1, PRKAG2, PRKAG3, PRKAR1A, PRKAR1B, PRKAR2A, PRKAR2B, PRKCA, PRKCB, PRKCD, PRKCE, PRKCG, PRKCH, PRKCI, PRKCQ, PRKCZ, PRKD1, PRKD2, PRKD3, PRKDC, PRKG1, PRKG2, PRKRA, PRKX, PROM1, PRPF19, PRPF4B, PRPS1, PRPS1L1, PRPS2, PSKH1, PSKH2, PTEN, PTK2, PTK2B, PTK6, PTK7, PTTG1, PTTG3P, PXK, RAB11FIP5, RAD18, RAD21, RAD50, RAD51, RAD51D, RAD52, RAD9A, RAF1, RBBP8, RBKS, RBM10, RBM6, RECQL5, RET, REV1, REV3L, RFK, RICTOR, RIF1, RIOK1, RIOK2, RIOK3, RIPK1, RIPK2, RIPK3, RIPK4, RNASEL, RNF4, RNF43, RNF8, ROCK1, ROCK2, ROR1, ROR2, ROS1, RP2, RPA1, RPA3, RPS6KA1, RPS6KA2, RPS6KA3, RPS6KA4, RPS6KA5, RPS6KA6, RPS6KB1, RPS6KB2, RPS6KC1, RPS6KL1, RPTOR, RRM1, RRM2B, RYK, SBK1, SBK2, SBK3, SCAMP5, SCYL1, SCYL2, SCYL3, SEM1_former_SHFM1, SEPHS2, SETD2, SETD7, SGK1, SGK2, SGK223, SGK3, SGK494, SH3BP4, SH3BP5, SH3BP5L, SHPK, SHPRH, SIK1_and_SIK1B, SIK2, SIK3, SIN3B, SLAMF6, SLK, SLX4, SMAD3, SMAD4, SMARCA2, SMARCA4, SMARCA5, SMG1, SNAI1, SNAI2, SNRK, SNX16, SNX9, SORD, SORD_and_SORD2P, SOX9, SPEG, SPHK1, SPHK2, SPTB, SRC, SRM, SRMS, SRPK1, SRPK2, SRPK3, SSRP1, STAT3, STAT5B, STK10, STK11, STK16, STK17A, STK17B, STK19, STK24, STK25, STK26, STK3, STK31, STK32A, STK32B, STK32C, STK33, STK35, STK36, STK38L, STK39, STK4, STK40, STKLD1, STRADA, STRADB, STYK1, SYK, TAB1, TAF1, TAF1_and_TAF1L, TAF1L, TAF9, TAOK1, TAOK2, TAOK3, TBCK, TBK1, TBRG4, TDP2, TEC, TECPR1, TEK, TESK1, TESK2, TEX14, TGFB1, TGFBI, TGFBR1, TGFBR2, TGFBR3, TIE1, TIGD6, TIGIT, TIMELESS, TJP2, TK1, TK2, TKFC, TLK1, TLK2, TM4SF1, TMEM139, TNFRSF14, TNFRSF18, TNFRSF4, TNFRSF9, TNFSF18, TNFSF4, TNFSF9, TNIK, TNK1, TNK2, TNNI3K, TOP2B, TOPBP1, TP53, TP53BP1, TP53RK, TPD52L3, TPK1, TPR, TPX2, TRIB1, TRIB2, TRIB3, TRIM24, TRIM27, TRIM28, TRIM33, TRIM67, TRIO, TRPM6, TRPM7, TRRAP, TSSK1B, TSSK2, TSSK3, TSSK4, TSSK6, TTBK1, TTBK2, TTK, TTN, TWF1, TWF2, TWIST1, TXK, TYK2, TYRO3, U2AF1_and U2AF1L5, UBA1, UBE2H, UBE2N, UCK1, UCK2, UCKL1, UGT2B7, UHMK1, ULK1, ULK2, ULK3, ULK4, USP7, USP9X, UVSSA, VRK1, VRK2, VRK3, VSIR, WDR59, WEE1, WEE2, WNK1, WNK2, WNK3, WNK4, WNT5A, WRN, XAB2, XRCC2, XRCC3, XYLB, YAP1, YES1, ZAK,

ZAP70, ZBED2, ZEB1, ZFP91, ZMYND8, ZNF230, ZNF547, ZNF589, ZNF594, ZNF658, ZNF775, ZPLD1, ZSWIM7, ZZEF1,

Supplemental Table 4 – genes in the DDR CRISPR screen

ABL1, ATAD5, ATM, ATR, BAP1, BARD1, BRCA1, BRCA2, BRCC3, C1orf86, CCNH, CDC14B, CDK12, CDK7, CLK2, DCLRE1B, DDB1, DNMT3A, EME2, ENDOV, ERCC1, ERCC2, ERCC3, ERCC8, ESCO2, FAAP20, FANCA, FANCC, FANCD2, FANCE, FANCM, G2E3, GEN1, GTF2H1, HELLS, HLTF, INO80D, LIG4, MAD2L2, MLH1, MLH3, MMS22L, MPLKIP, MSH6, MUM1, NBN, NEIL1, NEIL3, NTC, ORC5, PALB2, PAPD7, PARP1, PMS1, PNKP, POLD1, POLE, POLN, POLQ, POLR2F, PRKDC, PRPF19, PTEN, PWWP3A, RAD18, RAD21, RAD50, RAD51D, RAD52, RAD9A, RECQL5, REV1, REV3L, RIF1, RNF4, RNF8, RPA1, RPA3, RRM2B, SHFM1, SHPRH, SLX4, SMARCA2, SMARCA5, SMG1, SSRP1, TDP2, TENT4A, TIMELESS, TOP2B, TOPBP1, TP53, TP53BP1, UBA1, UBE2N, USP7, UVSSA, WRN, XAB2, XRCC2, XRCC3

Supplemental Figure 1 – pretreatment with cisplatin

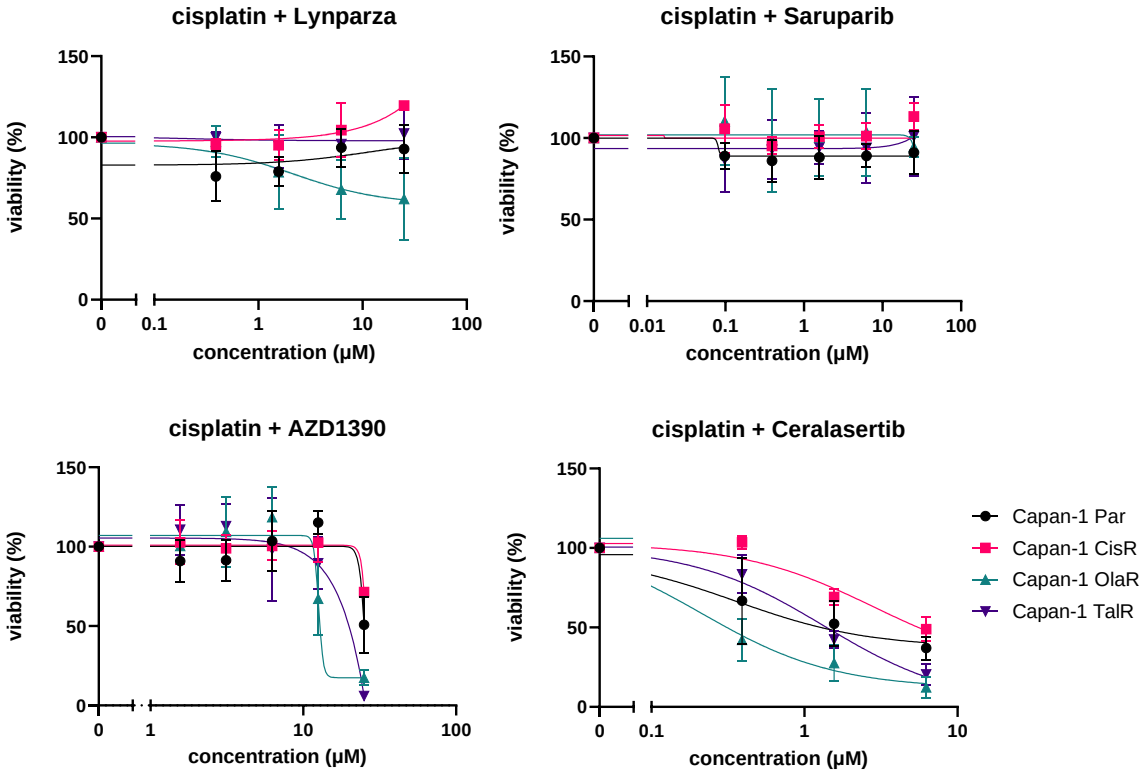

24-hour pretreatment with cisplatin does not sensitise to PARP, ATM, or ATR inhibitor. Cells were treated for 24 hours with 0.23 μM (~IC_{20}) cisplatin before addition of the other inhibitors. Cell viability was measured after 7 days of treatment with the inhibitors and was normalised against untreated control (n=3).

Supplemental Figure 2 – yH2AX and RAD51 foci formation after exposure to ATRi and/or PARPi

Cells were exposed for 4 hours before fixation. 60x magnification

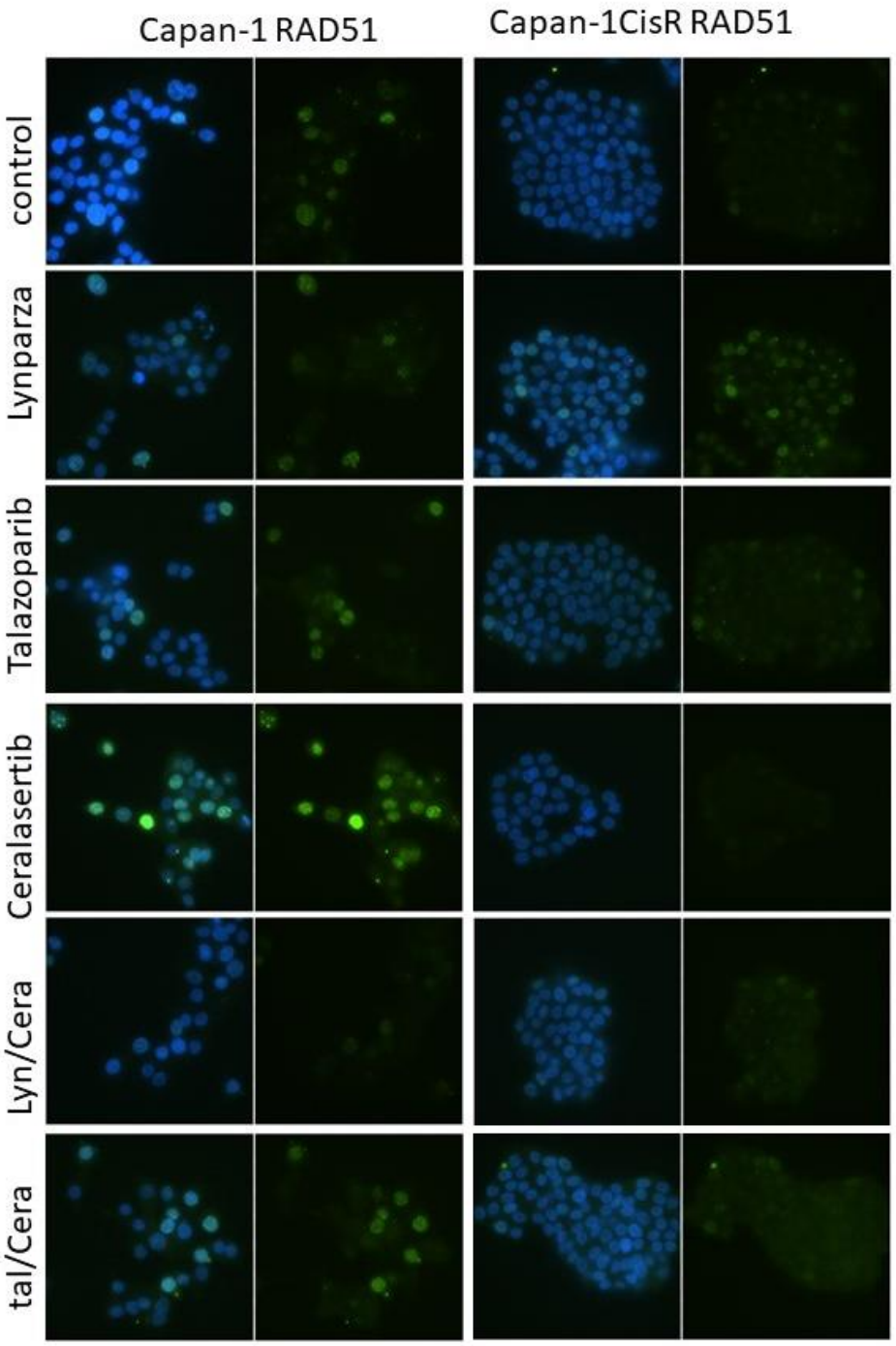

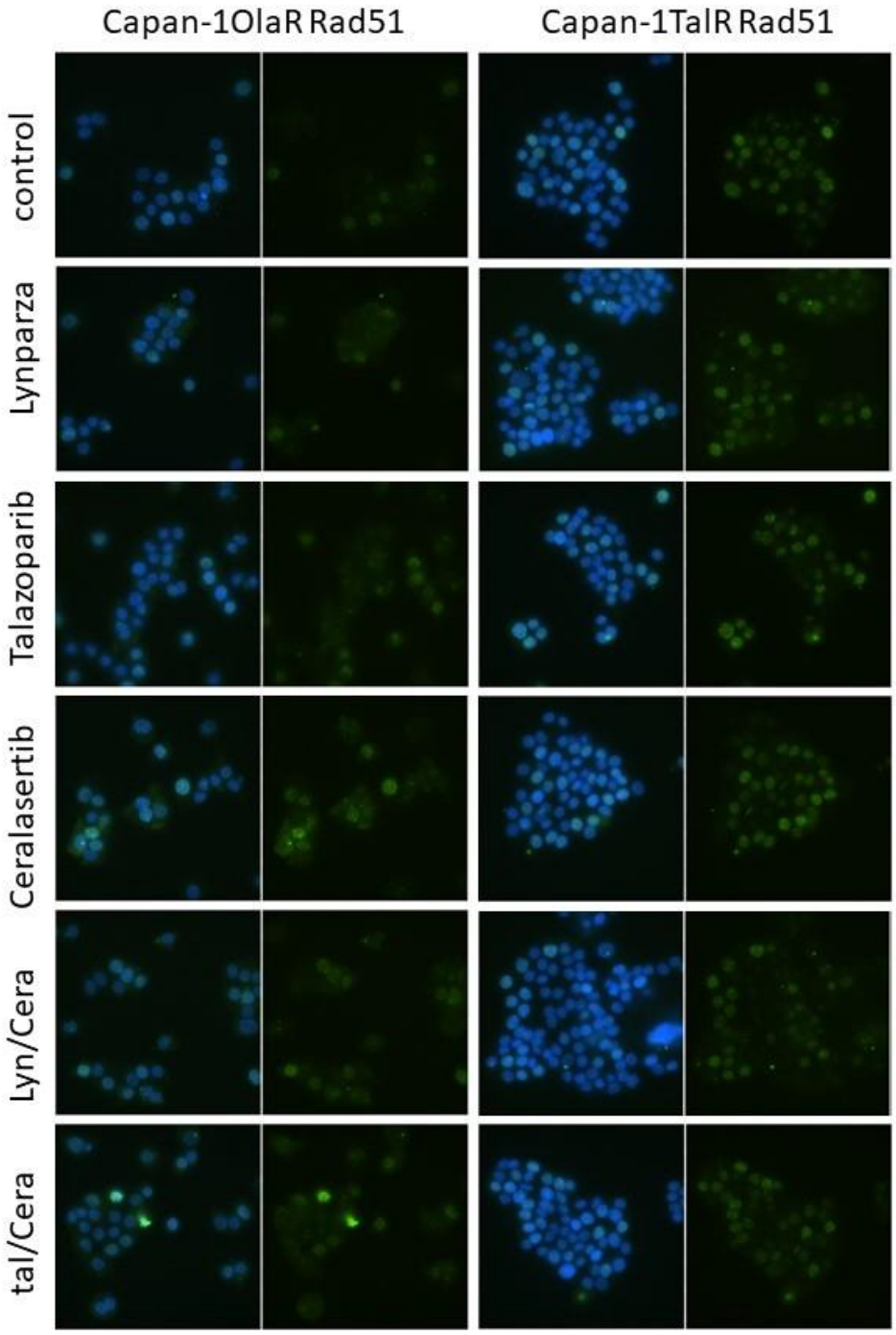
Capan-1OlaR Rad51
Capan-1TalR Rad51
control
Lynparza
Talazoparib
Ceralasertib
Lyn/Cera
tal/Cera

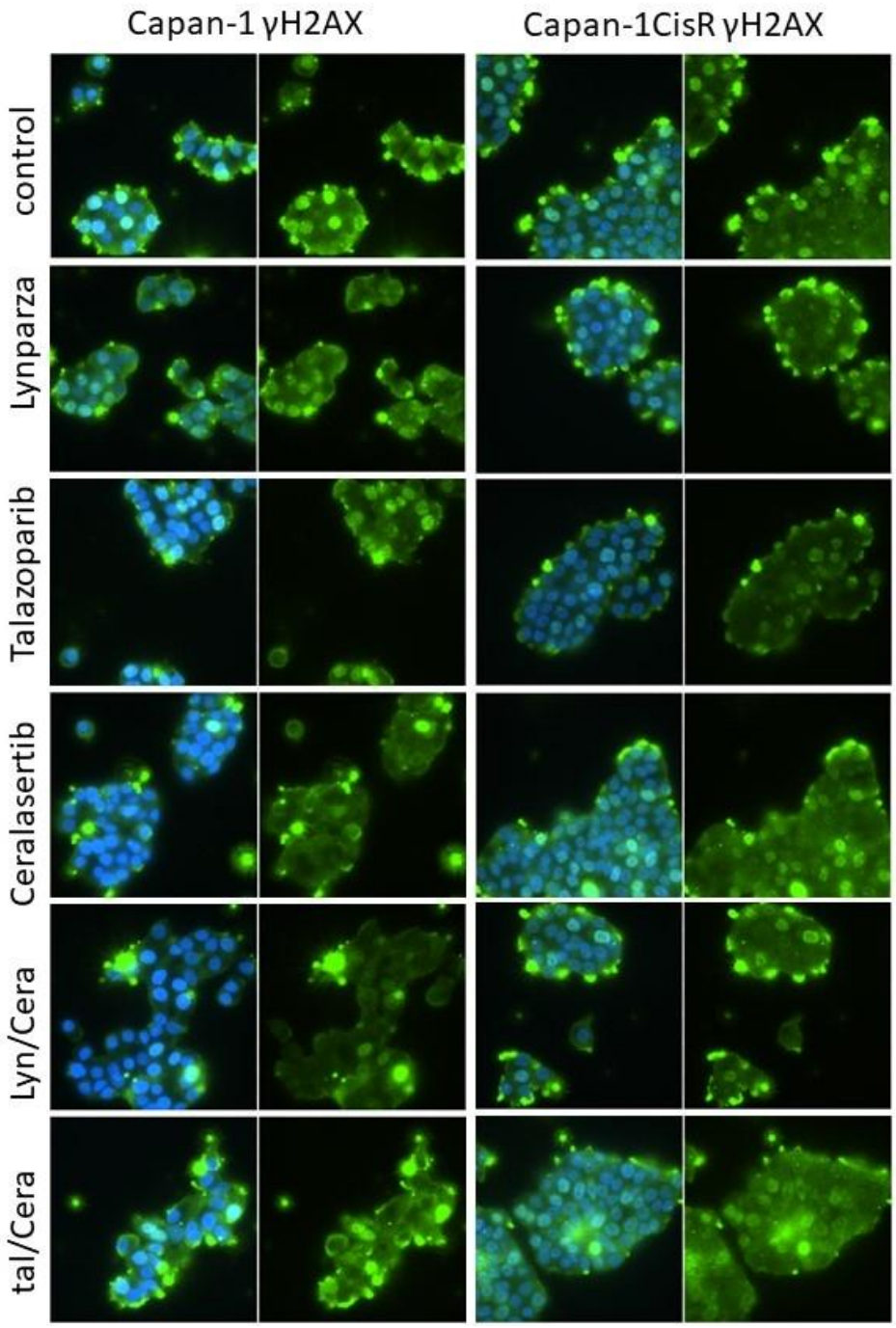
Capan-1 γH2AX
Capan-1CisR γH2AX
control
Lynparza
Talazoparib
Ceralasertib
Lyn/Cera
tal/Cera

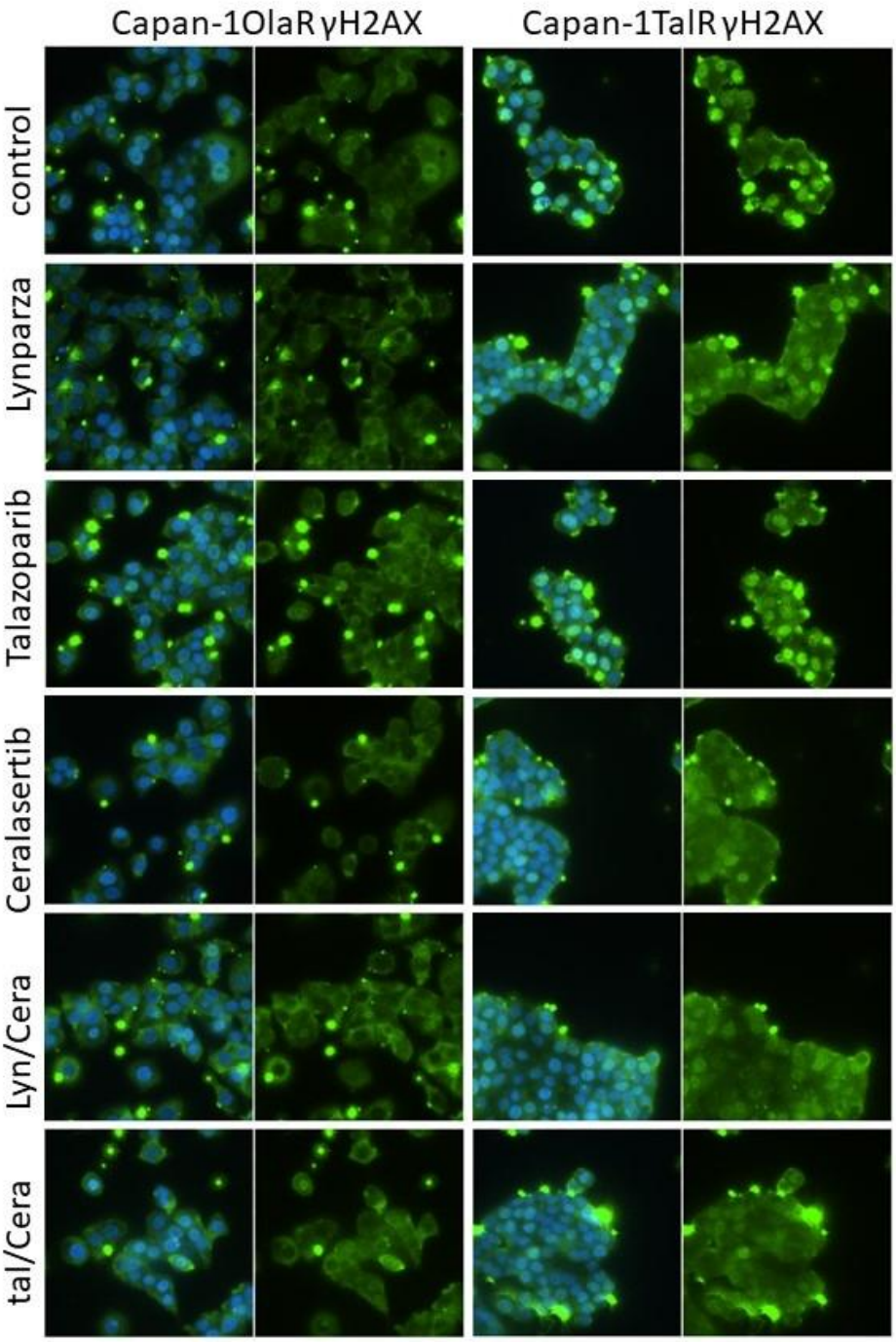
Capan-1OlaR γH2AX
Capan-1TalR γH2AX
control
Lynparza
Talazoparib
Ceralasertib
Lyn/Cera
tal/Cera

8 REFERENCES

Abad, E., Graifer, D., & Lyakhovich, A. (2020). DNA damage response and resistance of cancer stem cells. *Cancer Letters*, *474*. https://doi.org/10.1016/j.canlet.2020.01.008

Abbotts, R., & Wilson, D. M. (2016). Coordination of DNA Single Strand Break Repair. *Free radical biology & medicine*, *107*. https://doi.org/10.1016/j.freeradbiomed.2016.11.039

Alexander, J. L., & Orr-Weaver, T. L. (2016). Replication fork instability and the consequences of fork collisions from rereplication. *Genes & Development*, *30*(20). https://doi.org/10.1101/gad.288142.116

Alhmoud, J. F., Woolley, J. F., Moustafa, A.-E. A., & Malki, M. I. (2020). DNA Damage/Repair Management in Cancers. *Cancers*, *12*(4). https://doi.org/10.3390/cancers12041050

Arroyo-Olarte, R. D., Bravo Rodríguez, R., & Morales-Ríos, E. (2021). Genome Editing in Bacteria: CRISPR-Cas and Beyond. *Microorganisms*, *9*(4). https://doi.org/10.3390/MICROORGANISMS9040844

Asif, K., Memeo, L., Palazzolo, S., Frión-Herrera, Y., Parisi, S., Caligiuri, I., Canzonieri, V., Granchi, C., Tuccinardi, T., Rizzolio, F., Asif, K., Memeo, L., Palazzolo, S., Frión-Herrera, Y., Parisi, S., Caligiuri, I., Canzonieri, V., Granchi, C., Tuccinardi, T., & Rizzolio, F. (2021). STARD3: A Prospective Target for Cancer Therapy. *Cancers*, *13*(18). https://doi.org/10.3390/cancers13184693

AstraZeneca, A. B. (2014). *CHMP assessment report Lynparza*.

AstraZeneca, A. B. (2017). *NDA/BLA Multi-disciplinary Review and Evaluation NDA 208558 LynparzaTM (Olaparib)*. https://www.accessdata.fda.gov/drugsatfda_docs/nda/2017/208558Orig1s000MultidisciplineR.pdf

Bahar, E., Kim, J.-Y., Kim, H.-S., & Yoon, H. (2020). Establishment of Acquired Cisplatin Resistance in Ovarian Cancer Cell Lines Characterized by Enriched Metastatic Properties with Increased Twist Expression. *International Journal of Molecular Sciences*, *21*(20). https://doi.org/10.3390/ijms21207613

Bar-Even, A., Flamholz, A., Noor, E., Milo, R., Bar-Even, A., Flamholz, A., Noor, E., & Milo, R. (2012). Rethinking glycolysis: on the biochemical logic of metabolic pathways. *Nature Chemical Biology*, *8*(6). https://doi.org/10.1038/nchembio.971

Beek, L. v., McClay, É., Patel, S., Schimpl, M., Spagnolo, L., Oliveira, T. M. d., van Beek, L., McClay, É., Patel, S., Schimpl, M., Spagnolo, L., & Maia de Oliveira, T. (2021). PARP Power: A Structural Perspective on PARP1, PARP2, and PARP3 in DNA Damage Repair and Nucleosome Remodelling. *International Journal of Molecular Sciences*, *22*(10). https://doi.org/10.3390/ijms22105112

Begg, K., & Tavassoli, M. (2020). Inside the hypoxic tumour: reprogramming of the DDR and radioresistance. *Cell Death Discovery*, *6*(1). https://doi.org/10.1038/s41420-020-00311-0

Belostotsky, R., Pitt, J. J., & Frishberg, Y. (2012). Primary hyperoxaluria type III--a model for studying perturbations in glyoxylate metabolism. *Journal of molecular medicine*, *90*(12). https://doi.org/10.1007/s00109-012-0930-z

Bhardwaj, V., & He, J. (2020). Reactive Oxygen Species, Metabolic Plasticity, and Drug Resistance in Cancer. *International Journal of Molecular Sciences*, *21*(10). https://doi.org/10.3390/ijms21103412

Bhattacharjee, K., Nath, M., & Choudhury, Y. (2020). Fatty acid synthesis and cancer: Aberrant expression of the ACACA and ACACB genes increases the risk for cancer. *Meta Gene*, *26*, 100798-100798. https://doi.org/10.1016/j.mgene.2020.100798

Bi, L., Ren, Y., Feng, M., Meng, P., Wang, Q., Chen, W., Jiao, Q., Wang, Y., Du, L., Zhou, F., Jiang, Y., Chen, F., Wang, C., Tang, B., & Wang, Y. (2021). HDAC11 Regulates Glycolysis through the LKB1/AMPK Signaling Pathway to Maintain Hepatocellular Carcinoma Stemness. *Cancer Research*, *81*(8). https://doi.org/10.1158/0008-5472.CAN-20-3044

Biegała, Ł., Gajek, A., Marczak, A., Rogalska, A., Biegała, Ł., Gajek, A., Marczak, A., & Rogalska, A. (2023). Olaparib-Resistant BRCA2MUT Ovarian Cancer Cells with Restored BRCA2 Abrogate Olaparib-Induced DNA Damage and G2/M Arrest Controlled by the ATR/CHK1 Pathway for Survival. *Cells*, *12*(7). https://doi.org/10.3390/cells12071038

Bioinformatics, B. (2019). *OmicsBox – Bioinformatics Made Easy, BioBam Bioinformatics*. https://www.biobam.com/omicsbox

Blanc-Durand, F., Yaniz-Galende, E., Llop-Guevara, A., Genestie, C., Serra, V., Herencia-Ropero, A., Klein, C., Berton, D., Lortholary, A., Dohollou, N., Desauw, C., Fabbro, M., Malaurie, E., Bonichon-Lamaichhane, N., Dubot, C., Kurtz, J. E., Rauglaudre, G. d., Raban, N., Chevalier-Place, A.,…Leary, A. (2023). A RAD51 functional assay as a candidate test for homologous recombination deficiency in ovarian cancer. *Gynecologic Oncology*, *171*. https://doi.org/10.1016/j.ygyno.2023.01.026

Boj, S. F., Hwang, C.-I., Baker, L. A., Chio, I. I. C., Engle, D. D., Corbo, V., Jager, M., Ponz-Sarvise, M., Tiriac, H., Spector, M. S., Gracanin, A., Oni, T., Yu, K. H., Boxtel, R. v., Huch, M., Rivera, K. D., Wilson, J. P., Feigin, M. E., Öhlund, D.,…Tuveson, D. A. (2015). Organoid Models of Human and Mouse Ductal Pancreatic Cancer. *Cell*, *160*(1-2). https://doi.org/10.1016/j.cell.2014.12.021

Bray, F., Laversanne, M., Sung, H., Ferlay, J., Siegel, R. L., Soerjomataram, I., & Jemal, A. (2024). Global cancer statistics 2022: GLOBOCAN estimates of incidence and mortality worldwide for 36 cancers in 185 countries. *CA: A Cancer Journal for Clinicians*, *74*(3). https://doi.org/10.3322/caac.21834

Brenneman, M. A., Weiss, A. E., Nickoloff, J. A., & Chen, D. J. (2000). XRCC3 is required for efficient repair of chromosome breaks by homologous recombination. *Mutation Research/DNA Repair*, *459*(2). https://doi.org/10.1016/S0921-8777(00)00002-1

Caffo, O., Fallani, S., Marangon, E., Nobili, S., Cassetta, M. I., Murgia, V., Sala, F., Novelli, A., Mini, E., Zucchetti, M., & Galligioni, E. (2010). Pharmacokinetic study of gemcitabine, given as prolonged infusion at fixed dose rate, in combination with cisplatin in patients with advanced non-small-cell lung cancer. *Cancer Chemotherapy and Pharmacology*, *65*(6), 1197-1202. https://doi.org/10.1007/s00280-010-1255-7

Cahuzac, M., Péant, B., Mes-Masson, A.-M., & Saad, F. (2022). Development of Olaparib-Resistance Prostate Cancer Cell Lines to Identify Mechanisms Associated with Acquired Resistance. *Cancers*, *14*(16). https://doi.org/10.3390/cancers14163877

Caldecott, K. W. (2008). Single-strand break repair and genetic disease. *Nature Reviews Genetics*, *9*(8). https://doi.org/10.1038/nrg2380

Caldecott, K. W. (2024). Causes and consequences of DNA single-strand breaks. *Trends in biochemical sciences*, *49*(1). https://doi.org/10.1016/j.tibs.2023.11.001

Cannan, W. J., & Pederson, D. S. (2016). Mechanisms and Consequences of Double-strand DNA Break Formation in Chromatin. *Journal of cellular physiology*, *231*(1). https://doi.org/10.1002/jcp.25048

Cano, D. A., Hebrok, M., & Zenker, M. (2007). Pancreatic Development and Disease. *Gastroenterology*, *132*(2), 745-762. https://doi.org/10.1053/J.GASTRO.2006.12.054

Casale, F. (2004). Plasma concentrations of 5-fluorouracil and its metabolites in colon cancer patients. *Pharmacological Research*, *50*(2), 173-179. https://doi.org/10.1016/j.phrs.2004.01.006

Casolino, R., Paiella, S., Azzolina, D., Beer, P. A., Corbo, V., Lorenzoni, G., Gregori, D., Golan, T., Braconi, C., Froeling, F. E. M., Milella, M., Scarpa, A., Pea, A., Malleo, G., Salvia, R., Bassi, C., Chang, D. K., & Biankin, A. V. (2021). Homologous Recombination Deficiency in Pancreatic Cancer: A Systematic Review and Prevalence Meta-Analysis. *Journal of Clinical Oncology*, *39*(23). https://doi.org/10.1200/JCO.20.03238

Chandel, N. S. (2021). Glycolysis. *Perspectives in Biology*, *13*(5). https://doi.org/10.1101/cshperspect.a040535

Chandrasegaram, M. D., Gill, A. J., Samra, J., Price, T., Chen, J., Fawcett, J., & Merrett, N. D. (2017). Ampullary cancer of intestinal origin and duodenal cancer - A logical clinical and therapeutic subgroup in periampullary cancer. *World Journal of Gastrointestinal Oncology*, *9*(10). https://doi.org/10.4251/wjgo.v9.i10.407

Charlotte, A. (2023). *SomaSnake: A robust and interoperable end-to-end analysis pipeline for the interpretation of somatic NGS data*. https://gitlab.com/andhena/somasnake

Chaudhuri, A. R., & Nussenzweig, A. (2017). The multifaceted roles of PARP1 in DNA repair and chromatin remodelling. *Nature reviews. Molecular cell biology*, *18*(10). https://doi.org/10.1038/nrm.2017.53

Chen, H.-D., Guo, N., Song, S.-S., Chen, C.-H., Miao, Z.-H., & He, J.-X. (2020). Novel mutations in BRCA2 intron 11 and overexpression of COX-2 and BIRC3 mediate cellular resistance to PARP inhibitors. *American Journal of Cancer Research*, *10*(9), 2813-2831. /pmc/articles/PMC7539764/

/pmc/articles/PMC7539764/?report=abstract

https://www.ncbi.nlm.nih.gov/pmc/articles/PMC7539764/

Chen, X., Arciero, C. A., Wang, C., Broccoli, D., & Godwin, A. K. (2006). BRCC36 is essential for ionizing radiation-induced BRCA1 phosphorylation and nuclear foci formation. *Cancer Research*, *66*(10). https://doi.org/10.1158/0008-5472.CAN-05-4194

Chiorean, E., Guthrie, A., Philip, P., Swisher, E., Jalikis, F., Pishvaian, M., Berlin, J., Noel, M., Suga, J., Garrido-Laguna, I., DB, C., MR, R., M, D., S, B., AM, L., & HS., H. (2021). Randomized Phase II Study of PARP Inhibitor ABT-888 (Veliparib) with Modified FOLFIRI versus FOLFIRI as Second-line Treatment of Metastatic Pancreatic Cancer: SWOG S1513. *Clinical Cancer Research*, *27*(23). https://doi.org/10.1158/1078-0432.CCR-21-1789

Chiorean, E. G., Guthrie, K. A., Philip, P. A., Swisher, E. M., Jalikis, F., Pishvaian, M. J., Berlin, J., Noel, M. S., Suga, J. M., Garrido-Laguna, I., Cardin, D. B., Lew, D. L., Lowy, A. M., & Hochster, H. S. (2019). Randomized phase II study of second-line modified FOLFIRI with PARP inhibitor ABT-888 (Veliparib) (NSC-737664) versus FOLFIRI in metastatic pancreatic cancer (mPC): SWOG S1513. *Journal of Clinical Oncology*, *37*(15_suppl), 4014-4014. https://doi.org/10.1200/jco.2019.37.15_suppl.4014

Cho, S. M., Esmail, A., Raza, A., Dacha, S., & Abdelrahim, M. (2022). Timeline of FDA-Approved Targeted Therapy for Cholangiocarcinoma. *Cancers*, *14*(11). https://doi.org/10.3390/cancers14112641

Choi, J.-I., Jang, S. I., Hong, J., Kim, C. H., Kwon, S. S., Park, J. S., & Lim, J.-B. (2021). Cancer-initiating cells in human pancreatic cancer organoids are maintained by interactions with endothelial cells. *Cancer Letters*, *498*. https://doi.org/10.1016/j.canlet.2020.10.012

Chun, J., Buechelmaier, E. S., & Powell, S. N. (2013). Rad51 paralog complexes BCDX2 and CX3 act at different stages in the BRCA1-BRCA2-dependent homologous recombination pathway. *Molecular and Cellular Biology*, *33*(2). https://doi.org/10.1128/MCB.00465-12

Chun, Y. S., Pawlik, T. M., & Vauthey, J.-N. (2017). 8th Edition of the AJCC Cancer Staging Manual: Pancreas and Hepatobiliary Cancers. *Annals of surgical oncology*, *25*(4). https://doi.org/10.1245/s10434-017-6025-x

Conroy, T., Hammel, P., Hebbar, M., Abdelghani, M. B., Wei, A. C., Raoul, J.-L., Choné, L., Francois, E., Artru, P., Biagi, J. J., Lecomte, T., Assenat, E., Faroux, R., Ychou, M., Volet, J., Sauvanet, A., Breysacher, G., Fiore, F. D., Cripps, C.,…Bachet, J.-B. (2018). FOLFIRINOX or Gemcitabine as Adjuvant Therapy for Pancreatic Cancer. *New England Journal of Medicine*, *379*(25). https://doi.org/10.1056/NEJMoa1809775

Conroy, T., Pfeiffer, P., Vilgrain, V., Lamarca, A., Seufferlein, T., O'Reilly, E. M., Hackert, T., Golan, T., Prager, G., Haustermans, K., Vogel, A., & Ducreux, M. (2023). Pancreatic cancer: ESMO Clinical Practice Guideline for diagnosis, treatment and follow-up. *Annals of Oncology*, *34*(11). https://doi.org/10.1016/j.annonc.2023.08.009

Cooper, G. (2000). The Mechanism of Oxidative Phosphorylation. In *The Cell: A Molecular Approach*. Sunderland.

Cuneo, K. C., Morgan, M. A., Sahai, V., Schipper, M. J., Parsels, L. A., Parsels, J. D., Devasia, T., Al-Hawaray, M., Cho, C. S., Nathan, H., Maybaum, J., Zalupski, M. M., & Lawrence, T. S. (2019). Dose Escalation Trial of the Wee1 Inhibitor Adavosertib (AZD1775) in Combination With Gemcitabine and Radiation for Patients With Locally Advanced Pancreatic Cancer. *Journal of Clinical Oncology*, *37*(29). https://doi.org/10.1200/JCO.19.00730

D'Cruz, J. R., Misra, S., & Shamsudeen, S. (2024). *Pancreaticduodenectomy (Whipple Procedure)*. StatPearls Publishing. https://www.ncbi.nlm.nih.gov/books/NBK560747/

Darabi, S., Braxton, D. R., Xiu, J., Carneiro, B. A., Swensen, J., Antonarakis, E. S., Liu, S. V., McKay, R. R., Spetzler, D., El-Deiry, W. S., & Demeure, M. J. (2022). BRCA1/2 Reversion Mutations in Patients Treated with Poly ADP-Ribose Polymerase (PARP) Inhibitors or Platinum Agents. *Medicina*, *58*(12). https://doi.org/10.3390/medicina58121818

Dardare, J., Witz, A., Merlin, J.-L., Gilson, P., & Harlé, A. (2020). SMAD4 and the TGFβ Pathway in Patients with Pancreatic Ductal Adenocarcinoma. *International Journal of Molecular Sciences*, *21*(10). https://doi.org/10.3390/ijms21103534

Dasari, S., & Tchounwou, P. B. (2014). Cisplatin in cancer therapy: Molecular mechanisms of action. *European Journal of Pharmacology*, *740*. https://doi.org/10.1016/j.ejphar.2014.07.025

DeBerardinis, R. J., Lum, J. J., Hatzivassiliou, G., & Thompson, C. B. (2008). The Biology of Cancer: Metabolic Reprogramming Fuels Cell Growth and Proliferation. *Cell Metabolism*, *7*(1). https://doi.org/10.1016/j.cmet.2007.10.002

Debruyne, A. C., Okkelman, I. A., Heymans, N., Nobis, M., Borisov, S. M., & Dmitriev, R. I. (2023). Live microscopy of multicellular spheroids with the multi-modal near-infrared nanoparticles reveals differences in oxygenation gradients. *bioRxiv*. https://doi.org/10.1101/2023.12.11.571110

Demyan, L., Habowski, A. N., Plenker, D., King, D. A., Standring, O. J., Tsang, C., Surin, L. S., Rishi, A., Crawford, J. M., Boyd, J., Pasha, S. A., Patel, H., Galluzzo, Z., Metz, C., Gregersen, P. K., Fox, S., Valente, C., Abadali, S., Matadial-Ragoo, S.,…Weiss, M. J. (2022). Pancreatic Cancer Patient-Derived Organoids Can Predict Response to Neoadjuvant Chemotherapy. *Annals of surgery*, *276*(3). https://doi.org/10.1097/SLA.0000000000005558

Dhakhwa, R., & Kafle, N. (2016). Histopathologic analysis of pancreaticoduodenectomy specimen. *J Nepal Med Assoc.*, *55*(204), 79-85.

Dhillon, K. K., Swisher, E. M., & Taniguchi, T. (2011). Secondary mutations of BRCA1/2 and drug resistance. *Cancer Science*, *102*(4). https://doi.org/10.1111/j.1349-7006.2010.01840.x

Di Paolo, A., Lencioni, M., Amatori, F., Di Donato, S., Bocci, G., Orlandini, C., Lastella, M., Federici, F., Iannopollo, M., Falcone, A., Ricci, S., Del Tacca, M., & Danesi, R. (2008). 5-Fluorouracil Pharmacokinetics Predicts Disease-free Survival in Patients Administered Adjuvant Chemotherapy for Colorectal Cancer. *Clinical Cancer Research*, *14*(9), 2749-2755. https://doi.org/10.1158/1078-0432.CCR-07-1529

Dowden, H., & Munro, J. (2019). Trends in clinical success rates and therapeutic focus. *Nature Reviews Drug Discovery*, *18*(7). https://doi.org/10.1038/d41573-019-00074-z

Dréan, A., Williamson, C. T., Brough, R., Brandsma, I., Menon, M., Konde, A., Garcia-Murillas, I., Pemberton, H. N., Frankum, J., Rafiq, R., Badham, N., Campbell, J., Gulati, A., Turner, N. C., Pettitt, S. J., Ashworth, A., & Lord, C. J. (2017). Modeling Therapy Resistance in BRCA1/2-Mutant Cancers. *Molecular Cancer Therapeutics*, *16*(9). https://doi.org/10.1158/1535-7163.MCT-17-0098

Driehuis, E., Gracanin, A., Vries, R. G. J., Clevers, H., & Boj, S. F. (2020). Establishment of pancreatic organoids from normal tissue and tumours. *STAR protocols*. https://doi.org/10.1016/j.xpro.2020.100192

Driehuis, E., Hoeck, A. V., Moore, K., Kolders, S., Francies, H. E., Gulersonmez, M. C., Stigter, E. C. A., Burgering, B., Geurts, V., Gracanin, A., Bounova, G., Morsink, F. H., Vries, R., Boj, S., Es, J. V., Offerhaus, G. J. A., Kranenburg, O., Garnett, M. J., Wessels, L.,…Clevers, H. (2019). Pancreatic cancer organoids recapitulate disease and allow personalized drug screening. *Proceedings of the National Academy of Sciences of the United States of America*, *116*(52), 26580-26590. https://doi.org/10.1073/PNAS.1911273116

Ehrsson, H., Wallin, I., & Yachnin, J. (2002). Pharmacokinetics of Oxaliplatin in Humans. *Medical Oncology*, *19*(4), 261-266. https://doi.org/10.1385/MO:19:4:261

El-Mounadi, K., Morales-Floriano, M. L., & Garcia-Ruiz, H. (2020). Principles, Applications, and Biosafety of Plant Genome Editing Using CRISPR-Cas9. *Frontiers in Plant Science*, *11*, 56-56. https://doi.org/10.3389/FPLS.2020.00056/BIBTEX

Eskiler, G. G., Cecener, G., Egeli, U., & Tunca, B. (2018). Synthetically Lethal BMN 673 (Talazoparib) Loaded Solid Lipid Nanoparticles for BRCA1 Mutant Triple Negative Breast Cancer. *Pharmaceutical Research*, *35*(11). https://doi.org/10.1007/s11095-018-2502-6

Esmail, A., Badheeb, M., Alnahar, B. W., Almiqlash, B., Sakr, Y., Al-Najjar, E., Awas, A., Alsayed, M., Khasawneh, B., Alkhulaifawi, M., Alsaleh, A., Abudayyeh, A., Rayyan, Y., & Abdelrahim, M. (2024). The Recent Trends of Systemic Treatments and Locoregional Therapies for Cholangiocarcinoma. *Pharmaceuticals*, *17*(7). https://doi.org/10.3390/ph17070910

Feldmann, G., Rauenzahn, S., & Maitra, A. (2009). In vitro models of pancreatic cancer for translational oncology research. *Expert opinion on drug discovery*, *4*(4). https://doi.org/10.1517/17460440902821657

Feng, H., Ou, B.-c., Zhao, J.-k., Yin, S., Lu, A.-g., Oechsle, E., & Thasler, W. E. (2017). Homogeneous pancreatic cancer spheroids mimic growth pattern of circulating tumor cell clusters and macrometastases: displaying heterogeneity and crater-like structure on inner layer. *Journal of Cancer Research and Clinical Oncology*, *143*(9). https://doi.org/10.1007/s00432-017-2434-2

Fennema, E., Rivron, N., Rouwkema, J., van Blitterswijk, C., & Boer, J. D. (2013). Spheroid culture as a tool for creating 3D complex tissues. *Trends in Biotechnology*, *31*(2), 108-115. https://doi.org/10.1016/J.TIBTECH.2012.12.003

Fogh, J., Fogh, J. M., & Orfeo, T. (1977). One hundred and twenty-seven cultured human tumor cell lines producing tumors in nude mice. *Journal of the National Cancer Institute*, *59*(1). https://doi.org/10.1093/jnci/59.1.221

Foo, T. K., & Xia, B. (2022). BRCA1-Dependent and Independent Recruitment of PALB2–BRCA2–RAD51 in the DNA Damage Response and Cancer. *Cancer Research*, *82*(18). https://doi.org/10.1158/0008-5472.CAN-22-1535

Fragkos, M., Choleza, M., & Papadopoulou, P. (2023). The Role of γH2AX in Replication Stress-induced Carcinogenesis: Possible Links and Recent Developments. *Cancer Diagnosis & Prognosis*, *3*(6). https://doi.org/10.21873/cdp.10266

Fraser, M., Zhao, H., Luoto, K. R., Lundin, C., Coackley, C., Chan, N., Joshua, A. M., Bismar, T. A., Evans, A., Helleday, T., & Bristow, R. G. (2012). PTEN Deletion in Prostate Cancer Cells Does Not Associate with Loss of RAD51 Function: Implications for Radiotherapy and Chemotherapy. *Clinical Cancer Research*, *18*(4). https://doi.org/10.1158/1078-0432.CCR-11-2189

Frazier, M. L., Brown, N., Pathak, S., Mackay, B., Cleary, K., Olive, M., Byrd, D. R., Evans, D. B., & Levin, B. (1992). Human cell line from an adenocarcinoma of the ampulla of vater. *In Vitro Cellular & Developmental Biology - Animal*, *28*(3). https://doi.org/10.1007/BF02631083

Frenel, J.-S., Kim, J.-W., Berton-Rigaud, D., Asher, R., Vidal, L., Pautier, P., Ledermann, J. A., Penson, R. T., Oza, A. M., Korach, J., Huzarski, T., Pignata, S., Colombo, N., Park-Simon, T.-W., Tamura, K., Sonke, G. S., Freimund, A., Lee, C. K., & Pujade-Lauraine, E. (2020). 813MO Efficacy of subsequent chemotherapy for patients with BRCA1/2 mutated platinum-sensitive recurrent epithelial ovarian cancer (EOC) progressing on olaparib vs placebo: The SOLO2/ENGOT Ov-21 trial. *Annals of Oncology*, *31*. https://doi.org/10.1016/j.annonc.2020.08.952

Fu, X., Li, P., Zhou, Q., He, R., Wang, G., Zhu, S., Bagheri, A., Kupfer, G., Pei, H., & Li, J. (2024). Mechanism of PARP inhibitor resistance and potential overcoming strategies. *Genes & Diseases*, *11*(1). https://doi.org/10.1016/j.gendis.2023.02.014

Fukushima, N., & Fukayama, M. (2007). Mucinous cystic neoplasms of the pancreas: pathology and molecular genetics. *Journal of Hepato-Biliary-Pancreatic Surgery*, *14*(3). https://doi.org/10.1007/s00534-006-1168-3

Furusawa, T., Cavero, R., Liu, Y., Li, H., Xu, X., Andresson, T., Reinhold, W., White, O., Boufraqech, M., Meyer, T. J., Hartmann, O., Diefenbacher, M. E., Pommier, Y., & Weyemi, U. (2024). Metabolism-focused CRISPR screen unveils mitochondrial pyruvate carrier 1 as a critical driver for PARP inhibitor resistance in lung cancer. *Molecular Carcinogenesis*, *63*(6). https://doi.org/10.1002/mc.23705

Gajan, A., Sarma, A., Kim, S., Gurdziel, K., Wu, G. S., & Shekhar, M. P. (2021). Frontiers | Analysis of Adaptive Olaparib Resistance Effects on Cisplatin Sensitivity in Triple

Negative Breast Cancer Cells. *Frontiers in Oncology*, *11*. https://doi.org/10.3389/fonc.2021.694793

Ge, S. X., Jung, D., & Yao, R. (2020). ShinyGO: a graphical gene-set enrichment tool for animals and plants. *Bioinformatics*, *36*(8). https://doi.org/10.1093/bioinformatics/btz931

Gessler, L., Huraskin, D., Eiber, N., & Hashemolhosseini, S. (2024). The impact of canonical Wnt transcriptional repressors TLE3 and TLE4 on postsynaptic transcription at the neuromuscular junction. *Frontiers in Molecular Neuroscience*, *17*. https://doi.org/10.3389/fnmol.2024.1360368

Giglia-Mari, G., Zotter, A., & Vermeulen, W. (2011). DNA damage response. *Cold Spring Harbor Perspectives in Biology*, *3*(1). https://doi.org/10.1101/cshperspect.a000745

Gillespie, M. S., Ward, C. M., & Davies, C. C. (2023). DNA Repair and Therapeutic Strategies in Cancer Stem Cells. *Cancers*, *15*(6). https://doi.org/10.3390/cancers15061897

Gkountakos, A., Martelli, F. M., Silvestris, N., Bevere, M., Bellis, M. D., Alaimo, L., Sapuppo, E., Masetto, F., Mombello, A., Simbolo, M., Bariani, E., Milella, M., Fassan, M., Scarpa, A., & Luchini, C. (2023). Extrahepatic Distal Cholangiocarcinoma vs. Pancreatic Ductal Adenocarcinoma: Histology and Molecular Profiling for Differential Diagnosis and Treatment. *Cancers*, *15*(5). https://doi.org/10.3390/cancers15051454

Glicklis, R., Merchuk, J. C., & Cohen, S. (2004). Modeling mass transfer in hepatocyte spheroids via cell viability, spheroid size, and hepatocellular functions. *Biotechnology and Bioengineering*, *86*(6). https://doi.org/10.1002/bit.20086

Gohil, D., Sarker, A. H., & Roy, R. (2023). Base Excision Repair: Mechanisms and Impact in Biology, Disease, and Medicine. *International Journal of Molecular Sciences*, *24*(18). https://doi.org/10.3390/ijms241814186

Golan, T., Hammel, P., Reni, M., Cutsem, E. V., Macarulla, T., Hall, M. J., Park, J. O., Hochhauser, D., Arnold, D., Oh, D.-Y., Reinacher-Schick, A. C., Tortora, G., Algül, H., O'Reilly, E. M., McGuinness, D., Cui, K., Schlienger, K., Locker, G. Y., & Kindler, H. L. (2021). Overall survival from the phase 3 POLO trial: Maintenance olaparib for germline BRCA-mutated metastatic pancreatic cancer. *Journal of clinical oncology : official journal of the American Society of Clinical Oncology*, *39*(3_suppl), 378-378. https://doi.org/10.1200/JCO.2021.39.3_SUPPL.378

Gralewska, P., Gajek, A., Marczak, A., & Rogalska, A. (2021). Metformin Affects Olaparib Sensitivity through Induction of Apoptosis in Epithelial Ovarian Cancer Cell Lines. *International Journal of Molecular Sciences*, *22*(19). https://doi.org/10.3390/ijms221910557

Grossman, J. E., Muthuswamy, L., Huang, L., Akshinthala, D., Perea, S., Gonzalez, R. S., Tsai, L. L., Cohen, J., Bockorny, B., Bullock, A. J., Schlechter, B., Peters, M. L. B., Conahan, C., Narasimhan, S., Lim, C., Davis, R. B., Besaw, R., Sawhney, M. S., Pleskow, D.,…Hidalgo, M. (2022). Organoid Sensitivity Correlates with Therapeutic Response in Patients with Pancreatic Cancer. *Clinical cancer research : an official journal of the American Association for Cancer Research*, *28*(4), 708-708. https://doi.org/10.1158/1078-0432.CCR-20-4116

Guillén-Ponce, C., Blázquez, J., González, I., de-Madaria, E., Montáns, J., Carrato, A., Guillén-Ponce, C., Blázquez, J., González, I., de-Madaria, E., Montáns, J., & Carrato, A. (2017). Diagnosis and staging of pancreatic ductal adenocarcinoma. *Clinical and Translational Oncology*, *19*(10). https://doi.org/10.1007/s12094-017-1681-7

Guirouilh-Barbat, J., Lambert, S., Bertrand, P., & Lopez, B. S. (2014). Is homologous recombination really an error-free process? *Frontiers in Genetics*, *5*(JUN). https://doi.org/10.3389/FGENE.2014.00175

Gündel, B., Heuchel, R., & Löhr, M. (2023). Applying an automated image-based algorithm for phenotypical characterisation of cancer cell spheroids. *Pancreatology*, *23*. https://doi.org/10.1016/j.pan.2023.06.760

Gündel, B., Liu, X., Löhr, M., & Heuchel, R. (2021). Pancreatic Ductal Adenocarcinoma: Preclinical in vitro and ex vivo Models. *Frontiers in Cell and Developmental Biology*, *9*, 2991-2991. https://doi.org/10.3389/FCELL.2021.741162/XML/NLM

Guo, N., Li, M. Z., Wang, L. M., Chen, H. D., Song, S. S., Miao, Z. H., & He, J. X. (2022). Repeated treatments of Capan-1 cells with PARP1 and Chk1 inhibitors promote drug resistance, migration and invasion. *Cancer biology & therapy*, *23*(1), 69-82. https://doi.org/10.1080/15384047.2021.2024414

Han, Y., & Li, C.-W. (2019). Effect of metformin on PARP inhibitors-induced epithelial-mesenchymal transition and PD-L1 expression in triple-negative breast cancer. *Journal of Clinical Oncology*, *37*(15_suppl). https://doi.org/10.1200/JCO.2019.37.15_suppl.1063

He, C., Han, S., Chang, Y., Wu, M., Zhao, Y., Chen, C., & Chu, X. (2021). CRISPR screen in cancer: status quo and future perspectives. *American Journal of Cancer Research*, *11*(4), 1031-1031. /pmc/articles/PMC8085856/

/pmc/articles/PMC8085856/?report=abstract

https://www.ncbi.nlm.nih.gov/pmc/articles/PMC8085856/

He, J., Ford, H., Carroll, J., Douglas, C., Gonzales, E., Ding, S., Fearnley, I., & Walker, J. (2018). Assembly of the membrane domain of ATP synthase in human mitochondria. *Proceedings of the National Academy of Sciences of the United States of America*, *115*(12). https://doi.org/10.1073/pnas.1722086115

Hedrich, W. D., Panzica-Kelly, J. M., Chen, S.-J., Strassle, B., Hasson, C., Lecureux, L., Wang, L., Chen, W., Sherry, T., Gan, J., & Davis, M. (2020). Development and characterization of rat duodenal organoids for ADME and toxicology applications. *Toxicology*, *446*. https://doi.org/10.1016/j.tox.2020.152614

Herzog, M., Puddu, F., Coates, J., Geisler, N., Forment, J. V., & Jackson, S. P. (2018). Detection of functional protein domains by unbiased genome-wide forward genetic screening. *Scientific Reports*, *8*(1). https://doi.org/10.1038/s41598-018-24400-4

Hillemeyer, L., Espinoza-Sanchez, N. A., Greve, B., Hassan, N., Chelariu-Raicu, A., Kiesel, L., & Götte, M. (2022). The Cell Surface Heparan Sulfate Proteoglycan Syndecan-3 Promotes Ovarian Cancer Pathogenesis. *International Journal of Molecular Sciences*, *23*(10), 5793-5793. https://doi.org/10.3390/ijms23105793

Hirt, C. K., Booij, T. H., Grob, L., Simmler, P., Toussaint, N. C., Keller, D., Taube, D., Ludwig, V., Goryachkin, A., Pauli, C., Lenggenhager, D., Stekhoven, D. J., Stirnimann, C. U., Endhardt, K., Ringnalda, F., Villiger, L., Siebenhüner, A., Karkampouna, S., Menna, M. D.,…Schwank, G. (2022). Drug screening and genome editing in human pancreatic cancer organoids identifies drug-gene interactions and candidates for off-label therapy. *Cell Genomics*, *2*(2), 100095-100095. https://doi.org/10.1016/J.XGEN.2022.100095

Ho, J., Cruise, E. S., Dowling, R. J. O., & Stambolic, V. (2020). PTEN Nuclear Functions. *Cold Spring Harbor Perspectives in Medicine*, *10*(5). https://doi.org/10.1101/cshperspect.a036079

Höfer, S., Frasch, L., Putzker, K., Lewis, J., Sakhteman, A., The, M., Bayer, F. P., Müller, J., Hamood, F., & Kuster, B. (2024). Gemcitabine and ATR inhibitors synergize to kill PDAC cells by blocking DNA damage response. *bioRxiv*. https://doi.org/10.1101/2024.03.22.586243

Hopkins, T. A., Ainsworth, W. B., Ellis, P. A., Donawho, C. K., DiGiammarino, E. L., Panchal, S. C., Abraham, V. C., Algire, M. A., Shi, Y., Olson, A. M., Johnson, E. F., Wilsbacher, J. L., & Maag, D. (2019). PARP1 Trapping by PARP Inhibitors Drives Cytotoxicity in Both Cancer Cells and Healthy Bone Marrow. *Molecular Cancer Research*, *17*(2). https://doi.org/10.1158/1541-7786.MCR-18-0138

Hosein, A. N., Dougan, S. K., Aguirre, A. J., & Maitra, A. (2022). Translational advances in pancreatic ductal adenocarcinoma therapy. *Nature Cancer*, *3*(3). https://doi.org/10.1038/s43018-022-00349-2

Hou, S., Jin, W., Xiao, W., Deng, B., Wu, D., Zhi, J., Wu, K., Cao, X., Chen, S., Ding, Y., & Shi, H. (2019). Integrin α5 promotes migration and cisplatin resistance in esophageal squamous cell carcinoma cells. *American Journal of Cancer Research*, *9*(12), 2774-2788. https://www.ncbi.nlm.nih.gov/pmc/articles/PMC6943361/

Hruban, R. H., Takaori, K., Klimstra, D. S., Adsay, N. V., Albores-Saavedra, J., Biankin, A. V., Biankin, S. A., Compton, C., Fukushima, N., Furukawa, T., Goggins, M., Kato, Y., Kloppel, G., Longnecker, D. S., Luttges, J., Maitra, A., Offerhaus, G. J. A., Shimizu, M., & Yonezawa, S. (2004). An illustrated consensus on the classification of pancreatic intraepithelial neoplasia and intraductal papillary mucinous neoplasms. *The American journal of surgical pathology*, *28*(8), 977-987. https://doi.org/10.1097/01.PAS.0000126675.59108.80

Hu, Ye, Z., Qin, Y., Xu, X.-w., Yu, X.-j., Zhuo, Q.-f., & Ji, S.-r. (2021). Mutations in key driver genes of pancreatic cancer: molecularly targeted therapies and other clinical implications. *Acta Pharmacologica Sinica*, *42*(11). https://doi.org/10.1038/s41401-020-00584-2

Hu;, Chitnis, N., Monos, D., & Dinh, A. (2021). Next-generation sequencing technologies: An overview. *Human Immunology*, *82*(11). https://doi.org/10.1016/j.humimm.2021.02.012

Huang, S., Xing, Y., & Liu, Y. (2019). Emerging roles for the ER stress sensor IRE1α in metabolic regulation and disease. *The Journal of Biological Chemistry*, *294*(49). https://doi.org/10.1074/jbc.REV119.007036

Hutchinson, L., & Kirk, R. (2011). High drug attrition rates—where are we going wrong? *Nature Reviews Clinical Oncology*, *8*(4). https://doi.org/10.1038/nrclinonc.2011.34

Igarashi, S., Matsubara, T., Harada, K., Ikeda, H., Sato, Y., Sasaki, M., Matsui, O., & Nakanuma, Y. (2012). Bile duct expression of pancreatic and duodenal homeobox 1 in perihilar cholangiocarcinogenesis. *Histopathology*, *61*(2). https://doi.org/10.1111/j.1365-2559.2012.04218.x

Ihnen, M., zu Eulenburg, C., Kolarova, T., Qi, J. W., Manivong, K., Chalukya, M., Dering, J., Anderson, L., Ginther, C., Meuter, A., Winterhoff, B., Jones, S., Velculescu, V. E., Venkatesan, N., Rong, H.-M., Dandekar, S., Udar, N., Jänicke, F., Los, G.,…Konecny, G. E. (2013). Therapeutic Potential of the Poly(ADP-ribose) Polymerase Inhibitor Rucaparib for the Treatment of Sporadic Human Ovarian Cancer. *Molecular Cancer Therapeutics*, *12*(6). https://doi.org/10.1158/1535-7163.MCT-12-0813

Illumina. (2017). An introduction to Next-Generation Sequencing Technology. In. https://www.illumina.com/science/technology/next-generation-sequencing.html.

Illuzzi, G., Staniszewska, A. D., Gill, S. J., Pike, A., McWilliams, L., Critchlow, S. E., Cronin, A., Fawell, S., Hawthorne, G., Jamal, K., Johannes, J., Leonard, E., Macdonald, R.,

Maglennon, G., Nikkilä, J., O'Connor, M. J., Smith, A., Southgate, H., Wilson, J.,…Leo, E. (2022). Preclinical Characterization of AZD5305, A Next-Generation, Highly Selective PARP1 Inhibitor and Trapper. *Clinical Cancer Research*, *28*(21). https://doi.org/10.1158/1078-0432.CCR-22-0301

Imamura, Y., Mukohara, T., Shimono, Y., Funakoshi, Y., Chayahara, N., Toyoda, M., Kiyota, N., Takao, S., Kono, S., Nakatsura, T., & Minami, H. (2015). Comparison of 2D- and 3D-culture models as drug-testing platforms in breast cancer. *Oncology reports*, *33*(4). https://doi.org/10.3892/or.2015.3767

Ipsen, M. B., Sørensen, E. M. G., Thomsen, E. A., Weiss, S., Haldrup, J., Dalby, A., Palmfeldt, J., Bross, P., Rasmussen, M., Fredsøe, J., Klingenberg, S., Jochumsen, M. R., Bouchelouche, K., Ulhøi, B. P., Borre, M., Mikkelsen, J. G., & Sørensen, K. D. (2022). A genome-wide CRISPR-Cas9 knockout screen identifies novel PARP inhibitor resistance genes in prostate cancer. *Oncogene*, *41*(37). https://doi.org/10.1038/s41388-022-02427-2

Jamal, K., Galbiati, A., Armenia, J., Illuzzi, G., Hall, J., Bentouati, S., Barrell, D., Ahdesmäki, M., O'Connor, M. J., Leo, E., & Forment, J. V. (2022). Drug–gene Interaction Screens Coupled to Tumor Data Analyses Identify the Most Clinically Relevant Cancer Vulnerabilities Driving Sensitivity to PARP Inhibition. *Cancer Research Communications*, *2*(10). https://doi.org/10.1158/2767-9764.CRC-22-0119

James, N. E., Cantillo, E., Yano, N., Chichester, C. O., DiSilvestro, P. A., Hovanesian, V., Rao, R. S. P., Kim, K. K., Moore, R. G., Ahsan, N., & Ribeiro, J. R. (2019). Septin-2 is overexpressed in epithelial ovarian cancer and mediates proliferation via regulation of cellular metabolic proteins. *Oncotarget*, *10*(31). https://doi.org/10.18632/oncotarget.26836

Jang, D. H., Greenwood, J. C., Spyres, M. B., & Eckmann, D. M. (2017). Measurement of Mitochondrial Respiration and Motility in Acute Care: Sepsis, Trauma, and Poisoning. *Journal of intensive care medicine*, *32*(1). https://doi.org/10.1177/0885066616658449

Javle, M., E, S.-S., L, X., G, V., N, H., D, F., B, B., S, U., O, M., RA, W., & T, G. (2021). Olaparib Monotherapy for Previously Treated Pancreatic Cancer With DNA Damage Repair Genetic Alterations Other Than Germline BRCA Variants: Findings From 2 Phase 2 Nonrandomized Clinical Trials. *JAMA oncology*, *7*(5). https://doi.org/10.1001/jamaoncol.2021.0006

Jette, N. R., Kumar, M., Radhamani, S., Arthur, G., Goutam, S., Yip, S., Kolinsky, M., Williams, G. J., Bose, P., Lees-Miller, S. P., Jette, N. R., Kumar, M., Radhamani, S., Arthur, G., Goutam, S., Yip, S., Kolinsky, M., Williams, G. J., Bose, P., & Lees-Miller, S. P. (2020). ATM-Deficient Cancers Provide New Opportunities for Precision Oncology. *Cancers*, *12*(3). https://doi.org/10.3390/cancers12030687

Johansson, K. A., & Grapin-Botton, A. (2002). Development and diseases of the pancreas. *Clinical Genetics*, *62*(1), 14-23. https://doi.org/10.1034/J.1399-0004.2002.620102.X

Jong, E. J. M. d., Geest, L. G. v. d., Besselink, M. G., Bouwense, S. A. W., Buijsen, J., Dejong, C. H. C., Koerkamp, B. G., Heij, L. R., Hingh, I. H. J. T. d., Hoge, C., Kazemier, G., Laarhoven, H. W. M. v., Meijer, V. E. d., Stommel, M. W. J., Tjan-Heijnen, V. C. G., Iersel, L. B. J. V.-v., Wilmink, J. W., Geurts, S. M. E., & Vos-Geelen, J. d. (2022). Treatment and overall survival of four types of non-metastatic periampullary cancer: nationwide population-based cohort study. *HPB*, *24*(9). https://doi.org/10.1016/j.hpb.2022.01.009

Kalita, B., Sahu, S., Bharadwaj, A., Panneerselvam, L., Martinez-Cebrian, G., Agarwal, M., Mathew, S. J., Kalita, B., Sahu, S., Bharadwaj, A., Panneerselvam, L., Martinez-Cebrian, G., Agarwal, M., & Mathew, S. J. (2024). The Wnt-pathway corepressor TLE3 interacts with the histone methyltransferase KMT1A to inhibit differentiation in Rhabdomyosarcoma. *Oncogene*, *43*(7). https://doi.org/10.1038/s41388-023-02911-3

Kamarajah, S. K. (2018). Pancreaticoduodenectomy for periampullary tumours: a review article based on Surveillance, End Results and Epidemiology (SEER) database. *Clinical and Translational Oncology*, *20*(9). https://doi.org/10.1007/s12094-018-1832-5

Kanda, M., Matthaei, H., Wu, J., Hong, S.-M., Yu, J., Borges, M., Hruban, R. H., Maitra, A., Kinzler, K., Vogelstein, B., & Goggins, M. (2012). Presence of Somatic Mutations in Most Early-Stage Pancreatic Intraepithelial Neoplasia. *Gastroenterology*, *142*(4). https://doi.org/10.1053/j.gastro.2011.12.042

Kanda, M., Sadakari, Y., Borges, M., Topazian, M., Farrell, J., Syngal, S., Lee, J., Kamel, I., Lennon, A. M., Knight, S., Fujiwara, S., Hruban, R. H., Canto, M. I., & Goggins, M. (2013). Mutant TP53 in Duodenal Samples of Pancreatic Juice from Patients with Pancreatic Cancer or High-Grade Dysplasia. *Clinical gastroenterology and hepatology*, *11*(6). https://doi.org/10.1016/j.cgh.2012.11.016

Kaplan, A. R., & Glazer, P. M. (2020). Impact of hypoxia on DNA repair and genome integrity. *Mutagenesis*, *35*(1). https://doi.org/10.1093/mutage/gez019

Kaur, G., Evans, D. M., Teicher, B. A., & Coussens, N. P. (2021). Complex Tumor Spheroids, a Tissue-Mimicking Tumor Model, for Drug Discovery and Precision Medicine. *SLAS Discovery*, *26*(10). https://doi.org/10.1177/24725552211038362

Keniry, M., & Parsons, R. (2008). The role of PTEN signaling perturbations in cancer and in targeted therapy. *Oncogene*, *27*(41). https://doi.org/10.1038/onc.2008.248

Kennedy, M. W., Chalamalasetty, R. B., Thomas, S., Garriock, R. J., Jailwala, P., Yamaguchi, T. P., Kennedy, M. W., Chalamalasetty, R. B., Thomas, S., Garriock, R. J., Jailwala, P., & Yamaguchi, T. P. (2016). Sp5 and Sp8 recruit β-catenin and Tcf1-Lef1 to select enhancers to activate Wnt target gene transcription. *Proceedings of the National Academy of Sciences*, *113*(13). https://doi.org/10.1073/pnas.1519994113

Kim, J., Kim, J., & Bae, J.-S. (2016). ROS homeostasis and metabolism: a critical liaison for cancer therapy. *Experimental & Molecular Medicine*, *48*(11). https://doi.org/10.1038/emm.2016.119

Kim;, Min, A., Im, S.-A., Jang, H., Kim, Y. J., Kim, H.-J., Lee, K.-H., Kim, T.-Y., Lee, K. W., Oh, D.-Y., Kim, J.-H., & Bang, Y.-J. (2020). TDP1 and TOP1 Modulation in Olaparib-Resistant Cancer Determines the Efficacy of Subsequent Chemotherapy. *Cancers*, *12*(2). https://doi.org/10.3390/cancers12020334

Kim;, Xu, H., George, E., Hallberg, D., Kumar, S., Jagannathan, V., Medvedev, S., Kinose, Y., Devins, K., Verma, P., Ly, K., Wang, Y., Greenberg, R. A., Schwartz, L., Johnson, N., Scharpf, R. B., Mills, G. B., Zhang, R., Velculescu, V. E.,…Simpkins, F. (2020). Combining PARP with ATR inhibition overcomes PARP inhibitor and platinum resistance in ovarian cancer models. *Nature Communications*, *11*(1). https://doi.org/10.1038/s41467-020-17127-2

Kinoshita, K., Tsukamoto, Y., Hirashita, Y., Fuchino, T., Kurogi, S., Uchida, T., Nakada, C., Matsumoto, T., Okamoto, K., Motomura, M., Fukuchi, S., Sagami, R., Nagai, T., Gotoh, Y., Fukuda, K., Ogawa, R., Mizukami, K., Okimoto, T., Kodama, M.,…Hijiya, N. (2023). Efficient Establishment of Bile-Derived Organoids From Biliary Cancer

Patients. *Laboratory Investigation*, *103*(6). https://doi.org/10.1016/j.labinv.2023.100105

Klotz, D. M., Schwarz, F. M., Dubrovska, A., Schuster, K., Theis, M., Krüger, A., Kutz, O., Link, T., Wimberger, P., Drukewitz, S., Buchholz, F., Thomale, J., Kuhlmann, J. D., Klotz, D. M., Schwarz, F. M., Dubrovska, A., Schuster, K., Theis, M., Krüger, A.,…Kuhlmann, J. D. (2023-07-25). Establishment and Molecular Characterization of an In Vitro Model for PARPi-Resistant Ovarian Cancer. *Cancers 2023, Vol. 15, Page 3774*, *15*(15). https://doi.org/10.3390/cancers15153774

Kraus, W. L. (2015). PARPs and ADP-Ribosylation: Fifty Years… and Counting. *Molecular Cell*, *58*(6). https://doi.org/10.1016/j.molcel.2015.06.006

Krieger, T. G., Blanc, S. L., Jabs, J., Ten, F. W., Ishaque, N., Jechow, K., Debnath, O., Leonhardt, C. S., Giri, A., Eils, R., Strobel, O., & Conrad, C. (2021). Single-cell analysis of patient-derived PDAC organoids reveals cell state heterogeneity and a conserved developmental hierarchy. *Nature Communications*, *12*(1). https://doi.org/10.1038/S41467-021-26059-4

Kuo, Y.-C., Kou, H.-W., Hsu, C.-P., Lo, C.-H., & Hwang, T.-L. (2023). Identification and Clinical Significance of Pancreatic Cancer Stem Cells and Their Chemotherapeutic Drug Resistance. *International Journal of Molecular Sciences*, *24*(8). https://doi.org/10.3390/ijms24087331

Kyriazis, A. P., Kyriazis, A. A., Scarpelli, D. G., Fogh, J., Rau, M. S., & Lepera, R. (1982). Human pancreatic adenocarcinoma line Capan-1 in tissue culture and the nude mouse: morphologic, biologic, and biochemical characteristics. *American Journal of Pathology*, *106*(2), 250-260.

Lahiguera, Á., Hyroššová, P., Figueras, A., Garzón, D., Moreno, R., Soto-Cerrato, V., McNeish, I., Serra, V., Lazaro, C., Barretina, P., Brunet, J., Menéndez, J., Matias-Guiu, X., Vidal, A., Villanueva, A., Taylor-Harding, B., Tanaka, H., Orsulic, S., Junza, A.,…Viñals, F. (2020). Tumors defective in homologous recombination rely on oxidative metabolism: relevance to treatments with PARP inhibitors. *EMBO Molecular Medicine*, *12*(6). https://doi.org/10.15252/emmm.201911217

Lai, E., Ziranu, P., Spanu, D., Dubois, M., Pretta, A., Tolu, S., Camera, S., Liscia, N., Mariani, S., Persano, M., Migliari, M., Donisi, C., Demurtas, L., Pusceddu, V., Puzzoni, M., & Scartozzi, M. (2021). BRCA-mutant pancreatic ductal adenocarcinoma. *British Journal of Cancer*, *125*(10). https://doi.org/10.1038/s41416-021-01469-9

Lai, Z. W., Bolm, L., Fuellgraf, H., Biniossek, M. L., Makowiec, F., Hopt, U. T., Werner, M., Keck, T., Bausch, D., Sorio, C., Scarpa, A., Schilling, O., Bronsert, P., & Wellner, U. F. (2016). Characterization of various cell lines from different ampullary cancer subtypes and cancer associated fibroblast-mediated responses. *BMC Cancer*, *16*(1). https://doi.org/10.1186/s12885-016-2193-5

Latenstein, A. E. J., van der Geest, L. G. M., Bonsing, B. A., Groot Koerkamp, B., Haj Mohammad, N., de Hingh, I. H. J. T., de Meijer, V. E., Molenaar, I. Q., van Santvoort, H. C., van Tienhoven, G., Verheij, J., Vissers, P. A. J., de Vos-Geelen, J., Busch, O. R., van Eijck, C. H. J., van Laarhoven, H. W. M., Besselink, M. G., & Wilmink, J. W. (2020). Nationwide trends in incidence, treatment and survival of pancreatic ductal adenocarcinoma. *European Journal of Cancer*, *125*, 83-93. https://doi.org/10.1016/j.ejca.2019.11.002

Lau, C.-H., Tin, C., & Suh, Y. (2020). CRISPR-based strategies for targeted transgene knock-in and gene correction. *Faculty Reviews*, *9*. https://doi.org/10.12703/R/9-20

Lee, P. W. T., Koseki, L. R., Haitani, T., Harada, H., & Kobayashi, M. (2024). Hypoxia-Inducible Factor-Dependent and Independent Mechanisms Underlying Chemoresistance of Hypoxic Cancer Cells. *Cancers*, *16*(9). https://doi.org/10.3390/cancers16091729

Lee, T. H., & Kang, T. H. (2019). DNA oxidation and excision repair pathways. *International Journal of Molecular Sciences*, *20*(23). https://doi.org/10.3390/ijms20236092

Lévi, F., Metzger, G., Massari, C., Milano, G., Lévi, F., Metzger, G., Massari, C., & Milano, G. (2012). Oxaliplatin. *Clinical Pharmacokinetics*, *38*(1). https://doi.org/10.2165/00003088-200038010-00001

Li, H., Yang, Y., Hong, W., Huang, M., Wu, M., & Zhao, X. (2020). Applications of genome editing technology in the targeted therapy of human diseases: mechanisms, advances and prospects. *Signal Transduction and Targeted Therapy 2020 5:1*, *5*(1), 1-23. https://doi.org/10.1038/s41392-019-0089-y

Li, H. L., Gee, P., Ishida, K., & Hotta, A. (2016). Efficient genomic correction methods in human iPS cells using CRISPR–Cas9 system. *Methods*, *101*, 27-35. https://doi.org/10.1016/J.YMETH.2015.10.015

Li, R., Wu, X., Zhao, P., Xue, K., & Li, J. (2022). A pan-cancer analysis identifies HDAC11 as an immunological and prognostic biomarker. *The FASEB Journal*, *36*(7). https://doi.org/10.1096/fj.202101742RR

Li, W., Xu, H., Xiao, T., Cong, L., Love, M. I., Zhang, F., Irizarry, R. A., Liu, J. S., Brown, M., Liu, X. S., Li, W., Xu, H., Xiao, T., Cong, L., Love, M. I., Zhang, F., Irizarry, R. A., Liu, J. S., Brown, M., & Liu, X. S. (2014). MAGeCK enables robust identification of essential genes from genome-scale CRISPR/Cas9 knockout screens. *Genome Biology*, *15*(12). https://doi.org/10.1186/s13059-014-0554-4

Li, Y., Tang, S., Shi, X., Lv, J., Wu, X., Zhang, Y., Wang, H., He, J., Zhu, Y., Ju, Y., Zhang, Y., Guo, S., Yang, W., Yin, H., Chen, L., Gao, D., & Jin, G. (2023). Metabolic classification suggests the GLUT1/ALDOB/G6PD axis as a therapeutic target in chemotherapy-resistant pancreatic cancer. *Cell Reports Medicine*, *4*(9). https://doi.org/10.1016/j.xcrm.2023.101162

Liberti, M. V., & Locasale, J. W. (2016). The Warburg Effect: How Does it Benefit Cancer Cells? *Trends in biochemical sciences*, *41*(3). https://doi.org/10.1016/j.tibs.2015.12.001

Lin, J.-C., Liu, T.-P., & Yang, P.-M. (2020). CDKN2A-Inactivated Pancreatic Ductal Adenocarcinoma Exhibits Therapeutic Sensitivity to Paclitaxel: A Bioinformatics Study. *Journal of Clinical Medicine*, *9*(12). https://doi.org/10.3390/jcm9124019

Linehan, A., O'Reilly, M., McDermott, R., & O'Kane, G. M. (2024). Targeting KRAS mutations in pancreatic cancer: opportunities for future strategies. *Frontiers in Medicine*, *11*. https://doi.org/10.3389/fmed.2024.1369136

Liu, M., Quek, L.-E., Sultani, G., & Turner, N. (2016). Epithelial-mesenchymal transition induction is associated with augmented glucose uptake and lactate production in pancreatic ductal adenocarcinoma. *Cancer & Metabolism*, *4*(1). https://doi.org/10.1186/s40170-016-0160-x

Liu, X., Han, E. K., Anderson, M., Shi, Y., Semizarov, D., Wang, G., McGonigal, T., Roberts, L., Lasko, L., Palma, J., Zhu, G.-d., Penning, T., Rosenberg, S., Giranda, V. L., Luo, Y., Leverson, J., Johnson, E. F., & Shoemaker, A. R. (2009). Acquired Resistance to Combination Treatment with Temozolomide and ABT-888 Is Mediated by Both Base Excision Repair and Homologous Recombination DNA Repair Pathways. *Molecular Cancer Research*, *7*(10). https://doi.org/10.1158/1541-7786.MCR-09-0299

Liu, Y., Han, S., Li, Y., Liu, Y., Zhang, D., Li, Y., & Zhang, J. (2017). MicroRNA-20a contributes to cisplatin-resistance and migration of OVCAR3 ovarian cancer cell line. *Oncology Letters*, *14*(2). https://doi.org/10.3892/ol.2017.6348

Liu, Z., Dong, H., Cui, Y., Cong, L., & Zhang, D. (2020). Application of different types of CRISPR/Cas-based systems in bacteria. *Microbial Cell Factories 2020 19:1*, *19*(1), 1-14. https://doi.org/10.1186/S12934-020-01431-Z

Lloyd, R. L., Wijnhoven, P. W. G., Ramos-Montoya, A., Wilson, Z., Illuzzi, G., Falenta, K., Jones, G. N., James, N., Chabbert, C. D., Stott, J., Dean, E., Lau, A., Young, L. A., Lloyd, R. L., Wijnhoven, P. W. G., Ramos-Montoya, A., Wilson, Z., Illuzzi, G., Falenta, K.,…Young, L. A. (2020). Combined PARP and ATR inhibition potentiates genome instability and cell death in ATM-deficient cancer cells. *Oncogene*, *39*(25). https://doi.org/10.1038/s41388-020-1328-y

Longati, P., Jia, X., Eimer, J., Wagman, A., Witt, M. R., Rehnmark, S., Verbeke, C., Toftgård, R., Löhr, M., & Heuchel, R. L. (2013). 3D pancreatic carcinoma spheroids induce a matrix-rich, chemoresistant phenotype offering a better model for drug testing. *BMC Cancer*, *13*(1), 1-13. https://doi.org/10.1186/1471-2407-13-95/FIGURES/9

Luo, J. (2021). KRAS mutation in Pancreatic Cancer. *Seminars in Oncology*, *48*(1). https://doi.org/10.1053/j.seminoncol.2021.02.003

Luo, W., Wang, J., Chen, H., Ye, L., Qiu, J., Liu, Y., Wang, R., Weng, G., Liu, T., Su, D., Tao, J., Ding, C., You, L., & Zhang, T. (2023). Epidemiology of pancreatic cancer: New version, new vision. *Chinese Journal of Cancer Research*, *35*(5). https://doi.org/10.21147/j.issn.1000-9604.2023.05.03

Luo, Y., Cheng, Y., Wu, C., Ye, H., Chen, N., Zhang, F., Wei, H., & Xu, B. (2023). Pharmacokinetics, safety, and antitumor activity of talazoparib monotherapy in Chinese patients with advanced solid tumors. *Investigational New Drugs*, *41*(3), 503-511. https://doi.org/10.1007/s10637-023-01351-w

Ma, X., Dang, C., Min, W., Diao, Y., Hui, W., Wang, X., Dai, Z., Wang, X., & Kang, H. (2019). Downregulation of APE1 potentiates breast cancer cells to olaparib by inhibiting PARP-1 expression. *Breast Cancer Research and Treatment*, *176*(1). https://doi.org/10.1007/s10549-019-05189-w

Ma, Y., Zhang, L., & Huang, X. (2014). Genome modification by CRISPR/Cas9. *The FEBS Journal*, *281*(23), 5186-5193. https://doi.org/10.1111/FEBS.13110

Machado, N. O., Qadhi, H. a., & Wahibi, K. a. (2015). Intraductal Papillary Mucinous Neoplasm of Pancreas. *North American Journal of Medical Sciences*, *7*(5). https://doi.org/10.4103/1947-2714.157477

Mah, L.-J., El-Osta, A., Karagiannis, T. C., Mah, L.-J., El-Osta, A., & Karagiannis, T. C. (2010). γH2AX: a sensitive molecular marker of DNA damage and repair. *Leukemia*, *24*(4). https://doi.org/10.1038/leu.2010.6

Maier, C. F., Zhu, L., Nanduri, L. K., Kühn, D., Kochall, S., Thepkaysone, M.-L., William, D., Grützmann, K., Klink, B., Betge, J., Weitz, J., Rahbari, N. N., Reißfelder, C., & Schölch, S. (2021). Patient-Derived Organoids of Cholangiocarcinoma. *International Journal of Molecular Sciences*, *22*(16). https://doi.org/10.3390/ijms22168675

Makena, M. R., Gatla, H., Verlekar, D., Sukhavasi, S., Pandey, M. K., & Pramanik, K. C. (2019). Wnt/β-Catenin Signaling: The Culprit in Pancreatic Carcinogenesis and Therapeutic Resistance. *International Journal of Molecular Sciences*, *20*(17). https://doi.org/10.3390/IJMS20174242

Makoto, F., Shigenori, O., Kanako, S., & Masasuke, Y. (2014). Population of ATP synthase molecules in mitochondria is limited by available 6.8-kDa proteolipid protein (MLQ). *Genes to Cells*, *19*(2). https://doi.org/10.1111/gtc.12121

Mao, Z., Bozzella, M., Seluanov, A., & Gorbunova, V. (2008). Comparison of nonhomologous end joining and homologous recombination in human cells. *DNA Repair*, *7*(10), 1765-1765. https://doi.org/10.1016/J.DNAREP.2008.06.018

Marin, J. J. G., Monte, M. J., Macias, R. I. R., Romero, M. R., Herraez, E., Asensio, M., Ortiz-Rivero, S., Cives-Losada, C., Di Giacomo, S., Gonzalez-Gallego, J., Mauriz, J. L., Efferth, T., & Briz, O. (2022). Expression of Chemoresistance-Associated ABC Proteins in Hepatobiliary, Pancreatic and Gastrointestinal Cancers. *Cancers*, *14*(14). https://doi.org/10.3390/cancers14143524

Masoud, R., Reyes-Castellanos, G., Lac, S., Garcia, J., Dou, S., Shintu, L., Hadi, N. A., Gicquel, T., Kaoutari, A. E., Diémé, B., Tranchida, F., Cormareche, L., Borge, L., Gayet, O., Pasquier, E., Dusetti, N., Iovanna, J., & Carrier, A. (2020). Targeting Mitochondrial Complex I Overcomes Chemoresistance in High OXPHOS Pancreatic Cancer. *Cell Reports Medicine*, *1*(8). https://doi.org/10.1016/j.xcrm.2020.100143

Masters, J. R. (2002). HeLa cells 50 years on: the good, the bad and the ugly. *Nature Reviews Cancer*, *2*(4). https://doi.org/10.1038/nrc775

Masumori, N., Kunishima, Y., Hirobe, M., Takeuchi, M., Takayanagi, A., Tsukamoto, T., & Itoh, T. (2008). Measurement of Plasma Concentration of Gemcitabine and Its Metabolite dFdU in Hemodialysis Patients with Advanced Urothelial Cancer. *Japanese Journal of Clinical Oncology*, *38*(3), 182-185. https://doi.org/10.1093/jjco/hym171

McCluskey, J. T., Hamid, M., Guo-Parke, H., McClenaghan, N. H., Gomis, R., & Flatt, P. R. (2011). Development and functional characterization of insulin-releasing human pancreatic beta cell lines produced by electrofusion. *The Journal of Biological Chemistry*, *286*(25). https://doi.org/10.1074/jbc.M111.226795

McCombie, W. R., McPherson, J. D., & Mardis, E. R. (2019). Next-Generation Sequencing Technologies. *Perspectives in Medicine*, *9*(11). https://doi.org/10.1101/cshperspect.a036798

McEllin, B., Camacho, C. V., Mukherjee, B., Hahm, B., Tomimatsu, N., Bachoo, R. M., & Burma, S. (2010). PTEN Loss Compromises Homologous Recombination Repair in Astrocytes: Implications for Glioblastoma Therapy with Temozolomide or Poly(ADP-Ribose) Polymerase Inhibitors. *Cancer Research*, *70*(13). https://doi.org/10.1158/0008-5472.CAN-09-4295

McIntyre, C. A., Lawrence, S. A., Richards, A. L., Chou, J. F., Wong, W., Capanu, M., Berger, M. F., Donoghue, M. T. A., Yu, K. H., Varghese, A. M., Kelsen, D. P., Park, W., Balachandran, V. P., Kingham, T. P., D'Angelica, M. I., Drebin, J. A., Jarnagin, W. R., Allen, C. A. I.-D. P. J., & O'Reilly, E. M. (2020). Alterations in driver genes are predictive of survival in patients with resected pancreatic ductal adenocarcinoma. *Cancer*, *126*(17). https://doi.org/10.1002/cncr.33038

Mehibel, M., Xu, Y., Li, C. G., Moon, E. J., Thakkar, K. N., Diep, A. N., Kim, R. K., Bloomstein, J. D., Xiao, Y., Bacal, J., Saldivar, J. C., Le, Q.-T., Cimprich, K. A., Rankin, E. B., & Giaccia, A. J. (2021). Eliminating hypoxic tumor cells improves response to PARP inhibitors in homologous recombination–deficient cancer models. *The Journal of Clinical Investigation*, *131*(11). https://doi.org/10.1172/JCI146256

Mendes-Pereira, A. M., Martin, S. A., Brough, R., McCarthy, A., Taylor, J. R., Kim, J. S., Waldman, T., Lord, C. J., & Ashworth, A. (2009). Synthetic lethal targeting of PTEN mutant cells with PARP inhibitors. *EMBO Molecular Medicine*, *1*(6-7). https://doi.org/10.1002/emmm.200900041

Merighi, A., Gionchiglia, N., Granato, A., Lossi, L., Merighi, A., Gionchiglia, N., Granato, A., & Lossi, L. (2021). The Phosphorylated Form of the Histone H2AX (γH2AX) in the

Brain from Embryonic Life to Old Age. *Molecules*, *26*(23). https://doi.org/10.3390/molecules26237198

Meyer, T., Jahn, N., Lindner, S., Röhner, L., Dolnik, A., Weber, D., Scheffold, A., Köpff, S., Paschka, P., Gaidzik, V. I., Heckl, D., Wiese, S., Ebert, B. L., Döhner, H., Bullinger, L., Döhner, K., & Krönke, J. (2019). Functional characterization of BRCC3 mutations in acute myeloid leukemia with t(8;21)(q22;q22.1). *Leukemia*, *34*(2). https://doi.org/10.1038/s41375-019-0578-6

Michels, J., Vitale, I., Galluzzi, L., Adam, J., Olaussen, K. A., Kepp, O., Senovilla, L., Talhaoui, I., Guegan, J., Enot, D. P., Talbot, M., Robin, A., Girard, P., Oréar, C., Lissa, D., Sukkurwala, A. Q., Garcia, P., Behnam-Motlagh, P., Kohno, K.,…Kroemer, G. (2013). Cisplatin Resistance Associated with PARP Hyperactivation. *Cancer Research*, *73*(7). https://doi.org/10.1158/0008-5472.CAN-12-3000

Minami, F., Sasaki, N., Shichi, Y., Gomi, F., Michishita, M., Ohkusu-Tsukada, K., Toyoda, M., Takahashi, K., & Ishiwata, T. (2021). Morphofunctional analysis of human pancreatic cancer cell lines in 2- and 3-dimensional cultures. *Scientific Reports*, *11*(1). https://doi.org/10.1038/S41598-021-86028-1

Ming, M., & He, Y.-Y. (2012). PTEN in DNA damage repair. *Cancer Letters*, *319*(2). https://doi.org/10.1016/j.canlet.2012.01.003

Miura, K., Kimura, K., Amano, R., Yamazoe, S., Ohira, G., Murata, A., Nishio, K., Hasegawa, T., Yashiro, M., Nakata, B., Ohira, M., & Hirakawa, K. (2016). Establishment and characterization of new cell lines of anaplastic pancreatic cancer, which is a rare malignancy: OCUP-A1 and OCUP-A2. *BMC Cancer*, *16*(1). https://doi.org/10.1186/s12885-016-2297-y

Mo, W., & Zhang, J. (2012). Human ABCG2: structure, function, and its role in multidrug resistance. *Int J Biochem Mol Biol*, *3*(1), 1-27. https://pubmed.ncbi.nlm.nih.gov/22509477/

Mostafa, M. E., Erbarut-Seven, I., Pehlivanoglu, B., & Adsay, V. (2018). Pathologic classification of "pancreatic cancers": current concepts and challenges. *Chinese Clinical Oncology*, *6*(6). https://doi.org/10.21037/cco.2017.12.01

Mukherjee, A., Patterson, A. L., George, J. W., Carpenter, T. J., Madaj, Z. B., Hostetter, G., Risinger, J. I., & Teixeira, J. M. (2018). Nuclear PTEN Localization Contributes to DNA Damage Response in Endometrial Adenocarcinoma and Could Have a Diagnostic Benefit for Therapeutic Management of the Disease. *Molecular Cancer Therapeutics*, *17*(9). https://doi.org/10.1158/1535-7163.MCT-17-1255

Murai, J., Huang, S.-y. N., Das, B. B., Renaud, A., Zhang, Y., Doroshow, J. H., Ji, J., Takeda, S., & Pommier, Y. (2012). Differential trapping of PARP1 and PARP2 by clinical PARP inhibitors. *Cancer Research*, *72*(21). https://doi.org/10.1158/0008-5472.CAN-12-2753

Murai, J., Huang, S.-y. N., Renaud, A., Zhang, Y., Ji, J., Takeda, S., Morris, J., Teicher, B., Doroshow, J. H., & Pommier, Y. (2014). Stereospecific PARP trapping by BMN 673 and comparison with olaparib and rucaparib. *Molecular Cancer Therapeutics*, *13*(2). https://doi.org/10.1158/1535-7163.MCT-13-0803

Murphy, P., Armit, C., Hill, B., Venkataraman, S., Frankel, P., Baldock, R. A., & Davidson, D. R. (2022). Integrated analysis of Wnt signalling system component gene expression. *Development*, *149*(16). https://doi.org/10.1242/dev.200312

Naito, Y., Kuboki, Y., Ikeda, M., Harano, K., Matsubara, N., Toyoizumi, S., Mori, Y., Hori, N., Nagasawa, T., & Kogawa, T. (2021). Safety, pharmacokinetics, and preliminary efficacy of the PARP inhibitor talazoparib in Japanese patients with advanced solid

tumors: phase 1 study. *Investigational New Drugs*, *39*(6), 1568-1576. https://doi.org/10.1007/s10637-021-01120-7

Naumenko, N. V., Petruseva, I. O., & Lavrik, O. I. (2022). Bulky Adducts in Clustered DNA Lesions: Causes of Resistance to the NER System. *Acta Naturae*, *14*(4). https://doi.org/10.32607/actanaturae.11741

NCRI. (2024). *Survival statistics*. National Cancer Registry Ireland. Retrieved 18/06/2024 from https://www.ncri.ie/content/survival-statistics-new

Nelson, S. R., Zhang, C., Roche, S., O'Neill, F., Swan, N., Luo, Y., Larkin, A., Crown, J., & Walsh, N. (2020). Modelling of pancreatic cancer biology: transcriptomic signature for 3D PDX-derived organoids and primary cell line organoid development. *Scientific Reports*, *10*(1). https://doi.org/10.1038/s41598-020-59368-7

Nie, K., Li, J., He, X., Wang, Y., Zhao, Q., Du, M., Sun, H., Wang, J., Lyu, J., Fang, H., & Jin, L. (2020). COX6B2 drives metabolic reprogramming toward oxidative phosphorylation to promote metastasis in pancreatic ductal cancer cells. *Oncogenesis*, *9*(5), 51-51. https://doi.org/10.1038/s41389-020-0231-2

Nishimasu, H., Ran, F. A., Hsu, P. D., Konermann, S., Shehata, S. I., Dohmae, N., Ishitani, R., Zhang, F., & Nureki, O. (2014). Crystal structure of Cas9 in complex with guide RNA and target DNA. *Cell*, *156*(5), 935-949. https://doi.org/10.1016/j.cell.2014.02.001

Noorani, S., Nelson, S. R., Conlon, N. T., Meiller, J., Shcheglova, E., Usai, A., Stoof, J., Palanga, L., O'Neill, F., Roche, S., Cotter, M. B., Swan, N., & Walsh, N. (2022). Pancreatic Cancer 3D Cell Line Organoids (CLOs) Maintain the Phenotypic Characteristics of Organoids and Accurately Reflect the Cellular Architecture and Heterogeneity In Vivo. *Organoids*, *1*(2). https://doi.org/10.3390/organoids1020013

Noriko, M., Nagakatsu, H., Takeo, I., Izumi, O., Mitsuo, I., & Katsuhiko, Y. (2022). Identification of protease serine S1 family member 53 as a mitochondrial protein in murine islet beta cells. *Islets*, *14*(1). https://doi.org/10.1080/19382014.2021.1982325

O'Reilly, E. M., Lee, J. W., Zalupski, M., Capanu, M., Park, J., Golan, T., Tahover, E., Lowery, M. A., Chou, J. F., Sahai, V., Brenner, R., Kindler, H. L., Yu, K. H., Zervoudakis, A., Vemuri, S., Stadler, Z. K., Do, R. K. G., Dhani, N., Chen, A. P., & Kelsen, D. (2020). Randomized, Multicenter, Phase II Trial of Gemcitabine and Cisplatin With or Without Veliparib in Patients With Pancreas Adenocarcinoma and a Germline BRCA/PALB2 Mutation. *Journal of clinical oncology : official journal of the American Society of Clinical Oncology*, *38*(13), 1378-1388. https://doi.org/10.1200/JCO.19.02931

Obrist, F., Michels, J., Durand, S., Chery, A., Pol, J., Levesque, S., Joseph, A., Astesana, V., Pietrocola, F., Wu, G. S., Castedo, M., & Kroemer, G. (2018). Metabolic vulnerability of cisplatin-resistant cancers. *The EMBO Journal*, *37*(14). https://doi.org/10.15252/embj.201798597

Ohike, N., Kim, G. E., Tajiri, T., Krasinskas, A., Basturk, O., Coban, I., Bandyopadhyay, S., Morohoshi, T., Goodman, M., Kooby, D. A., Sarmiento, J. M., & Adsay, N. V. (2010). Intra-ampullary Papillary-Tubular Neoplasm (IAPN). *American Journal of Surgical Pathology*, *34*(12), 1731-1748. https://doi.org/10.1097/PAS.0b013e3181f8ff05

Olaoba, O. T., Adelusi, T. I., Yang, M., Maidens, T., Kimchi, E. T., Staveley-O'Carroll, K. F., & Li, G. (2024). Driver Mutations in Pancreatic Cancer and Opportunities for Targeted Therapy. *Cancers*, *16*(10). https://doi.org/10.3390/cancers16101808

Ooi, A. T., & Gomperts, B. N. (2015). Molecular Pathways: Targeting Cellular Energy Metabolism in Cancer via Inhibition of SLC2A1 and LDHA. *Clinical Cancer Research*, *21*(11). https://doi.org/10.1158/1078-0432.CCR-14-1209

Oya, Y., Imaizumi, K., & Mitsudomi, T. (2024). The next-generation KRAS inhibitors…What comes after sotorasib and adagrasib? *Lung Cancer*, *194*. https://doi.org/10.1016/j.lungcan.2024.107886

Pandol, S. J. (2010). Anatomy. In *The Exocrine Pancreas*. Morgan & Claypool Life Sciences. https://www.ncbi.nlm.nih.gov/books/NBK54134/

Papa, S., Martino, P. L., Capitanio, G., Gaballo, A., De Rasmo, D., Signorile, A., & Petruzzella, V. (2012). The Oxidative Phosphorylation System in Mammalian Mitochondria. *Advances in Experimental Medicine and Biology*. https://doi.org/10.1007/978-94-007-2869-1_1

Park, Chen, Chou, J. F., Varghese, A., Yu, K., Wong, W., Capanu, M., Balachandran, V., McIntyre, C. A., Dika, I. E., Khalil, D. N., Harding, J. J., Ghalehsari, N., McKinell, Z., Chalasani, S., Makarov, V., Selenica, P., Pei, X., Lecomte, N.,…O'Reilly, E. M. (2020). Genomic Methods Identify Homologous Recombination Deficiency in Pancreas Adenocarcinoma and Optimize Treatment Selection. *Clinical cancer research : an official journal of the American Association for Cancer Research*, *26*(13). https://doi.org/10.1158/1078-0432.CCR-20-0418

Park, J., Kim, S. I., Jeong, S. Y., Kim, Y., Bookman, M. A., Kim, J.-W., Kim, B.-G., & Lee, J.-Y. (2022). Second-line olaparib maintenance therapy is associated with poor response to subsequent chemotherapy in BRCA1/2-mutated epithelial ovarian cancer: A multicentre retrospective study. *Gynecologic Oncology*, *165*(1). https://doi.org/10.1016/j.ygyno.2022.02.002

Park;, Yamamoto, T. M., Li, H., Alcivar, A. L., Xia, B., Wang, Y., Bernhardy, A. J., Turner, K. M., Kossenkov, A. V., Watson, Z. L., Behbakht, K., Casadei, S., Swisher, E. M., Mischel, P. S., Johnson, N., & Bitler, B. G. (2020). Amplification of the mutation-carrying BRCA2 allele promotes RAD51 loading and PARP inhibitor resistance in the absence of reversion mutations. *Molecular Cancer Therapeutics*, *19*(2), 602-613. https://doi.org/10.1158/1535-7163.MCT-17-0256

Parsels, L., Engelke, G., Parsels, J. D., Flanagan, S., Zhang, Q., Tanska, D., Wahl, D. R., Canman, C. E., Lawrence, T. S., & Morgan, M. A. (2021). Combinatorial Efficacy of Olaparib with Radiation and ATR Inhibitor Requires PARP1 Protein in Homologous Recombination-Proficient Pancreatic Cancer - PubMed. *Molecular Cancer Therapeutics*, *20*(2). https://doi.org/10.1158/1535-7163.MCT-20-0365

Partyka, O., Pajewska, M., Kwaśniewska, D., Czerw, A., Deptała, A., Budzik, M., Cipora, E., Gąska, I., Gazdowicz, L., Mielnik, A., Sygit, K., Sygit, M., Krzych-Fałta, E., Schneider-Matyka, D., Grochans, S., Cybulska, A. M., Drobnik, J., Bandurska, E., Ciećko, W.,…Kozłowski, R. (2023). Overview of Pancreatic Cancer Epidemiology in Europe and Recommendations for Screening in High-Risk Populations. *Cancers*, *15*(14). https://doi.org/10.3390/cancers15143634

Pasello, M., Giudice, A. M., & Scotlandi, K. (2020). The ABC subfamily A transporters: Multifaceted players with incipient potentialities in cancer. *Seminars in Cancer Biology*, *60*. https://doi.org/10.1016/j.semcancer.2019.10.004

Patel, R. P., Kuhn, S., Yin, D., Hotz, J., Maher, F. A., Robey, R. W., Gottesman, M. M., & Horibata, S. (2021). Cross-resistance of cisplatin selected cells to anti-microtubule agents: Role of general survival mechanisms. *Translational Oncology*, *14*(1). https://doi.org/10.1016/j.tranon.2020.100917

Pavlova, N. N., & Thompson, C. B. (2016). The Emerging Hallmarks of Cancer Metabolism. *Cell Metabolism*, *23*(1). https://doi.org/10.1016/j.cmet.2015.12.006

Petropoulos, M., Karamichali, A., Rossetti, G. G., Freudenmann, A., Iacovino, L. G., Dionellis, V. S., Sotiriou, S. K., Halazonetis, T. D., Petropoulos, M., Karamichali, A., Rossetti, G.

G., Freudenmann, A., Iacovino, L. G., Dionellis, V. S., Sotiriou, S. K., & Halazonetis, T. D. (2024). Transcription–replication conflicts underlie sensitivity to PARP inhibitors. *Nature*, *628*(8007). https://doi.org/10.1038/s41586-024-07217-2

Pettitt, S. J., Krastev, D. B., Brandsma, I., Dréan, A., Song, F., Aleksandrov, R., Harrell, M. I., Menon, M., Brough, R., Campbell, J., Frankum, J., Ranes, M., Pemberton, H. N., Rafiq, R., Fenwick, K., Swain, A., Guettler, S., Lee, J.-M., Swisher, E. M.,…Lord, C. J. (2018). Genome-wide and high-density CRISPR-Cas9 screens identify point mutations in PARP1 causing PARP inhibitor resistance. *Nature Communications*, *9*(1). https://doi.org/10.1038/s41467-018-03917-2

Pettitt, S. J., Rehman, F. L., Bajrami, I., Brough, R., Wallberg, F., Kozarewa, I., Fenwick, K., Assiotis, I., Chen, L., Campbell, J., Lord, C. J., & Ashworth, A. (2013). A Genetic Screen Using the PiggyBac Transposon in Haploid Cells Identifies Parp1 as a Mediator of Olaparib Toxicity. *PLOS ONE*, *8*(4). https://doi.org/10.1371/journal.pone.0061520

Pfizer Europe, M. E. (2019). *Assessment report Talzenna*. https://www.ema.europa.eu/en/documents/assessment-report/talzenna-epar-public-assessment-report_en.pdf

Pilarski, R. (2019). The Role of BRCA Testing in Hereditary Pancreatic and Prostate Cancer Families. *American Society of Clinical Oncology Educational Book*(39). https://doi.org/10.1200/EDBK_238977

Porter, R. L., Magnus, N. K. C., Thapar, V., Morris, R., Szabolcs, A., Neyaz, A., Kulkarni, A. S., Tai, E., Chougule, A., Hillis, A., Golczer, G., Guo, H., Yamada, T., Kurokawa, T., Yashaswini, C., Ligorio, M., Vo, K. D., Nieman, L., Liss, A. S.,…Ting, D. T. (2019). Epithelial to mesenchymal plasticity and differential response to therapies in pancreatic ductal adenocarcinoma. *Proceedings of the National Academy of Sciences*, *116*(52). https://doi.org/10.1073/pnas.1914915116

Prabhu, K. S., Kuttikrishnan, S., Ahmad, N., Habeeba, U., Mariyam, Z., Suleman, M., Bhat, A. A., & Uddin, S. (2024). H2AX: A key player in DNA damage response and a promising target for cancer therapy. *Biomedicine & Pharmacotherapy*, *175*. https://doi.org/10.1016/j.biopha.2024.116663

Prasad, C. B., Prasad, S. B., Yadav, S. S., Pandey, L. K., Singh, S., Pradhan, S., & Narayan, G. (2017). Olaparib modulates DNA repair efficiency, sensitizes cervical cancer cells to cisplatin and exhibits anti-metastatic property. *Scientific Reports 2017 7:1*, *7*(1), 1-15. https://doi.org/10.1038/s41598-017-13232-3

Principe, D. R. (2022). Precision Medicine for BRCA/PALB2-Mutated Pancreatic Cancer and Emerging Strategies to Improve Therapeutic Responses to PARP Inhibition. *Cancers*, *14*(4). https://doi.org/10.3390/CANCERS14040897

Qian, Y., Gong, Y., Fan, Z., Luo, G., Huang, Q., Deng, S., Cheng, H., Jin, K., Ni, Q., Yu, X., & Liu, C. (2020). Molecular alterations and targeted therapy in pancreatic ductal adenocarcinoma. *Journal of Hematology and Oncology*, *13*(130). https://doi.org/10.1186/s13045-020-00958-3

Qiu, L., Li, R., Wang, Y., Lu, Z., Tu, Z., & Liu, H. (2024). PTEN inhibition enhances sensitivity of ovarian cancer cells to the poly (ADP-ribose) polymerase inhibitor by suppressing the MRE11-RAD50-NBN complex. *British Journal of Cancer*. https://doi.org/10.1038/s41416-024-02749-w

Rabl, J. (2020). BRCA1-A and BRISC: Multifunctional Molecular Machines for Ubiquitin Signaling. *Biomolecules*, *10*(11). https://doi.org/10.3390/biom10111503

Rahib, L., Smith, B. D., Aizenberg, R., Rosenzweig, A. B., Fleshman, J. M., & Matrisian, L. M. (2014). Projecting cancer incidence and deaths to 2030: The unexpected burden of

thyroid, liver, and pancreas cancers in the united states. In (Vol. 74, pp. 2913-2921): American Association for Cancer Research Inc.

Rahman, M., Hasan, M. R., Rahman, M., & Hasan, M. R. (2015). Cancer Metabolism and Drug Resistance. *Metabolites*, *5*(4). https://doi.org/10.3390/metabo5040571

Rajkumar, P., Mathew, B. S., Das, S., Isaiah, R., John, S., Prabha, R., & Fleming, D. H. (2016). Cisplatin Concentrations in Long and Short Duration Infusion: Implications for the Optimal Time of Radiation Delivery. *Journal of Clinical and Diagnostic Research : JCDR*, *10*(7). https://doi.org/10.7860/JCDR/2016/18181.8126

Ranjha, L., Howard, S. M., & Cejka, P. (2018). Main steps in DNA double-strand break repair: an introduction to homologous recombination and related processes. *Chromosoma*, *127*(2), 187-214. https://doi.org/10.1007/s00412-017-0658-1

Rath, D., Amlinger, L., Rath, A., & Lundgren, M. (2015). The CRISPR-Cas immune system: Biology, mechanisms and applications. *Biochimie*, *117*. https://doi.org/10.1016/j.biochi.2015.03.025

Ren, B., Liu, X., & Suriawinata, A. A. (2019). Pancreatic Ductal Adenocarcinoma and Its Precursor Lesions: Histopathology, Cytopathology, and Molecular Pathology. *The American Journal of Pathology*, *189*(1), 9-21. https://doi.org/10.1016/J.AJPATH.2018.10.004

Rhim, A. D., & Stanger, B. Z. (2010). Molecular Biology of Pancreatic Ductal Adenocarcinoma Progression: Aberrant Activation of Developmental Pathways. *Progress in molecular biology and translational science*, *97*. https://doi.org/10.1016/B978-0-12-385233-5.00002-7

Ro, C., Chai, W., Yu, V. E., & Yu, R. (2013). Pancreatic neuroendocrine tumors: biology, diagnosis, and treatment. *Chinese Journal of Cancer*, *32*(6). https://doi.org/10.5732/cjc.012.10295

Romero-Calvo, I., Weber, C. R., Ray, M., Brown, M., Kirby, K., Nandi, R. K., Long, T. M., Sparrow, S. M., Ugolkov, A., Qiang, W., Zhang, Y., Brunetti, T., Kindler, H., Segal, J. P., Rzhetsky, A., Mazar, A. P., Buschmann, M. M., Weichselbaum, R., Roggin, K., & White, K. P. (2019). Human organoids share structural and genetic features with primary pancreatic adenocarcinoma tumors. *Molecular Cancer Research*, *17*(1), 70-83. https://doi.org/10.1158/1541-7786.MCR-18-0531/81528/AM/HUMAN-ORGANOIDS-SHARE-STRUCTURAL-AND-GENETIC

Romero-Garcia, S., Lopez-Gonzales, J. S., Baez-Viveros, J. L., Aguilar-Cazares, D., & Prado-Garcia, H. (2011). Tumor cell metabolism: an integral view. *Cancer biology & therapy*, *12*(11). https://doi.org/10.4161/cbt.12.11.18140

Romero, N., Swain, P., Neilson, A., & Dranka, B. P. (2021). *Improving Quantification of Cellular Glycolytic Rate Using Agilent Seahorse XF Technology [white paper]*. Agilent Technologies.

Rudolph, J., Jung, K., Luger, K., Rudolph, J., Jung, K., & Luger, K. (2022). Inhibitors of PARP: Number crunching and structure gazing. *Proceedings of the National Academy of Sciences*, *119*(11). https://doi.org/10.1073/pnas.2121979119

Rudolph, J., Roberts, G., Luger, K., Rudolph, J., Roberts, G., & Luger, K. (2021). Histone Parylation factor 1 contributes to the inhibition of PARP1 by cancer drugs. *Nature Communications*, *12*(1). https://doi.org/10.1038/s41467-021-20998-8

Sakai, W., Swisher, E. M., Karlan, B. Y., Agarwal, M. K., Higgins, J., Friedman, C., Villegas, E., Jacquemont, C., Farrugia, D. J., Couch, F. J., Urban, N., & Taniguchi, T. (2008). Secondary mutations as a mechanism of cisplatin resistance in BRCA2-mutated cancers. *Nature*, *451*(7182), 1116-1120. https://doi.org/10.1038/nature06633

Sánchez-Garrido, M., Habegger, K., Clemmensen, C., Holleman, C., Müller, T., Perez-Tilve, D., Li, P., Agrawal, A., Finan, B., Drucker, D., Tschöp, M., DiMarchi, R., & Kharitonenkov, A. (2016). Fibroblast activation protein (FAP) as a novel metabolic target. *Molecular Metabolism*, *5*(10). https://doi.org/10.1016/j.molmet.2016.07.003

Sarmiento, J. M., Nagorney, D. M., Sarr, M. G., & Farnell, M. B. (2001). PERIAMPULLARY CANCERS: Are There Differences? *Surgical Clinics of North America*, *81*(3). https://doi.org/10.1016/S0039-6109(05)70142-0

Sasaki, Y., Inouchi, T., Nakatsuka, R., Inoue, A., Masutani, M., & Nozaki, T. (2024). Activated NAD+ biosynthesis pathway induces olaparib resistance in BRCA1 knockout pancreatic cancer cells. *PLOS ONE*, *19*(4). https://doi.org/10.1371/journal.pone.0302130

Schmidt, M. L., Donninger, H., & Clark, G. J. (2014). Ras Regulates SCFβ-TrCP Protein Activity and Specificity via Its Effector Protein NORE1A. *The Journal of Biological Chemistry*, *289*(45). https://doi.org/10.1074/jbc.M114.594283

Schulz, A., Meyer, F., Dubrovska, A., & Borgmann, K. (2019). Cancer Stem Cells and Radioresistance: DNA Repair and Beyond. *Cancers*, *11*(6). https://doi.org/10.3390/cancers11060862

Sears, C. R., Cooney, S. A., Chin-Sinex, H., Mendonca, M. S., & Turchi, J. J. (2016). DNA damage response (DDR) pathway engagement in cisplatin radiosensitization of non-small cell lung cancer. *DNA Repair*, *40*. https://doi.org/10.1016/j.dnarep.2016.02.004

Shalem, O., Sanjana, N. E., & Zhang, F. (2015). High-throughput functional genomics using CRISPR–Cas9. *Nature Reviews Genetics*, *16*(5), 299-311. https://doi.org/10.1038/nrg3899

Shichi, Y., Gomi, F., Sasaki, N., Nonaka, K., Arai, T., & Ishiwata, T. (2022). Epithelial and Mesenchymal Features of Pancreatic Ductal Adenocarcinoma Cell Lines in Two- and Three-Dimensional Cultures. *Journal of Personalized Medicine*, *12*(5). https://doi.org/10.3390/jpm12050746

Shruthi, S., & Shenoy, K. B. (2024). Cisplatin Resistance in Cancer Therapy: Causes and Overcoming Strategies. *ChemistrySelect*, *9*(25). https://doi.org/10.1002/slct.202401449

Singh, M. P., Cho, H. J., Kim, J.-T., Baek, K. E., Lee, H. G., & Kang, S. C. (2019). Morin Hydrate Reverses Cisplatin Resistance by Impairing PARP1/HMGB1-Dependent Autophagy in Hepatocellular Carcinoma. *Cancers*, *11*(7). https://doi.org/10.3390/cancers11070986

Skuta C, P, B., & D, S. (2014). InCHlib – interactive cluster heatmap for web applications. *Journal of Cheminformatics*, *6*(44).

Spiegel, J. O., Houten, B. V., & Durrant, J. D. (2021). PARP1: Structural insights and pharmacological targets for inhibition. *DNA Repair*, *103*. https://doi.org/10.1016/j.dnarep.2021.103125

Stewart, M. D., Vega, D. M., Arend, R. C., Baden, J. F., Barbash, O., Beaubier, N., Collins, G., French, T., Ghahramani, N., Hinson, P., Jelinic, P., Marton, M. J., McGregor, K., Parsons, J., Ramamurthy, L., Sausen, M., Sokol, E. S., Stenzinger, A., Stires, H.,…Allen, J. (2022). Homologous Recombination Deficiency: Concepts, Definitions, and Assays. *The Oncologist*, *27*(3). https://doi.org/10.1093/oncolo/oyab053

Stine, Z. E., Schug, Z. T., Salvino, J. M., & Dang, C. V. (2021). Targeting cancer metabolism in the era of precision oncology. *Nature Reviews Drug Discovery*, *21*(2). https://doi.org/10.1038/s41573-021-00339-6

Stoof, J., Harrold, E., Mariottino, S., Lowery, M. A., & Walsh, N. (2021). DNA Damage Repair Deficiency in Pancreatic Ductal Adenocarcinoma: Preclinical Models and Clinical Perspectives. *Frontiers in Cell and Developmental Biology*, *9*. https://doi.org/10.3389/FCELL.2021.749490

Summers, K. C., Shen, F., Potchanant, E. A. S., Phipps, E. A., Hickey, R. J., & Malkas, L. H. (2011). Phosphorylation: The Molecular Switch of Double-Strand Break Repair. *International Journal of Proteomics*, *2011*(1). https://doi.org/10.1155/2011/373816

Sun, L., Evsikova, C. M. d., Bian, K., Achille, A., Telles, E., Pei, H., & Seto, E. (2018). Programming and Regulation of Metabolic Homeostasis by HDAC11. *EBioMedicine*, *33*. https://doi.org/10.1016/j.ebiom.2018.06.025

Surveillance Research Program, N. C. I. (2024). *SEER*Explorer: An interactive website for SEER cancer statistics [Internet]*. https://seer.cancer.gov/statistics-network/explorer/.

Suurmeijer, J. A., Soer, E. C., Dings, M. P. G., Kim, Y., Strijker, M., Bonsing, B. A., Brosens, L. A. A., Busch, O. R., Groen, J. V., Halfwerk, J. B., Slooff, R. A. E., van Laarhoven, H. W. M., Molenaar, I. Q., Offerhaus, G. J. A., Morreau, H., van de Vijver, M. J., Fariña Sarasqueta, A., Verheij, J., Besselink, M. G.,…de Guerre, L. (2022). Impact of classical and basal-like molecular subtypes on overall survival in resected pancreatic cancer in the SPACIOUS-2 multicentre study. *British Journal of Surgery*, *109*(11). https://doi.org/10.1093/bjs/znac272

Taherian, M., Wang, H., & Wang, H. (2022). Pancreatic Ductal Adenocarcinoma: Molecular Pathology and Predictive Biomarkers. *Cells*, *11*(19). https://doi.org/10.3390/cells11193068

Takimoto, C. H., Graham, M. A., Lockwood, G., Ng, C. M., Goetz, A., Greenslade, D., Remick, S. C., Sharma, S., Mani, S., Ramanathan, R. K., Synold, T. W., Doroshow, J. H., Hamilton, A., Mulkerin, D. L., Ivy, P., Egorin, M. J., & Grem, J. L. (2007). Oxaliplatin Pharmacokinetics and Pharmacodynamics in Adult Cancer Patients with Impaired Renal Function. *Clinical Cancer Research*, *13*(16), 4832-4839. https://doi.org/10.1158/1078-0432.CCR-07-0475

Tanaka, K., Kawai, S., Fujii, E., Yano, M., Miyayama, T., Nakano, K., Terao, K., & Suzuki, M. (2023). Development of rat duodenal monolayer model with effective barrier function from rat organoids for ADME assay. *Scientific Reports*, *13*(1). https://doi.org/10.1038/s41598-023-39425-7

Tang, M., Bolderson, E., O'Byrne, K. J., & Richard, D. J. (2021). Tumor Hypoxia Drives Genomic Instability. *Frontiers in Cell and Developmental Biology*, *9*. https://doi.org/10.3389/fcell.2021.626229

Tang, Y., Hou, J., Li, G., Song, Z., Li, X., Yang, C., Liu, W., Hu, Y., & Xu, Y. (2014). ABCG2 regulates the pattern of self-renewing divisions in cisplatin-resistant non-small cell lung cancer cell lines. *Oncology reports*, *32*(5). https://doi.org/10.3892/or.2014.3470

Tarcan, Z. C., Esmer, R., Akar, K. E., Bagci, P., Bozkurtlar, E., Saka, B., Armutlu, A., Sahin Ozkan, H., Ozcan, K., Taskin, O. C., Kapran, Y., Aydin Mericoz, C., Balci, S., Yilmaz, S., Cengiz, D., Gurses, B., Alper, E., Tellioglu, G., Bozkurt, E.,…Adsay, N. V. (2024). Intra-ampullary Papillary Tubular Neoplasm (IAPN): Clinicopathologic Analysis of 72 Cases Highlights the Distinctive Characteristics of a Poorly Recognized Entity. *The American journal of surgical pathology*. https://doi.org/10.1097/PAS.0000000000002275

Tarsounas, M., Davies, A. A., & West, S. C. (2004). RAD51 localization and activation following DNA damage. *Philosophical Transactions of the Royal Society B: Biological Sciences*, *359*(1441), 87-87. https://doi.org/10.1098/RSTB.2003.1368

Tarsounas, M., Davies, D., & West, S. C. (2003). BRCA2-dependent and independent formation of RAD51 nuclear foci. *Oncogene 2003 22:8*, *22*(8), 1115-1123. https://doi.org/10.1038/sj.onc.1206263

Teng, Q.-X., Lei, Z.-N., Wang, J.-Q., Yang, Y., Wu, Z.-X., Acharekar, N. D., Zhang, W., Yoganathan, S., Pan, Y., Wurpel, J., Chen, Z.-S., & Fang, S. (2024). Overexpression of ABCC1 and ABCG2 confers resistance to talazoparib, a poly (ADP-Ribose) polymerase inhibitor. *Drug Resistance Updates*, *73*. https://doi.org/10.1016/j.drup.2023.101028

Terns, M. P., & Terns, R. M. (2011). CRISPR-based adaptive immune systems. *Current Opinion in Microbiology*, *14*(3), 321-327. https://doi.org/10.1016/J.MIB.2011.03.005

The Galaxy Community, Afgan, E., Nekrutenko, A., Grüning, B. A., Blankenberg, D., Goecks, J., Schatz, M. C., Ostrovsky, A. E., Mahmoud, A., Lonie, A. J., Syme, A., Fouilloux, A., Bretaudeau, A., Nekrutenko, A., Kumar, A., Eschenlauer, A. C., DeSanto, A. D., Guerler, A., Serrano-Solano, B.,…Briggs, P. J. (2022). The Galaxy platform for accessible, reproducible and collaborative biomedical analyses: 2022 update. *Nucleic Acids Research*, *50*(W1). https://doi.org/10.1093/nar/gkac247

Tibbetts, R. S., Cortez, D., Brumbaugh, K. M., Scully, R., Livingston, D., Elledge, S. J., & Abraham, R. T. (2000). Functional interactions between BRCA1 and the checkpoint kinase ATR during genotoxic stress. *Genes & Development*, *14*(23). https://doi.org/10.1101/gad.851000

Tiriac, H., Belleau, P., Engle, D. D., Plenker, D., Deschênes, A., Somerville, T. D. D., Froeling, F. E. M., Burkhart, R. A., Denroche, R. E., Jang, G. H., Miyabayashi, K., Young, C. M., Patel, H., Ma, M., Lacomb, J. F., Palmaira, R. L. D., Javed, A. A., Huynh, J. C., Johnson, M.,…Tuveson, D. A. (2018). Organoid profiling identifies common responders to chemotherapy in pancreatic cancer. *Cancer Discovery*, *8*(9), 1112-1129. https://doi.org/10.1158/2159-8290.CD-18-0349

Tobalina, L., Armenia, J., Irving, E., O'Connor, M. J., & Forment, J. V. (2021). A meta-analysis of reversion mutations in BRCA genes identifies signatures of DNA end-joining repair mechanisms driving therapy resistance. *Annals of Oncology*, *32*(1). https://doi.org/10.1016/j.annonc.2020.10.470

Tong, Y., Sun, M., Chen, L., Wang, Y., Li, Y., Li, L., Zhang, X., Cai, Y., Qie, J., Pang, Y., Xu, Z., Zhao, J., Zhang, X., Liu, Y., Tian, S., Qin, Z., Feng, J., Zhang, F., Zhu, J.,…Ding, C. (2022). Proteogenomic insights into the biology and treatment of pancreatic ductal adenocarcinoma. *Journal of Hematology & Oncology 2022 15:1*, *15*(1). https://doi.org/10.1186/s13045-022-01384-3

Torres, M. P., Rachagani, S., Souchek, J. J., Mallya, K., Johansson, S. L., & Batra, S. K. (2013). Novel Pancreatic Cancer Cell Lines Derived from Genetically Engineered Mouse Models of Spontaneous Pancreatic Adenocarcinoma: Applications in Diagnosis and Therapy. *PLOS ONE*, *8*(11). https://doi.org/10.1371/journal.pone.0080580

Tuli, R., Shiao, S. L., Nissen, N., Tighiouart, M., Kim, S., Osipov, A., Bryant, M., Ristow, L., Placencio-Hickok, V. R., Hoffman, D., Rokhsar, S., Scher, K., Klempner, S. J., Noe, P., Davis, M. J., Wachsman, A., Lo, S., Jamil, L., Sandler, H.,…Hendifar, A. (2019). A phase 1 study of veliparib, a PARP-1/2 inhibitor, with gemcitabine and radiotherapy in locally advanced pancreatic cancer. *EBioMedicine*, *40*, 375-381. https://doi.org/10.1016/j.ebiom.2018.12.060

Uhlén, M., Fagerberg, L., Hallström, B. M., Lindskog, C., Oksvold, P., Mardinoglu, A., Sivertsson, Å., Kampf, C., Sjöstedt, E., Asplund, A., Olsson, I., Edlund, K., Lundberg, E., Navani, S., Szigyarto, C. A.-K., Odeberg, J., Djureinovic, D., Takanen, J. O., Hober, S.,…Pontén, F. (2015). Tissue-based map of the human proteome. *Science*, *347*(6220). https://doi.org/10.1126/science.1260419

Vaitsiankova, A., Burdova, K., Sobol, M., Gautam, A., Benada, O., Hanzlikova, H., & Caldecott, K. W. (2022). PARP inhibition impedes the maturation of nascent DNA strands during DNA replication. *Nature Structural & Molecular Biology*, *29*(4). https://doi.org/10.1038/s41594-022-00747-1

Valdiglesias, V., Giunta, S., Fenech, M., Neri, M., & Bonassi, S. (2013). γH2AX as a marker of DNA double strand breaks and genomic instability in human population studies. *Mutation research*, *753*(1). https://doi.org/10.1016/j.mrrev.2013.02.001

Valle, J., Wasan, H., Palmer, D. H., Cunningham, D., Anthoney, A., Maraveyas, A., Madhusudan, S., Iveson, T., Hughes, S., Pereira, S. P., Roughton, M., & Bridgewater, J. (2010). Cisplatin plus Gemcitabine versus Gemcitabine for Biliary Tract Cancer. *New England Journal of Medicine*, *362*(14). https://doi.org/10.1056/NEJMoa0908721

van Staveren, W. C. G., Solís, D. Y. W., Hébrant, A., Detours, V., Dumont, J. E., & Maenhaut, C. (2009). Human cancer cell lines: Experimental models for cancer cells in situ? For cancer stem cells? *Biochimica et Biophysica Acta (BBA) - Reviews on Cancer*, *1795*(2), 92-103. https://doi.org/10.1016/J.BBCAN.2008.12.004

Wagh, V., Joshi, P., Jariyal, H., & Chauhan, N. (2020). ATM and ATR Checkpoint Kinase Pathways: A Concise Review. *Advances in Human Biology*, *10*(2). https://doi.org/10.4103/AIHB.AIHB_78_19

Wallez, Y., Dunlop, C. R., Johnson, T. I., Koh, S.-B., Fornari, C., Yates, J. W. T., Fernández, S. B. d. Q., Lau, A., Richards, F. M., & Jodrell, D. I. (2018). The ATR Inhibitor AZD6738 Synergizes with Gemcitabine In Vitro and In Vivo to Induce Pancreatic Ductal Adenocarcinoma Regression. *Molecular Cancer Therapeutics*, *17*(8). https://doi.org/10.1158/1535-7163.MCT-18-0010

Wang, C., Zhang, W., Fu, M., Yang, A., Huang, H., & Xie, J. (2015). Establishment of human pancreatic cancer gemcitabine-resistant cell line with ribonucleotide reductase overexpression. *Oncology reports*, *33*(1). https://doi.org/10.3892/or.2014.3599

Wang, G., Chen, A., Wu, Y., Wang, D., Chang, C., Yu, G., Wang, G., Chen, A., Wu, Y., Wang, D., Chang, C., & Yu, G. (2022). Fat storage-inducing transmembrane proteins: beyond mediating lipid droplet formation. *Cellular & Molecular Biology Letters 2022 27:1*, *27*(1). https://doi.org/10.1186/s11658-022-00391-z

Wang, J., Kho, D. H., Zhou, J.-Y., Davis, R. J., Wu, G. S., Wang, J., Kho, D. H., Zhou, J.-Y., Davis, R. J., & Wu, G. S. (2017). MKP-1 suppresses PARP-1 degradation to mediate cisplatin resistance. *Oncogene*, *36*(43). https://doi.org/10.1038/onc.2017.197

Wang, Y., Wang, K., Zhang, H., Jia, X., Li, X., Sun, S., & Sun, D. (2023). Cell death-related biomarker SLC2A1 has a significant role in prognosis prediction and immunotherapy efficacy evaluation in pan-cancer. *Frontiers in Genetics*, *13*. https://doi.org/10.3389/fgene.2022.1068462

Wang, Z., Jia, R., Wang, L., Yang, Q., Hu, X., Fu, Q., Zhang, X., Li, W., & Ren, Y. (2022). The Emerging Roles of Rad51 in Cancer and Its Potential as a Therapeutic Target. *Frontiers in Oncology*, *12*. https://doi.org/10.3389/fonc.2022.935593

Wangpaichitr, M., Theodoropoulos, G., Nguyen, D. J. M., Wu, C., Spector, S. A., Feun, L. G., & Savaraj, N. (2021). Cisplatin Resistance and Redox-Metabolic Vulnerability: A

Second Alteration. *International Journal of Molecular Sciences*, *22*(14). https://doi.org/10.3390/ijms22147379

Ward, I. M., & Chen, J. (2001). Histone H2AX Is Phosphorylated in an ATR-dependent Manner in Response to Replicational Stress. *Journal of Biological Chemistry*, *276*(51). https://doi.org/10.1074/jbc.C100569200

Washington, M. K., Goldberg, R. M., Chang, G. J., Limburg, P., Lam, A. K., Salto-Tellez, M., Arends, M. J., Nagtegaal, I. D., Klimstra, D. S., Rugge, M., Schirmacher, P., Lazar, A. J., Odze, R. D., Carneiro, F., Fukayama, M., & Cree, I. A. (2021). Diagnosis of digestive system tumours. *International Journal of Cancer*, *148*(5). https://doi.org/10.1002/ijc.33210

Watanabe, S., Yogo, A., Otsubo, T., Umehara, H., Oishi, J., Kodo, T., Masui, T., Takaishi, S., Seno, H., Uemoto, S., & Hatano, E. (2022). Establishment of patient-derived organoids and a characterization-based drug discovery platform for treatment of pancreatic cancer. *BMC Cancer 2022 22:1*, *22*(1), 1-12. https://doi.org/10.1186/S12885-022-09619-9

Wei, K., & Hackert, T. (2021). Surgical Treatment of Pancreatic Ductal Adenocarcinoma. *Cancers*, *13*(8). https://doi.org/10.3390/cancers13081971

Wiedenheft, B., Sternberg, S. H., & Doudna, J. A. (2012). RNA-guided genetic silencing systems in bacteria and archaea. *Nature 2012 482:7385*, *482*(7385), 331-338. https://doi.org/10.1038/nature10886

Wijk, L. M. v., Nilas, A. B., Vrieling, H., & Vreeswijk, M. P. G. (2022). RAD51 as a functional biomarker for homologous recombination deficiency in cancer: a promising addition to the HRD toolbox? *Expert Review of Molecular Diagnostics*, *22*(2). https://doi.org/10.1080/14737159.2022.2020102

Wong, C. H., Siah, K. W., & Lo, A. W. (2019). Estimation of clinical trial success rates and related parameters. *Biostatistics*, *20*(2). https://doi.org/10.1093/biostatistics/kxx069

Wu, H., Fu, M., Wu, M., Cao, Z., Zhang, Q., & Liu, Z. (2024). Emerging mechanisms and promising approaches in pancreatic cancer metabolism. *Cell Death & Disease*, *15*(8). https://doi.org/10.1038/s41419-024-06930-0

Wu, S., Zhou, J., Zhang, K., Chen, H., Luo, M., Lu, Y., Sun, Y., & Chen, Y. (2020). Molecular Mechanisms of PALB2 Function and Its Role in Breast Cancer Management. *Frontiers in Oncology*, *10*. https://doi.org/10.3389/fonc.2020.00301

Wu, X., Song, W., Cheng, C., Liu, Z., Li, X., Cui, Y., Gao, Y., & Li, D. (2023). Small molecular inhibitors for KRAS-mutant cancers. *Frontiers in Immunology*, *14*. https://doi.org/10.3389/fimmu.2023.1223433

Xu, J., Gao, Y., Luan, X., Li, K., Wang, J., Dai, Y., Kang, M., Lu, C., Zhang, M., Lu, C. X., Kang, Y., & Xu, C. (2022). An effective AKT inhibitor-PARP inhibitor combination therapy for recurrent ovarian cancer. *Cancer Chemotherapy and Pharmacology*, *89*(5). https://doi.org/10.1007/s00280-022-04403-9

Xu, J., Peng, H., & Zhang, J.-T. (2007). Human multidrug transporter ABCG2, a target for sensitizing drug resistance in cancer chemotherapy. *Current medicinal chemistry*, *14*(6). https://doi.org/10.2174/092986707780059580

Xue, Y., Vanoli, A., Balci, S., Reid, M. M., Saka, B., Bagci, P., Memis, B., Choi, H., Ohike, N., Tajiri, T., Muraki, T., Quigley, B., El-Rayes, B. F., Shaib, W., Kooby, D., Sarmiento, J., Maithel, S. K., Knight, J. H., Goodman, M.,…Adsay, V. (2016). Non-ampullary–duodenal carcinomas: clinicopathologic analysis of 47 cases and comparison with ampullary and pancreatic adenocarcinomas. *Modern Pathology*, *30*(2). https://doi.org/10.1038/modpathol.2016.174

Yamashita, T., Inui, T., Yokota, J., Kawakami, K., Morinaga, G., Takatani, M., Hirayama, D., Nomoto, R., Ito, K., Cui, Y., Ruez, S., Harada, K., Kishimoto, W., Nakase, H., & Mizuguchi, H. (2021). Monolayer platform using human biopsy-derived duodenal organoids for pharmaceutical research. *Molecular Therapy. Methods & Clinical Development*, *22*. https://doi.org/10.1016/j.omtm.2021.05.005

Yin, T., Wei, H., Gou, S., Shi, P., Yang, Z., Zhao, G., & Wang, C. (2011). Cancer Stem-Like Cells Enriched in Panc-1 Spheres Possess Increased Migration Ability and Resistance to Gemcitabine. *International Journal of Molecular Sciences*, *12*(3). https://doi.org/10.3390/ijms12031595

Ying, H., Elpek, K. G., Vinjamoori, A., Zimmerman, S. M., Chu, G. C., Yan, H., Fletcher-Sananikone, E., Zhang, H., Liu, Y., Wang, W., Ren, X., Zheng, H., Kimmelman, A. C., Paik, J.-h., Lim, C., Perry, S. R., Jiang, S., Malinn, B., Protopopov, A.,…DePinho, R. A. (2011). Pten is a major tumor suppressor in pancreatic ductal adenocarcinoma and regulates an NF-κB-cytokine network. *Cancer Discovery*, *1*(2). https://doi.org/10.1158/2159-8290.CD-11-0031

Yokose, T., Kitago, M., Matsuda, S., Sasaki, Y., Masugi, Y., Nakamura, Y., Shinoda, M., Yagi, H., Abe, Y., Oshima, G., Hori, S., Yusuke, F., Nakano, Y., Endo, Y., Abe, K., Tokino, T., & Kitagawa, Y. (2020). Combination of KRAS and SMAD4 mutations in formalin-fixed paraffin-embedded tissues as a biomarker for pancreatic cancer. *Cancer Science*, *111*(6). https://doi.org/10.1111/cas.14425

Yu, J. S. L., & Yusa, K. (2019). Genome-wide CRISPR-Cas9 screening in mammalian cells. *Methods*, *164-165*, 29-35. https://doi.org/10.1016/J.YMETH.2019.04.015

Zaal, E. A., & Berkers, C. R. (2018). The Influence of Metabolism on Drug Response in Cancer. *Frontiers in Oncology*, *8*. https://doi.org/10.3389/fonc.2018.00500

Zamanian, M. Y., Golmohammadi, M., Yumashev, A., Hjazi, A., Toama, M. A., AbdRabou, M. A., Gehlot, A., Alwaily, E. R., Shirsalimi, N., Yadav, P. K., & Moriasi, G. (2024). Effects of metformin on cancers in experimental and clinical studies: Focusing on autophagy and AMPK/mTOR signaling pathways. *Cell Biochemistry and Function*, *42*(4). https://doi.org/10.1002/cbf.4071

Zampieri, L. X., Sboarina, M., Cacace, A., Grasso, D., Thabault, L., Hamelin, L., Vazeille, T., Dumon, E., Rossignol, R., Frédérick, R., Sonveaux, E., Lefranc, F., & Sonveaux, P. (2021). Olaparib Is a Mitochondrial Complex I Inhibitor That Kills Temozolomide-Resistant Human Glioblastoma Cells. *International Journal of Molecular Sciences*, *22*(21). https://doi.org/10.3390/ijms222111938

Zeeberg, K., Cardone, R. A., Greco, M. R., Saccomano, M., Nøhr-Nielsen, A., Alves, F., Pedersen, S. F., & Reshkin, S. J. (2016). Assessment of different 3D culture systems to study tumor phenotype and chemosensitivity in pancreatic ductal adenocarcinoma. *International Journal of Oncology*, *49*(1). https://doi.org/10.3892/ijo.2016.3513

Zhang, Y., Esmail, A., Mazzaferro, V., Abdelrahim, M., Zhang, Y., Esmail, A., Mazzaferro, V., & Abdelrahim, M. (2022). Newest Therapies for Cholangiocarcinoma: An Updated Overview of Approved Treatments with Transplant Oncology Vision. *Cancers*, *14*(20). https://doi.org/10.3390/cancers14205074

Zhang, Z., Zhang, H., Liao, X., & Tsai, H.-i. (2023). KRAS mutation: The booster of pancreatic ductal adenocarcinoma transformation and progression. *Frontiers in Cell and Developmental Biology*, *11*. https://doi.org/10.3389/fcell.2023.1147676

Zhao, J., Lai, L., Ji, W., & Zhou, Q. (2019). Genome editing in large animals: current status and future prospects. *National Science Review*, *6*(3), 402-420. https://doi.org/10.1093/NSR/NWZ013

Zhao, Y., Ye, X., Xiong, Z., Ihsan, A., Ares, I., Martínez, M., Lopez-Torres, B., Martínez-Larrañaga, M.-R., Anadón, A., Wang, X., & Martínez, M.-A. (2023). Cancer Metabolism: The Role of ROS in DNA Damage and Induction of Apoptosis in Cancer Cells. *Metabolites*, *13*(7). https://doi.org/10.3390/metabo13070796

Zhao, Y., Zhang, L.-X., Jiang, T., Long, J., Ma, Z.-Y., Lu, A.-P., Cheng, Y., & Cao, D.-S. (2020). The ups and downs of Poly(ADP-ribose) Polymerase-1 inhibitors in cancer therapy–Current progress and future direction. *European Journal of Medicinal Chemistry*, *203*. https://doi.org/10.1016/j.ejmech.2020.112570

Zheng, F., Zhang, Y., Chen, S., Weng, X., Rao, Y., & Fang, H. (2020). Mechanism and current progress of Poly ADP-ribose polymerase (PARP) inhibitors in the treatment of ovarian cancer. *Biomedicine & Pharmacotherapy*, *123*. https://doi.org/10.1016/j.biopha.2019.109661

Zhou, T., Xie, Y., Hou, X., Bai, W., Li, X., Liu, Z., Man, Q., Sun, J., Fu, D., Yan, J., Zhang, Z., Wang, Y., Wang, H., Jiang, W., Gao, S., Zhao, T., Chang, A., Wang, X., Sun, H.,…Liu, J. (2023). Irbesartan overcomes gemcitabine resistance in pancreatic cancer by suppressing stemness and iron metabolism via inhibition of the Hippo/YAP1/c-Jun axis. *Journal of Experimental & Clinical Cancer Research*, *42*(1). https://doi.org/10.1186/s13046-023-02671-8

Zhou, X., Gao, H., Guo, Y., Chen, Y., & Ruan, X. (2018). Knocking down Stard3 decreases adipogenesis with decreased mitochondrial ROS in 3T3-L1 cells. *Biochemical and biophysical research communications*, *504*(2). https://doi.org/10.1016/j.bbrc.2018.06.030

Zhou, X., Hu, K., Bailey, P., Springfeld, C., Roth, S., Kurilov, R., Brors, B., Gress, T., Buchholz, M., An, J., Wei, K., Peccerella, T., Büchler, M. W., Hackert, T., & Neoptolemos, J. P. (2021). Clinical Impact of Molecular Subtyping of Pancreatic Cancer. *Frontiers in Cell and Developmental Biology*, *9*. https://doi.org/10.3389/fcell.2021.743908

Zihlif, M., Hameduh, T., Bulatova, N., & Hammad, H. (2023). Alteration in the expression of the chemotherapy resistance-related genes in response to chronic and acute hypoxia in pancreatic cancer. *Biomedical Reports*, *19*(6). https://doi.org/10.3892/br.2023.1670

Zimmermann, M., Murina, O., Reijns, M. A. M., Agathanggelou, A., Challis, R., Tarnauskaitė, Ž., Muir, M., Fluteau, A., Aregger, M., McEwan, A., Yuan, W., Clarke, M., Lambros, M. B., Paneesha, S., Moss, P., Chandrashekhar, M., Angers, S., Moffat, J., Brunton, V. G.,…Durocher, D. (2018). CRISPR screens identify genomic ribonucleotides as a source of PARP-trapping lesions. *Nature*, *559*(7713). https://doi.org/10.1038/s41586-018-0291-z